# Development of Backdrivable Hydraulic Actuators Using Magnetorheological Fluids

# 磁性流体を用いたバックドライブ可能な油圧アクチュエータの開発

**February 2017**

**Gonzalo AGUIRRE DOMINGUEZ**

**アギーレ ドミンゲス ゴンサロ**

# Development of Backdrivable Hydraulic Actuators Using Magnetorheological Fluids

# 磁性流体を用いたバックドライブ可能な油圧アクチュエータの開発

**February 2017**

**Waseda University**

**Graduate School of Creative Science and Engineering**

**Department of Modern Mechanical Engineering**

**Research on Intelligent Machines**

**Gonzalo AGUIRRE DOMINGUEZ**

**アギーレ ドミンゲス ゴンサロ**

*To my family, friends,*
*and Hande Ünlü*

# ACKNOWLEDGEMENTS

With my deepest appreciation to those who made this dissertation possible.

I would like to extend my most sincere gratitude to my Ph.D. supervisor Professor Dr. Shigeki Sugano –at Department of Modern Mechanical Engineering, School of Creative Science and Engineering at Waseda University– for his guidance, encouragement, and above all, for giving me the opportunity to join his distinguished research team. I also express my thankfulness to Prof. Atsuo Takanishi, Prof. Jun Ohya, Prof. Mitsuo Umezu, Prof. Tetsuya Ogata, Prof. Hiroyasu Iwata, and Prof. Eiji Iwase for their contribution in improving this work.

The Japanese government-sponsored Monbukagakusho Scholarship and the NEDO SAMURAI fund, which made my study and research in Japan financially possible.

My supervisor Dr. Mitsuhiro Kamezaki for all discussions, constructive criticism, and inspiration that made this research original and focused. My team members, especially Morgan French and He Shan for their hard work, efforts, and patience that made the practical evaluation of my research possible. As well as Kenshiro Otsuki and Peizhi Zhang for their selfless commitment and engagement during my final year. Members from Sugano Lab., specially to Dr. Alexander Schmitz, Dr. Sophon Somlor, and Tito Pradhono for challenging my ideas in our fruitful discussions. The Sugano Lab. secretaries, Yoko Ono and Kyoko Arai for their support.

The Leading Program for Embodiment Informatics and all its members for a nurturing environment to conduct my research, allowing me to work surrounded by brilliant and motivated minds. I would like to thank all the professors for their wise input and motivation to conduct my research, and look for other applications beyond the scope of it.

FTECH company which supplied the parts used at my experiments. Their timely delivery, along with the expertise of Mr. Masayuki, enabled the successful realisation of the prototypes.

Dr. Hande Ünlü, my loving wife, for her constant encouragement, her never-ending patience, and above all, for helping realise my dreams with her unconditional support.

My beloved family for their love and support despite the long distance. To my father Oscar Aguirre Ramirez who taught me the basic concepts of engineering that later inspired me to become one. To my mother Nora Araceli Dominguez Lerma, for her constant encouragement to pursue the highest standards. To my brother, Oscar Aguirre Dominguez for helping me focus my goals, and motivating me to continue working hard to achieve them.

Tokyo, 1 December 2016
*Gonzalo Aguirre Domínguez*

# ABSTRACT

In recent years, the widespread of robotic technology outside factories has brought along a rising interest in deploying robots in construction and disaster relief operations, to minimise the risk and hazards for humans in such environments. For these applications, it is indispensable to ensure the safety for robots, their environment, and the people around them. Therefore, several systems for robust safe robotic actuation have been designed. Nevertheless, most of them are aimed at small power systems for human collaboration, and do not meet the requirements of more demanding applications. In the future, systems need to provide them with mobility to navigate through obstacles, energy efficiency for longer periods of operation, versatility to perform many tasks, backdrivability to ensure safety, and simplified control to operate in challenging conditions. Given the practical necessity, this research focuses on the development of actuators with high power densities and soft actuation capabilities for mobile robotic applications. In so far, state-of-art research on safe actuators with high power output appears to offer limited alternatives, with some systems being able to provide some of the characteristics mentioned above, but none to offer a feasible and practical integration of all of them. This research tries to overcome the observed disadvantages of current devices, by proposing a new concept for safe high power actuation. It is hypothesised that it is possible achieve all the requirements above by effectively combining the properties of electro-hydrostatic systems and MR fluids.

After researching current literature on MR fluid based actuators, it was found that the most suitable alternative for such system was to use annular flow piston dampers, because of their high forces and compact movable heads. However, after analysing most common designs, it was discovered that they lacked customization options, and probably have inefficient magnetic circuits. This motivates the conceptualization of an alternative configuration inspired by toroidal electromagnets, which consists of a novel array of MR valves, contained within the piston head. The device is theorised to offer better energy efficiency by increasing the interaction area between the MR fluid and the magnetic field, and less magnetic leakage by exploiting the material properties the materials used in its construction. In order to test this novel idea a piston prototype is designed, built, and tested. The experiments show that the prototype is able to precisely control the output force of the actuator with fast response times, proving the feasibility of the toroidal magnetic circuit, and highlighting its potential in force control applications to provide a wider range of customisation options. Nevertheless, its measured force and energy efficiency were very limited when compared to the conventional system.

In order to better understand the observed performance, mathematical models for the new actuator was constructed. Unlike current complex models, the mechanical, electromagnetic, and hydraulic models for the new actuator are constructed using simplified equations, based on the reluctance method, and an approximation of the Buckingham Reiner equation. This makes it possible to understand the relations between relevant parameters of the actuator, in order to identify the key parameters of the system. However, during the validation of the models the results showed a significant discrepancy with the experimental data, probably caused by the assumptions used in the electromagnetic model. Thus, a

magnetic Finite Element Method (FEM) analysis was conducted to confirm this. The analysis shows unaccounted magnetic leakage in the circuit. After, integrating the results of the analysis into the model equations, the prediction improved. However, its accuracy can be improved, probably by finding accurate values for the material properties used in the model.

The observations obtained from the modelling and simulations provide valuable information about ways to improve the performance of the prototype. Using this information, a new conceptual prototype is designed. An analysis, based on an iterative search for valid permutations of parameters, revealed that there is an optimal relation between the magnetic flux density, and the active area exposed to the MRF. It also identified the key parameters relating these properties, which are then optimised. The results from the new prototype show that the optimisation procedure successfully improve the performance of the prototype, achieving twice the original force and twelve fold energy efficiency.

The improved prototype of the system is connected to a gear pump, to test the performance of the proposed system as an actuator. The results of the experiments reveal that the speed and force of the actuator can be controlled independently achieving accuracy of 98% on the output force, even during collisions, outside the friction deadband, where force is still uncontrollable. Additionally, the small correlation between speed and force reveals its potential to realise different operation modes. A proposal for an intelligent control strategy using these operation modes makes clear how future applications could achieve faster reaction times, improved backdrivability, and better energy efficiency.

As a final step, the theory behind the linear prototype is adapted into the conceptualization of a rotatory device. The new concept yields two different prototypes based on a traditional vane motor. They realise backdrivable operation by using passages through the vane and centre shaft. The results show that the unique hydraulic vane motor with 4Nm is a successful adaptation of the original concept, demonstrating the versatility and adaptability of the technology. In the future this technology can be implemented not only in collaborative robots for construction and disaster relief, but also in many other solutions for mobile applications where compact high power and safe actuation are a critical necessity.

The theoretical and empirical evidence presented in this study shows that it is feasible to develop a backdrivable hydraulic actuator using MR fluids that simultaneously provides high power output and intrinsically soft actuation characteristics. Introducing a new toroidal array of MR valves in the piston head makes it possible to achieve a greater degree of configuration options when compared to other conventional systems. Nevertheless, technical limitations, such as high friction, weight and integration of the hydraulic components into a single unit, prevent the immediate application of the system in safety critical tasks. These limitations can be overcome using practical know-how of hydraulic systems, such as seal-less designs, and fully integrated hydrostatic transmission models to improve the friction performance, weight and size of the actuator. Future studies should also refine the mathematical models in order to provide solid basis for the development of an intelligent control system, which can make full use of the capabilities of this device. Finally, it is necessary to implement the system in a concrete application to evaluate its performance in different practical tasks. I hope that in the future this device can reach its full potential to bridge the gap in actuation system, offering many solutions for mobile applications where high power and safe backdrivable actuation are necessary.

# CONTENTS

# List of Tables

# List of Figures

# List of Equations

# List of Abbreviations and Acronyms

ANSYS → Analysis System (program)

CAD → Computer Aided Design (program)

DAQ → Data Acquisition

EM → Electromagnet

EMC → Electromagnet Current

EMI → Electromagnetic Interference

EMV → Electromagnet Voltage

ER → Electrorheological

FEM → Finite Element Method

GUI → Graphical User Interface

MR → Magnetorheological

MRA → magnetorheological actuator

MRF → Magnetorheological Fluid

MRPA → Magnetorheological Piston Actuator

pHRI → Physical Human Robot Interaction

PTFE → Polytetrafluoroethylene

PV → Pump Voltage

PWM → Pulse Width Modulation

PID → Proportional Integral Derivative (controller)

SEA → Series Elastic Actuators

SDA → Series Dissipative Actuators

VDC → Volts Direct Current

# 1 Introduction

The advent of the digital age brought along a new industrial revolution based on automation and robotics. Since then, the remarkable increase in factory quality and productivity has led to the thriving success of robots in the manufacturing industry. Which in time has also sparked the interest to expand the applications of this technology into variety of new areas. Industries, such as pharmaceutical, biochemical and food are among many, which have adapted manufacturing systems into several forms of automation in their own processes.

Following these developments, recent years have brought along the emergence of robotic applications outside industrial environments. Now it is possible to see humanoid robots, such as Pepper, providing information in stores, Roombas helping to vacuum the house, and Google autonomous cars cruising the streets of California. In this way, robotic technology has evolved to a point where it starts intermingling with human society, affecting our everyday tasks and along our lives. However, different from controlled industrial settings, human environments present many new challenges to robotic technology. Navigation in unknown environments, task adaptability and learning, and safe physical human-robot (pHRI) interaction are a few examples of the problems that are currently being tackled.

In the near future, safe robot interaction will be of paramount importance to guarantee that no harm will occur to humans, the robot, and its close environment. This trend will drive

the development of new actuation systems for a variety of applications. Nevertheless, in order to ensure the applicability and feasibility of these technologies, it is necessary to develop systems that:

- provide safe actuation to interact with their environment
- address the requirements of current and future robotic applications

## 1.1 Motivation

In so far, the current research on safe robotic actuators has mainly focused on in the service and home environments. These actuation systems aim to provide a very safe pHRI with relatively low force. However, little attention has been drawn to safe actuation with a high power output. The lack of research in this area has overlooked other potential applications that may benefit from this technology.

In most current heavy-duty applications, operational safety guidelines and procedures are commonplace. Several passive mechanisms have been developed to avoid or isolate the risk of injury or harm of personal while operating the machine. These mechanisms basically work by minimizing the occurrence of dangerous situations for humans. However, there are limited systems that prevent the machine from damaging its environment or even itself. In most cases, it falls within the expertise and skills of the operator to minimise these risks. However, future autonomous or semi-autonomous robots for heavy-duty tasks must implement more sophisticated mechanisms to prevent uncontrolled dangerous interactions. Thus, there is a plausible need for the development of safe actuators with high power output, which can address the requirements of a new generation of heavy-duty robots.

### 1.1.1 Practical Application

Construction, disaster relief, mining, and oil industries are some examples were robot technology has great potential for future deployment. Typically, the work done in this ambit involves heavy-duty tasks, some of which also carry many environmental and occupational risks and dangers. In such scenarios, robots can perform the work instead of humans, minimizing the hazard and potentially saving many lives. However, safe actuators have rarely been designed and used for these type of systems.

The implementation of safe actuators in this type of applications brings several advantages. Limiting the force used during the operation of heavy equipment could prevent catastrophic damage to the environment and the robot during uncontrollable collisions. Implementing backdrivability of the end effectors in robots would allow a more simple control during manipulation tasks involving multiple limbs. This could be particularly useful for robots implementing multiple arms. Moreover, in inter-robot collaborative applications, this will ensure the safety of the agents operating in close distance. In tele-operated environments, this could also become a crucial part of the control loop, since a fast and reliable communication is not always possible. Additionally, this simplified control is particularly useful in environments with limited visibility. In these cases, it is not always possible to send precise commands, or rely on computer vision strategies to compensate for dangerous actions. These are few of the possible applications for this kind of technology. However, as robotic applications make their way in other similar industries the need for this type of actuation systems will continue to grow.

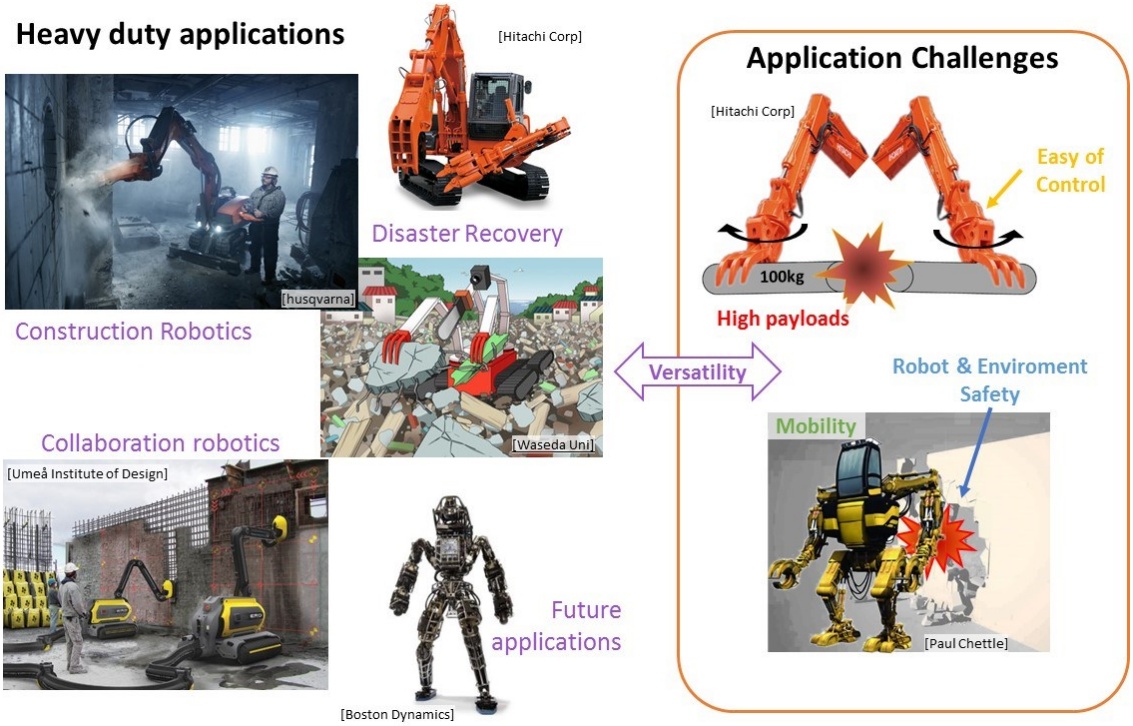


Figure 1-1. Possible applications for safe actuation systems and their challenges

## 1.1.2 Technology Gap

These kind of applications have very different requirements than their factory, service and home oriented counterparts, as shown in Figure 1-1. The tasks performed by these applications normally require higher payload capacity than the one used in manufacturing and

service environments. Additionally, most of these machines need to have a certain degree of mobility. They must be able to move, or be transported, easily from one place to the next, in order to complete their tasks efficiently. They are also required to operate extended periods of time on batteries or fuel, which requires good energy efficiency. At the same time, some applications need to be compact enough to facilitate their movement in constrained spaces. In order to develop safe actuators suitable for these type of applications new solutions are needed.

Currently, most robotic applications are built with highly rigid conventional servo systems that are good for precise speed and position control, but perform poor in terms of safety. Therefore, they have to employ complex control schemes to overcome this rigidity and achieve safe actuation. However, these solutions are limited by the bandwidth of the controller, which can lead to potentially harmful situations that arise due to the complexity of the environment and the interaction itself.

Nowadays, a new trend focuses on the development of systems, which can provide some level of collision safety thorough their particular mechanical properties. Generally, this intrinsic safety is achieved by using soft or light materials in the construction of the robot limbs. Other alternatives implement some mechanism in their drivetrain to provide a level of backdrivability, i.e. they intrinsically allow their outputs to be driven by an external agent. This backdrivable property is usually realised by a mechanism that either stores or dissipates the energy produced by external forces. In other words, these systems are capable of absorbing excess energy coming from the interaction forces with the environment. These actuators have been widely investigated in academia, as well as by the industry. However, there is only limited deployment of such systems in robotic applications for heavy-duty tasks.

One of the reasons behind the slow penetration of backdrivable technologies in heavy-duty applications is that most of the current technologies have not been developed for hydraulic systems. Most of the applications in used in heavy-duty tasks employ hydraulic actuators to achieve the high power densities needed. Nevertheless, the adoption of hydraulic actuators in robotic applications is relatively new, and somehow limited due to the many challenges they present. Compared to their electromechanic counterparts, these systems are still difficult to control, and maintain. Therefore, further research in hydraulic actuation is needed in order to spread the adoption of such system in many areas of robotics.

In so far, there are few examples in literature that have explored the implementation of compliant or backdrivable mechanisms in hydraulic systems. Among them, there are three relevant examples listed below:

- Electro-hydrostatic actuator with enhanced backdrivability
- Magnetorheological Dampers
- Magnetorheological Power Actuation System

A more in-depth description of these approaches is covered in chapter 2. Nevertheless, none of these approaches is able to successfully combine adjustable backdrivability with high output forces in an integrated mobile system. The development of such system would enable the creation of safe and reliable robotic applications for heavy-duty tasks, which are not currently available in the market, as seen in Figure 1-2. Therefore,

**the motivation of this research is,** *to equip mobile robotic applications with a suitable actuation system to safely undertake heavy-duty tasks in collaborative environments*


Figure 1-2. Research motivation: current gap in actuation technology

## 1.2 Theory and Hypothesis

As it has been previously discussed, there are relatively few alternatives to realise backdrivable actuation systems with high power density. Hydraulics systems are the technological choice for most heavy-duty task, since they can deliver very high force-weight ratios. Unfortunately, these systems are normally very stiff, even when compared with

electromechanical devices. Additionally, until now it has been challenging to implement safe control mechanisms for them.

In literature, hydraulic backdrivable systems based on magnetorheological fluids (MRFs) have been recently tested with satisfactory results. These systems provide the means to precisely control the system backdrivability with very fast response times. Unfortunately, there has not been a successful example of a fully integrated actuator with high power output. On the other hand, electro-hydrostatic actuators offer a compact form factor for hydraulic actuation, but lack the necessary mechanisms to adjust the amount of backdrivability in the system. Based on premises, the main theory behind this research can be summarised as:

- **electro-hydrostatic actuators** *are compact hydraulic devices with high output forces*
- **magnetorheological fluids** *can be used to achieve safe hydraulic actuation.*

Hypothetically, there should be a way to successfully combine the compact and efficient design of electro-hydrostatic actuators with the backdrivable properties of MRFs. A careful integration of both technologies could help to realise a new type of actuator that addresses the current technological gap between safe backdrivable motion and high power actuation. In this respect, **the main hypothesis of this research is**:

*it is possible to develop a compact device with a powerful yet safe force output by effectively combining the properties of electro-hydrostatic systems and MR fluids.*

## 1.3 Objective

The successful implementation of an actuation system with the characteristics mentioned above requires the development of several parts. A complete actuation system consists basically of an energy source, a transducer (commonly known as actuator), and a control unit.

As it can be seen in Figure 1-3, in the case of an electro-hydrostatic actuator the power supply can be considered as the complete hydraulic circuit, including the motor and pump; the control system including the sensor inputs and control output signals. On the other hand, the transducer is typically a piston or a rotatory motor. There are other important elements to the circuit, such as accumulator, filter, and sensors, among others. They have been omitted in this drawing for simplification purposes.

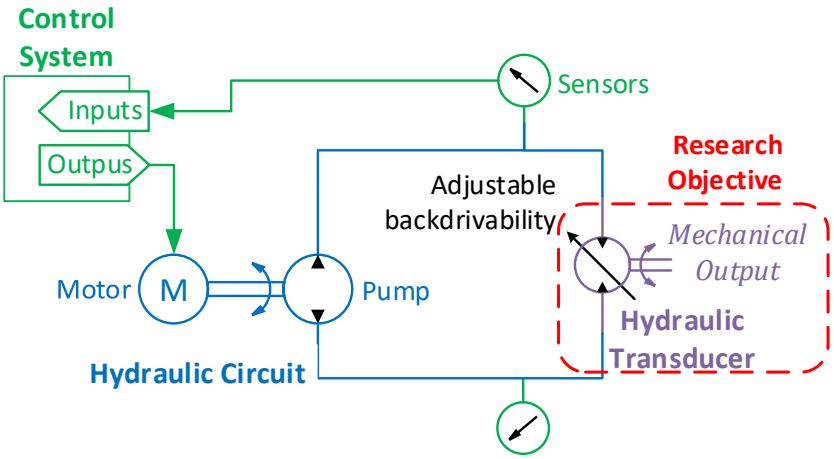


Figure 1-3. Main parts of a hydraulic actuation system, and the main research objective

Although all the parts of the system are essential for correct functionality of the actuator, the transducer plays a relevant role in its operation. It is in this part where the energy from the pressurised fluids is transformed in mechanical motion. Therefore, its correct design and implementation will greatly influence the overall performance of the system, including the backdrivable properties of the actuator.

**Thus, the concrete objective of this research is,** *to design and develop backdrivable actuators based in MR fluids that efficiently use hydraulic power to generate safe and powerful output forces.*

## 1.4 Sub Objectives

In order to realise a useful actuator for a variety of situations it is important to take into consideration the requirements of current and future applications of this technology. In order to achieve this, it is necessary to go beyond a simple proof of the feasibility of this research's hypothesis, and lay the necessary groundwork that allows the effective implementation of this technology. As a result, four milestones were set for the development of this study.

- Propose an actuator design: analyse the current technologies, in order to propose a suitable MR actuator design. The design must address the requirements previously described: high forces, backdrivable output, mobility, and versatility to adapt to many tasks.
- Model the actuator: in order to have the necessary guidelines to apply or optimise the actuator to any possible applications.

- Evaluate actuator performance: in order to validate the hypothesis of this research, and establish the quantitative feasibility of the technology, as well as to envision potential applications for it. Here it is also equally necessary to test and benchmark the technology against state-of-the-art alternatives.
- Introduce an alternative design: in order to demonstrate how the technology can be adapted to other known actuator configurations.

These objectives provide the necessary framework to provide a complete and satisfactory output from this research. Nevertheless, one must not forget that the development of new technology usually involves an iterative process. This allows not only to refine the quality of the technology but also to gain a deeper insight of its functionality and potential applications.

## 1.5 Research Methodology

As it can be inferred from the objectives described above, the evaluation of the research's hypothesis will be carried through an iterative process based on an analytical and empirical evaluation of the proposed technology. For this reason, the research was conducted in two main iterations, consisting of both analytical and empirical approaches. This approach is summarized in the diagram showed in Figure 1-4.

In an initial step, a prototype is conceptualised after analysing the shortcomings of current technologies. Later, the prototype is built and tested to evaluate the feasibility of the technology. On a second iteration, the design is improved through a comprehensive analysis of the original prototype. The resulting stable prototype is then tested and compared with state-of-the-art designs. The steps carried out in these two iterations are described in detail below.

1) Background Research Survey: previous research about compliant actuator is done in detail. With this information the requirements and the gap in the research is clearly defined. From the research it is clear that MRF based actuators (MRA) are intrinsically safe due to their backdrivable capabilities, low output inertia, and high operational bandwidth. They also exhibit high torque to mass ratio, short response times, and precise control of the output force making them suitable for applications in pHRI [1]. Moreover, because of their relatively simple construction and resistance to wear they present a high potential for deployment and commercialization at low cost [2], [3]. However their application in the robotics field is still quite limited, and

until now they are mostly used as haptic systems [4] and assistive devices [5]. Based on these findings, the conceptual design of a new MR actuator based on a piston is presented.

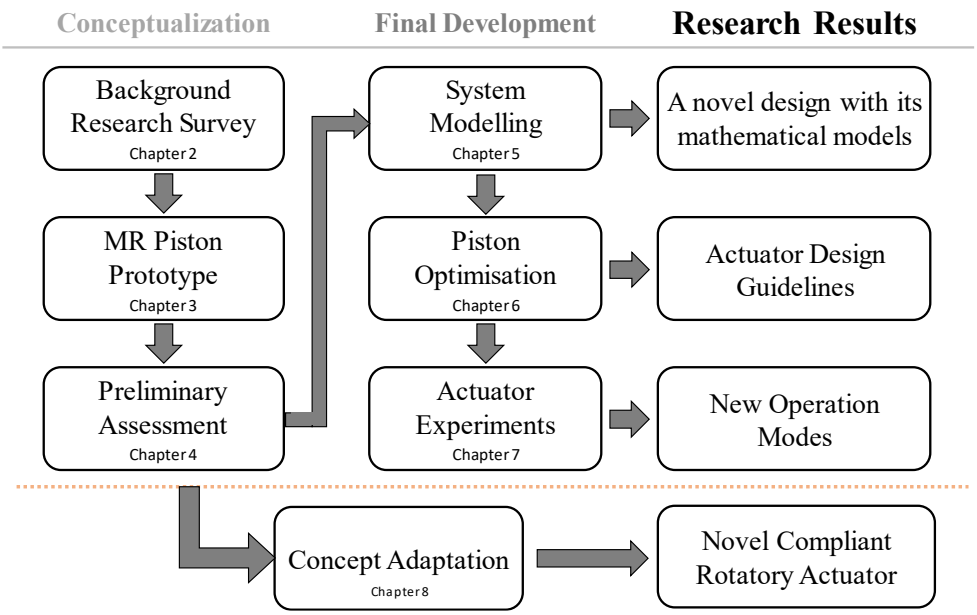


Figure 1-4. Overview of the steps involved in the research methodology

2) MR Piston Prototype: using a simplified equation the concept for a new piston head prototype is develop in this section. The principle of operation of the novel toroidal configuration for the piston head, as well as the parts involved in its construction are described in detail.

3) Preliminary Assessment: the passive performance of the device is analysed in order to evaluate its feasibility for active testing. Additionally, a benchmark against current actuators based on an annular design is introduced.

4) System Modelling: In order to understand the performance of the actuator the modelling of the electromagnetic circuit and the hydraulic system is done. The model is constructed using simple equations that provide an explicit solution to the parameter of the device. The models show the areas of opportunity for optimisation, but also the current limitations of the device. After comparing the results of the model with the previous step, it is clear that there are several discrepancies. To further refine the models, a FEM analysis is also performed. From it, it is possible to understand the mechanics of the electromagnetic circuit, and find additional points were the model could be improved.

5) Piston Optimisation: with the results from the model and the experimental evaluation, an iterative optimisation in Matlab is done. The optimisation study reveals that there are parameters with optimal values, while others depend on the application constrains. Additionally, other mechanical improvements, as well as an optimised piston head geometry are summarised in this section.

6) Actuator Experiments: The performance of the new optimised prototype is tested both passively and actively. The results are benchmarked against state-of-art actuators. The experiments aim to evaluate the actuator performance as a whole and determine the force, speed, and backdrivable capabilities of the device.

7) Compliant Rotatory Actuator: in this final chapter, the knowledge gathered from the work done previously is transferred into a new rotational prototype. The design is used to prove how the concepts learned in the previous iterations can be applied to other similar hydraulic transducers. Additionally, this new design opens the door for new applications of the technology. The efficiency of this design allows for further miniaturization, and much simpler integration of the device in future applications.

In resume, this study focusses on the conceptualization and development of a new type of hydraulic actuators based on an electro-hydrostatic system using MR fluids. These devices aim to address the shortcomings of current actuation technologies, which until now cannot provide mobile robots with suitable actuator to safely undertake heavy-duty tasks in collaborative environments. In order to overcome this, the novel prototypes combine the high power of hydraulics with the inherent safety provided by the MR fluids. These characteristics should allow a high force output with backdrivable active motion. This research aims to provide insights into the feasibility and potential application of these devices in real world applications.

# 2 Background Research

In this chapter covers a survey about the relevant current research done in safe actuation and hydraulic systems. The chapter begins by introducing the core safety technologies currently used in robots, defining the common terminology used in the field to avoid any misconceptions. Later, a more in-depth analysis of several safety systems explains the current state-of-the-art technologies covering their advantages, and shortcomings. At this point, electrorheological (ER) and magnetorheological (MR) fluids are introduced, and the basic concepts about actuators based on these smart materials are covered. To conclude, implementations of different systems using MR fluids are introduced and compared with current technologies to determine the shortcomings of these devices and the challenges that this work aims to overcome.

In resume, the main objectives of this chapter are to survey state of the art research to understand technologies used in safe actuation, find implementations of safe hydraulic actuators, determine shortcomings of current systems, and find the basis for a suitable technological alternative to develop a system that can theoretically overcome these problems.

## 2.1 Types of Safety Mechanisms

In conventional robotic applications stiff mechanisms has been used in order to achieve precise control of the trajectory and speed of the end effectors. These actuation systems have

allowed robots to perform repetitive tasks at very high speeds with remarkable precision. However, such rigid systems prone to damage when collisions occur. And while the robot may be expendable (yet expensive), collisions pose a serious danger to people close to the robot. For this reason, current research has focused in the development of force control strategies that compensate or mitigate the dangers of rigid mechanisms.

On the other hand, living organisms have evolved with a different kind of actuation means. The musculoskeletal system, found in developed vertebrae, do not only allow them to accurately execute speed and positioning control tasks, but also to provide a certain degree of safety while doing them. These characteristics are achieved by making use of elastic muscles, soft skin, spongy bone (cancellous bone), and cartilages.

These elements make it possible to control how their bodies store or dissipate energy generated during their interaction with the environment, protecting our bodies from injury. For example, muscles are able to store elastic energy by tensing and relaxing, i.e. adjusting the stiffness of the limbs. In this way, the muscles can store the energy caused by an external contact, and use it to return to the original position after it. While the viscous damping in the muscles maintains the stability during fast interactions and absorbs the impact from shocks. On the other hand, the skin is able to dissipate the energy from an impact to protect the inner tissues. These mechanisms act together to provide safety to the body.

### 2.1.1 Active vs Passive Safety

From the earlier discussion, it can be seen that in order to implement safety in robotic applications there are basically two main strategies, which have been widely documented research. **Active safety** uses complex control strategies to provide a level of safety in conventional rigid servo systems found in most robotic applications [6]. Some of these strategies try to emulate the properties observed in biological system. Impedance and admittance control is a force regulation strategy that models the interaction forces between the actuator and its environment as a spring, damper, mass system [7]. This approach has been researched in detail, finding several kinds of implementations such as unified [8], hybrid [9], and sensors based [10] strategies, among others. These can now be found in several robots and systems [11], including medical applications [12]. However, such strategies are limited to frequencies below the bandwidth of the controller used [13], [14]. Leading to potential dangerous situations that arise during the complex interaction between robots and humans.

The limitations found in active control systems have driven the development of alternative solutions. These strategies aim to provide an intrinsic level of safety by using mechanisms that mimic the safety properties found in biological systems. In this sense, these mechanisms constantly provide **passive safety** thorough out the interaction of the robot with its environment. However, most of these systems suffer from a trade-off between performance and position accuracy, making them less suitable for precise position control applications [15]. Nevertheless, they offer significant advantages for legged, human interaction, medical and rehabilitation robotic applications.

Passive safety can be easily realised by implementing soft skin around the moving parts of the robot [10], making them lighter [16] to avoid strong impacts [17], or adding some energy absorption element in the drive train, such spring or dampers. While these designs provide a reasonable level of safety, when compared with traditional systems, the properties of the system are fixed during the design. Lacking the possibility to adapt to different situations restricts the range of applications in which they can be deployed.

The simplicity of the applications above is appealing for applications where the speed, force, and precision necessary to perform a task does not change. However, a more versatile approach is needed in order to provide safety over a wider range of combinations of these variables. In this case, it is necessary to develop actuators that can provide adjustable safety mechanisms. This is typically achieved by introducing an adjustable spring or damping element to the drive train of the actuator or robotic system. While these elements add to the complexity of the system, they allow to control the level of safety by changing their mechanical properties. However, before detailing the way these mechanisms work, it is necessary to have a common understanding of the mechanical properties that affect the safety of a system. In order to do this, the concepts of compliance and backdrivability will be introduced.

## 2.2 Adjustable Backdrivability and Compliance

In recent years, *compliance* and *backdrivability* have been widely used in the field of safe actuation [15]. They are both recognised as important and desirable characteristics of actuators aim for force interaction. As in shoulders of humanoid robots [18]. Although sometimes used interchangeably, these terms need to be clearly defined in order to understand their role in the actuator functionality and safety.

Firstly, it must be understood that conventional servo systems are consider unsafe due to their rigidity. This is due to the fact that, during dynamic interactions with external agents they transfer all the kinetic energy and electromechanical forces directly to their end effectors. Moreover, during static interaction the friction in their gears and motors causes the mechanisms to be stiff. These characteristics make them particularly dangerous during unexpected collisions, where high interaction forces are involved.

To solve this problem, safety strategies are implemented directly in the mechanical design of the actuation system. Among them the most widely used mechanism is *backdrivability*, which, as it names implies, *intrinsically allows the output of a system to be driven by external agents*. As a result, backdrivability allows systems to absorb excess energy coming from the interaction forces with the environment, making them less prone to damage themselves or their surrounding environment. Typically, this desirable property has been realised by a mechanism that either stores or dissipates the energy produced by external forces. In this respect, the first implementation mostly uses springs, to achieve *compliant* actuation. In other words, a *compliant system implements elastic elements to absorb and release energy resulting from interaction forces*. *Thus, compliance can be regarded as a type of backdrivability*. This and other implementations of backdrivability are discussed ahead.

### 2.2.1 Series of Elastic Actuators

This type of actuator uses spring elements in series with the drivetrain, as seen in the figure below. This concept was introduced by Prat and Williamson in [19].

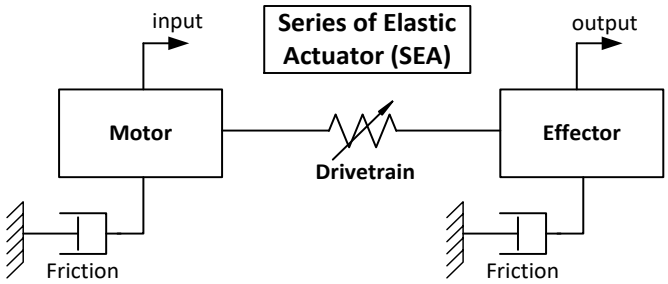


Figure 2-1. SEA – Series of Elastic Actuator Diagram

The biggest advantage of this type of backdrivability is that it stores the energy resulting from the interaction. The energy can be released later in a controlled or explosive manner to achieve different actuation properties. This is really useful to increase the energy efficiency

during walking tasks [20] in robots [21], and to create explosive force in throwing [22] or jumping [23] [24] tasks respectively.

Among these type of actuators it is worth to mention the following designs: VS-joint, a non-linear mechanisms for robot arms [25]. MACEPPA [26], a mechanism used in passive walking with adjustable equilibrium position using two motors. A mechanical impedance adjuster [27] used in a robot arm [28]. As well as vsaUT-II which employs a leaf spring with a movable fulcrum point [29].

All the designs mention above In this case there is a trade-off between backdrivability and ease of control [30]. In other words, the more backdrivable they are the more difficult is to achieve stable positioning. This characteristic can reduce their safety due to the uncontrolled oscillations caused by the spring.

### 2.2.2 Series of Dissipative Actuators

This type of actuator use an energy dissipation element in their drive trains. As a result, they offer a trade-off between backdrivability and efficiency. The more energy is dissipated is less efficient, but more movable. This model has been analysed and discussed in detail in the field of hydraulic actuation [31]. The figure below show their model.

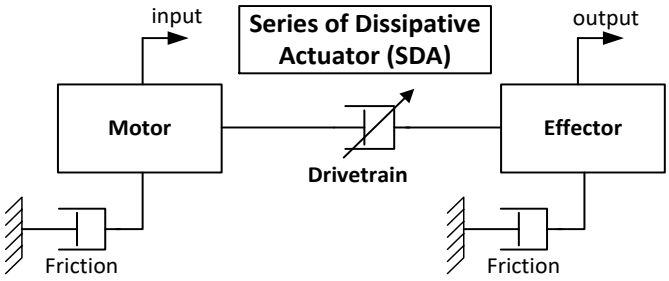


Figure 2-2. SDA- Series of Dissipative Actuator diagram

The series of dissipative actuator makes them more suitable for critical safety tasks due to the lack of oscillations. By safely dissipating the energy of impacts they ensure that it does not come back to damage the object affected by them.

The most common type of devices using this configuration are dampers. They are used to reduce oscillations, absorb energy, mitigate seismic vibrations [32], among other applications. Depending on their configuration within a system, they have been used as rehabilitation devices [33], to cite a few examples.

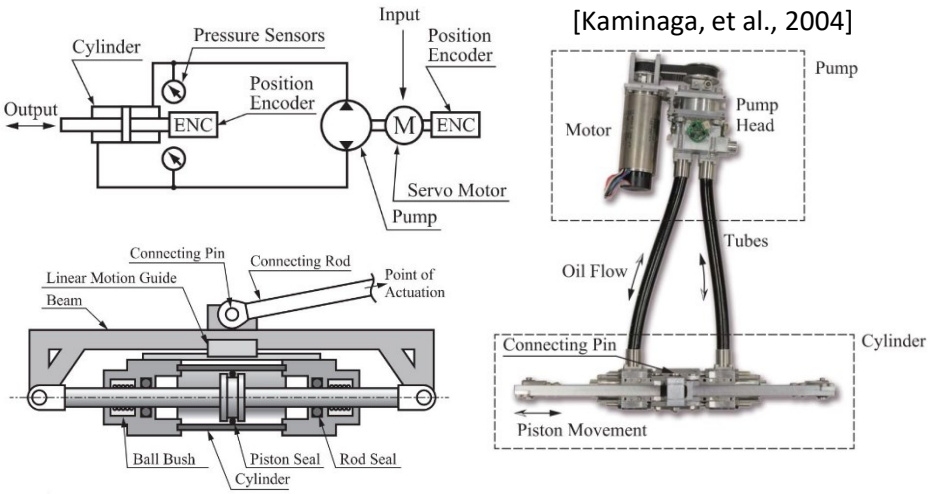


Figure 2-3. Electro-Hydrostatic Actuator with backdrivable output

Among these devices, an electro-hydrostatic actuator [34] has successfully achieve a combination of hydraulic power with backdrivable motion by introducing small leakage in the hydraulic circuit [35]. In this way it can achieve a certain degree of backdrivability by balancing the hydrostatic forces between the pump and the actuator. This approach is straightforward to implement, and provides forces that match conventional hydraulic actuators. However, it lacks the ability to adjust the backdrivability of the system, limiting its adaptability to perform different tasks.

## 2.3 Electro- & Magneto-rheological Fluids

Electrorheological (ER) and magnetorheological (MR) fluids are a type of smart materials that exhibit changes in their rheological, i.e. viscosity, when they are stimulated by an external voltage or magnetic field respectively. ER fluids usually require very large voltages in order to operate, which are difficult to control. Nevertheless, they require small currents, which makes them relatively safe when compared to MR fluids.

On the other hand, MR fluids are able to exhibit larger changes in their rheological properties, which allows widen the range of forces they can generate. These properties make them more suitable for high power applications with backdrivable motion, where high and low forces are necessary. In order to implement MR fluids, it is first necessary to understand how they work, and how applications exploit their characteristics in order to achieve different actuation behaviours.

MRFs have small ferromagnetic particles, suspended in a liquid medium, as shown in Figure 2-4. These particles react to magnetic fields, aligning themselves forming chains across the field lines and changing the apparent viscosity of the fluid. The stronger resistance to movement is observed usually when force/pressure is exerted perpendicular to the direction of the magnetic field.

This makes it possible to control the rheological properties of the MRFs using electromagnets [36]. This system exploits this property to smoothly control the exerted force, while achieving an intrinsic backdrivable operation [37], as described in the next section.

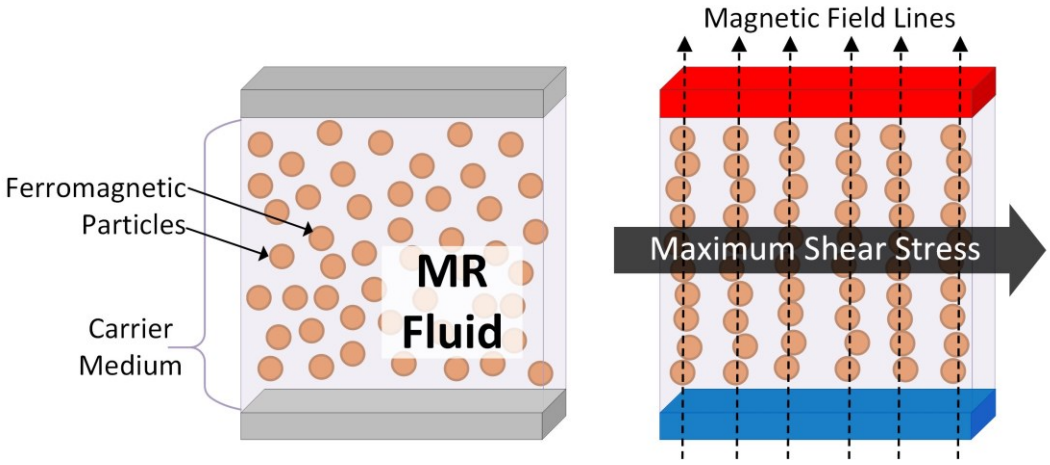


Figure 2-4. Magnetorheological fluids basic constitution and principle of operation

In the market there are already several commercial fluids used in a variety of applications. Among them one of the most commonly used in research for the design, prototyping, and testing of magnetorheological devices are the ones provided by Lord Corporation.

### 2.3.1 MRF Operation Modes

Depending on how MRF are used their operating principle can be divided in three modes: shear, flow, and squeeze. They are described according to their characteristics and form of flow [38]. Exploiting the characteristics of these modes allows the realisation of different applications and systems.

1) Valve Mode

In this mode the MRF flows between fixed surfaces. The magnetic field is perpendicular to the flow. The pressure necessary to overcome the shear stress between the surfaces is proportional to the magnetic field applied.

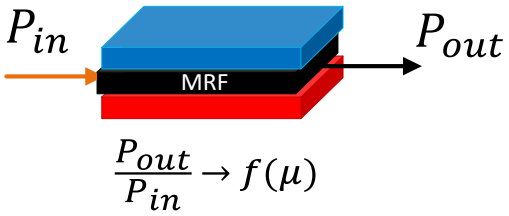


Figure 2-5. Valve mode for the MRF

2) Shear Mode

The MRF is trapped between moving surfaces. In this case the force amount of force transmitted between the surfaces is proportional to the magnetic field, and to a less degree the speed difference between them.

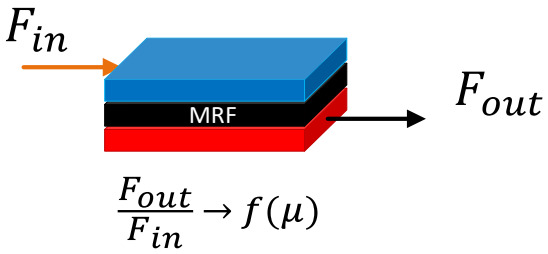


Figure 2-6. Shear mode for the MRF

3) Squeeze Mode

Usually in this mode the MRF is trapped between moving surfaces, e.g. an elastic pouch. This force necessary to deform the shape of the surfaces is proportional to the magnetic field.

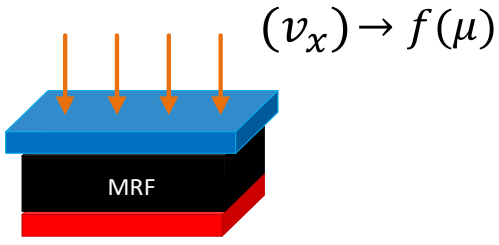


Figure 2-7. Squeeze mode for the MRF

This operation mode is usually useful for haptic devices such as the virtual reality glove [39], or a tactile device for medical training [40].

In all the operating modes the changes in force necessary to produce a change are proportional not only to the magnetic field acting on the MRF, but also to the speed at which

the change is occurring. Depending on how they are used they can have different characteristics for the same purpose [41].

### 2.3.2 Direction of the Magnetic field

As it was mention before, it is very important to consider the direction of the field. The orientation of the field significantly affects the performance [42]. Therefore, there are methods that try to overcome this by adding changes in the flow direction [43], or random paths in crowded [44] or porous media [45]. This phenomenon will be explained in more detail on subsequent sections during the development of the actuator.

## 2.4 MRF Based Actuators

The development of magnetorheological actuators has produced several kind of devices [46]. These devices can be divided into clutch, damper, and valve type actuators. Several configurations of these actuators have been constructed and evaluated with different degrees of success, and some have also been integrated into applications to demonstrate their potential, even in mobile applications [47]. Some novel combinations such as artificial muscles have also been introduced [48]. In the research field most of the active MRF based devices have been developed to provide compliant rotatory motion, such as in the case of MR clutches. Now we will focus in the three most common types of uses.

### 2.4.1 MR Clutches

The clutch type devices operate in a similar way to a friction clutch does. However, instead of relying on physical contact between the two rotatory plates, they employ MR fluid trapped between the plates to adjust the amount of torque transmitted to the output.

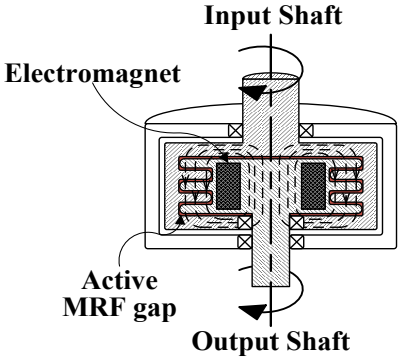


Figure 2-8. Magnetorheological Clutch

These devices have fast response times that can quickly minimise the system inertia, while keeping high torque performance. Although it's construction can be quite simple, they still present several challenges, such high hysteresis [49], difficult modelling [50], and low power to weight ratio. Shafer and Kermani have successfully develop and tested a clutch for human friendly manipulation, however their modelling and control is still somewhat challenging [51], show in Figure 2-9. In the same line of work, they have also presented the application of these devices for small haptic interfaces [52].

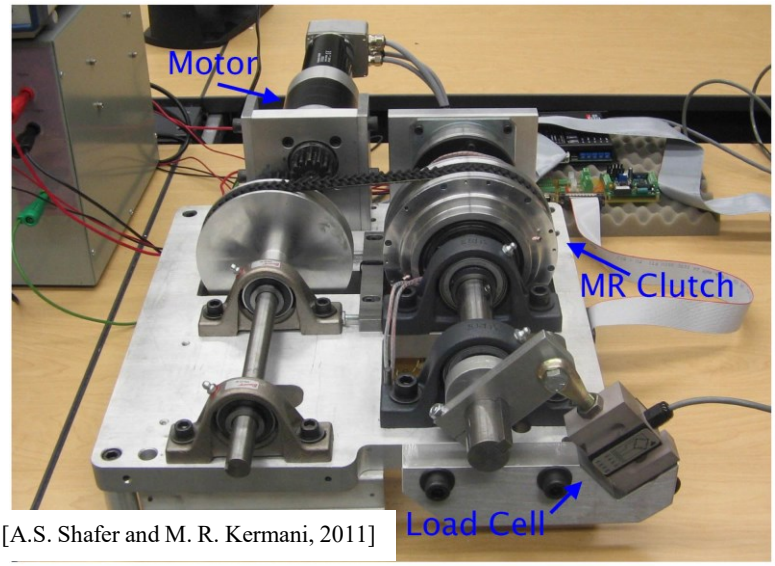


Figure 2-9. Experimental setup used to test a magnetorheological clutch attached with a motor.

This type of devices have successfully been implemented as an actuator [53]. In this isolated study, a series of clutch actuators was used to construct a robot arm. The resulting prototype prove the feasibility of the concept. However, it lack the necessary power and size to be successfully implemented in the intended robotic applications.

However, they have shown promising results in many areas such as assistive devices [5], shown in Figure 2-10. As well as in promising medical applications [54], and rehabilitation devices [55]. Another advantage is the possibility to create normally closed clutches [56] to suit specific tasks where normally opened clutch will be liability, as well as to adjust the operation point to optimise the energy consumption. They versatility allows them to double as brakes as well [57]. The list of applications could continue growing; however, the common denominator of these devices is that none can provide enough torque to drive a powerful system. Moreover,

most of the devices in this category do have means to provide integrated active power. In other words, they all must act passively, or be connected to an electric motor in order to output power.

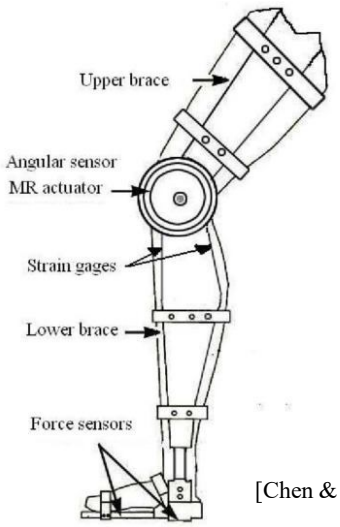


[Chen & Liao, 2006]

Figure 2-10. Leg exoskeleton using a MR clutch

Nevertheless, Dirk et al [58] were able to develop a Clutch-Drive-System that successfully combined a clutch with a shiftable electromotive actuator. While promising this actuator has not been tested comprehensively tested, its output power is somewhat limited, and it shows limited capacity to control its backdrivability and torque in an independent way.

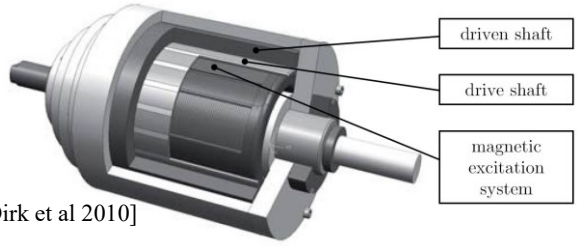


[G. Dirk et al 2010]

Figure 2-11. Clutch-Drive-System schematic showing an integrated motor and clutch

Additionally, the direction in which the clutch acts can be changed depending on the design of the plates. In this way, it is possible to create devices with omnidirectional action, such as the spherical haptic device constructed by Han and Choi [59].

### 2.4.2 MR Valves

Finally, the valve type actuators can control the pressure drop of the MRF flowing through them. These devices have been widely researched, and now they efficiency and construction

have been greatly improved [60]. Typically they are used as bypass valves for hydraulic pistons in order to achieve the functionality of adaptive passive dampers [44].

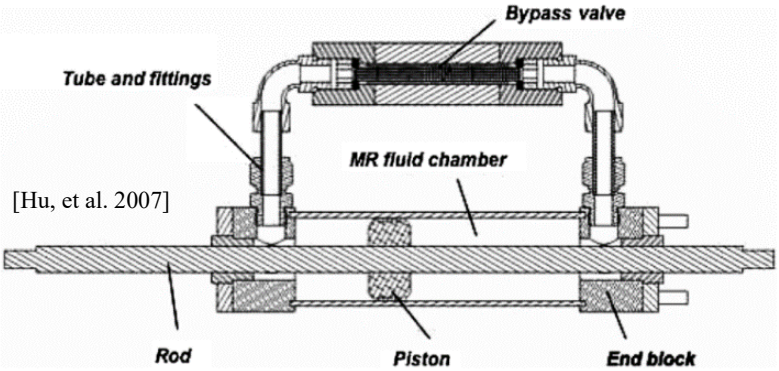


Figure 2-12. Magnetorheological damper using a bypass valve

They employ different configurations in order to enhance the pressure drop, for example using a multi-stage radial flow, [61], or a modified flanges to direct and concentrate the magnetic flux [62]. Other design include variable geometry mechanisms to mechanically adjust the flow [63].

There have been few applications for this technology to create actuators. One example is based on a miniature device to produce high forces with very small displacement [64]. In a different study, Yoo and Wereley have used high efficient valves to construct a bridge hydraulic circuit in a Wheatstone configuration to control the pressure supplied to a piston actuator, resulting in an active linear device [65], shown in Figure 2-13.

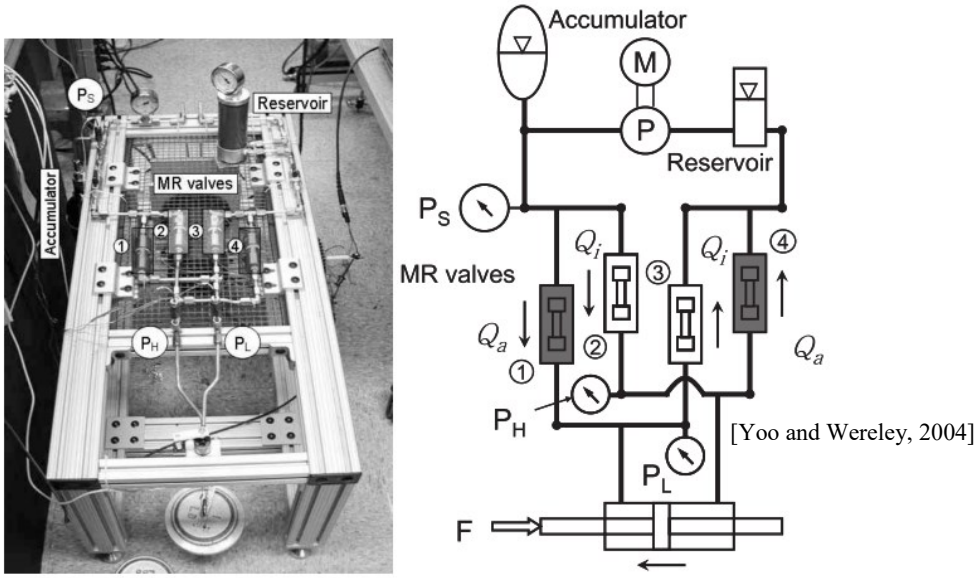


Figure 2-13. Magnetorheological Hydraulic Power Actuation System

However, in these configurations the MR valves are attached as external components, increasing the amount of MR fluid necessary to fill the system, and adding complexity to the overall system. Since the MRF is expensive and heavy, it limits the applications of such devices in portable cost efficient systems. Moreover, the current devices has been only reported to achieve small forces 36N at 1.6A with an efficiency of 80%.

### 2.4.3 MR Dampers

Other kind of devices are the damper type [66] [67]. These have been studied extensively, and now are commercially available for high-end automotive applications and their seats [68], as well as sold as adaptive damping systems. They operate in a similar way to traditional dampers, with the difference that they can change their damping constant by varying the viscosity of the liquid passing through or around the piston head using electromagnets.

There are several configurations [69] but most of them involve using an annular gap configuration, realised either by concentric holes in the piston head [70], or a gap between the piston and the cylinder wall. Among the most common configurations, the following have been widely researched in literature.

1) Dash-Pot Dampers

This is the most common type of damper [71]. The piston head lets fluid move between the walls of the piston head and the piston cylinder [72]. As it can be seen in the figure below

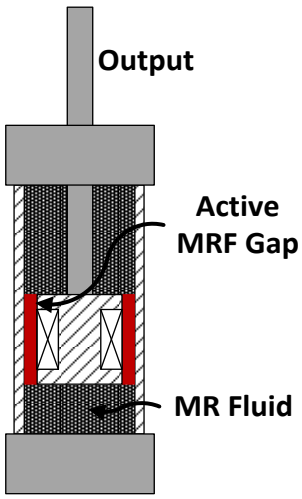


Dash-Pot Type

Figure 2-14. Types of MR dampers

Some of these devices has been modified in order to achieve unique characteristics, such as integrated position sensing with an energy regeneration mechanism [73].

2) Wall Dampers

They flow moving through their walls, which makes them particularly unsuitable for operation in fast moving applications. They have been particularly study in combination with other modes of operation. However, in all cases their mechanical design makes them particular difficult to implement in combination with active power applications using a pumping system.

3) Bi-fold Dampers

This kind of dampers are a subset of the wall dampers. In their case the fluid movement is restricted by using serpentine like passages between the main chamber and the wall chamber [74]. They produce more force than conventional wall dampers. However, the electromagnetic circuit is embedded in the piston cap, which could potentially restrict a pressurised flow from a pump, in the case of active motion.

4) Annular Gap Dampers

This is the most common type of dampers, thus they have been particularly and extensively researched [68]. They employ a bobbin shaped valves inside their head, as it can be seen in the Figure 2-15. However, they are known to have different types of configurations that help them tune their characteristics [75].

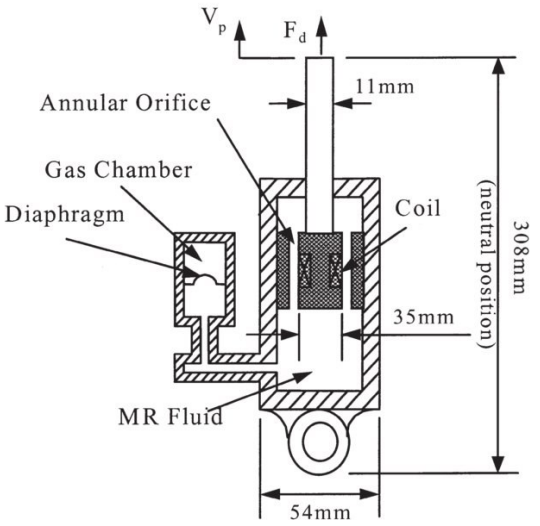


Figure 2-15. Magnetorheological damper with annular piston head

This type of dampers has the advantage of full mobility compared to their counterparts. This makes them especially suitable for motion applications. Another advantage is that they exhibit the highest forces due to the operation mode, which induces fast moving flows through their gaps. Additionally, extensive research has been conducted, which makes them well documented and reliable, to the point they are now commercially available in many applications. They have also been combined with other types to generate interesting configurations [76]. Moreover, research is also being conducted in their applications for soft robotics, using some innovative configurations [77].

## 2.5 Discussion & Remarks

The research in backdrivable systems has led to the development of several actuation technologies for safe interaction. Nonetheless, most of the current applications are for small power actuation. Very limited research has been conducted in the field of safe backdrivable power actuation with a high force output. New technology is needed to fill this current gap. The current analysis revealed that the most reliable way to implement safe actuation is to use to alter the mechanical properties of the system. By doing this, the system would be able to safely react in the event of fast changing conditions and situations, such as impacts. However, even by implementing mechanical compliance, the mass and inertia of a system will limit the safety of the system, since their effect will negatively affect the safe performance of the system. In the future, new systems should include a mechanism to minimise these effects. Only then, will a system will truly be safe. A summary of these technologies is shown in Table 2-I.

TABLE 2-I. SUMMARY OF CURRENT SAFE ACTUATION TECHNOLOGIES

| System | | | Safe/ Adjustable | High Active power | Efficiency | Integration | Control | Versatility |
|---|---|---|---|---|---|---|---|---|
| Active Compliance | | | Δ✓ unsafe | ○○○✓ | ○○○ | ○○○ | ○ | ○○○ |
| Mechanical Compliance | SEA Series of Elastic Actuators | VSA MACCEPA Impedance Adj. PPAM | ○○✓ vibration | <1kN✓ | ○○○○ | ○○○ | ○ | ○○ |
| | SDA Series of Dissipative Actuators | MR clutches | ○○○✓ | 7Nm weak | ○○ | ○○ | ○○ | ○○ |
| | | MR clutch drive | ○○○✓ | 24Nm weak | ○ | ○○○ | ○ | ○ |
| | | Bypass dampers | ○○○✓ | >>1KN | ○○ | ○ complex | ○○ | ○○ |
| | | MR Dampers | ○○○✓ | >>1KN passive | ○○ | ○○ | ○○ | ○○ |
| | | Elec. Hydrostatic Actuator | ○ fixed | >>1KN✓ | ○○○ | ○○○ | ○○ | ○○ |
| | | MR Hydraulic power actuator | ○○✓ | >1KN✓ | ○○ | ○ complex | ○○ | ○ |

Currently the research is pointing towards the use of hydraulic systems to develop compact actuators with high power output. While these systems are extremely effective in generating high forces, their efficiency and applicability is quite limited. The correct implementation of such systems will greatly influence their performance and usability in a real application. This is a critical point that must be considered if this technology is to be implemented in a particular application.

MR fluids are an alternative solution to implement backdrivable operation in hydraulic systems. In recent years, this technology has been successfully applied in cars dampers, as well as in building damping systems. This type of fluids offers many advantages such as high response times, and wide range of changes in yield stress. Nevertheless, they still struggle to find widespread application in more fields. This is partially caused by the stability of these suspensions over time or high stress, the difficulty to accurately control them, and finally, their cost. In the future, more research is necessary to overcome these challenges, making the implementation of these fluids a feasible reality.

## 2.6 Chapter Summary

A background survey on the state-of-art technologies for safe actuation was conducted. The results showed that mechanically implemented backdrivability offers inherently safe actuation when compared to active (software based) strategies, which are limited by the control loop bandwidth. Most mechanically backdrivable devices are based on series of elastic actuators SEA. However, this approach is prone to uncontrolled oscillations, which can be potentially dangerous in high power systems. In this respect, series of dissipative actuators, SDA, are preferred since they disperse the energy resulting from interactions. This type of actuation is particularly suitable for hydraulic systems, which are known to have high power densities in medium and large applications.

As far as the background research covered there are currently two backdrivable applications implementing such mechanism. An electro-hydrostatic-actuator EHA provides high power output. However, the backdrivability cannot be adjusted since it is determined by the coupling in hydraulic circuit and the friction of its components. On the other hand, a magnetorheological hydraulic actuation system takes advantage of the smart fluid properties to quickly adjust the output force and backdrivability of a hydraulic piston. Nevertheless, the system was design and tested for a low power output. It also requires a high number of

components to operate, making it difficult to integrate and miniaturise. Moreover, having many components increases the probability of failure, reducing its reliability and safety. In order to overcome these limitations a new kind of actuation system is necessary.

# 3 MR PISTON ACTUATOR

The next generation of robotic applications is expected to increase productivity and release humans from dangerous and exhausting tasks in a variety of fields. In order to provide this future high power mobile robots with the required adjustable safety it is necessary to develop a new actuation system. Current hydraulic applications are used to provide high power for heavy duty tasks. However, current systems lack a combination of high power and adjustable backdrivability. These reasons motivated the development of the magnetorheological piston actuator (MRPA). Based on the findings from the background research this actuator builds on the advantages found in previous actuation systems, while striving to provide solutions for some of the problems that afflict them.

The development of the MRPA requires different parts, from the hydraulic system, to the instrumentation and control system. Nevertheless, as it was mention in the introduction chapter, this study focuses mostly on the conceptualization and implementation of the hydraulic transducer. The correct implementation of this part is crucial to the performance and functionality of the MRPA. In this respect, the successful implementation of this part, will not only determine the feasibility of the proposed idea, but also its reach and limitations.

This chapters is based in a previously published work [78] and it describes in detail the conceptualization, design and manufacturing of the first MRPA prototype. First, the general

concept and principle of operation behind the actuator is presented. Then, an analysis of the current technology of MR pistons provides a comprehensive understanding of the available options for the concrete implementation of the actuator. Moreover, the analysis also uncovers some limitations in the current technology. This motivates the proposal of a new kind of MR piston head, which is specifically design to meet the requirements of adjustable backdrivable actuation. The novel design is inspired by the functionality of magnetorheological valves and the magnetic efficiency of a toroidal electromagnet.

The design of the MRPA prototype is based on the novel configuration for the piston head and the factors affecting its performance. However, in order for the actuator to perform adequately it is also necessary to take into account other important considerations such as friction, integration, ease of assembly. These and other practical design points are presented and discussed in detail in this chapter.

## 3.1 System Concept

The MRPA aims to combine the high power of hydraulic actuators with the safety of MR fluid systems. In order to achieve this a novel electro-hydrostatic-actuator (EHA) using a MRF is proposed. A schematic of the basic system is shown in Figure 3-1.

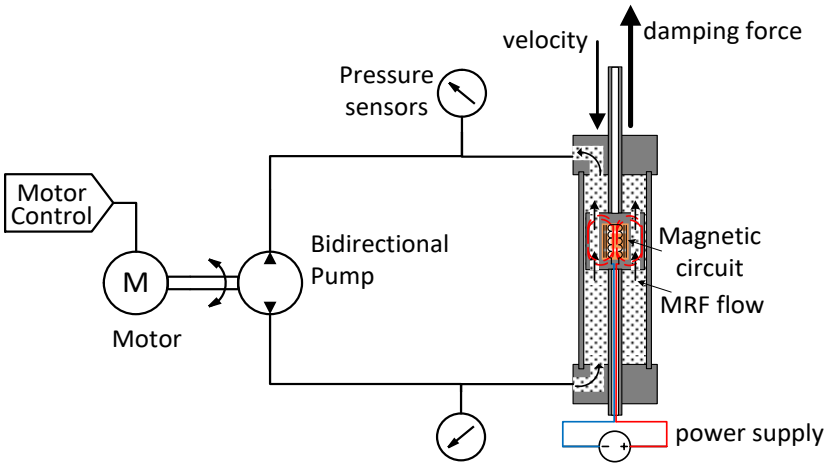


Figure 3-1. Schematic of the MRPA – Magnetorheological Piston Actuator

The MRPA basically consists of a hydraulic unit and a MR piston connected in a typical EHA configuration [79]. The hydraulic unit compromises an electric motor and an integrated bidirectional pumping system including all the necessary hydraulic components for its operation. However, different from traditional hydraulic systems the MRPA utilises MRFs, instead of hydraulic oils, to achieve actuation with adjustable stiffness.

### 3.1.1 Principle of Operation

The MRPA operates in a similar way to a conventional EHA, where a bidirectional hydraulic pump is used to provide the necessary flow and pressure to drive the piston. In these actuators the pressure difference and flow generated by the pump is controlled by adjusting the torque and speed of the electric motor respectively. This makes it possible to achieve a reliable control without the need of complex and expensive flow valves.

In conventional the displacement of the piston is equal to the fluid propelled by the pump at fixed system pressure. However, the MRPA uses a piston head with passages that allow the pressurised liquid to flow in a controlled manner from one chamber of the head to the other, as in can be seen inside the piston head in Figure 3-1 and Figure 3-2.

In this case, the pressure difference on both sides of the piston head depends on the viscosity and flow of the liquid passing through these passages. By using MRF, instead of oil, it is possible to control this pressure difference by varying the apparent viscosity of the fluid in the passages. This configuration makes it virtually possible to set the actuator force by adjusting the magnetic field in the passages, and the speed of the piston head by adjusting the flow rate, $Q_p$, generated by the pumping system. Additionally, it also delivers many advantages such as fast response times, and considerable force range, seen in MR damping base systems. However, there are also many challenges due to the magnetic and rheological behaviour of the MRF and materials used to construct them. Therefore, selecting appropriate parameters when designing these actuators will greatly influence their performance.

### 3.1.2 MR Piston Head Design

The most important part of the new concept is the design of the piston head. Inside the piston head of the MR damper there is an electromagnet, which is used to induce a magnetic field perpendicular to the fluid flow. This maximises the effect on the magnetic field on the MRF. By controlling the current in the coil, it is possible to change the yield stress of the MRF inside the passage, increasing the pressure gradient between chambers. The output force of the actuator depends on the flow rate, the viscosity of the fluid, and the magnetically induced yield stress of the MRF inside the MRP passages. In this way, it is possible to modify the damping response to a controlled magnetic field by selecting the geometry of the passage, electromagnets, and coils, as well as the magnetic properties of the construction materials, and the rheological properties of MRF. In order to design a piston with optimal backdrivability,

efficient power, versatile customisation options, and high output forces is necessary to understand the fundamental parameters affecting these properties.

In section 2.4.3-*MR Dampers* several configurations of this devices were introduced. Among them the annular configuration was found to be one of the most adequate configurations for this type of system. The schematic below shows in detail a MR damper piston head with its main hydraulic parameters.

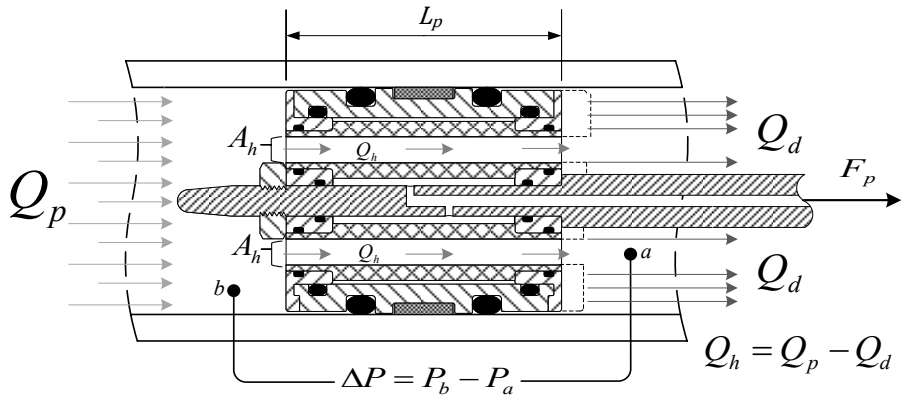


Figure 3-2 Hydraulic diagram showing operational principle of MRPA

These dampers operate in flow mode, letting the fluid move through the passages inside the piston head. In this way, they can achieve higher forces than other configurations, while keeping the friction forces to a minimum.

Several mathematical models have been proposed to model the force generated by these devices [80] [81]. However, most of them require complex computations, tables, requiring considerable modifications to adapt to a particular geometry. A more straightforward approach to understand the relations of parameters in the MR damper is to use an approximation to the Buckingham-Reiner approximation [82]. Equation 3-1 gives the pressure difference in a simplified set of parameters.

$$\Delta P = \frac{8\eta L_p Q_h}{A_h r_{gap}^2} + \frac{8\tau_y L_p{}'}{3r_{gap}}$$

Equation 3-1. Pressure difference derived from the Buckingham-Reiner equation

The first term in the right hand side represents the pressure generated by the Newtonian flow. This pressure depends mostly on the viscosity of the fluid, the flow rate, and the dimensions of the passages. On the other hand, the second term of the right hand side is related

to the visco plastic behaviour of the MRF. Which means it does not contribute to the pressure difference when there is not magnetic field. This term is mostly affected by the magnetically induced yield stress, $\tau_y$, and the length of the passages. As a result, the minimum force of the MR piston, i.e. zero field, is determined by size of the passages, while the maximum force is determined by the length of the passages.

The objective of the piston head is to minimise the viscous forces to achieve better backdrivability, while maximizing its force output. In other words, it is necessary to minimise the Newtonian term of this equation, and maximise the viscous one. To achieve this, we analyse the typical structure of an annular piston configuration, as seen in Figure 3-3.

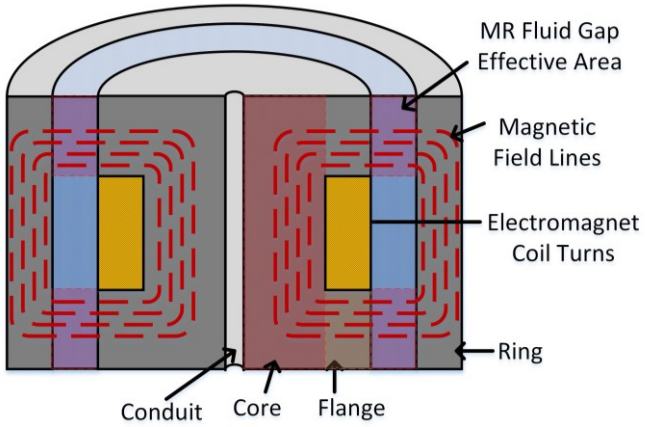


Figure 3-3. Annular piston head of an MR Damper

As it can be seen, the annular piston head has a compact and simple design that allows for a high number of coil turns and a relatively big passage hole. This makes it a good alternative to for most commercial applications. However, it has several disadvantages that make it not suitable to achieve the goals of this research:

- It has limited amount of parameters that can be configure. This limits its versatility to satisfy the requirements of different applications.
- The area where the magnetic field interacts with the MRF is rather limited. This theoretically reduces the visco plastic dependant force, thus limiting the maximum forces of the actuator.
- The magnetic circuit configuration is prone to electromagnetic leakage through the top of the bobbin core or the sides of the ring. This can potentially reduce the efficiency of the electromagnetic circuit. Moreover, it could also lead to undesirable friction between the walls of the piston cylinder and the piston head.

These reasons motivated the development of a novel piston head configuration specifically design to meet the goals outlined in this research.

## 3.2 Toroidal Piston Head

The new configuration, inspired by toroidal electromagnets, is the key part of the new actuator. Toroidal electromagnets typically have higher magnetic fields, and less magnetic leakage when compared to designs using conventional straight solenoids.

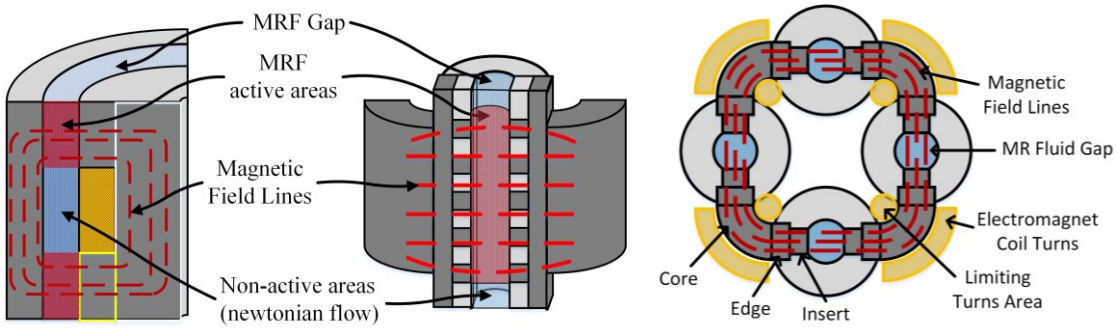


Figure 3-4. Annular piston head vs novel toroidal configuration

As shown in Figure 3-4 the proposed toroidal head design consists of alternating electromagnets and passages forming a circular array of MR valves, which is fully integrated inside the piston head. The reduction in the number of components decreases de possibility of failure in a system intended for safe actuation, and at the same time, it increases the space efficiency when compared to other piston alternatives such as bypass dampers.

The toroidal array creates a contained circular magnetic field, similar to the one observed in toroids. This prevents magnetic leakage that can reduce the efficiency of the actuator. Moreover, this enhances backdrivability, since any leakage of the magnetic field could cause unnecessary friction between the piston walls and the piston head.

As it can be seen this new configuration, allows for more configuration options since the number, size and shape of the passages and electromagnet cores can be tuned to meet the application parameters. Finally, the most important point is that it allows for a larger area of interaction between the MRF and the magnetic field. This theoretically should provide better utilization of the field, leading to higher output forces. However, an extended analysis is necessary to establish the different trade-offs between the combination of several parameters, and to determine design guidelines for this new design.

### 3.2.1 Electromagnetic Circuit Design

The electromagnetic circuit of the toroidal piston head, is used to control the magnetic field in the MRF. As shown in Figure 3-4, it consists of 4 plugs, and 4 electromagnets, with their respective cores and coil windings, placed next to each other to create a close circular magnetic path similar to a toroid.

The successful implementation of the electromagnetic circuit will ensure that an optimal magnetic field density, with a stable current, is generated at the gap of the passages. The magnetic field density should be high enough to reach high yield stress values of the MRF, without having to use currents that will overheat the coils. However, it must not reach the region where the yield stress begins to saturate. Otherwise, the energy efficiency and the linearity of the output force will drastically decrease. In order to achieve these objectives, a careful selection of the materials and dimensions of the different sections of the electromagnetic circuit is necessary.

#### 3.2.1.1 Material Selection

The choice of materials for the electromagnetic circuit is important to ensure that enough field is produced using minimum current. This will extend the MRP's force range. There are basically two type of materials used in the construction of electromagnetic circuits.

1) Permeable Materials: This kind of materials are particularly suited to allow the magnetic field move through them. The most common are ferromagnetic materials, which are inexpensive, and heavily used as electromagnet cores. However, there are materials that exhibit better permeability by using doping with certain elements, alloying with other materials, or using special treatments to align their internal structures. These are used in more demanding applications.

2) Non-Permeable Materials: These materials prevent the magnetic field to flow through them. Commonly, all of them exhibit permeability values close to the permeability of free space. For this prototype, these materials are based on aluminium alloys.

In most high performance applications, the electromagnetic cores are manufactured using special alloys that has a high magnetic permeability and relatively low coercivity, which also helps to enhance the induction of a magnetic field while keeping the hysteris of the magnetic circuit low. However, in systems using magnetorheological fluids it is not only necessary to

generate a high magnetic field, but also to ensure that the field focuses in the MRF fluid passages. In order to achieve this, the plugs were manufactured using permeable and non-permeable materials. Aluminium is used to prevent the magnetic flux from leaving the desired path, while permeable materials are necessary to conduct the flux into the plug passages. Each of the sections of the electromagnetic core must be design taking into consideration its role in the toroidal circuit.

### 3.2.2 Magnetorheological Valve Sections

The proposed configuration for the prototype consists of 4 MR valves aligned in a circular way. Increasing the number of passages enhances the backdrivability of the piston, by maximizing the gap size inside the piston head. Figure 3-5 shows the toroidal design sections.

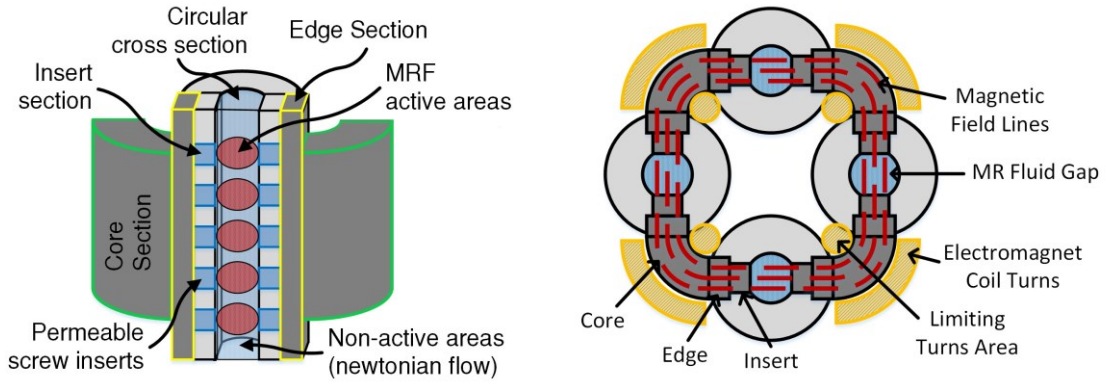


Figure 3-5. Front and top section schematics of the toroidal valve array

1) Core Section: It is constructed with permeable materials, and is where the electromagnet coils are winded. The 4 cores generate the electromagnetic field to control the yield stress of the MRF.

2) Edge Section: The edge sections are part of the core; however, they are considered a separate section due to their different dimensions. Their purpose is to secure the core against the insert sections, and to act as an enclosure for the electromagnet windings.

3) Insert Section: It is used to transport the magnetic field into the passages of the plug. Insert screws were attached to the plug walls in order to keep the MRF from leaking into the piston head. This configuration ensures a high sealing performance.

4) Magnetorheological Fluid Gap Section: The MR fluid gap sections serve as passages for the MRF to move freely from one side of the piston head to the other, allowing

the MRP to achieve an inherently mechanically compliant design. The combined area and geometry of the four gaps determines the minimum force of the actuator, since is directly related to the Newtonian flow of the force equation.

### 3.2.3 Manufacturing and Assembly

For the construction of most electromagnetic actuators, materials with high magnetic permeability and low coercivity are preferred. They allow the induction of a high magnetic flux, by reducing the hysteresis of the circuit. Therefore, Permalloy 78 was chose for the electromagnet main electromagnet cores. Soft iron screws were chosen for the plug inserts respectively. On the other hand, aluminium, with a low permeability, was chosen, for the rest of the components in the circuit, to contain the field and direct it towards the desired path. The properties of these materials are summarised in Table 3-I.

TABLE 3-I - MATERIALS USED IN THE MAGNETIC CIRCUIT

| *Part* | *Material* | *Relative Permeability* |
|---|---|---|
| Electromagnetic Core | Permalloy 78 | $\mu_p = 56000\ \mu_0$ |
| Plugs | Aluminium | $\mu_a = 1\ \mu_0$ |
| Plug Inserts | Soft Iron | $\mu_i = 2000\ \mu_0$ |

The magnetic permeability of vacuum is equal to, μ0= 4π×10−7 V·s/(A·m)

Consequently, the plugs that form the passages were constructed in aluminium, with holes filled with tightly sealed iron inserts that direct the field into the passages of the actuator. Figure 3-6 shows the manufactured toroidal piston head.

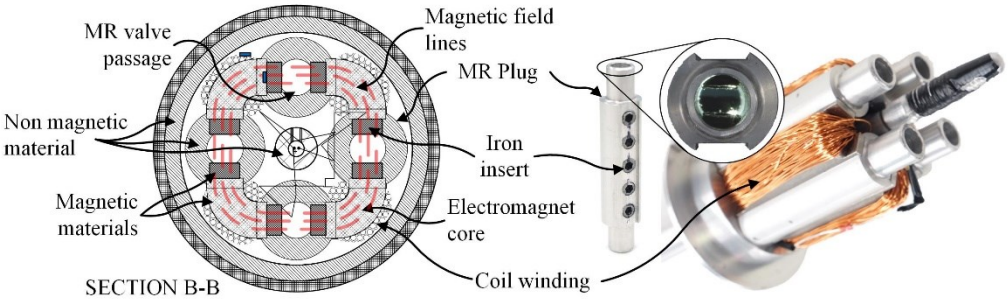


Figure 3-6. MRP head showing inner toroidal array and its top section schematic

## 3.3 MR Piston Design

A schematic of the MRP from is shown in Figure 3-7. Its construction is very similar to conventional pistons. However, different from conventional pistons, the MRPA has a toroidal

piston head, which allow the MRF to flow between the piston chambers, and control the magnetic field to adjust rapidly and precisely the damping factor respectively.

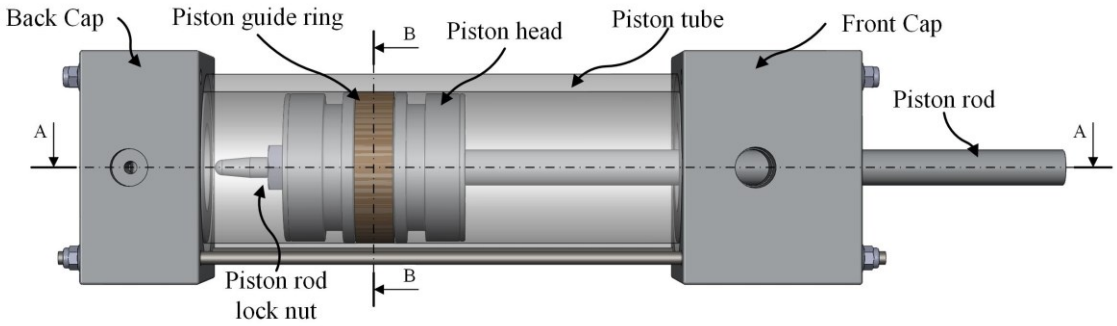


Figure 3-7. Drawing of MRP showing its most relevant parts

The MRP has been designed considering not only the performance of this electromagnetic circuit, but also taking into account requirements for compliant actuation, friction and seal performance, ease of assembly for testing, as well as other aspects for optimal performance of the MRF.

### 3.3.1 Actuation Oriented Design

The MRP consists mainly of parts found in both standard hydraulic pistons and other MR damping systems, as shown in Figure 3-8. For instance, the front and back caps have been fitted with hydraulic ports, A and B, and other necessary features in order to be able to pump MRF to drive the MRP as a conventional hydraulic piston. In this way, it is possible to provide the necessary flow and pressure to the MRF inside the piston to generate linear motion. This configuration makes it possible to connect the MRP to the external pump, and to easily slide back and forward with few friction coming only from the piston seals.

In a similar way, an accumulator is used in order to accommodate the MRF volume displaced by the piston rod when moving in and out of the piston. This device absorbs also the pressure fluctuations that a pump could generate if attached, and provides additional safety during impacts.

Finally, the piston head does not only contain the toroidal MR valve assembly, but also the necessary temperature sensor, seals and fixtures. Around it the conventional O-ring seals have been removed, and replace with a single wear ring to maintain alignment during actuation

motion. In this direction there are other design features that make this MRP uniquely suitable for the intended application.

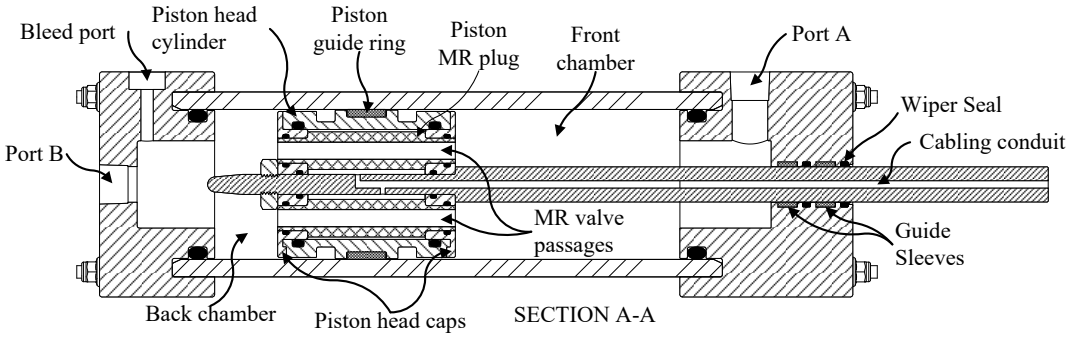


Figure 3-8. Schematic of Section A-A of the MRP showing its functional parts

### 3.3.2 MR Fluid Oriented Design

The MRP head encloses the passages that connect the piston chambers, along with all the permeable parts of the magnetic circuit. It is made of specifically of aluminium to stop any field from leaking outside of it. This prevents the MRF from generating undesirable friction between the wall and piston head, allowing the MRP to freely slide back and forward. Along with the piston head cover, the cylinder wall, piston caps and piston rod are also made of aluminium.

The MR fluid is a non-colloidal solution based on mineral oil. It has additives that ensure a low sedimentation of the ferromagnetic particles, as well as for reducing the friction caused by them. However, materials such as natural rubber and silicone are weak against such components. For this reason, nitrile rubber based sealings are used. Additionally, Teflon based components are used in the wipers and wear rings to reduce the abrasive action of the fluid.

### 3.3.3 Friction and Seal System Design

In compliant robotic applications friction is a key factor that reduces the backdrivable capabilities of the system, negatively affecting the overall safety. In most hydraulic actuators the friction comes from the sealing system. However, the sealing system is a crucial part of these actuators, since it ensures optimal performance by minimising leakage of the pressurised fluid. Moreover, it also ensures that the hydraulic fluid does not get contaminated by foreign materials in the working environment. In this respect, the sealing system design plays the important role to minimise friction while maintaining the actuator functionality. Therefore, a compromise between friction and sealing capacity is critical for such application.

In order to meet both requirements, low friction Polytetrafluoroethylene (PTFE) wear rings were used in the piston head and piston rod, while nitrile rubber O-rings and wiper seals were used only in the piston rod to seal and avoid pollution of the MRF.

### 3.3.4 Design for Assembly and Testing

The piston was constructed with removable caps fixed with tie rods, allowing easy assembly, and disassembly for testing. It also features a bleed port, which is necessary during the filling process. It is used to remove unwanted air from the system that negatively impacts the performance of MRFs during operation. Finally, the piston head was sealed to prevent air in the cabling conduit from leaking into the piston chambers polluting the MRF.

## 3.4 Prototype Design and Construction

The prototype was design using Dassault Systèmes CAD software SOLIDWORKS. The main parameters of its design and construction are shown here in Table 3-II.

TABLE 3-II - PARAMETERS FOR CONSTRUCTION OF MRP

| ***Parameter*** | ***Value*** |
|---|---|
| Core middle radius, $r_{core}$ | 6 mm |
| Electromagnet edge, $l_{edge}$ | 2 mm |
| Air gap, $l_{gap}$ | 6 mm |
| Plug insert length, $l_{insert}$ | 3 mm |
| Core cross section area, $S_{core}$ | 259 mm$^2$ |
| EM edge cross section area, $S_{edge}$ | 329 mm$^2$ |
| Air gap cross section area, $S_{gap}$ | 179 mm$^2$ |
| Inserts cross section area, $S_{insert}$ | 20.2 mm$^2$ |
| Total no. of windings, $N$ | 240 turns |
| Number of passages, $N_p$ | 4 |
| Passage diameter, $D_p$ | 6 mm |
| Passage length, $L_p$ | 50 mm |

At the moment, the prototype was built as proof of concept, to study its feasibility and potential performance in future applications. A careful redesign using the model provided in this paper, along with other known optimization techniques should make possible to scale it down and adapt it for specific applications.

The prototype was manufactured according the tolerance and specifications found in the design handbook of pistons [83].

In order to assemble the piston several steps needed to be done. Including the assemble of the toroidal electromagnetic valves, the sealing system of all the parts, including the rod, the filling process of the complete assembly, as well as the necessary instrumentation and cabling necessaries to monitor the sensors of the piston.

The most relevant part is the assembly of the toroidal head. In order to ensure that the plugs stay in place it was necessary to ensure the tight alignment of all elements. The seals in the toroidal head were also selected to prevent leakage into the piston head. Otherwise the coil windings could cause a shortcut despite the nonconductive nature of the MR fluid.

## 3.5 Filling System

Air contamination can cause reduce performance of the MR fluid. They lower the yield stress response to a magnetic field. Moreover, in the case of a hydraulic actuator they may cause cavitation, which could damage the pump and piston. Therefore, it is necessary to have a system to adequately extract any air bubbles that might be trapped during the fluid filling process. Using a vacuum pump is possible to get rid of the air inside the piston. The main system used in this research works as shown in Figure 3-9.

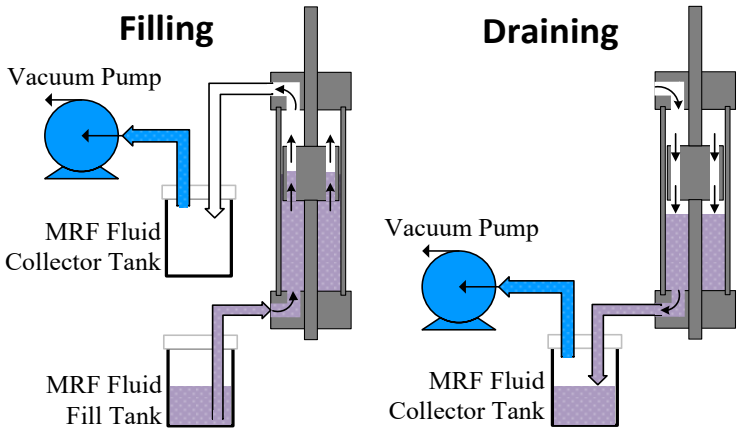


Figure 3-9. Piston filling and draining system schematics

During the filling process, the vacuum pump creates a pressure difference that allows the MRF ascend through the piston from the bottom. This vacuum generated also allows the air dissolved in the MRF fluid to expand and boil out. As a result is possible to have not only the piston but also the MRF free of air. Additionally, this system also aids to quickly fill the piston, including the small spaces that otherwise would be neglected.

The draining process of the piston works in the same way, but in this case the vacuum is generated at the bottom of the piston to force the fluid out of it. A typical setup used in the draining process is shown in Figure 3-10.

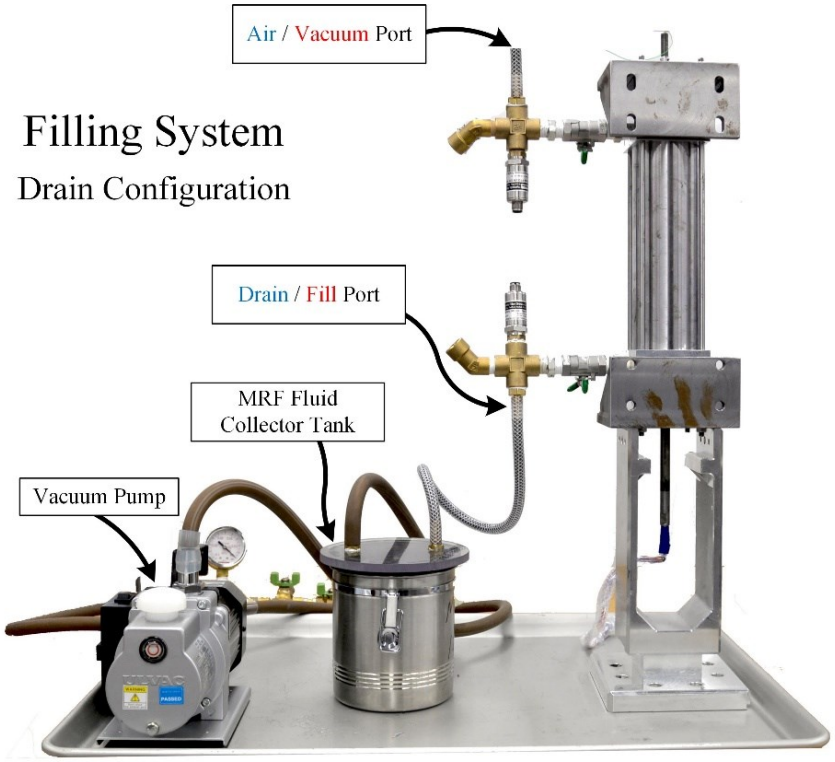


Figure 3-10. Piston draining setup used in experiments

## 3.6 Conventional Annular Head Design

MR dampers have typically been constructed having annular gaps around a solenoid. This allows for a relatively simple construction with few parts. In order to compare the performance of the prototype designed in this section, a conventional design based on an annular gap is introduced here.

A common kind of MR dampers designs use an annular gap formed by a solenoid core and a wall inside the piston head acting as a flux return path. The key advantage of this design is its simple construction with a relatively big core cross section that allows for a high magnetic flux density. Its main disadvantage is that the active length of the gap is a fraction of the total piston head length, somehow compensated by the relatively long circumference of the annulus.

### 3.6.1 Sections of the Annular Piston Head

1) Conduit Section: It is a hollow area inside the solenoid core used for the power and sensor cables. Since it does not contribute to the magnetic circuit performance, its dimensions are kept to a minimum, also to maintain the structural strength of the MRP.

2) Core Section: It is the central part of the solenoid bobbin and in covers the same functions as in the toroidal design.

3) Flange Section: While acting as a frame for the coil, it directs the magnetic field outwards towards the MRF gap. Typically, it has a rectangular shape, but here it can has been changed to accommodate more windings while keeping its magnetic performance.

4) Transmit Section: It provides an additional cross section area for the magnetic flux and MRF to interact. In this way is possible to set an independent dimension for bobbin flange to study the effects of the flux density vs. interaction area on the output force.

5) Magnetorheological Fluid Gap Section: Analogue to the toroidal design, this section allows the free flow of MRF between the piston chambers, and the annular gap area determines the minimal force of the piston head.

6) Ring Section: This part of the design allows the magnetic flux to return through the bobbin flanges.

### 3.6.2 Construction of the Annular Head

The annular head was design, as it can be seen in the appendix, with the size of the toroidal head, to have a fair way to compare both. The materials, seals and dimensions also are adjusted to closely match the other prototype. Unfortunately, it is difficult to produce an equivalent gap size since the dimensions are not matching with the hydraulic diameter.

## 3.7 Discussion & Remarks

The proposed system consists of an electro-hydrostatic-actuator. This closed system has never been used before with magnetorheological fluids to create a backdrivable actuator.

Among the advantages are that it does not require any valves to control the direction and flow rate of the MRF, making the system compact, cheap, and efficient. Additionally, it allows generating high pressures with relatively small electrical motors. Nevertheless, this kind of system poses several challenges for its correct implementation. For instance, the pressure and flow rate of the system entirely depend on the pump control. In order to achieve a control performance that equals to that of the valve based system, it is necessary to implement a more complex control system. Such system could possibly increase the instrumentation and development costs of the overall actuator.

Another important consideration that could affect the performance of these systems is the lack of an efficient cooling mechanism. The lack of tank reduces the size and weight of the system considerably. However, it is normally inside the tank where the pressurised fluids are cooled down. This cooling is necessary to ensure the correct operation of the hydraulic fluids, by avoiding evaporation, changes in viscosity due to temperature, and possible overheating of the overall system. This must also be addressed when implementing the system, by including a radiator inside the hydraulic loop. Despite all this shortcomings, EHA has been successfully implemented in several safety critical applications such as airplanes. These applications have proven their advantages as compact yet powerful actuation systems. Thus, they are the ideal technology for the development of this actuator.

As it was described in the introduction, the most important part of the EHA is the hydraulic transducer (actuator). In this case, a hydraulic piston was selected, given its simple construction and implementation when compared to other hydraulic actuators. Its geometry allows to easily increasing the force output by adjusting the piston diameter size. However, it is important to point out that this technology could theoretically be implemented in other types of actuators, such a rotatory types. Future works should try to work on different possibilities in order to bring this technology into other applications.

Among the different MR damper designs currently available in research and industry, the annular type was selected as the base for this research. This type of damper offers the highest force range observed with a relatively simple construction. Moreover, this configuration fulfilled some basic implementation requirements, such as friction performance, compact size, and unconstructed access for the fluid coming from hydraulic ports. Nevertheless, other possible implementation must be fully assessed to determine its feasibility for operation with

this new system. Moreover, a comparative study of other prototypes will bring a more comprehensive benchmark against the toroidal system proposed in this study.

In this chapter, the toroidal configuration was conceptualised as an alternative to the current annular technology. This configuration aims to address some of the theoretical concerns over the implementation of MR dampers in an active system. The toroidal configuration should theoretically increase the effective area where the MRF and magnetic field interact, increasing the output force of the piston. The close toroidal circuit should also limit the magnetic leakage that could occur between the piston wall and the piston head, improving the friction performance of the piston. Finally, this configuration should offer a wider range of configuration options to meet the requirements of specific applications. At the moment, all these claims are based only on theoretical assumptions. Therefore, it is imperative to perform a mathematical and experimental analysis of these claims, in order to determine their veracity and quantitatively assess their advantages. It is also important to mention that the toroidal configuration has been theoretically described in a patent [84], and evaluated in a series of experiments [85] conducted previous to this research. Nevertheless, these isolated studies did not fully analysed the potential of this configuration, and only covered a small fraction of the experimental and theoretical data presented in this study. Moreover, despite best efforts to find them, the existence of these publications were only available to this author at the end of this research.

At the moment, the practical design and construction of the MR piston was done using standard technology in hydraulic systems. Therefore, the performance of the system could be limited by several factors, including the sealing performance, size of the piston, hydraulic losses, and material choice. In the future, it will be necessary to make use of state-of-art hydraulic technology in order to develop a system that can optimally perform in all areas.

## 3.8 The Chapter Summary

The novel actuator concept it is introduced. It is based in an electro-hydrostatic-actuator compromising a magnetorheological piston directly connected to an integrated pumping system. The pumping system employs an electric motor that drives a bidirectional pump to control the speed and pressure of magnetorheological fluid (MRF) to the piston. Since these fluids change their apparent viscosity when subject to a magnetic field, it is possible to use an electromagnet in the piston head to precisely control the output force. In this way, it is possible to

independently control the piston speed using the electric motor speed, while the output force is controlled by the electromagnets inside the piston head.

An analysis of the current MR dampers alternatives revealed that the most suitable type of MR piston for this system is the annular type. However, this type of damper has several disadvantages, which make it not suitable for the requirements of the new system. It was found that these pistons underuse the active area in the piston head, are prone to magnetic flux leakage, and offer few parameters available for customization. This could potentially lead to decreased force range, poor performance, and limited versatility to meet different application requirements. Therefore, a new type of MR piston head was necessary for the new actuator.

A novel piston head inspired by the toroidal electromagnets was introduced. The design consists of an array of 4 MR valves placed in a circular configuration. This setup allows to overcome the disadvantages of the previous prototype by providing a larger active area, minimised magnetic leakage, and the possibility to select the number, size and geometry of the passages inside the piston head. The new piston head was constructed using permeable and non-permeable materials to ensure that the electromagnetic circuit performs optimally.

Finally, the MR piston was design built and constructed taking into account the necessary considerations for optimal actuation performance. The MR piston design has the necessary features to connect to pump, and sustain the pressure and force variations that could occur during operation. The materials and features are design to allow the MRF fluid to operate under optimal conditions, while keeping it seal inside the piston. At the same time, the sealing system was design to minimise the friction, allowing for maximum backdrivability and optimal seal performance. The new system is also easy to assemble and setup. Making the testing procedure faster and more flexible for future implementations.

# 4 Performance Assessment

The magnetorheological piston actuator (MRPA) is a new type of backdrivable hydraulic actuator consisting of an electro-hydrostatic-system and a MR piston. The need for a MR piston that will suit this actuator lead to the development of a novel toroidal piston head design. This configuration has the possibility to overcome many of the limitations of annular piston head designs. However, such a MR damper configuration has no precedent in research. In order to measure the damping force performance of this first prototype, several experiments are necessary. These experiments evaluate the MRP alone, i.e. without being connected to the pump, in order to benchmark the performance of the toroidal piston head design against conventional annular system. The experiments' design and execution is described in detail in this chapter. This work has been partly discussed in previous publications [78] and [86].

In general, the experiments were conducted using two different test benches. First, a universal testing machine is used to evaluate the passive force performance of the piston head. Since this machine is normally used for materials' testing, it can safely drive the piston with very high forces. However, it had several disadvantages. Among them, the lack of a synchronisation mechanism with external data sources, i.e. other sensors, limited the

experimental accuracy of results. Therefore, a subsequent integrated testing setup was design and constructed to perform the experiments in a more suitable manner. All the experiments conducted in this chapter evaluate only the passive performance of both prototypes.

## 4.1 Early Experimental Setup

In all the experiments, the pistons are fixed while the rod is driven back and forward using the linear actuator with a 10kN load cell attached between them. During the tests the universal machine or the linear actuator drives the piston at a constant speed, while the position, force, current, temperature and pressure values are recorded using a data acquisition board. At the moment, the temperature inside the piston head is kept constant at room temperature (20–30°C). The current in the electromagnet is manually set using an 800W digital power supply. The force measured is positive when the piston is pushed, and negative when pulled. The stroke range is set to 80 mm (from the total 110 mm) for security reasons, setting the start position, when the piston is close to its compressed state.

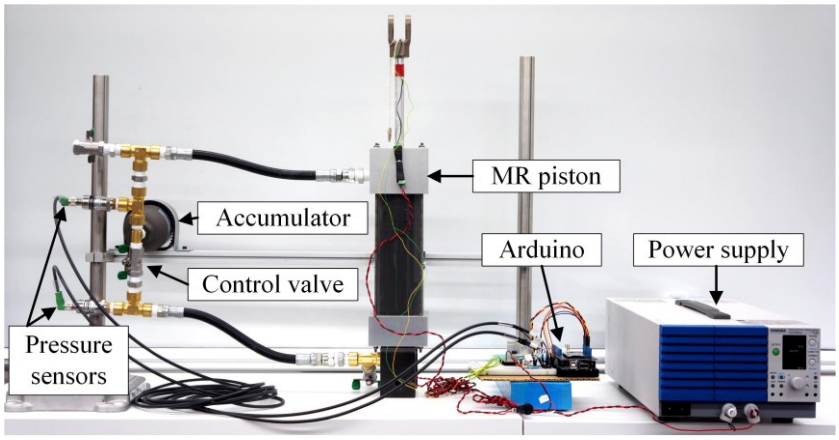


Figure 4-1. Early experimental setup: sensors and data acquisition system

The piston setup, shown in Figure 4-1, was firstly used to evaluate the toroidal piston head. In this setup, is fixed by the lower base while the rod was driven at a speed using a clevis end attached to the driving part of the universal machine with a 10kN load cell. Since the piston has only one rod, an accumulator is also used to accommodate the volume it displaces as it enters the piston. In order to take into account the effect of the accumulator in the system, the static force of the actuator was measured at different positions, and then subtracted from the resultant force.

### 4.1.1 Instrumentation & Data Acquisition System

The instrumentation setup used in this test bench were divided in two parts. One compromise of a microcontroller connected to the current, temperature and pressure sensors. While the force, position and speed are implemented in the universal testing machine. An schematic of this systems can be seen in Figure 4-2.

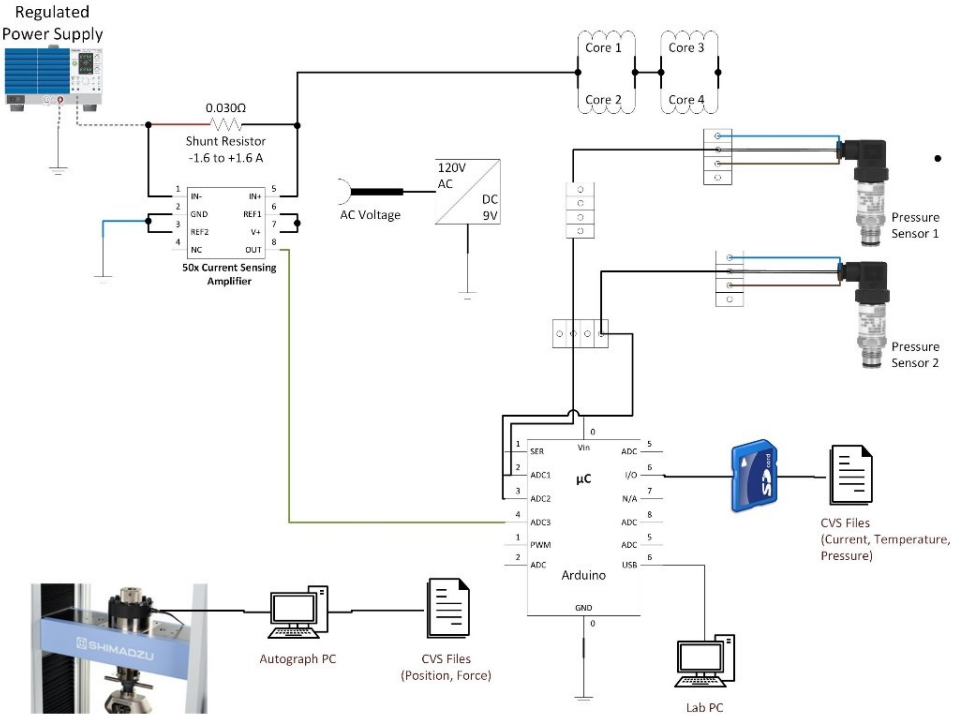


Figure 4-2. Early experimental setup: schematic of the sensor and controllers

An Arduino Mega ADK records the data in cyclical manner. The program uses a serial interface to communicate with the user. The program normally displays the average values of the variables. During the logging operation the display is stopped and only a status symbol, "*" is display to indicate that data is being logged. If buffer overruns occur the program will display a warning with its number at the end of the logging command.

### 4.1.2 Universal Testing Machine

The universal testing machine (UTM) is usually used for testing material strength. The strong forces and controlled speed make it ideal for testing the piston. During the tests the universal machine drives the piston at constant speed, usually 500mm/min (8.33mm/s), and records the position and the force applied. The test bench is shown in Figure 4-3.

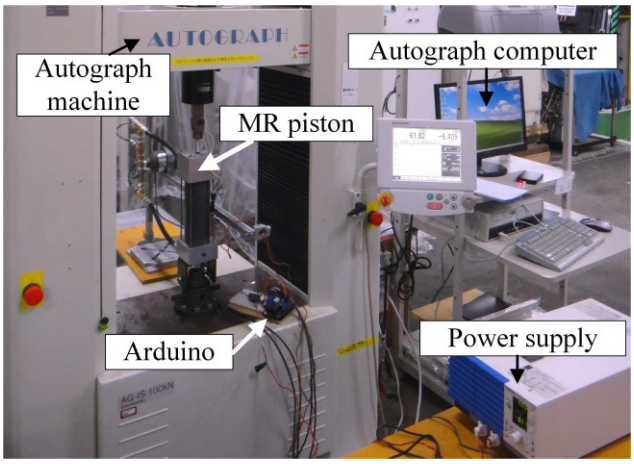


Figure 4-3. Early experimental setup: UTM test bench

The force measured is positive when the piston is pulled, and negative when compressed. The stroke range is set to 85 mm for security reasons, marking zero when the piston is close to its fully compressed state.

In order to attach the piston to the machine it was necessary to have a special jig manufacture for the lower base. On the top, a hinge with a screw is used to attach the piston rod to the load cell of the UTM.

## 4.2 Early Experimental Results

The experimental setup, shown in Figure 4-3, was used to evaluate the performance of the actuator. The round of experiments compromises a friction test to measure the minimum backdrivability force, force range test to evaluate the maximum force of the piston, and a step response test to determine the reaction time of the system.

### 4.2.1 Friction Measurement & Accumulator Compensation

The friction experiments were conducted with MR piston filled with MRF 132 DG from Lord Corp. This MRF has a nominal viscosity, μ, of 0.112 ± 0.02 Pa–s@40℃, and a maximum yield stress of approximately 45kPa at 700 mT. The piston was driven at 100mm/min (1.66mm/sec) with the control valve open to allow fluid to move freely, allowing to measure the friction of the system.

The result of the preliminary measurements are shown in top part of Figure 4-4. This measurements represent the raw forces exhibit by the actuator without magnetic field.

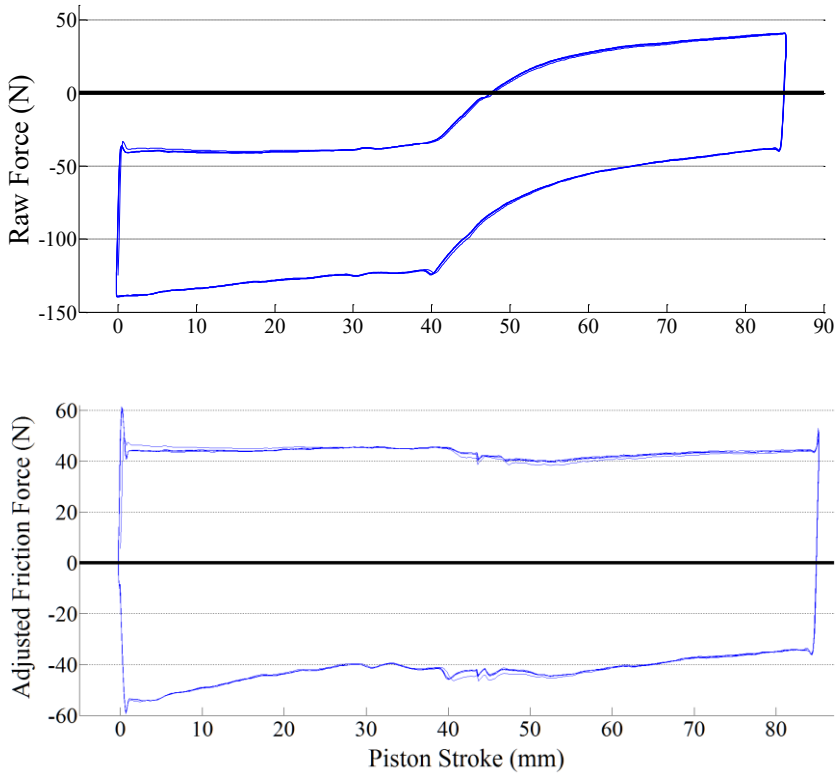


Figure 4-4. Accumulator effect and its compensation in early setup

As it can be observed from the graph as the piston moves to the back of the cylinder the compression force increases. This is caused by the change of volume in the accumulator, which increases the internal pressure of the system. Since the piston head areas are different, the built pressure will create a force opposite to compression. The actuator force reaches zero at the point when the friction and pressure force are in balance, which occurs at approximately 47mm.

In order to compensate for the effect of the accumulator, samples of the static forces at different strokes positions were taken. The samples were smoothed and adjusted to match zero at the most extended position of the piston. The result is subtracted from raw force tests to estimate the piston forces. The adjusted friction data is shown in the lower part of the Figure 4-4. As it can be seen, the adjusted values show a constant friction force as expected from this test.

### 4.2.2 Piston Force Test

The piston is cyclically pushed and pulled at 500mm/min (8.33mm/sec), while the current is gradually increased from 0 to 3A in 1A increments. Figure 4-5 shows that the MR piston is able to generate 400N of force at 3A of current, which is a very conservative value to prevent

overheating. However, it can generate up to an excess of 1kN for a short time when a current of 7A is used. This current should induce a field higher than 500mT which bring the MRF used at about 65% of its maximum shear stress.

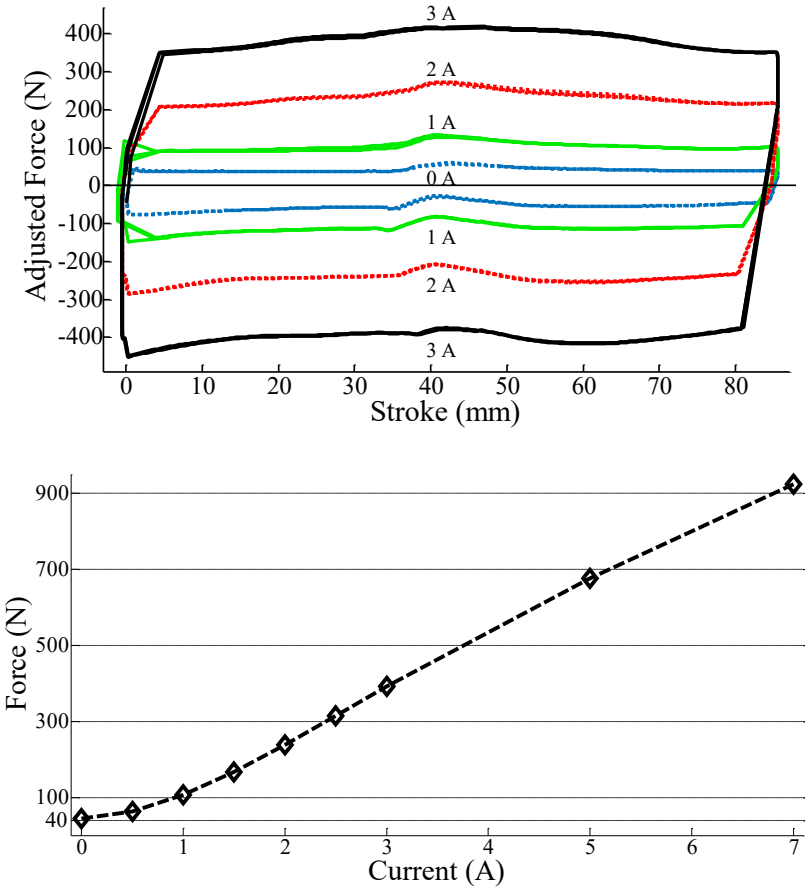


Figure 4-5. Early results: adjusted force vs stroke, force vs current at 500mm/min

The adjusted force values show that the accumulator causes force disturbances around half the stroke. This effect is possibly caused by the movement of the poppet valve in the port of the accumulator. Preloading the cylinder pressure might attenuate this undesirable effect.

### 4.2.3 Step Response

The test was performed at 500mm/min in the extending direction using two different current steps, 0.5A and 3.0A. The time and force were recorded to determine the response of the system to a small and big step changes.

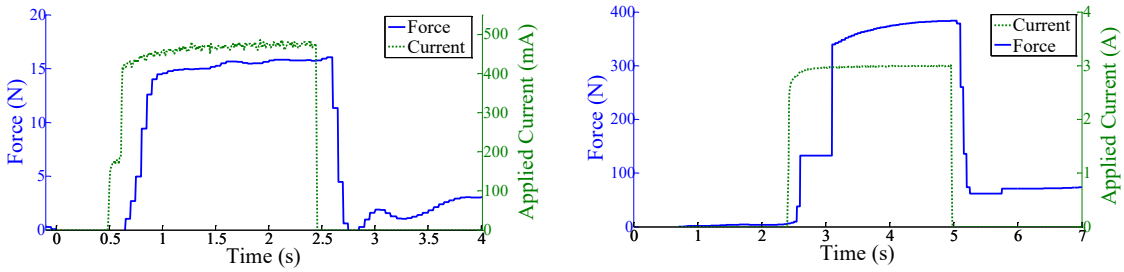


Figure 4-6. Early results: Force step response to 500mA and 3A current steps

As it can be seen on the top part in Figure 4-6, the current prototype shows a time constant of about 200ms for the 500mA step. However, it was not possible to obtain a precise measurement for the 3A step, since speed controller of the universal testing machine causes variations in the force measurements. At the moment, the cores of the system are connected in series to avoid overheating of the cables in the conduit. However, this configuration increases the time constant of the system, which can be observed in the slow response of the system. A much faster response could be achieved by reducing the inductance, and other common techniques [87] for MR based actuators. Nevertheless, it is possible that the large response time of the MR piston could be caused by a synchronisation error in the timestamps of the data.

## 4.3 Upgraded Experimental Setup

Different from previous setup, a new test bench was set to have a more control over the parameters of the driving system. As it can be appreciated in Figure 4-7 the new test setup is based on a linear actuator and a central data acquisition board. In this way, it is possible to more accurately control the force and speed of the test, as well as to solve the synchronisation issues between the data collected by the UTM and the Arduino microcontroller.

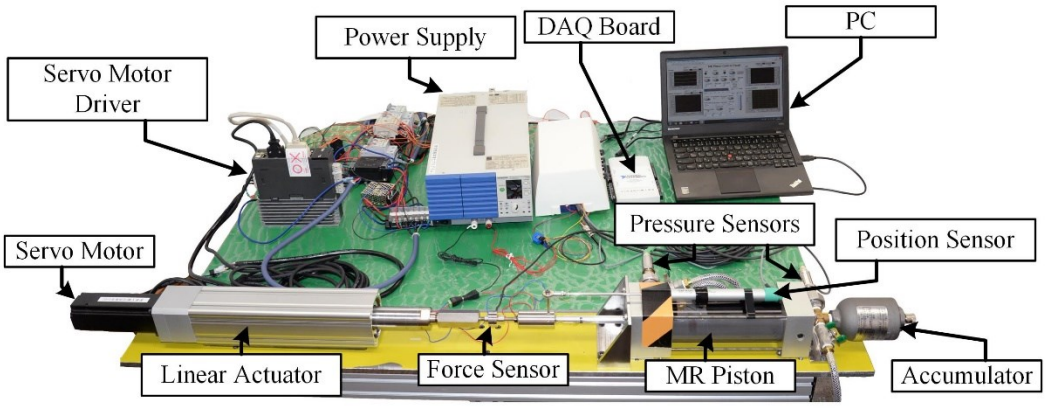


Figure 4-7. Upgraded experimental setup: test bench

### 4.3.1 Electromagnet Controller

A new electromagnet controller to accurately set the current of the coils. In contrast with the previous setup the current now can be set in an automated way in order to perform more complex tests, as well as for developing a force controller for the MR piston. This controller is responsible for regulating and keeping constant the current supplied to the electromagnetic circuit inside the piston head. It consists of a 48 VDC power supply, a full bridge PWM driver, and a current sensor. Unfortunately, due to the low inductance of the coil, and the 2kHz frequency of the PWM, it is challenging to measure the pulsating currents in the electromagnet.

### 4.3.2 Linear Actuator

An ASD-A2-0421 400W AC servo motor system from Delta drives the 2kN ball screw rod type linear actuator, LEY63. It is used to smoothly control the speed and force applied to the MRPA during the passive experiments, described in the subsequent section.

### 4.3.3 Instrumentation & Data Acquisition System

Along with the current sensors for the electromagnet and pump currents, the following sensors were added to monitor the performance of the MRPA. A 2kN load cell, eLU-2000N, from IMADA is installed at the tip of the piston rod to measure the force of the actuator. It is connected to an ez-Connect amplifier to provide an analog reading. Two 250bar pressure sensors from Parker, PTDVB2501B1C2, are connected next to the MRPA ports to accurately monitor the pressure changes inside both piston chambers. A linear potentiometer, GEFRAN PZ34-A-150, is placed on top of the piston, and attached to the piston rod, to monitor the position and speed of the piston rod.

Finally, a NI USB 6212 data acquisition (DAQ) board from National Instruments is connected to a PC to log all the data from the sensors, as well as to control the electromagnet, pump driver, and the linear actuator. This system allows for logging simultaneously all the inputs and outputs from the system at 1 kHz, to avoid the synchronization errors from previous studies. A LabVIEW GUI, shown on the top right side in Figure 4-8, was designed to monitor the system variables, log these variables into a file, implement the force and speed controllers, as well as to operate the system in a semi-automatic way during the experiments.

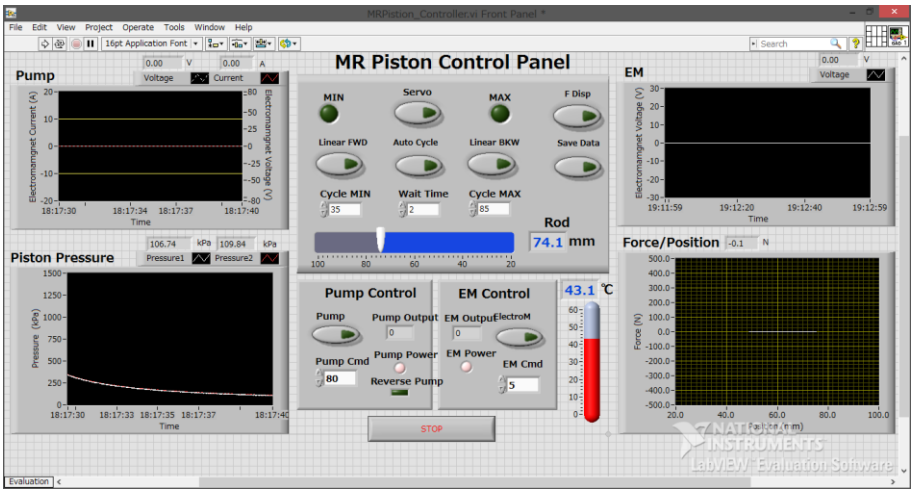


Figure 4-8. Graphical User Interface implemented in LabVIEW

## 4.4 Revised Experimental Results

The new experimental setup is used to conduct new experiments in the prototype. However, other problems related to the piston configuration were previously found during the assessment experiments. These problems need to be address before proceeding to the new experiments. The modifications will ensure a better understanding of the piston properties.

### 4.4.1 New Accumulator Compensation Method

The accumulator causes the internal pressure of the piston to rise as the piston rod enters the cylinder, creating an offset force that pushes the piston outwards. In order to obtain meaningful force measurements, it is necessary to compensate its effects.

In the previous experimental setup, static force measurements were used to compensate for this effect. However, the adjusted forces were not consistent, as shown in Figure 4-5. This problem was caused because the static measurements could not account for the static friction force. At the time, the accumulator and the pressure sensors were also placed far away from the piston, further disturbing the measurements, and compensation efforts.

In this iteration, the accumulator was placed close to the piston, as shown in Figure 4-7. In order to account for the static friction a new compensation strategy uses force measurements at slow speed.

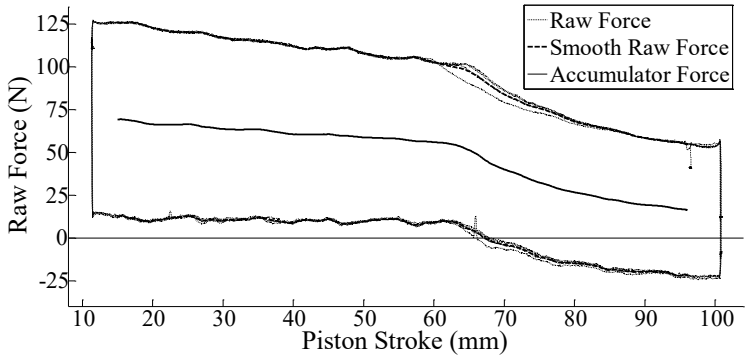


Figure 4-9. New compensation method: raw force vs stroke

The force values from the pulling and pushing motions are added together to cancel the movement related forces, i.e. the zero field damping force, and the dynamic friction of the piston. Finally, the resultant force is smoothed using a lowess filter, and subtracted from all measurements in both configurations within a stroke of 50mm. The resultant accumulator force is shown in Figure 4-9.

Using this procedure measurement for the annular and toroidal piston prototype were conducted. The adjusted force measurements are shown in Figure 4-10. As the figure shows, the adjusted forces are more stable, and the effect of the accumulator is considerably reduced when compared with previous strategy.

Nonetheless, the effects of the accumulator in the system performance are still significant. A more detailed analysis of the force measurements also showed that the effect of the accumulator is not identical during the pushing and pulling motions. This could be caused by the construction of the accumulator, which generates different flow patterns when the MRF enters or exits.

In future prototypes a double rod design could be used to eliminate the need for an accumulator, simplifying the force control, and reducing the device size and weight. However, this could negatively affect the backdrivability of piston by increasing its friction.

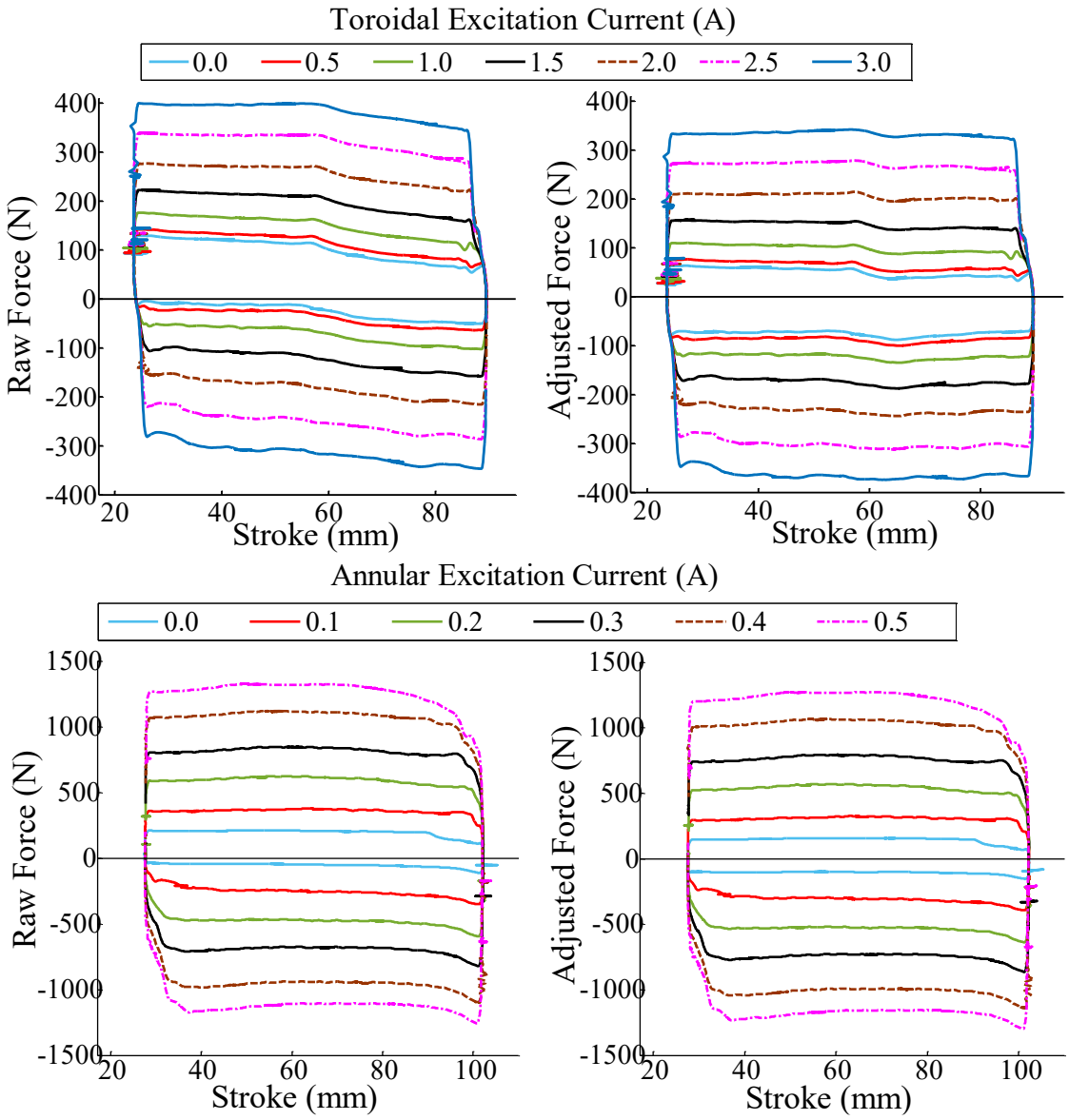


Figure 4-10. Forces vs stroke of annular and toroidal head

### 4.4.2 Friction Force Measurements

The friction was estimated at 70N during steady force push-pull operations at low speeds. The current friction performance should be improved in order to enhance the backdrivability of the actuator.

### 4.4.3 Piston Force Measurements

In this experiment, the piston is cyclically driven at four different speeds 10, 20, 30, and 50mm/s. In each iteration, the current is increased from 0.0 to 3.0A in 0.5A increments for the toroidal design, and 0.0 to 0.5A in 0.1 increments for the annular design.

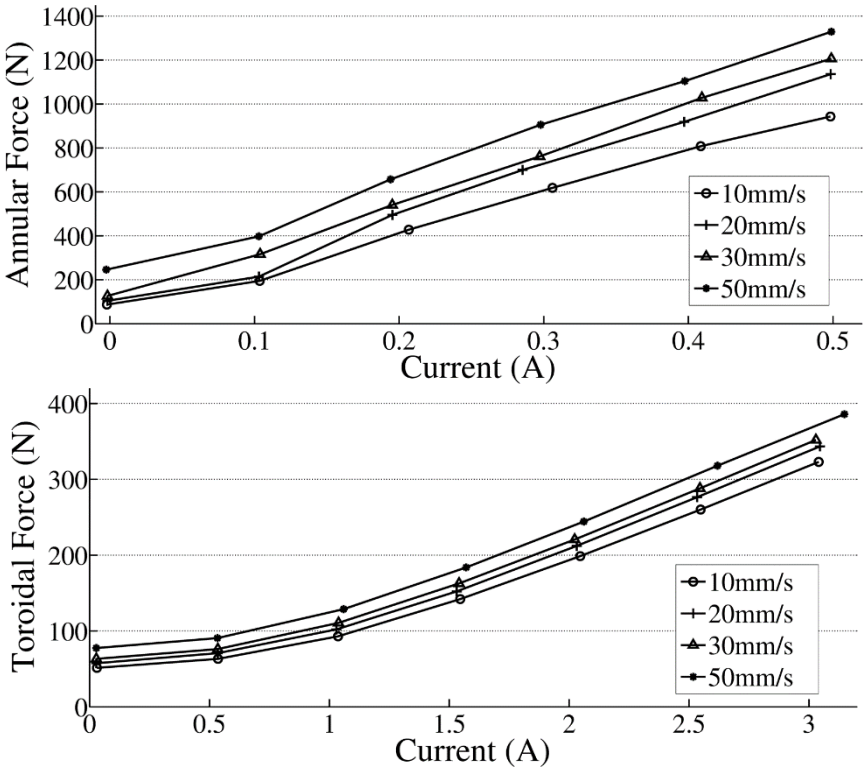


Figure 4-11. Force vs current curves at different speeds for both designs

The results, shown in Figure 4-11 and the summary in Table 4-I, indicate that the peak forces of the current prototype, under nominal current ranges (i.e. safe for the coils), are about one third of the conventional annular design. This is because the annular design has higher number of windings in the coil, which help it to achieve such forces, as well as higher energy efficiency.

TABLE 4-I - MR PISTON PERFORMANCE PARAMETERS

| | | |
|---|---|---|
| Peak Force [current] | 607 N [5.0A] | 1136 N [0.5A] |
| Power @ 300N | 24.3 W | 0.3 W |

Power and force values taken at 20mm/s
5A were applied to toroidal for a short period of time

Nonetheless, as shown in Table 4-I, the toroidal design can also achieve high forces when excited with high currents for a short period of time. This fact hints that an optimization of the magnetic circuit, as well as the geometry of the passages could be used to achieve comparable results to the conventional annular design.

The results of the toroidal forces appear to be more stable and consistent throughout the current range when compared to the annular design. While this problem could be caused by the torque and speed controllers in the linear actuator, it points towards an easier control for the

proposed prototype. A more powerful and robust test setup, using a hydraulic piston might be necessary in order to improve the tests for the annular type.

### 4.4.4 Force vs Speed Test

The force speed curves are used to see the stability of the force in response to a sinusoidal position input. The speed response is evaluated at a top speed of 120mm/s, limiting the current to 0.3A for the annular type. The curves in the toroidal design are more independent from the piston speed, and exhibit lower hysteresis, when compared to its annular counterpart. This result is unexpected since the gap cross section of the annular design is bigger, which it would normally lead to lower damping related forces. This could be caused by the empty seal grooves of the toroidal head, which were not included during the manufacturing of the annular head. Nevertheless, this shows the ability of the toroidal prototype to keep more stable forces throughout this speed range.

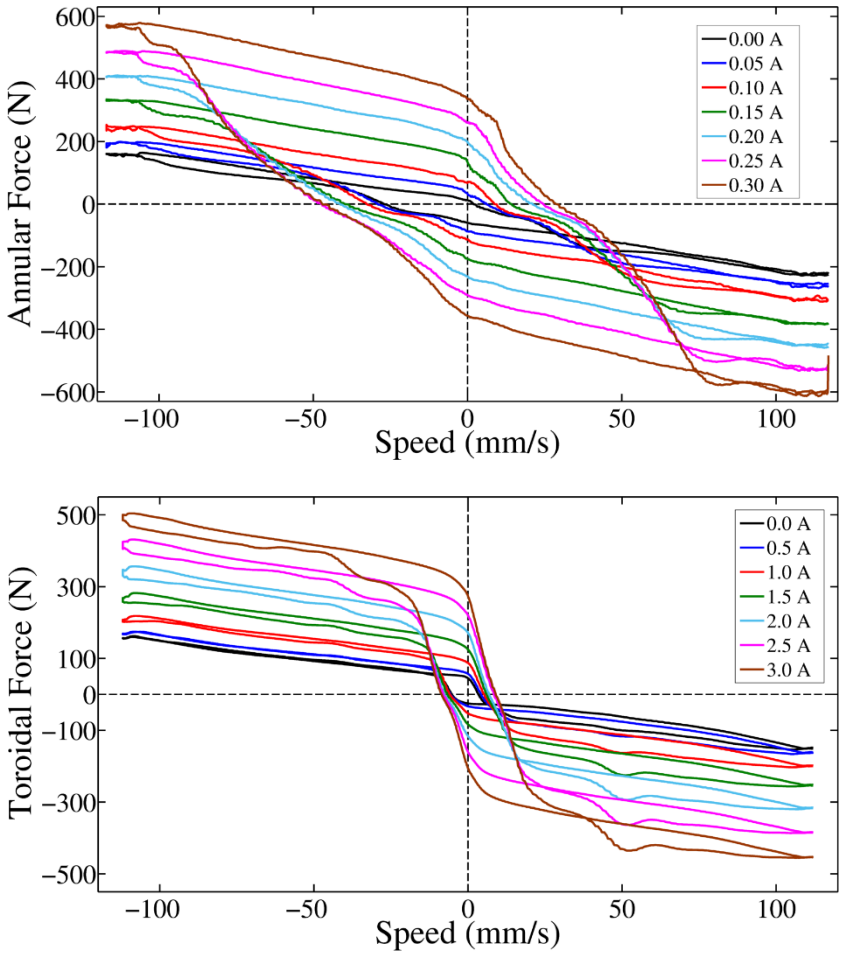


Figure 4-12. Force vs speed curves at different currents for both designs

Finally, it is worth to note that the resultant curves exhibit a linear behaviour, since both pistons were design to operate in the quasilinear region of the MRF yield stress curve. There, an easier relation between the output force and the controlled magnetic field can be achieved. Moreover, both designs are far from the saturation limit of the permeable materials, where the permeability value rapidly decreases. This further improves their response time performance, as it will be shown below.

### 4.4.5 Current Step Response

In previous experimental setup, the response time was estimated at 200ms, which was unusually slow when compared to other MR devices. The probable cause of the problem was the synchronization of the force results coming from a universal testing machine, and the rest of the sensor data collected by an Arduino board. For this reason, in this new test bench all the measurements are simultaneously sampled using a data acquisition board. The new test was done at 10mm/s using 1.0A and 0.07A steps for the toroidal and annular designs respectively, which correspond to a 70N force step from their zero field damping force on both designs.

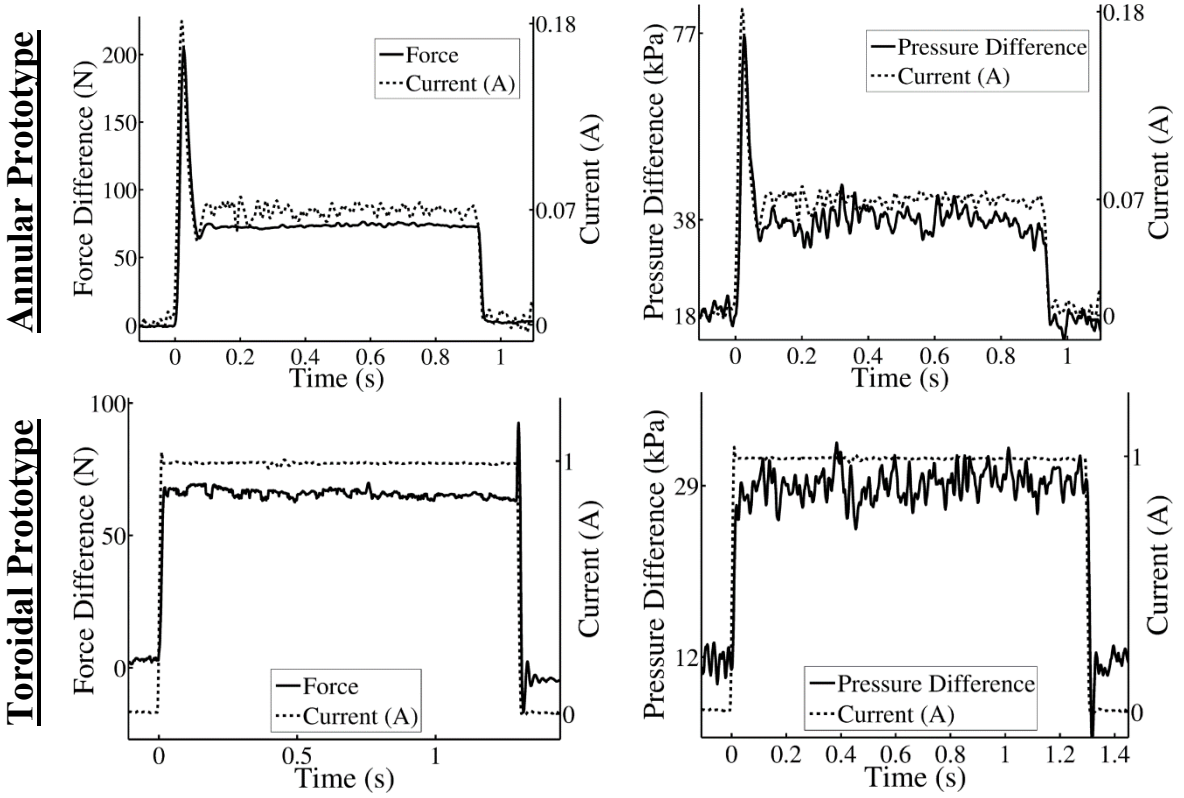


Figure 4-13. Current step input responses for annular and toroidal prototypes

Figure 4-13 shows the force and pressure responses to a current set input. The toroidal force and pressure responses to a 0.0–1.0A step is 57N→122N and 12kPa→29kPa, and occur within 20ms and 30ms respectively. While the annular force and pressure response to a 0.0–0.07A step are 92N→165N and 18kPa→38kPa, occurring both within 12ms. These results show that despite a fast initial response, the higher inductance in the annular core causes an overshoot in its current, allowing the toroidal design to reach the steady state value 5 times faster with less ripple. These values make the toroidal design a suitable alternative for force control applications, such as contact forces in pHRI. The fast response can be attributed to the low coercivity values of the materials used in the electromagnetic core. In the case of the annular design, the overshoot problem can be compensated using a current controller to obtain the optimal response seen in current damper designs.

The pressure difference, shown in the right part of Figure 4-13, is calculated by the difference of the values measured by two pressure sensors connected next to the piston ports. The new position of the sensors in the setup was crucial to this measurement, since in previous attempts it was not possible to collect this data. In general, the pressure response is slightly slower than the force, and its behaviour is apparently independent of the effect of the accumulator, so they could be a suitable alternative as the force feedback for the device. Nevertheless, pressure sensors have typically noisier signals than force sensors, as it can be seen from the graphs.

### 4.4.6 Hysteresis Performance

These experiments were performed with the objective to determine the performance of the toroidal magnetic circuit with respect to varying currents. In this test, the piston was driven at 500mm/sec (8.33mm/sec) and the current was raised from 0A to 3A, and then decreased back to 0A using 0.5A steps.

From the results, shown in Figure 4-14, it can be concluded that the actuator has very low hysteresis, when compared to similar actuators found in literature, showing its potential to achieve a good degree of controllability. This characteristic can be attributed to the small size of the cores, and the low coercivity of the Permalloy 78 used in their construction.

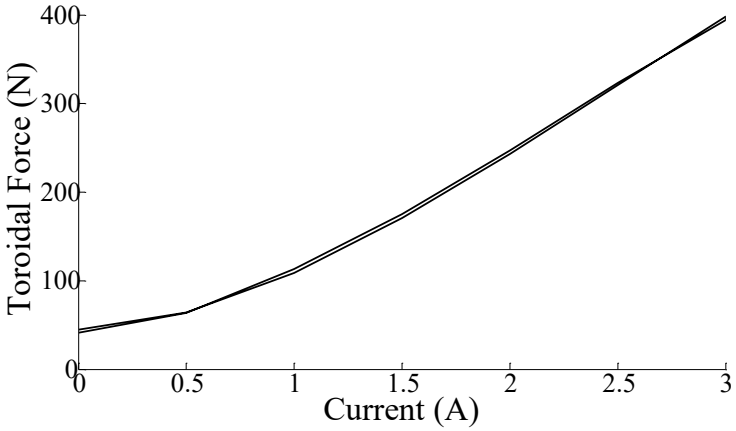


Figure 4-14. Hysteresis measurement performed at 500mm/min

The results also show that between 0 to 1.0A the force has a strong non-linear behaviour. This is caused by the material properties, and the relation between the Newtonian and yield stress induced forces. After 1.0A the permeability of the material should have reached a more stable value, and the yield stress of the MRF becomes the dominant force, allowing to enter the linear region of the device. These characteristics will have to be taken into account for the future design of the force controller, where a compensation strategy such as piecewise linear controller [88] [89] could be used.

## 4.5 Force Control Experiments

Because it is important to evaluate the prototype in a real control application a force controller was implemented. The description of the tuning and the experiments is described below in detail.

### 4.5.1 Force Controller Parameters

A PID controller was programed in LabVIEW to produce the control output signal to drive the piston. The inputs and outputs of the controller are handled by the DAQ board NI USB-6212. To achieve the necessary driving current, the control output signal is amplified using a chopper current controller, TI LMD18245.

### 4.5.2 Force Control Sine

All the sine waves have same amplitude of 50N, but different frequencies from 0.5Hz to 5Hz. The results in Figure 4-15 show the ability of the proposed prototype to accurately track

the sine inputs, with no significant difference compared to the annular prototype. In the case of the 2Hz input the annular design exhibits a small ripple. Similarly, in 5Hz, both designs tend to produce higher ripples, with the toroidal design starting to lose track at the end of the stroke where the accumulator pressure is higher. The cause of the ripple is variations of the frequency of the controller since it is not implemented in real time. Despite these problems, the proposed head achieves smoother force control up to 2Hz.

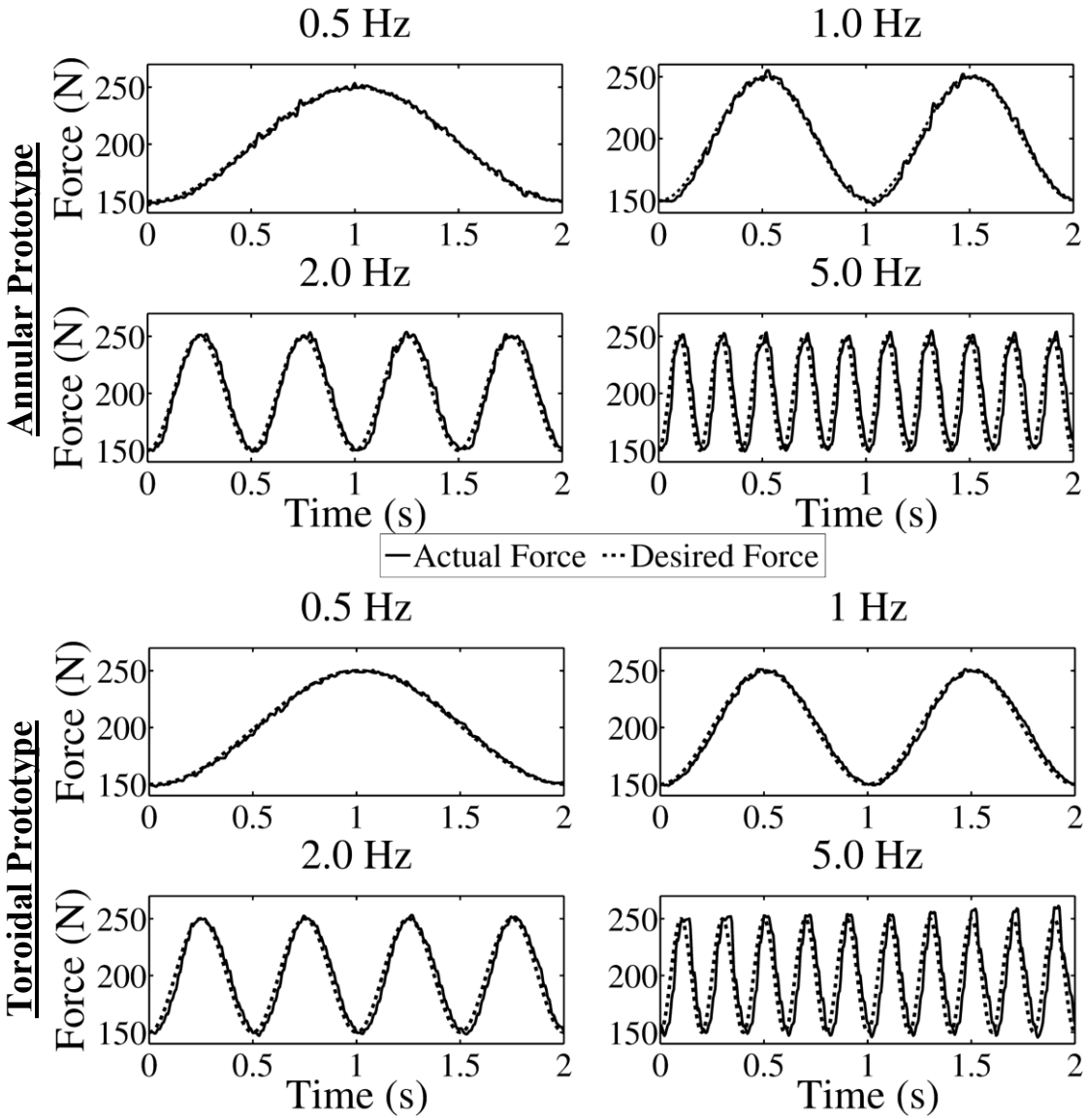


Figure 4-15. Force control performance to a sinusoid - annular (top) and toroidal (bottom)

### 4.5.3 Force Control Step

In the experiment a square step of 100N, and four sine waves are used as inputs.

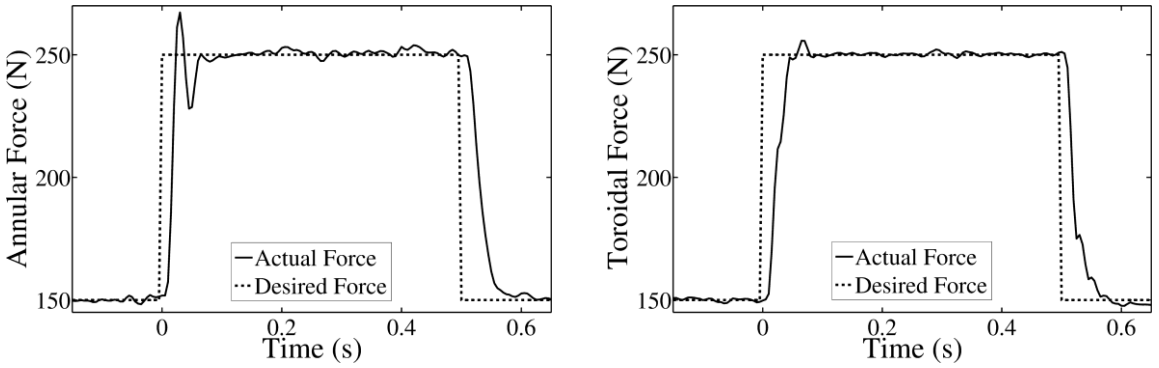


Figure 4-16. Force controller response to a 100N step input

In the case of the step response, as expected from previous experiments, the annular design is slightly faster in the rising edge, 20ms against 45ms to reach final value; while the falling edge is the same 60ms for both. However, it still shows a reduced 8% overshoot. These problems are probably caused by the difference in driving currents. On the other hand, the steady state value of the toroidal type appears to be more stable, which is a necessary characteristic for force interaction applications. The PID controller successfully improved the response from both prototypes, and partially suppressed the effect of the accumulator. However, its performance is still limited to low frequency inputs. Perhaps a more complete strategy such as [90], can be used in more demanding applications.

## 4.6 Discussion & Remarks

The passive performance of the toroidal configuration prototype was tested in order to assess its feasibility as a transducer for the MRPA. The results from this experiments showed that the piston was capable to achieve high forces and a relatively fast step response. In this way, the piston was proven to be a feasible alternative for implementation in the MRPA.

Nevertheless, these results were not congruent with the performance of similar MR based designs, such as the annular MR damper (used as a benchmark). This problem was first attributed to the measurement strategy in the test setup. New measurements compared the toroidal and annular piston heads performance. It was found that the forces of the toroidal prototype are more stable over the current and speed ranges. This is thanks to the toroidal design, which allows the piston head to operate within the quasilinear region of materials in the core

and the MR fluid. The results to a current step showed that despite a fast initial response, the higher inductance in the annular core causes an overshoot in its current, allowing the toroidal design to reach the steady state value 5 times faster with less ripple. In both cases, the step response time was now calculated to be between 20ms and 30ms. These values are more in line with similar MRF based actuators.

The force control tests of the actuator show its capacity to perform well using a simple PID controller. In this case, the actuator was able to accurately flow the sinusoidal force input up to 5Hz, with minimal disturbance. During these experiments, it was also establish that the toroidal prototype has an equally satisfactory performance when compared with its annular counterpart. Additionally, it is noteworthy that the controller was able to compensate for the asymmetrical force caused by the accumulator expansion. Nevertheless, these experiments only demonstrate the passive performance of the actuator. At a later stage, it will be necessary also to evaluate its performance when connected to the full hydraulic circuit. Then, a full evaluation of the complete system will bring light to the possibilities and capabilities of this new system.

The positive results point some of the advantages of the toroidal design over its counterpart. However, it was evident that the new configuration was still underperforming even after the test setup was fixed. The reasons behind the limited performance of the prototype are believed to be related to the magnetic circuit construction. The use of steel inserts in the MR plugs maybe creating a non-uniform field inside the passages. This reduces the area of interaction between the MRF and the piston head, affecting its performance. Additionally, it is also possible that magnetic saturation maybe occurring in some parts of the magnetic circuit. Moreover, if this saturation is big enough it could lead not only to decreased performance but also to magnetic leakage, increasing the friction of the prototype.

Concerning the friction performance, the current prototype has a remarkable performance for a piston of this size. This is was achieve by avoiding the use of tight seals around the piston head, and the Teflon based wear rings for the head and rod. These modifications certainly have a negative impact in the efficiency of the system by increasing the MRF leakage around the piston head. The exact amount of leakage was not evaluated in this research. Perhaps, there is an optimal balance between these characteristics that would allow the piston to perform better according to the requirements of a specific task. On the other hand, there is the possibility to further reduce the friction without significantly impact the sealing performance. The piston wall could be polished, and perhaps treated with special materials to improve its friction performance.

Additionally, small rod sizes could also be used if the stroke of the piston is short enough to avoid bending of the rods. Finally, materials suitable to interact with the MRFs could be used in the wear rings in order to provide adequate lubrication and movement for the piston head.

Finally, there are some parts of the prototype that need improvement, such as the accumulator, and single rod design. These cause an asymmetric output force, as well as poor backdrivable performance respectively. These problems need to be solved before the prototype can realise its full potential.

## 4.7 Chapter Summary

A test setup based on a universal testing machine (UTM) was primarily used to test the passive damping force of the actuator. The results from this experiments showed that the piston was a feasible alternative to the annular prototype. However, discrepancies in the measurement results were attributed to the data acquisition setup. Since it was based in two separate data collection systems, it could be possible that synchronisation errors in the timestamps of the measured data were not correct. A second setup based on the centralised DAQ board for all measurements was used to address these issues. The new setup also included other mechanical and technical considerations, as well as a linear actuator to precisely control the applied speed and force, in order to improve the experiments and measurements.

A new round of experiments shows that while the response performance of the prototype is similar to state-of-art designs, its force performance is limited. The force curves of the toroidal prototype also appear to have a higher linearity and are more stable during several tests. In this way the feasibility of the prototype is confirm, and some of its advantages are clearly defined. However, there are some areas that need improvement such as the maximum force performance and energy efficiency, where the prototype lags behind current designs.

The new test setup also included a current controller for the electromagnetic circuit. This controller allowed the implementation of a force control strategy for the MRP. Experiments including a sinusoidal and force step input were performed. The results show that performance of both prototypes is similar in both experiments, with the annular prototype performing slightly better at 5Hz sinusoidal input. Nevertheless, the overshoot in the annular prototype was observed again in this test.

All the results have shown the feasibility of the new toroidal configuration as an alternative to the conventional toroidal configuration. Nevertheless, its performance is still limited by several factors. For instance, the mechanical design of the piston has room for improvement. Specially, the accumulator needs to be eliminated to stabilise the force readings. The friction in the seals needs to be changed to improve the backdrivability of the piston. Additionally, it is believe that the dimensions of the electromagnetic circuit as well as the passages of the toroidal array need to be optimised. Therefore, it is necessary to improve the model of the MR piston to understand how these parameters affect its performance, so that they can be optimised to meet specific systems requirements.

# 5 System Modelling

The new toroidal configuration of the MR piston has been shown to be a feasible alternative to the conventional systems. During a preliminary evaluation of the first prototype, this configuration showed potential for improvement in aspects. In order to realise this potential, it is necessary to have an understanding of the underlying principles of this actuator. Although some equations were introduced during the design phase, they only cover a small fraction of the phenomena involved in the operation of the MRP. In order to model all the parameters of the actuator it is necessary to construct complete models for the electromagnetic, hydraulic, and magnetorheological functions of this system.

This chapter describes in detail how a comprehensive model of actuator was constructed. The models presented in this chapter are based on previous work published in [91]. The models presented here attempt to provide a simplified understanding of the actuator using explicit equations. In this way, it is possible to more easily find the relations between relevant performance parameters. It is important to note that it is not within the scope of these models to provide a precise method to calculate the output variables of the actuator, but to provide a straightforward way to estimate its performance. This kind of modelling will enable streamlining the design process of this new type of actuator, allowing future designers to match the output force and backdrivability requirements of particular applications.

As it was described in previous sections, the MRP is similar to conventional piston and dampers. In this sense, it can be modelled in a similar way as previous systems. Thus, in order to derive an equation for the damping force an analysis of the hydraulic, magnetorheological, and the electromagnetic models is presented in this section.

## 5.1 Hydraulic Model

Figure 5-1 shows the hydraulic model schematics with the main variables involved in the modelling of the piston flow and forces. The operation of the piston head can be described as follows. As the piston head is pushed backwards by an external force, $F_e$, at a constant speed, $v_p$, it displaces a volume of MRF at a rate, $Q_d$. The displaced fluid crosses from chamber *a* to *b* at a rate, $Q_h$, creating the pressure difference between the chambers $\Delta P$. Omitting the friction force, this pressure creates a force $F_p$, opposite to the movement of the piston.

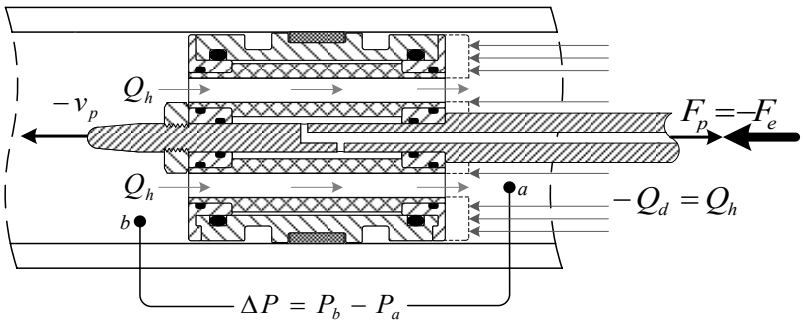


Figure 5-1. Schematic diagram of the piston head for the mathematical models

Because the MRF fluid can be assumed to be incompressible, applying the law of conservation of mass we have that the flow in the passages is equal to the displaced fluid. Given the piston area, $A_p$, and piston rod area, $A_r$, the flow is

$$Q_d = -Q_h = (A_p - A_r)v_p$$

Equation 5-1. Volumetric flow in the piston head passages

It is important to note that due to the single rod design, the fluid displaced by the piston rod has to be compensated using an accumulator. This accumulator for simplicity is not included in this analysis.

In the absence of magnetic field, the MRF fluid behaves like a Newtonian fluid. In case we neglect the transient pressure variations generated by changes in the flow, the pressure can be assumed to be uniform on each piston chamber. Since all the passages are identical, then

flow rate across them can be considered equal, and the pressure drop across a single hole is given by the Poiseuille equation,

$$\Delta P' = \frac{8\eta L_p}{\pi r_{gap}^4}\frac{Q_h}{N_p}$$

Equation 5-2. Poiseuille equation for the pressure gradient under laminar flow

Because the pressure and flow are uniform in the chambers and piston holes, Equation 5-1 and Equation 5-2 can be combined making possible to write the pressure difference in terms of the piston velocity,

$$\Delta P = \frac{-8(A_p - A_r)\eta L_p}{\pi r_{gap}^4 N_p} v_p$$

Equation 5-3. Newtonian pressure difference for a damper with circular passages

### 5.1.1 Visco-Plastic Hydraulic Models

In order to model the visco-plastic behaviour several methods [80] have been proposed. Wang and Gordaninejad presented accurate results using the Herschel-Bulkley model [92]. A non-dimensional analysis used by Wereley and Pang [93], presented satisfactory results using an implicit equation. However, the first one requires complex computations and tables, while the latter is difficult to apply to the complex geometry of the toroidal head. Since our objective is to develop an efficient model to evaluate the performance of the damper for constant velocity input, the Bingham model is widely used in many cases including dampers [94]. In this case, it is chosen for its simplicity to predict the force in steady state conditions with a high degree of accuracy.

### 5.1.2 Bingham Model

A simplified approach based on the Bingham model is preferred for its simplicity in steady state conditions, and high degree of accuracy for fluids with variable yield stress [95].

In the Bingham model, the MRF is considered to have a yield stress, $\tau_y$. In this case, the MRF will not flow, until the pressure is high enough to induce a stress higher than the yield stress. Therefore, the constitutive equation of the Bingham model is given as a discontinuous equation,

$$\dot{\gamma} = 0 \qquad \tau \leq \tau_y$$
$$\tau = \tau_y + \eta\dot{\gamma} \quad \tau > \tau_y$$

Equation 5-4. Constitutive equation of the Bingham model

An approximate solution to the Buckingham-Reiner equation for laminar flow of Bingham fluids in pipes presented by Eberl & Eberl [82], gives the pressure drop across the piston head as,

$$Q = \frac{\pi D^4 \Delta P}{128 L_p \eta} - \frac{\tau_y \pi D^3}{24\eta}$$

Equation 5-5. Approximate solution to Buckingham-Reiner eq. for laminar flow of Bingham fluids

Solving for ΔP and substituting the corresponding variables,

$$\Delta P = \frac{8\eta L_p}{\pi r_{gap}^4} \frac{Q_h}{N_p} - \frac{8\tau_y L_p{}'}{3 r_{gap}} sign(v_p)$$

Equation 5-6. Pressure difference derived from the Buckingham-Reiner equation

The first term on the right hand side of Equation 5-6 is the contribution of the Poiseuille flow to the pressure gradient, same as in Equation 5-3. This drop is related to the nominal viscosity of the MRF, $\eta$, the geometrical parameters of the toroidal assembly, and the flow rate $Q_h$ in the head passages,

On the other hand, the second term on the right hand side shows the velocity independent contribution from magnetically induced yield stress, $\tau_y$. It is important to notice that this equation is convenient, since it allows to separately calculate the Newtonian, as well as the visco-plastic behaviour of the MRF. It also includes two different lengths, $L_p$ and $L_p'$, for each term of the equation. In this way, it can be used to analyse passages where the magnetic field does not affect the complete length of the gap, as with the device that it is being modelled.

## 5.2 Magnetorheological Fluid Model

The prototype was filled with MRF 132DG from LORD Corp. with a nominal viscosity, μ, of 0.042 ± 0.02 Pa–s@40°C, and a maximum yield stress of approximately 35kPa, which is developed at around 700 mT. The parameters necessary to model the visco-plastic behaviour of the fluid where obtained from the curves provided in the datasheet of the manufacturer.

$$H = 122168\mathrm{B}^3 + 136184\mathrm{B}$$

Equation 5-7. Fitted eq. for magnetisation B-H curve provided for MRF 132DG from Lord Corp.

$$\tau_y = 9.5 \times 10^{-13} H^3 - 1 \times 10^{-6} H^2 + 0.41\mathrm{H} - 1150$$

Equation 5-8. Fitted eq. for yield stress curve provided for MRF 132DG from Lord Corp.

These equations estimate the shear stress for the hydraulic model given that the magnetic flux density inside the actuator passages, B, is known. They assume that the maximum yield stress can be reached with a flux density of 0.7 Tesla.

## 5.3 Electromagnetic Model

As it has been described in the previous section, the force in the system is the result of varying the magnetic field generated by the electromagnets, the apparent viscosity of the MRF, and finally in the flow rate between the chambers in the piston. In this section, we cover the analysis of the electromagnetic model.

### 5.3.1 Reluctance Model

The reluctance model is used to estimate the average magnetic flux density, B, necessary for the calculation of the yield stress. Previously, a simplified model of the piston's magnetic circuit was done in [91], [96].

The reluctance method is analogue to an electrical circuit, as explain in [97]. The following equation is the counterpart of the Ampere's law,

$$\Phi\mathcal{R} = NI$$

Equation 5-9. Simplified equation used in the reluctance method to estimate flux in a closed path.

Where the electromotive force (NI), the reluctance (R), and the magnetic flux (Φ) are analogue to the voltage, resistance and current in electrical circuits. Likewise, the resistance in every path of the circuit is directly proportional to the length, and inversely proportional to the cross-sectional area.

$$\mathcal{R} = {}^{l}/_{\mu S}$$

Equation 5-10. General reluctance form for a material of constant cross section

The reluctance method provides a good estimation of the magnetic flux. However, its accuracy varies according to the estimation of the material parameters, as well as the assumptions used when determining the magnetic flux path. In this paper the magnetic permeability of the materials is assumed to be constant, the air gaps are neglected in the calculations, and the geometry of the flux path has been simplified.

### 5.3.2 Toroidal Piston Head Configuration

The following figure shows the relevant parts of a section of the electromagnet circuit.

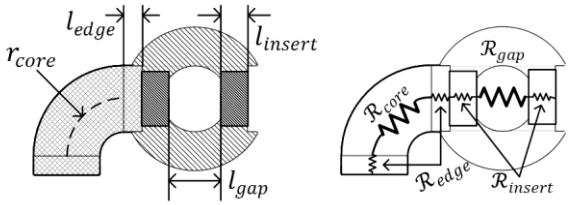


Figure 5-2. Section of the electromagnetic circuit, used in the reluctance model

In order to obtain the combined resistance of the electromagnetic circuit first the reluctances, of each segment are calculated as follows. The core reluctance can be calculated using the centreline radius as follows,

$$\mathcal{R}_{core} = {}^{l_{core}}\!/_{\mu_{core} S_{core}} = {}^{2\pi r_{core}}\!/_{4\mu_p S_{core}}$$

Equation 5-11. Reluctance of the core section

The edge reluctance has a constant square cross-section

$$\mathcal{R}_{edge} = {}^{l_{edge}}\!/_{\mu_p S_{edge}}$$

Equation 5-12. Reluctance of edge section

The reluctance across the passage was calculated by modelling a cylinder of height, h, and radius, $r_{gap}$, as follows,

$$\mathcal{R}_{gap} = \int_{-r_{gap}}^{r_{gap}} \frac{dr}{\mu_{gap} 2h\sqrt{{r_{gap}}^2 - r^2}} = \frac{1}{2\mu_{gap} h} \sin\left(\frac{r_{gap}}{r}\right)\Big|_{-r_{gap}}^{r_{gap}}$$

$$\mathcal{R}_{gap} = \frac{\pi}{2\mu_{gap} h}$$

Equation 5-13. Reluctance of the gap section

From the resultant equation it is understood that the reluctance of a circular gap is independent of its radius. Since the magnetic permeability of the MRF is higher than the aluminium, the magnetic flux going through the sections of the aluminium plug can ignored.

The inserts are 5 steel bolts, thus the reluctance is given by

$$\mathcal{R}_{insert} = {}^{l_{insert}}/_{5 * \mu_i S_{insert}}$$

Equation 5-14. Reluctance of the insert section

The complete reluctance can be calculated by summing all the individual reluctances necessary to close the magnetic circuit.

$$\mathcal{R}_{total} = 4\left(\mathcal{R}_{core} + 2\mathcal{R}_{edge} + \mathcal{R}_{gap} + 2\mathcal{R}_{insert}\right)$$

Equation 5-15. Total reluctance of toroidal magnetic circuit

The magnetic flux can be calculated using eq. 1, and the magnetic flux density at the gap is calculated as follows,

$$B_{gap} = {}^{\Phi}/_{S_{gap}} = {}^{\mathrm{NI}}/_{\mathcal{R}_{total} S_{gap}}$$

Equation 5-16. Magnetic flux density at the gap

However, given the non-uniform cross-section of the passages it is necessary to consider an equivalent area for the gap. Since the flux has to travel through the full length of the passage ($2r_{gap}$), it is possible to combine Equation 5-10 and Equation 5-13 and solve for *S*, to obtain

$$\mathrm{S}_{gap} = {}^{4r_{gap}h}/_{\pi}$$

Equation 5-17. Cross-section area at the gap

As it was mention before, the accuracy of the model depends to great extent on the estimation of the parameters. In this specific case, it is particularly sensitive to the cross section of the gap affected by the magnetic field.

### 5.3.3 Annular Piston Head Configuration

Similar to the toroidal head the annular head was modelled using the reluctance system. The parameters are done according the figures in the appendix.

## 5.4 Model Based Estimations

In order to test the accuracy of the model a simulation in Matlab was done to verify the results. The details of the simulation are explained in detail in the subsequent sections.

### 5.4.1 Matlab Simulation

A simulation using Matlab was conducted taking into consideration the equations developed in the previous section. The steady damping force over a given speed range was evaluated for different currents, ranging from 0A to 5A. The results are shown in Figure 5-3.

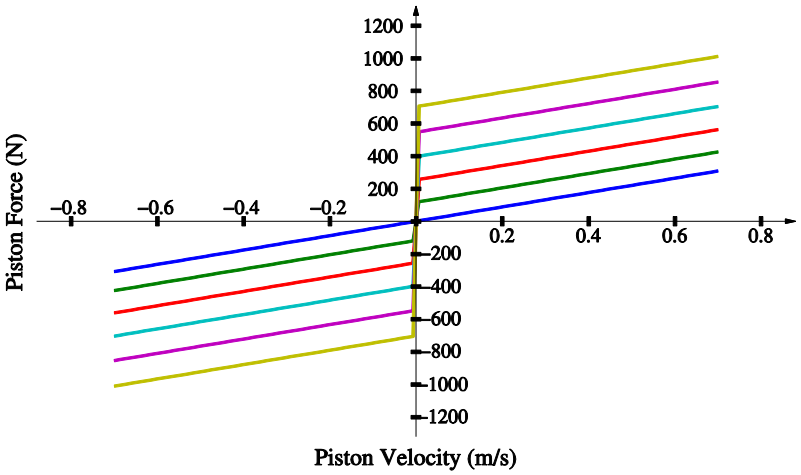


Figure 5-3. Velocity related piston force for various current settings

In the figure the friction force is not considered, therefore the minimum force shown represents the theoretical force induced exclusively by the Newtonian flow, i.e. no current. The operational range of the piston is between 0 and 1000N when operating up to 5 amperes and a speed of 700mm/s.

### 5.4.2 Magnetic Flux Density in Gap

In order to validate the predictions of the model, measurements in the electromagnetic circuit are performed. The measurements are done by placing a hall sensor in the centre of the plug. At the moment, the plug is not filled with MRF, but rather empty. Therefore, the estimation of the magnetic field is done by using the magnetic permeability of vacuum at the centre of the gap.

The results, shown in Figure 5-4, show the estimation done with the vacuum permeability, as well as the estimation done in the case the MR valve passage was filled with MRF. In the

case of air, it was estimated around 50mT. The MRF has much higher permeability, therefore the estimation with MRF is in the order of 300mT.

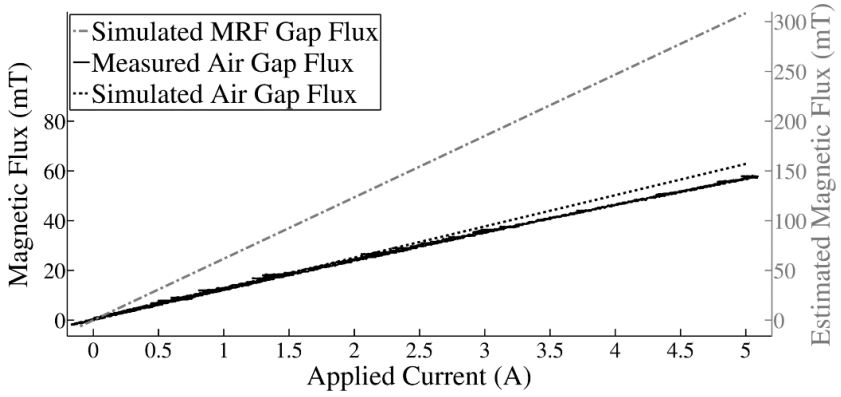


Figure 5-4. Comparison of simulated and measured magnetic flux densities at air gap

As it can be see from the simulated air gap flux density, the results of the model agree with the experimental measurements. There is a slight deviation at the end, this can be possibly attributed to the saturation of the magnetic circuit. Other explanation maybe related to a possible magnetic flux leakage inside the toroidal electromagnet.

### 5.4.3 Passive Force Comparison

The friction force was estimated at approximately 40N. It was experimentally measured by moving the piston at a speed of 0.833mm/s. The friction force was added to the simulation in order to compare its results with the experimental data. The results are shown in Figure 5-5. Force vs current curve comparison between the experimental and simulated data at a speed of 8.33mm/s.

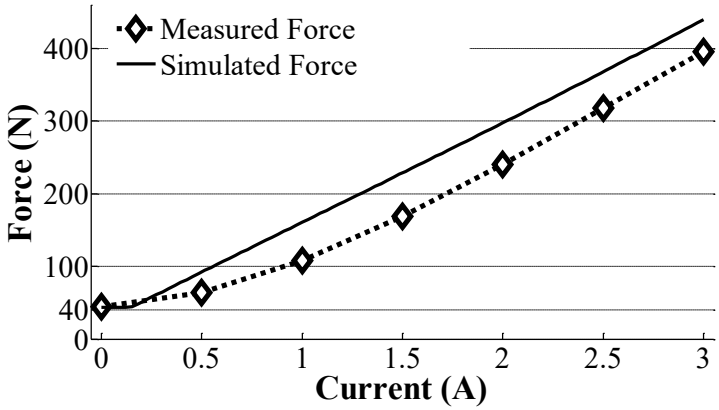


Figure 5-5. Force vs current curve comparison between the experimental and simulated data at a speed of 8.33mm/s

As it can be seen, the simulation force accurately predicts the force behaviour of the prototype. The discrepancy observed in the measurements can be primarily explained by the estimation of the effect of the accumulator in the system, however the simplifications used in the mathematical model cannot be completely discarded as another possible cause. In order to clarify this problem, a new design for the piston using two rods is necessary.

The limit of 5 amperes is the maximum allowed current that ensures the integrity of the cores. Higher currents could be possible but only for small periods of time, therefore they were not included in this study.

The forces at different current settings do not increment linearly with the current. This is expected since the yield stress curve of the MRF has a logarithmic behaviour, which saturates around 0.8T at the gap.

### 5.4.4 Parameter Sensitivity

At the moment, the model results considerably vary depending on the material properties and dimensions input in the model. These large variations are described as parameter sensitivity. In order to improve it, it is necessary to have accurate measurements of the properties of the materials. Additionally, is necessary to evaluate the margin of error incurred when a certain deviation is introduced. However, this study is outside the scope of the discussions in this research.

## 5.5 Simulation of Electromagnetic Circuit

Given the complex geometry of the prototype, a precise modelling of the electromagnetic circuit of the toroidal head is challenging. As mentioned earlier, the current mathematical model provides a reasonable estimation of its behaviour in steady state conditions within the quasilinear range of the material magnetic properties. However, in order to be able to precisely estimate the force of the actuator in every condition, it is necessary to build a solution taking into account the following points:

- Magnetic flux leakage between the core edges
- Parallel flux paths through the non-magnetic materials
- Non-linear, and saturation effects of magnetic materials

### 5.5.1 Finite Element Method

The finite element method allow the calculation of the magnetic field by creating a mesh around the objects, and trying to minimise the difference between each iteration that the mesh is refined. The accuracy of the simulation depends on the parameters input in the simulation. Currently the easiest way is to use a suit program, but one can write its own. It has been successfully used to model this type actuators [98].

### 5.5.2 FEM Simulation with ANSYS

In order to account for these factors a simulation using finite element method software ANSYS, is prepared. The 3D model is done in SolidWorks, then directly imported in to ANSYS. It only includes the cores with their coils, plugs with their inserts, and the MRF inside the passages. The magnetization curves (B-H curves) provided by the material manufactures, were inputted accordingly. The results from a magnetostatic analysis with a current sweep from 0.5 to 3.0 amperes with 0.5 amperes increments are shown in Figure 5-6.

### 5.5.3 Simulation Results

As it was expected, the magnetic field inside the passages is not uniform. It is stronger between each pair of inserts, clearly visible in the plug sections at different excitations, especially on the light orange regions of the 3.0 A iteration. This fact is also confirmed by the sinusoidal curves on the graph.

The graph also shows that the average values for the magnetic density are about 30% lower than the theoretical values in the previous section. The most likely cause is the magnetic leakage in the inner part, and to a less extend in the outer part of the assembly. As it can be seen on the top views of the electromagnetic circuit. At the moment, the cause of this leakage is still unknown. The most likely cause is the close distance between the core edges, when compared to the large MRF gap in the passages. Additionally, the simulation shows that the magnetic flux density inside the electromagnets cores is low, reaching only about 200mT at the centre, which implies that they are underused.

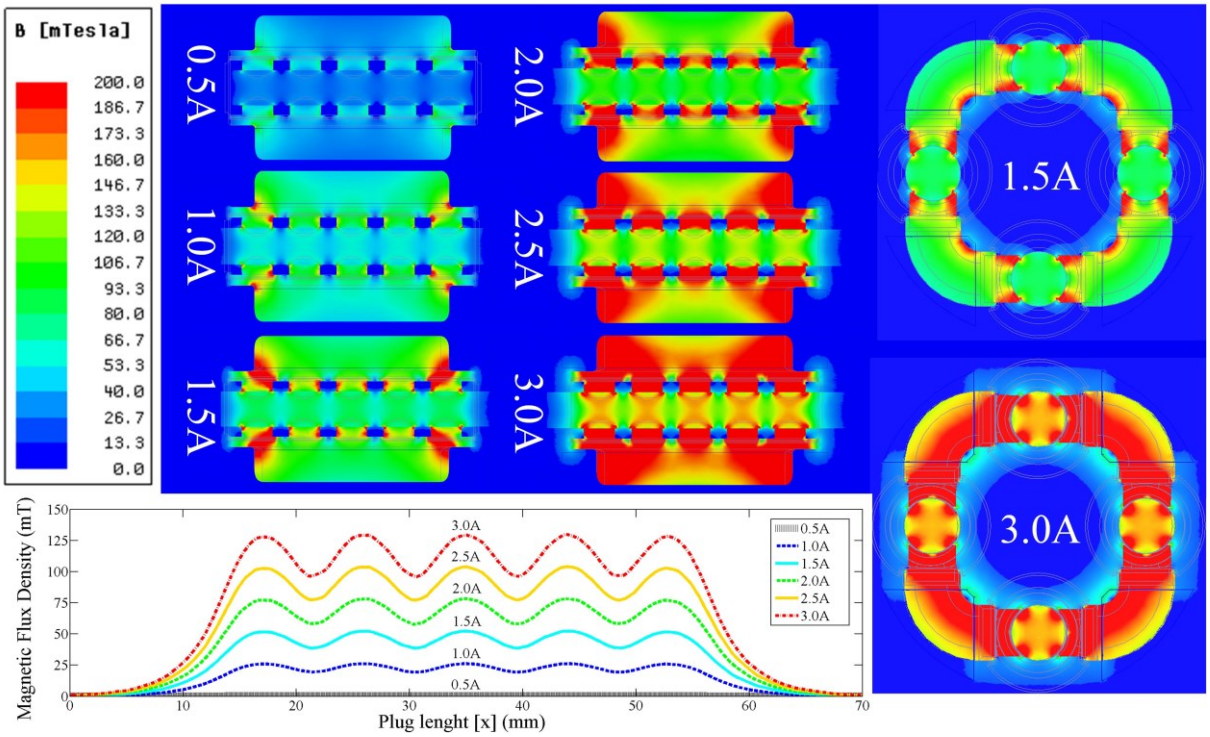


Figure 5-6. FEM simulation showing the magnetic flux density distribution across the centre plug passage.

In the future, the dimensions of the electromagnetic core need to be optimised by balancing the space for the coils, the maximum saturation value of the core material, and the desired flux density at the gap, taking into consideration the requirements of a particular application. Additionally, the passages need to be simplified, by changing their geometry. A square shape could help to simplify the model, if a proper seal between the materials in the passages can be achieved. The new shape will also allow the inserts to be exchanged for a uniform wall to create a uniform field inside the passages. Finally, the magnetic flux leakage should be included in the design equations, in order to minimise it.

It is also important to note that in the current prototype, the permeability for the electromagnets was the most important selection criteria for the material, because it was necessary to generate a large magnetic flux with a limited space for the coils, i.e. a small electromotive force. However, the magnetic saturation parameter of the material must also be considered during the design process in order to achieve a more compact, and optimal design.

## 5.6 Force Estimation based on Simulation

Using the magnetic flux values at the centre of the MRF gap, shown in the plots of Figure 5-6, it is possible to calculate the pressure drop across the piston head by modifying Equation 5-6, to include the data from the simulation as follows,

$$\Delta P = \frac{8\eta L_p}{\pi r_{gap}^4}\frac{Q_h}{N_p} - \frac{8}{3r_{gap}} sign(v_p) \int_0^{L_p} \tau_y(B)\,\mathrm{dx}$$

Equation 5-18. Piston force estimation based on FEM results

The new force values from the FEM data are plotted and compared with the data from previous experiments in Figure 5-7. The new results are closer to the measured data for low current values; however, at higher currents the discrepancy becomes more significant.

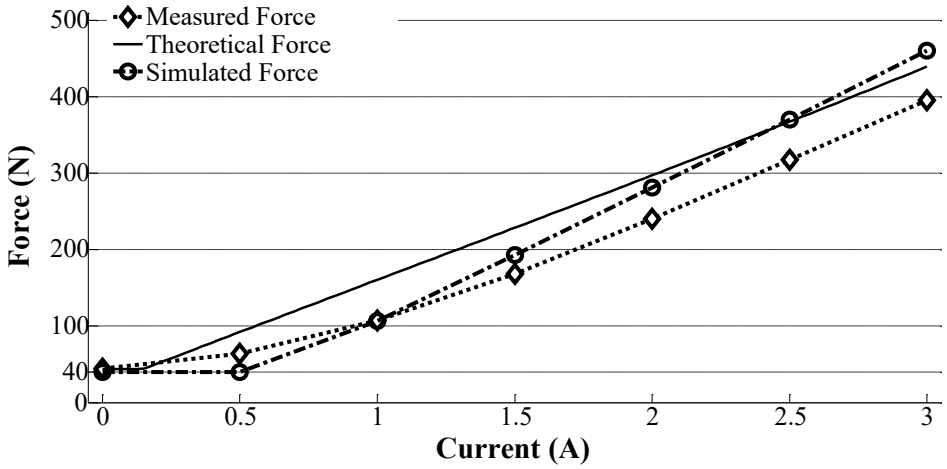


Figure 5-7. Comparison between the theoretical, simulated and measured piston forces vs currents at 500mm/min.

Assuming that the FEM results correctly account for the leakage, and the non-linearities of the materials (i.e. saturation values, and the variable permeability in the B-H curves), the problem can be attributed to the inaccuracy of the material parameters used in the simulation, the yield stress calculation for the MRF, or the simplified equation to calculate the pressure drop. A more precise characterization of the magnetic alloys and the MRF, together with the redesign of the plugs in the piston head, might prove useful to further improve the accuracy of the model.

## 5.7 Discussion & Remarks

This chapter covered the modelling of the MRPA. Given its novelty, a comprehensive mathematical analysis of the electromagnetic, hydraulic, and visco-plastic characteristics of this actuator has never been reported in research before. This research introduced all these necessary models. As with most electromagnetic actuators, the magnetic field can be approximated using the reluctance model to simply the necessary calculations. On the other hand, the visco-plastic, hydraulic, model of the actuator was done using an approximate solution to the Buckingham-Reiner equation. Finally, the magnetorheological model was constructed using curve fits for the data provided by the manufacturer. The resulting equations are used to accurately predict force trends of the output forces. This can be used to estimate the performance of other configuration for these actuators before they are constructed.

Additionally, the models presented in this research allow to model of all domains of this actuator with explicit equations. This allows for a more direct understanding of the characteristics and parameters of the new actuator. Moreover, the possibility to independently model all parameters allows analysing and understanding the relations between the main parameters affecting each performance parameter of the MRPA. Nevertheless, the approximations used to construct these models introduce further deviations from the real performance of the actuator, as shown by the experimental results.

In order to understand and improve the accuracy of the results, it was necessary to use a FEM simulation of the magnetic field. The analysis shows that the mathematical model can estimate the trend of the magnetic field. Nevertheless, the magnetic field appears to have an uneven pattern inside the plugs. This causes the overall average value to differ from that of the mathematical equations, which assume a uniform field across the gap. Using the average value from the FEM simulation dramatically improve the results from the mathematical models. This proves the accuracy, and usability of the simplified mathematical models presented in this research. Nevertheless, there is room for improvement, and some modifications are necessary in order to improve the predictions of the models.

The overall accuracy of the models can be improve dramatically by having precise data on the materials used in the construction of the prototype. Not only the construction material data is necessary, but also a more precise measurement of the magnetorheological properties of the MRF will help to improve these results. Finally, in order to reduce the number of

assumptions used in the model it is necessary to revise the geometry of the piston. This will allow for a more simple and accurate model of the device.

## 5.8 Chapter Summary

The experimental results from previous chapter showed that the current MR piston prototype had potential to improve its performance. In order to realise this potential, a more accurate model of the actuator was necessary. Therefore, the hydraulic, visco-plastic, electromagnetic, and magnetorheological models were created using explicit equations.

The behaviour of MR fluids has been typically modelled using complex equations derived for visco-plastic flow. They normally attempt to obtain an exact calculation for the force of these devices. However, they normally incur in difficult to solve implicit equations or tables, which can only be applied to a particular geometry. On the other hand, the Bingham model offers a simplified, yet accurate modelling for such devices. Therefore, the hydraulic and visco-plastic models are based in an approximate solution to the Buckingham-Reiner equation. In this way, it was possible to obtain an explicit equation to calculate the Newtonian and yield stress related pressure drops across the piston head. This allows to model different geometries, including the toroidal passages, with ease. In order to calculate the necessary yield stress for the Bingham model an electromagnetic and magnetorheological model of the fluid were necessary to complete the system.

MR fluids are normally complex to model. Therefore, their properties are normally calculated using experimental data. In this research, the data from the manufacturer was fitted magnetic and yield stress curves. Lastly, the electromagnetic model was done based in the reluctance model. This approach is based on an analogy to electrical circuits. It allows to easily and accurately estimating the magnetic flux density at the gap.

The results from the model are a good estimate of the experimental measurements. However, there appears to be a constant discrepancy in the approximation. In order to identify the cause of this problem a finite element method simulation for the magnetic field was employed. The results from this simulations shows that the magnetic field varied across the plug passages. Moreover, there was also significant magnetic leakage in the magnetic cores, which affects the performance of the actuator. In order to obtain the force from these results, the equations were modified to integrate the values. The recalculated theoretical performance

of the actuator is closer to the measured performance in the low current range. However, the discrepancy increases with the current. This indicates that the problem might also be related to the estimation of the material parameters.

# 6 Piston Optimisation

The novel toroidal configuration for the MR piston head had been experimentally tested and then mathematically modelled. The results shows that while the MR piston is able to display high forces with fast response times, its potential appears to be yet limited by several factors. The experimental data and observations in Chapter 4 exposed several mechanical flaws that affect the force symmetry, backdrivability, as well as the ease of construction of the prototype. On the other hand, the models constructed in Chapter 5, revealed that the geometry of the current toroidal assembly is not optimal, causing not only field leakage and low forces, but also preventing an accurate modelling of the actuator.

In this chapter, the discussions made in previous works [96], [99] are expanded to provide detailed solutions to the problems found during the experimentation of the 1st prototype. Additionally, a study of the key design parameters inside the electromagnetic circuit provides insight into the relations between different parameters. This analysis reveals possible areas for improvement of the design, which later will be the targets for a mathematical optimisation.

In order to validate the results from the optimisation, a new prototype is constructed, and its passive force performance is benchmarked against the previous iteration of the MR piston. The experimental testing will evaluate the effectiveness of the optimisation, and it will bring light into the true potential of the toroidal piston head. Moreover, this comprehensive

optimisation of the prototype can serve as a guideline for the design, optimisation, and construction of MR pistons. While most of the concepts are aimed to the toroidal design, they can also be easily adapted to other similar kind of actuators. This will enable the adaption of the MRPA technology into a wider range of applications, beyond the scope of this research.

## 6.1 Summary of Findings

The experiments and analysis presented in Chapters 4 and 5 encountered a several areas of opportunity where the MR piston could be improved. The following list contains some of the most relevant findings.

1) Single Rod Design: Using a single rod piston design was selected to minimise the size of the actuator. However, this causes uneven forces between the pushing and pulling motions. Moreover, it creates the need for an accumulator to accommodate the piston rod volume as it enters or leaves the piston.

2) Accumulator: It is needed in a single rod piston design, to accommodate the changing piston rod volume. However, due to its constructions and the dynamics of the hydraulic fluid, it can generate unexpected pressure variations as liquids enters or leaves the accumulator chamber. Additionally, in the case of the MRF it can accumulate ferromagnetic particles as they start to sediment after a long period of time. This can cause even further changes in the pressure dynamics, and alter the mixture balance of the MRF fluid.

3) Round plug passages: This shape is simple to manufacture and seal. However, it creates an uneven magnetic flux that is difficult to model with conventional techniques. Moreover, this design makes it very difficult to implement a complete bi-material construction, therefore steel screw inserts had to be used to transmit the magnetic field into the plug passages.

4) Screw inserts: they were necessary to transport the magnetic field from the cores into the passages. However, they do not cover the complete surface of the passage, which leaves unused space for interaction between the MRF and the magnetic field. Moreover, they also cause a non-uniform magnetic field that it is concentrated between the screw inserts. This makes the electromagnetic circuit difficult to model.

5) Dimensions of the core: The cores were design to maximise the total magnetic flux. Since the Permalloy 78 has a limited magnetic flux density, it was necessary to increase the cross-section area in order to be as close as possible in size to the cross section of the MRF gap. However, the finite element simulation showed that the electromagnets cores were underused most of the time, despite the fact that the coil windings were done to fill all the available space. Therefore, it could be assumed that there was a relation between the core size, and the windings space. Additionally, this also suggested that not only magnetic permeability but also saturation of the construction materials are important design parameters.

6) Other findings: several improvement points include the friction from the seals, the fillings system, the seals of the piston head, among others.

## 6.2 Mechanical Optimisation

The previous piston was constructed in the same way a conventional piston, including the necessary ports, seals, wipers, guides, and rods, as shown in Figure 6-1. In order to improve its usability in real robotic compliant applications the piston design has been optimised in several ways as described below.

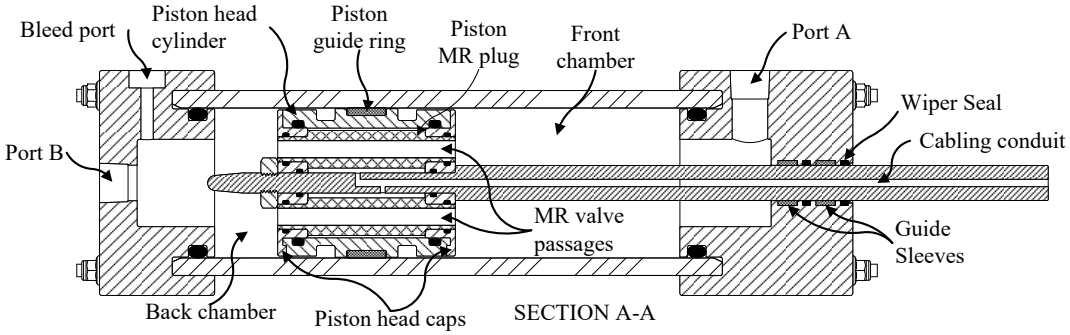


Figure 6-1. Schematic of Section A-A of the MRP showing its functional parts

### 6.2.1 Friction Reduction

Friction plays a very important role in the performance of backdrivable actuators. It increases the actuators minimum force, causing wear, inefficiency, and low safety. The modifications below are used to ensure optimal performance:

- Teflon coated faces are used in the rod seals and head wear ring to eliminate the stick-slip effect.

- The wall of the piston cylinder has been surfaced treated with a chrome plating.
- Low friction ball bearings have been used instead of wear rings in the piston rod.
- Piston rod with smaller diameter to minimise contact.

### 6.2.2 Double Rod Design

The single rod system used in the previous design was convenient from the design point of view. However, in order to accommodate for the volume changes caused by the rod entering/ leaving the MRP it was necessary to use an accumulator. The accumulator in the system causes undesired changes in the pressure and force measurements during the operation of the MRP. It also adds additional weight and size to the overall system, making less portable and safe. A double rod design eliminates the need for an accumulator, which complicates the force control, and can cause pollution. For these reasons, it was necessary to implement a double rod system. Additionally, the additional rod helps to keep the alignment of the head.

Nevertheless, the double rod design presents some fundamental disadvantages. For instance, it increases the system complexity by increasing the amount of parts. Additionally, the tolerances of the manufacturing process have revised and ensured to prevent misalignments between moving parts. The additional seals and rod also create additional friction in the system, reducing its compliance. On the other hand, it allows for a reduction in the rod diameter while keeping the head aligned, and giving extra space for cabling. Despite all this, the double rod system presents better opportunities to develop a more stable and reliable system, with much better controllability than its single rod counterpart.

### 6.2.3 Usability Considerations

The piston has been redesigned taking into consideration the requirements for MRFs, ease of assembly for testing, as well as reduction in complexity. MRAs can decrease their efficiency when exposed to air, due to the compressibility of air, and the lower magnetic permeability that it has. In order to ensure that the MRF is free of air, the piston caps, and their ports has been designed with tilted surface for the air to easily bleed from the top while filling the piston with a vacuum pump.

The system has also been designed to allow for a quick reconfiguration of the main components. Other improvements include a removable sealing pack for fast seal

reconfiguration, and a piston head design without any fasteners (aside from the piston rods) or soldered parts by using self-aligning symmetrical components.

## 6.3 Redesign of the Electromagnetic Circuit

The most important part of the MR piston is the new toroidal piston head, which was specifically design to meet the requirements of the MRPA for backdrivable hydraulic actuation with high power output. Nevertheless, its performance in previous experiments was subpar with the conventional annular piston head design. The problem was largely attributed to the dimensions and configuration of the electromagnetic circuit.

As it can be seen in left side of Figure 6-2, the current toroidal prototype uses screw inserts and has a circular passage shape. These features have been found to limit the performance of the circuit. Moreover, its modelling revealed that the shape and configurations of the passages made it difficult to understand and redesign. Therefore, before the toroidal circuit can be optimised, a new configuration needs to be implemented.

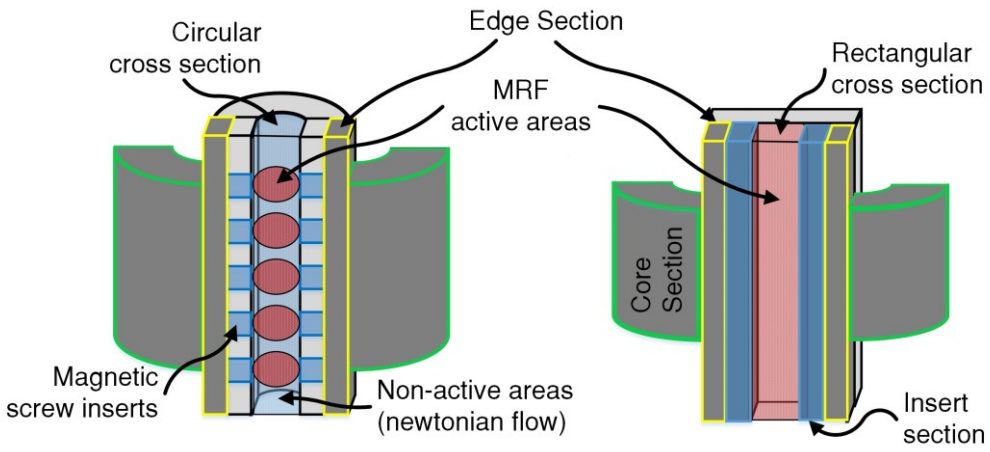


Figure 6-2. Toroidal electromagnetic circuit redesign

### 6.3.1 Magnetorheological Valve Sections

The toroidal piston head configuration consists of 4 MR valves aligned in a circular way. They are formed by intercalating passages and electromagnets. The main components of a single valve, shown in Figure 6-2, are explained below along with the necessary changes.

1) Core Section: It is constructed with permeable materials, and is where the electromagnet coils are winded. The 4 cores generate the electromagnetic field to control the yield stress of the MRF. A balance between the core size and the space

winding s must be achieved in order to have the necessary coils to generate enough electromotive force while having enough cross-sectional area not to saturate the core when high magnetic fluxes are necessary.

2) Edge Section: The edge sections are part of the core; however, they are considered a separate section due to their different dimensions. Their purpose is to secure the core against the insert sections, and to act as an enclosure for the electromagnet windings. For the new iteration, this area has been reduced in order to have additional space for the insert section.

3) Insert Section: This is a part of the plug that is built of permeable material. It is used to transport the magnetic field into the passages of the plug. In this iteration, the screws have been replaced by a complete wall. This wall is firmly attached with screws to the other non-permeable plug walls in order to keep the MRF from leaking into the piston head. In previous iterations, Figure 6-2 left side, permeable insert screws were used, since this configuration ensured a high sealing performance. In this way, new square shaped passages are created now.

4) Magnetorheological Fluid Gap Section: The MR fluid gap sections serve as passages for the MRF to move freely from one side of the piston head to the other, allowing the MRP to achieve an inherently mechanically compliant design. The combined area and geometry of the four gaps determines the minimum force of the actuator, since is directly related to the Newtonian flow of the force equation.

## 6.4 New Toroidal Design Model

The initial toroidal design was inspired by the advantages of toroidal cores, which have higher magnetic fields, and lower magnetic leakage than straight solenoids. Their biggest advantage lies in a larger active length for the magnetic field and the MRF to interact, when compared to the annular design where it is limited to the flanges of the bobbing. Theoretically, this translates into higher forces, which depend on the length, $L_p$', as shown by the right term of the output force equation.

By manipulating this length, along with the effective piston area ($A_p$-$A_r$), number, and radius of passages ($N_p$, $r_{gap}$), it is possible to have more design flexibility to achieve the desired magnetic flux density in the gaps. To understand the relation between parameters, the design

was simplified using a permeable material for the wall of the passages, instead of small screw inserts. Additionally, the areas of the gaps has been changed from circular to a rectangular shape. These modifications allow for a larger active length, and a simpler mathematical model, simplifying the assembly and increasing the space efficiency. It is important to note that the Newtonian ($L_p$) and magnetic yield stress ($L_p$') related lengths in Eq. 1 are still needed to account for the piston head cover length. Although the effect of using a single length might be negligible at low piston speeds, $v_p$, when excitation current is low, and the speed higher its effect becomes more apparent.

### 6.4.1 New Toroidal Reluctance Model

The reluctance and hydraulic models have to be revised in order to account for the modifications done during the mechanical redesign.

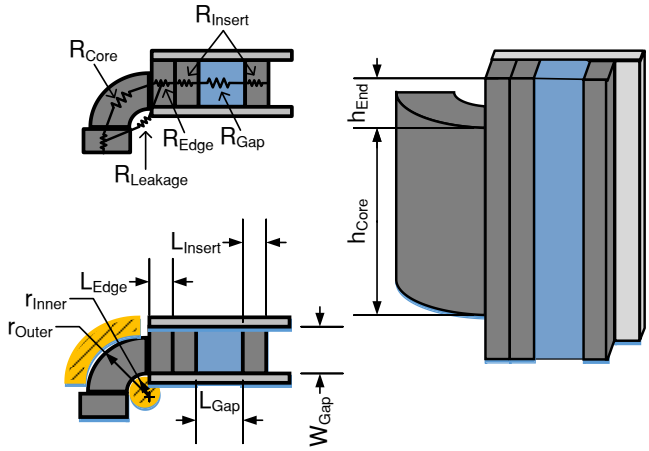


Figure 6-3. Annular EM circuit section schematic with reluctance names and dimensions

Identical to the equations presented before, the main reluctance equation is,

$$B = {}^{NI}/_{RA'}$$

Equation 5-9. Simplified equation used in the reluctance method to estimate flux in a closed path.

Where $R$ is the combined reluctance of the electromagnetic circuit, and $A$' is the cross section area, where the magnetic flux density $B$ is being calculated.

The reluctance of any section of the full electromagnetic circuit is defined by its length, $l$, magnetic permeability, $\mu$, and cross sectional area perpendicular to the magnetic flow, $A$',

$$R = {}^{l}/_{\mu A'}$$

Equation 5-10. General reluctance form for a material of constant cross section

Assuming that the mean magnetic flux goes through the geometric centre of each section, their reluctances can be easily define by using the dimension shown in Figure 6-3.

$$R_{core} = \frac{\pi(r_{inner} + r_{outer})}{4\mu_{alloy}h_{core}(r_{outer} - r_{inner})}$$

Equation 6-1. Core section reluctance of new toroidal prototype

The core equation in this case is identical to previous equation.

$$R_{insert} = \frac{2L_{insert}}{\mu_{alloy}(h_{core} + 2h_{end})W_{gap}}$$

Equation 6-2. Insert section reluctance of new toroidal prototype

It has been significantly simplified since the inserts were substituted for a complete wall. In this way, there is no need to estimate the reluctance of a section with materials having different permeabilities.

$$R_{edge} = \frac{2L_{edge}}{\mu_{alloy}(h_{core} + 2h_{end})W_{gap}}$$

Equation 6-3. Edge section reluctance of new toroidal prototype

The edge reluctance equations has also not changed

$$R_{gap} = \frac{L_{gap}}{\mu_{fluid}(h_{core} + 2h_{end})W_{gap}}$$

Equation 6-4. Gap section reluctance of new toroidal prototype

The square gap shape has also helped to further simplify the reluctance of the

$$R_{leakage} = \frac{\sqrt{2r_{inner}^2}}{\mu_{air}(h_{total})(2r_{inner})} = \frac{1}{\sqrt{2}\,\mu_{air}(h_{core} + 2h_{end})}$$

Equation 6-5. Approximate air gap magnetic leakage reluctance

Given the symmetry of the magnetic circuit and combining these equations, the magnetic flux density at the toroidal gap can be obtained, using $R_p$ as the combined reluctance of the plug as, and $A_{Tgap}$ as the cross section area of the toroidal gap,

Development of the original reluctance equation can be done using a simplified circuit as seen in the next figure and explain by the equation below. This solution is based in the equivalent tension between two points of the circuit and the integration of the cross sectional area of the gap.

$$B_{Tgap} = \frac{NI}{A_{Tgap}} \frac{R_{Leakage}}{R_p R_{Core} + R_{Core} R_{Leakage} + R_{Leakage} R_p}$$

Equation 6-6. Magnetic flux density for the rectangular toroidal gap

$$R_p = R_{gap} + 2R_{insert} + 2R_{edge}$$

Equation 6-7. Combined plug reluctance

It is important to note that, the plug equation assumes that no magnetic flux travels through the walls of the valve plug. This assumption is true as long as the width of the gap, Wgap, allows for enough space to keep the magnetic flux density in the gap well below the saturation value of the MRF.

$$A_{Tgap} = (h_{core} + 2h_{end}) W_{gap}$$

Equation 6-8. Cross section area of the valve gap

It is assumed that the magnetic flux will evenly permeate the edge and insert sections of the MR valve.

### 6.4.2 New Toroidal Hydraulic Model

The hydraulic model was solved using the same approximate solution to the Buckingham-Reiner equation. Shown below again for the readers convenience,

$$F = \frac{-8\left(A_p - A_r\right)^2 \eta L_p}{A_{gap} r_{gap}^2} v_p - \frac{8\tau_y L_p' \left(A_p - A_r\right)}{3 r_{gap}} sign(v_p)$$

Equation 6-9. Piston force equation based on Buckingham-Reiner approximation

Where $A_p$ and $A_r$ are the areas of the piston head and the rod respectively. The right side of the equation represents the force induced by the magnetically controlled yield stress of the MRF, which can be considered independent of the flow rate, i.e. the piston movement, as long as the flow is laminar. While the left side of the equation represents the Newtonian force, which depends of the flow rate, i.e. the configuration of the piston holes. This equation can be used to estimate the force of both piston configurations by correctly choosing, $L_p'$, MRF active gap length, $L_p$, total length of the gap, $A_{gap}$, the area of the piston gap which is perpendicular to the flow, and $r_{gap}$, the radius of the equivalent hydraulic diameter.

The hydraulic parameters of the toroidal configuration are,

$$L'_p = h_{core} + 2h_{end}$$

Equation 6-10. Active length of the valve wall affected by the magnetic field

$$L_p = L'_p + 2h_{cap}$$

Equation 6-11. Total length of the valve wall

This is the length of were the MRF interacts with the walls while travelling through the piston head. It is related to the Newtonian force generated by the viscous interaction of the MRF inside the passages, which is speed dependant.

$$A_{gap} = 4L_{gap}W_{gap}$$

Equation 6-12. Entire area of the piston gap, compromising four passages

$$r_{gap} = \frac{D_H}{2} = \frac{L_{gap}W_{gap}}{L_{gap} + W_{gap}}$$

Equation 6-13. Hydraulic radius for a rectangular duct

The new equations uses the hydraulic diameter concept to calculate the pressure in a rectangular duct. However, this diameter can be modified to match many other common shapes. This makes the model of the actuator very versatile, allowing it to be immediately applied to different configurations of piston heads.

## 6.5 Annular Piston Head

In order to have a more complete comparison with the MR piston a conventional annular piston head is also analysed and modelled. MR dampers have typically been constructed in this way, having annular gaps around a solenoid. This allows for a relatively simple construction with few parts.

The design presented here has been improved to have better performance by modifying the transmit section of the solenoid, as shown in Figure 6-4. A comparative description of the annular piston head sections explains how they work to complete the electromagnetic circuit.

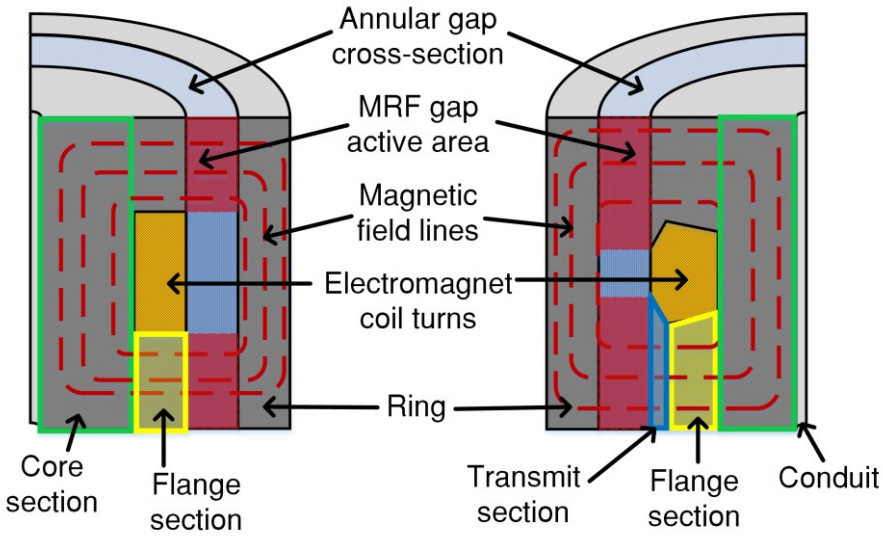


Figure 6-4. Annular electromagnetic circuit redesign

1) Conduit Section: It is a hollow area inside the solenoid core used for the power and sensor cables. Since it does not contribute to the magnetic circuit performance, its dimensions are kept to a minimum, also to maintain the structural strength of the MRP.

2) Core Section: It is the central part of the solenoid bobbin and in covers the same functions as in the toroidal design.

3) Flange Section: While acting as a frame for the coil, it directs the magnetic field outwards towards the MRF gap. Typically, it has a rectangular shape, but here it can has been changed to accommodate more windings while keeping its magnetic performance.

4) Transmit Section: It provides an additional cross section area for the magnetic flux and MRF to interact. In this way is possible to set an independent dimension for bobbin flange to study the effects of the flux density vs. interaction area on the output force.

5) Magnetorheological Fluid Gap Section: Analogue to the toroidal design, this section allows the free flow of MRF between the piston chambers, and the annular gap area determines the minimal force of the piston head.

6) Ring Section: This part of the design allows the magnetic flux to return through the bobbin flanges.

The reluctance and hydraulic models used to calculate the force of the annular prototype are described below. These models are based in the modified version of a conventional annular prototype.

### 6.5.1 Annular Reluctance Model

The electromagnetic circuit for the modified annular design was done using the reluctance model. Similar to the toroidal prototype the dimensions and parameters of the materials used in its construction play an important role in its ability to generate the necessary flux density at the MRF gap.

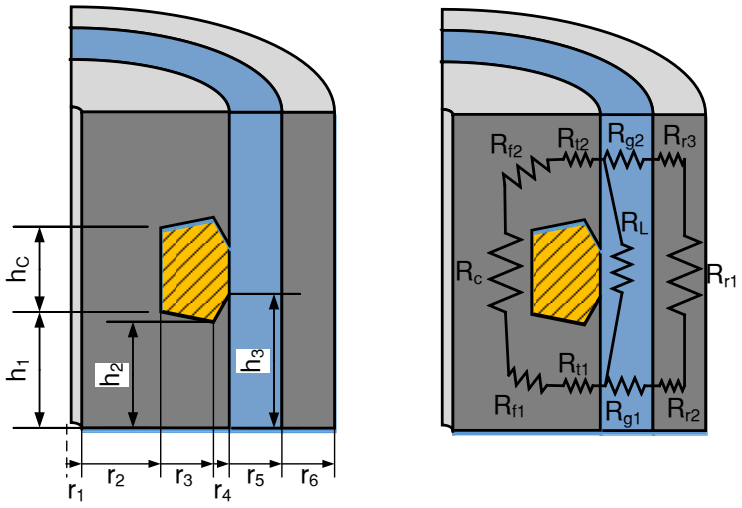


Figure 6-5. Annular EM circuit section schematic with reluctance names and dimensions

The annular head equations are derived from the schematic in Figure 6-5, and using Equation 5-9 in a similar way than in the toroidal configuration.

$$R_c = \frac{h_c + h_1}{\mu_{alloy}\pi(r_2^2 - r_1^2)}$$

Equation 6-14. Annular core reluctance

$$R_{t1,2} = \int_{r_3}^{r_4} \frac{dr}{\mu 2\pi r h} = \frac{1}{2\pi\mu}\int_{r_3}^{r_4} \frac{dr}{mr^2 + (h_2 - mr_3)r}$$

$$= \frac{\ln({}^{r_4 h_2}/_{r_3 h_3})}{2\mu_{alloy}\pi(h_2 - mr_3)},\ m = \frac{h_3 - h_2}{r_4 - r_3}$$

Equation 6-15. Transmit reluctance

The transit is not a constant section as with the flange section, for this reason its equation is develop in a general form.

$$R_{g1,2} = \int_{r_4}^{r_5} \frac{dr}{\mu 2\pi r h_3} = \frac{\ln({}^{r_5}/_{r_4})}{2\mu_{fluid}2\pi h_3}$$

Equation 6-16. Annular gap reluctance

The magnetic flux moves along the transmit area into the gap affecting only the area of the gap directly in contact with the metal surface.

$$R_{r1} = \frac{h_c + 2h_1 - h_3}{\mu_{alloy}\pi(r_6^2 - r_5^2)}$$

Equation 6-17. Annular ring reluctance

$$R_{r2,3} = \int_{r_5}^{\frac{r_5 + r_6}{2}} \frac{dr}{\mu 2\pi r h_3} = \frac{\ln\left({}^{r_5 + r_6}/_{2 * r_5}\right)}{\mu_{alloy}2\pi h_3}$$

Equation 6-18. Annular ring entrance reluctance

$$R_L = \frac{h_c + 2h_1 - h_3}{\mu_{fluid}\pi(r_5^2 - r_4^2)}$$

Equation 6-19. Annular leakage reluctance

Leakage in the annular electromagnetic circuit is assumed to occur inside the MRF itself. When the magnetic flux travels between the transmit section walls along the MRF, it becomes parallel to the MRF flow. In this case, the contribution of the magnetically induced force is almost zero as described in next section.

For the flange section, the cross section area is constant, and the total reluctance of the magnetic circuit is given by,

$$A'_{f1} = A'_{f2} \ , \qquad r_2 h_1 = r_3 h_2$$

$$R_{f1,2} = \int_{\frac{r_1+r_2}{2}}^{r_3} \frac{dr}{\mu 2\pi r(^{r_2 h_1}/_{r})} = \frac{2r_3 - r_1 - r_2}{\mu_{alloy} 4\pi r_2 h_1}$$

Equation 6-20. Annular leakage reluctance

The flange section can also be calculated using Equation 6-15, given that it is a particular case of a similar geometry.

$$R_{total} = R_c + 2R_{f1,2} + 2R_{t1,2} + (R_x || R_L)$$

Equation 6-21. Total reluctance of the annular electromagnetic circuit

Where the combined reluctance of the gap section and ring, $R_x$, is.

$$R_x = 2R_{g1,2} + 2R_{r2,3} + R_{r1}$$

Equation 6-22. Combined reluctance of the ring and gap section in annular design

In this exercise the gap reluctance is calculated assuming that most of the magnetic flux goes across an area, $A'_{Agap}$, equal to the transmit cross section area at the mid-section of the annulus, and that the leakage can be estimated by the middle distance inside the MRF gap. Therefore, based on Eq. 42 the magnetic flux in the annular gap can be estimated as,

$$B_{Agap} = \frac{NI}{A_{Agap} R_{total}} \frac{R_L}{R_x + R_L}$$

Equation 6-23. Magnetic flux density at centre of the annular circular gap

$$A_{Agap} = \pi(r_5 + r_4) h_3$$

Equation 6-24. Cross section area centre of the annular circular gap

### 6.5.2 Annular Hydraulic Model

Similar to the toroidal model Equation 6-9 can be used to estimate the force of the prototype. However, it is necessary to use the following hydraulic parameters to account for the different geometry of the piston head.

$$L'_p = 2h_3$$

Equation 6-25. Active length of the annular gap wall affected by the magnetic field

$$L_p = h_c + 2h_1 + 2h_{cap}$$

Equation 6-26. Total length of the annular gap

$$A_{gap} = \pi(r_5^2 - r_4^2)$$

Equation 6-27. Total area of the annular gap

$$r_{gap} = \frac{D_H}{2} = r_5 - r_4$$

Equation 6-28. Hydraulic diameter of an annular gap

## 6.6 Performance Parameter Analysis

In the past, several attempts were made to optimise the device dimensions using different combinations of cost functions, targeting key performance parameters such as force range, volume, and net magnetic flux densities at several sections.

Unfortunately, no conclusive results were obtained from this approach, since the correlation of parameters appears to cause a great number of local minima. To overcome this problem an analysis of the fundamental relations, restrictions, dependencies between parameters is needed.

### 6.6.1 Design Specification

The analysis is done following the specifications of Table 6-I.

TABLE 6-I. DESIGN SPECIFICATION OF NEW MR PISTON

| | |
|---|---|
| Stroke | 136mm |
| Piston Head height | 50mm |
| Piston diameter | 60mm |
| Rod diameter | 10mm |
| Maximum current | 3A |
| Minimum material thickness | 1.2 mm |
| Wire thickness | 0.4 mm |
| Wire packing efficiency ($\eta_w$) | 42% |

The wire packing efficiency was obtained from previous empirical evidence

First, the piston head size is set to match the dimensions of the previous prototype in order to compare the performance improvement, also a minimum material thickness is set for all dimensions, in order to withstand the high forces generated by the piston, as shown in the table below.

### 6.6.2 Coil Windings Space

The smallest space around the core determines the number of turns that produce the necessary magnetic field. The calculation for the number of coil turns that can be placed on any of both designs can be done by,

$$\mathrm{N} = \eta_w \left( {}^{A_{coil}}/_{A_{wire}} \right)$$

Equation 6-29. Number of coils as a function of coil space

Where $A_{coil}$ is the limiting area for the electromagnetic coil turns to fit, shown in yellow colour in Equation 6-3, and $A_{wire}$ is the cross section area of the wire used in the windings, which is specified in Table I. The circular packing efficiency, $\eta_w$, was determined previously through experimental results by manually winding the electromagnetic cores.

### 6.6.3 Importance of Magnetic Saturation

Normally materials with a high permeability have been used in MRAs. In previous work, the importance of the material selection in magnetorheological actuators was also stressed through a discussion about the properties of magnetically soft materials such as Permalloy. Which can generate high magnetic field intensities with lower magnetomotive forces (i.e. N·I), as well as low residual magnetization, due to its high magnetic permeability, and low coercivity. In other words, they can generate high magnetic field intensities with very low currents.

However, during the design process, also the importance of their saturation limits was realised. Insomuch that when selecting a material, a careful consideration of these three properties is crucial to meet the application requirements. In electromagnets with compact gap designs and small currents, materials with high permeability are preferred. On the other hand, systems requiring large magnetic fields in gaps with big cross sections will benefit from materials with a high saturation values, in order to wide their output force range.

Therefore, since large magnetic flux densities in the gaps are required to generate larger forces, the core will benefit from materials with a high saturation values. As a result, for the construction of the magnetic circuit Permendur was chosen instead of Permalloy 78. Permendur has still a reasonable permeability helping it maintain a low reluctance, thus a compact yet powerful circuit can be constructed. Subsequently, in this iteration, the MRPA was constructed using Permendur, which will allow for higher magnetic flux densities, (for higher forces) in larger gaps (lower damping factor), while maintaining a compact size. Table 6-II shows the relevant parameters of the materials used in previous and new models.

TABLE 6-II - PROPERTIES OF PREFERRED MAGNETIC ALLOYS

| ***Material*** | $\boldsymbol{\mu_m}$ ***Maximum Permeability*** | $\boldsymbol{B_{max}}$ ***(Tesla) Magnetic Saturation*** |
|---|---|---|
| K-M31 | $2500\mu_0$ | 1.25 T |
| Permalloy 78 | $100000\mu_0$ | 0.80 T |

The permeability of free space, $\mu_0$, is equal to $4\pi \cdot 10^{-7} H/m$

### 6.6.4 Gap Active Area and Force Output Relation

As it can be seen from Equation 6-9, the output force of the actuator is mostly related to both the yield stress of the MRF, and the length of the active gap area it affects. Thus, the longer gaps the higher the output forces should be. However, a closer look at the magnetic flux density Equation 6-6 & Equation 6-23, for the toroidal and annular designs respectively, reveals that increasing the interaction length the magnetic flux density at the gap to drop. In order to make the relationship between these values clearer, an analysis of the trend between the active area and the resultant force was done by varying several dimensions.

## 6.7 Optimisation of Parameters

The optimisation of parameters was carried out using an iterative Matlab® program to search all valid permutations that satisfy the conditions set in the analysis developed in previous sections. This approach allows for flexibility when setting optimisation targets such as force ranges, net magnetic flux densities, and saturations at several sections, and limits in specific dimensions, since it allows to directly observe parameters dependencies, and make decision based on the trade-offs offer by each individual design.

### 6.7.1 Matlab Program

A Matlab program runs in an iterative way to examine the possible combinations of all the variables in the model. A GUI was also provided in Matlab to assess the final results displaying simplify figures of the model results.

## 6.8 Optimisation Results and Validation

The program was run with the relevant parameters as follows. Using this approach it was found that the core width, $W_{core}= r_{outer}–W_{inner}$, and the gap width, $W_{gap}$, were the most critical dimensions for the toroidal designs.

Figure 6-6 shows how both dimensions have an optimal point where the magnetic flux density achieves a maximum output force. In the first case, the area of the core increases the available magnetic flux.

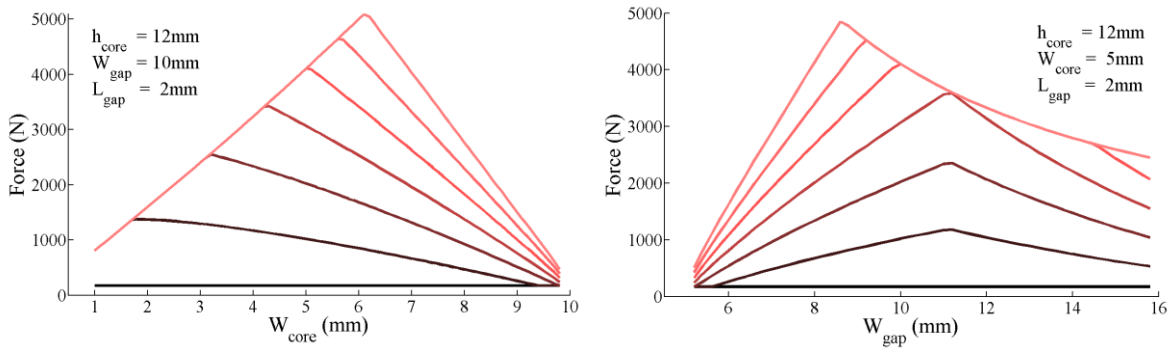


Figure 6-6. Estimated output force for performance parameters with optimal ranges, toroidal design

Here the width of the core is defined as, $W_{core}= r_{outer}–W_{inner}$. The simulation was done with 0-3A excitation current, and 1mm/sec piston speed. It is possible to observe the saturation of the magnetic circuit where the light red line overlaps the other. However, there is a point where the size of the core restricts the number of windings that it can fit. Similarly, the gap width increases the active surface, which drives the output force. This trend continues until the big area causes the magnetic flux density to drop.

Other important parameters were the core height, $h_{core}$, which should always be increased to the maximum possible value in order to increase the flux density of the circuit. Finally, the gap length, $L_{gap}$, is used to determine the minimum zero current force. In this case, it is also

preferred to have long gaps to decrease the forces even at high operational piston speeds, while maintaining a target maximum force.

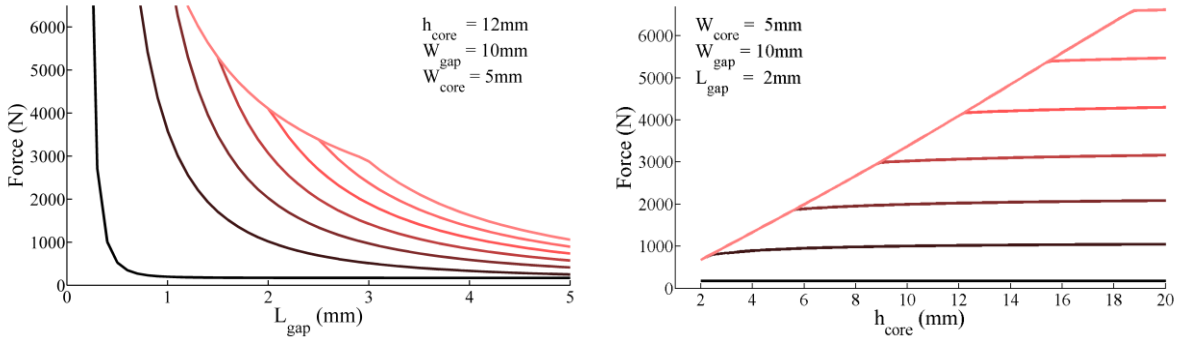


Figure 6-7. Estimated output force for performance parameters with trade-off relationship, toroidal design

As it is shown in Figure 6-7, it is clear that both parameters do not have an optimal region of operation. They rather have a dependency with the maximum available space. Thus, they have to be selected according to the design specifications to meet.

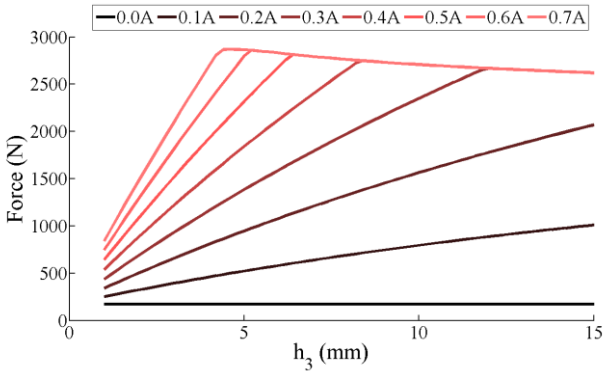


Figure 6-8. Relationship between the simulated output force and the transmit height, h3, in the annular design of the piston head.

In case of the annular design, shown in Figure 6-8, the transmit height, $h_3$, has a minimum value where the relation between the field density and the interaction area achieve maximum performance. After this point, further increasing the transmit area has relatively little effect on the output.

Using a simple cost function to maximise the force range, a set of parameters for each design was chosen. These parameters were then adjusted to comply with other manufacturing constrains, and the results are shown in the tables below.

TABLE 6-III - RESULTING DIMENSIONS AND PARAMETERS

| Annular Design | |
|---|---|
| ***Parameter*** | ***Value*** |
| $h_c$ | 35.4 mm |
| $h_1$ | 4.8 mm |
| $h_2$ | 2.9 mm |
| $h_3$ | 4.0 mm |
| $r_1$ | 2 mm |
| $r_2$ | 10 mm |
| $r_3$ | 16.7 mm |
| $r_4$ | 18.7 mm |
| $r_5$ | 20.8 mm |
| $r_6$ | 23 mm |
| $h_{cap}$ | 5.0 mm |
| Windings N | 850 turns |

| Toroidal Design | |
|---|---|
| ***Parameter*** | ***Value*** |
| $r_{inner}$ | 6 mm |
| $r_{outer}$ | 10.8 mm |
| $W_{gap}$ | 10 mm |
| $L_{insert}$ | 2.7 mm |
| $L_{edge}$ | 1 mm |
| $L_{gap}$ | 2 mm |
| $h_{core}$ | 12 mm |
| $h_{end}$ | 13 mm |
| $h_{cap}$ | 2.5 mm |
| Windings N | 388 turns |

## 6.9 Experimental Validation

The construction of the next prototype was done based on the results from the simulation. After the annular and toroidal piston prototypes are built, they were tested using a similar test bench to the one using the universal testing machine. However, modifications were done in order to fit the double rod design. The constructed prototypes and these experiments are described below.

### 6.9.1 New Piston Designs

In order to have equal testing conditions for both piston head configurations, the new MR piston was design in a modular way. This makes possible to change the piston head configuration without changing any additional components. Sections of both MR pistons are shown in Figure 6-10 and Figure 6-9.

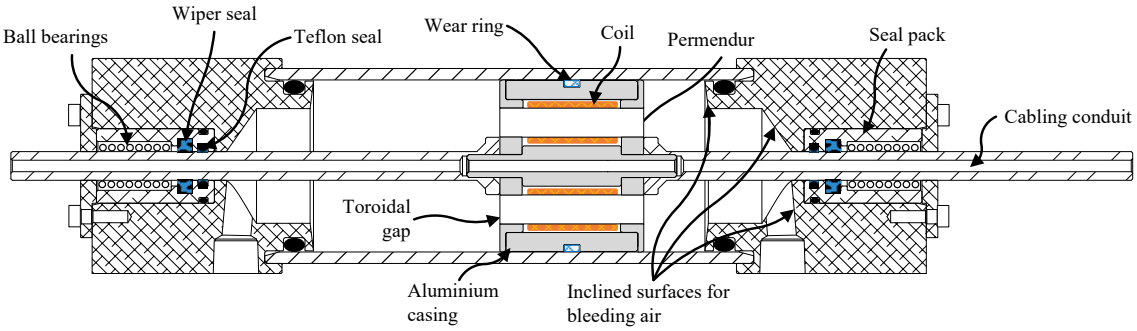


Figure 6-9. Optimised MR piston showing a toroidal configuration

The toroidal piston configuration, Figure 6-9, shows the passages of the MR valves. Compared to the previous iterations, these passages are now wider to allow for a similar amount of flow, yet they are thinner to minimise the resistance of the magnetic circuit. This allows keeping a same degree of backdrivability while enhancing the magnetic flux density at the gap. The electromagnet cores are not visible in this section since they are at a different angle. Nevertheless, it is possible to see the edge of the electromagnet cores projected next to the passages. In this section, it is also possible to see the inclined surfaces that facilitate de-airing of the piston during the filling process; as well as the new sealing system including the modular rod seals and the wear ring in the piston head.

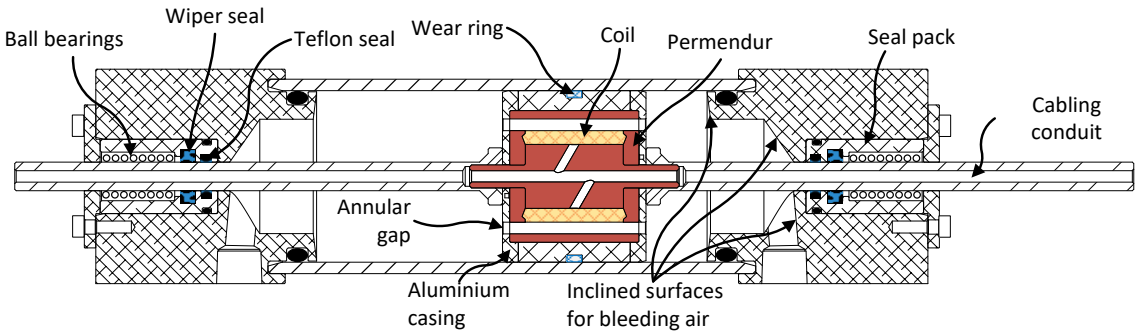


Figure 6-10 Optimised MR piston showing an annular configuration

Different from the toroidal head configuration, the annular piston configuration shows in red the permeable materials of the core bobbin and the ring that acts as a return path for the magnetic flux. Apart from this difference the rest of the elements in the MR piston remain the same as in the toroidal configuration.

### 6.9.2 Piston Heads

The resultant piston head configurations were constructed using the materials described in previous section. For it assembly was necessary to protect the coil windings from the contact with the electromagnetic cores. Otherwise, small movements could remove the enamel and cause a short circuit in the coils. Therefore, insulating tape on the edge walls, along with thermofit material in the inner part of the core, are used to protect the coil in case of the toroidal design.

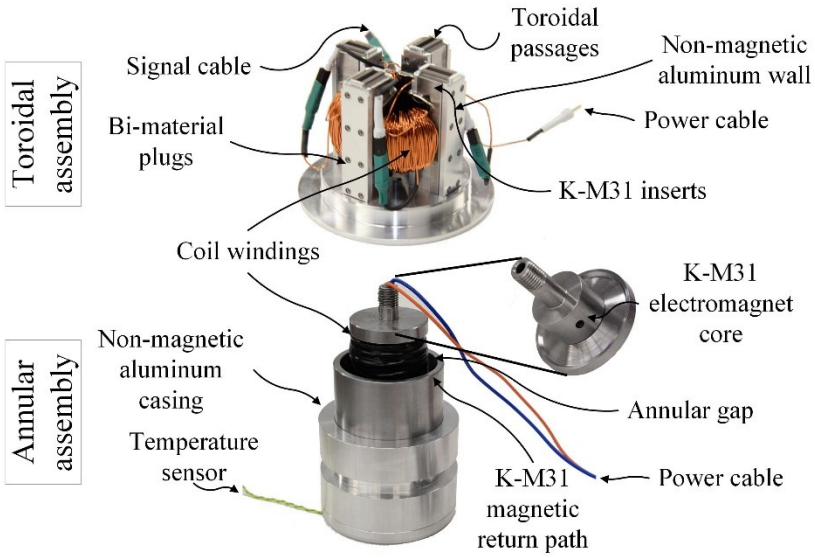


Figure 6-11. Optimised piston heads with new materials

On the other hand, insulation tape around the complete bobbin for the annular design ensures the stability of the coil circuit. Figure 6-11 shows the final piston head configurations. In the picture is possible to see the permeable and non-permeable materials used in the construction of both prototypes.

### 6.9.3 Test Setup for Maximum Force

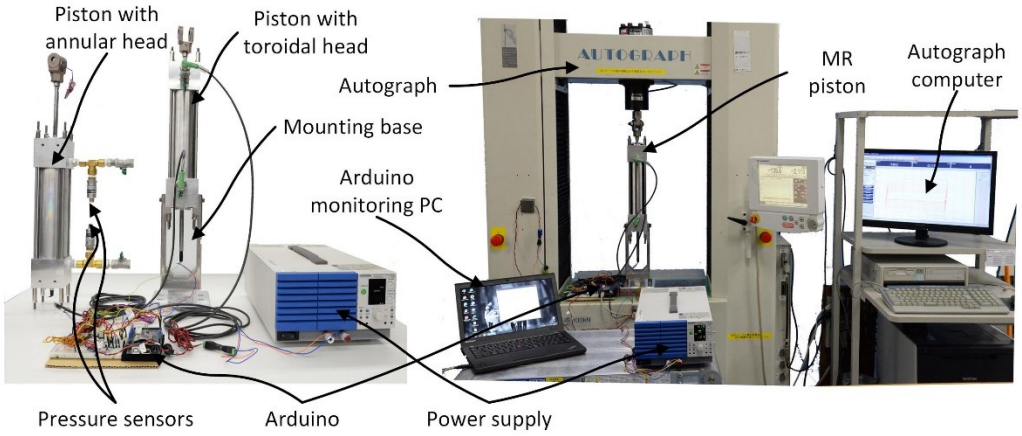


Figure 6-12. Experimental setup used to test the maximum force of optimised piston

The original setup included a universal testing machine in order to evaluate the passive performance of the MR piston at a wide range of forces. Therefore, as an initial test and in order to benchmark the results of the optimisation with the previous prototype results, the same setup is used. Nevertheless, a new mounting base is needed in order to accommodate the length of the additional piston rod.As with the previous setup, the piston is fixed while the universal

testing machine drives it back and forward, along a 70mm stroke for security, at a constant speed, as seen in Figure 6-12.

The position, driving force, electromagnet current, pressure values, and temperature are recorded, while temperature is kept constant (30–40°C) to ensure consistent measurements. The coil current is manually set using a digital power supply.

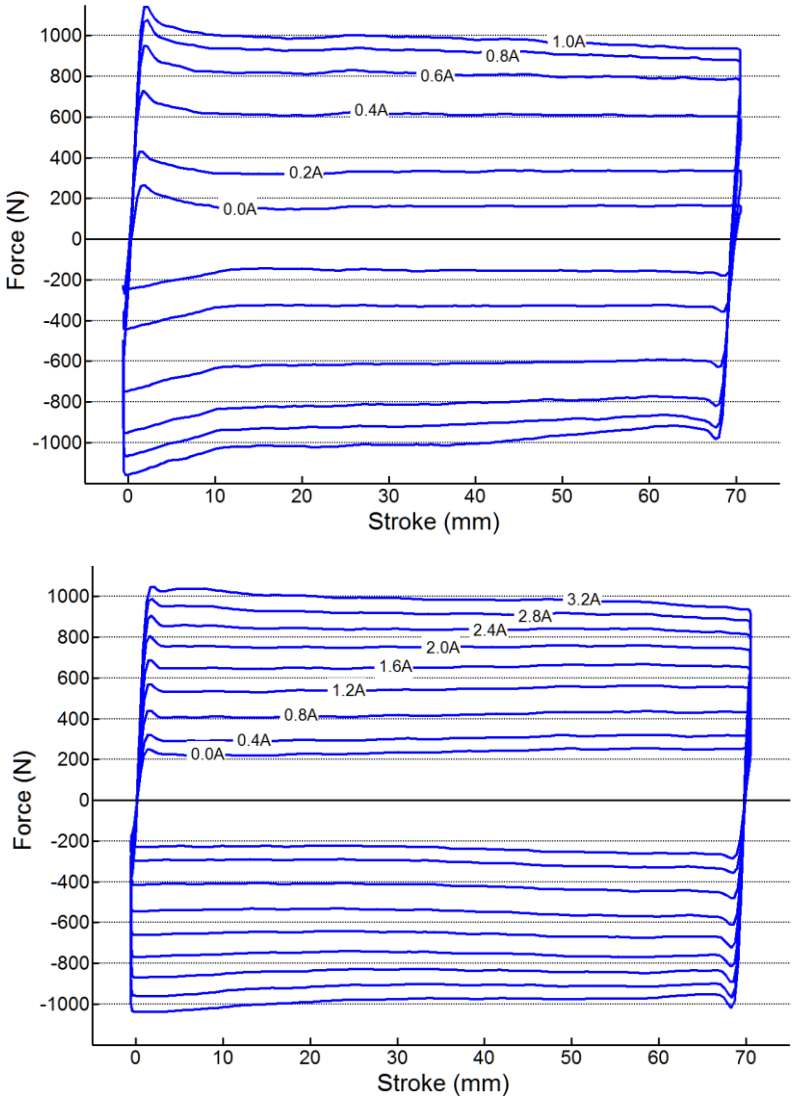


Figure 6-13. Annular and toroidal force vs stroke over different currents at 500mm/min

The results of both prototypes are shown in Figure 6-13. The graphs show that the optimisation lead to an increased in peak force of 71%, 12 times better energy efficiency, when compared to the old design that needed 5A to produce 677N. The force values of both the toroidal and annular designs are similar. However, the toroidal design has a more stable force to current characteristic, at the expense of energy efficiency due to the larger active gap area to be saturated.

#### 6.9.3.1 Force vs Current

Three different piston speeds are used, 100mm/min, 500mm/min, and 1000min/min. In each the current is increased at regular steps from 0.00 to 1.2A, and 0.00A to 3.2A for the annular and toroidal designs respectively.

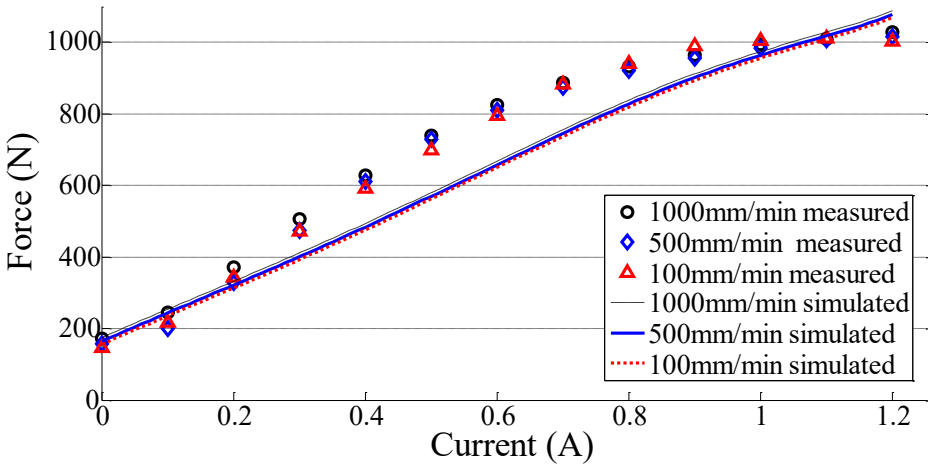


Figure 6-14. Annular design piston force vs current characteristic of at different speeds

The results show that increasing the magnetomotive force (i.e. coil windings) by 60%, leads to an increase of 71% in peak force, 12 times better energy efficiency, and more than twice the force to weight ratio when considering the piston's head weight. The values of the toroidal design, are similar to the conventional annular design.

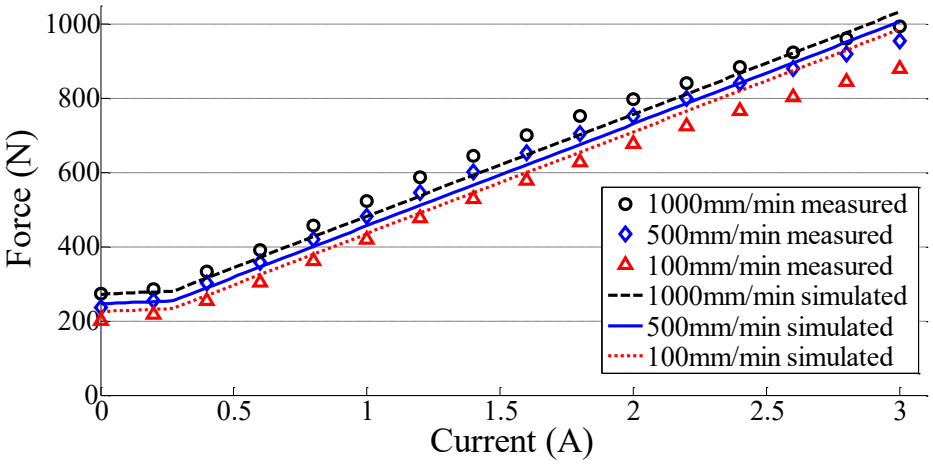


Figure 6-15. Toroidal design piston force vs current characteristic of at different speeds

However, the toroidal design exhibits a potential to achieve higher forces with a 50% better force to weight ratio, but at the expense of 2.5 times energy efficiency due to the larger active area to be saturated.

The graphs show that the speed has a bigger effect on the output force of the toroidal design. This is caused by the flow dependant Newtonian force, which is inversely proportional to the cross section area of the gap that it is more than 3 times bigger in the annular design. This also explains the difference in the zero field force of the both designs. In this respect, the annular design seems to be better suited for compliant actuation, since it allows for bigger gap areas, which minimises the Newtonian force, and reduces the speed dependent behaviour for better controllability, while keeping a satisfactory peak force performance.

On the other hand, it appears that the effects of the magnetic saturation of the core material, as well as the non-linear behaviour of the MRF yield stress are more pronounce in the annular configuration, making it more difficult to control. This is an important point for the toroidal prototype, since it means that it can avoid the saturation of the MR fluid and the materials of the electromagnetic core. This feature allows it to achieve a wider range of linear force. Moreover, this also means that the toroidal design has the potential to develop higher forces by varying the core and coil configurations, without sacrificing force performance, ultimately allowing for a greater degree of customisation options to meet different system requirements.

The minimum damping force of the new MR piston is considerable higher than the previous design despite the substantial modifications done. This is most likely caused by the stainless steel used for the cylinder and rods, which despite being rated as non-magnetic it shows a small but noticeable amount of magnetic permeability. Other reasons also include the double rod design, and tighter tolerances in the piston head.

It is important to note that despite the efforts to improve the estimation of the forces using the mathematical models. The simulated forces still show some discrepancy with test results.

#### 6.9.3.2 Force Hysteresis Curve

This test was performed at 500mm/min over an extended current range to measure the influence of high currents in the residual magnetisation of the electromagnetic circuit. This allows to observe the hysteresis parameter on the piston force. A low hysteresis means that the

K-M31 magnetic alloy can perform well in MR devices intended for safe pHRI, where fast control strategies are preferred for safety.

In both tests the force range of the graphs has been aligned in order to more easily compare the hysteris curves. But it must be clear that the excitation currents are different, since the energy efficiency of the prototypes is different as it was discussed before. The annular was tested with a current of 0.0–1.4A using 0.2A steps, while the toroidal with a current of 0.0–4.5A using 0.5A steps.

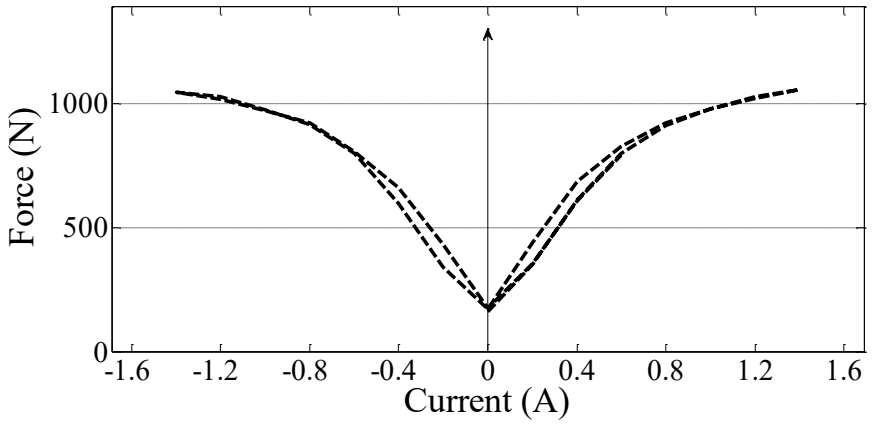


Figure 6-16. Hysteresis characteristic of force vs current curves for the annular design

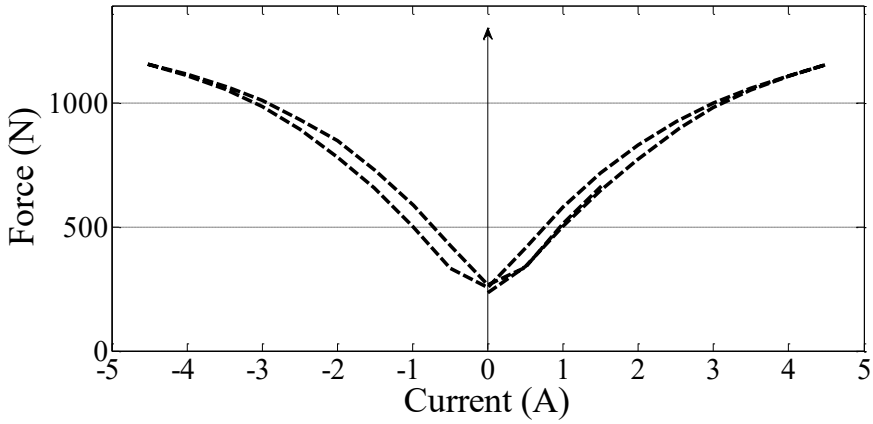


Figure 6-17. Hysteresis characteristic of force vs current curves for the toroidal design

The performance of both designs is good, with the annular design having a slight smaller hysteresis. Here is also possible to appreciate that the saturation limit of the toroidal design start approaching at 4.5 amperes, however there is still room to increase the force with higher current, while keeping a good linear characteristics.

### 6.9.4 Finite Element Method Evaluation

In order to understand the reason behind the difference between the experimental data, and the results obtained from the measurements, a FEM analysis was performed using ANSYS software. For the analysis the values in Table 6-I, Table 6-II and Table 6-III, together with the manufacture 3D CAD models were used. However, the B-H magnetic curves for the Permendur and MRF-132DG were input directly into the software.

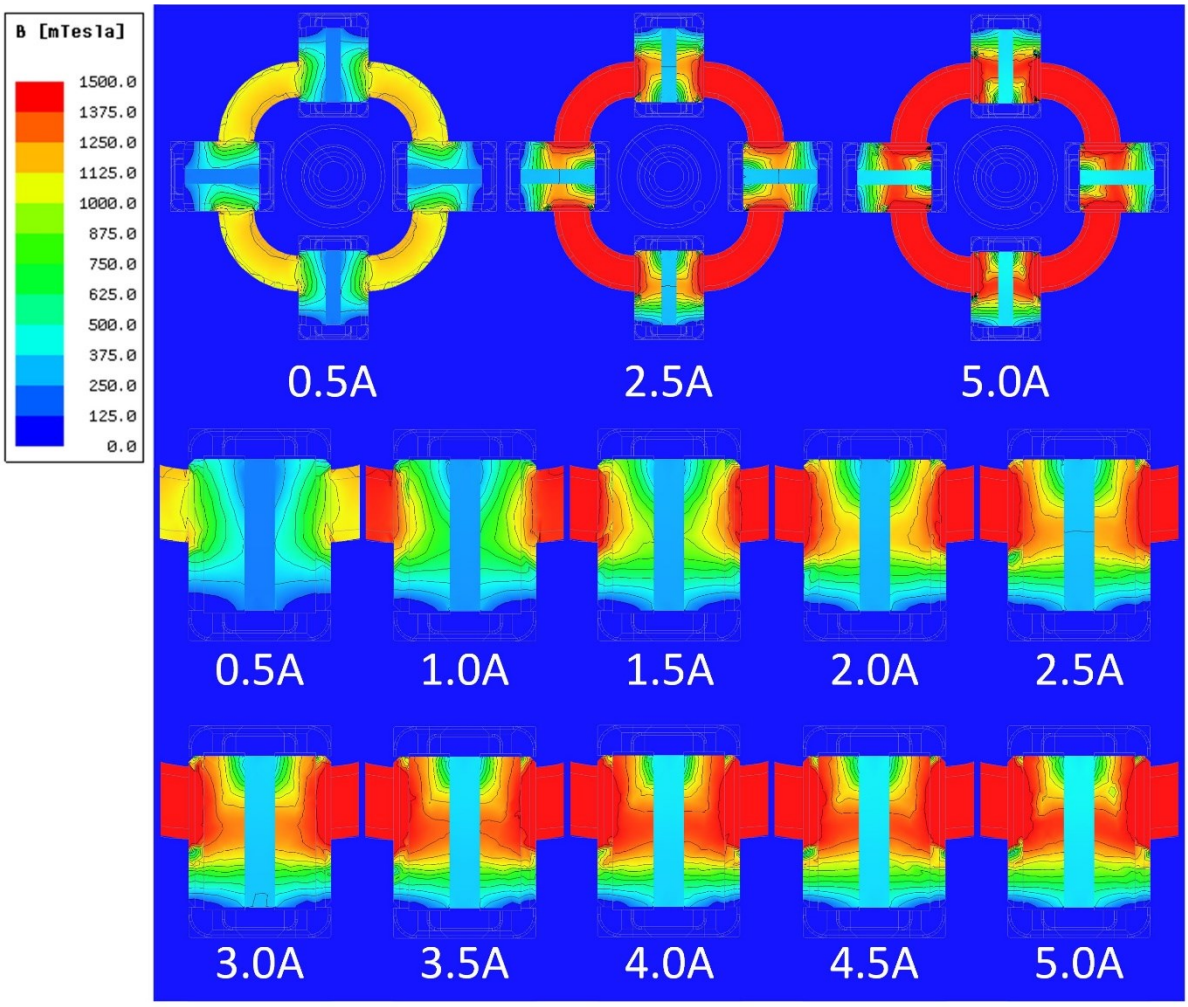


Figure 6-18. FEM simulation for toroidal design top sections, excitation current of 0.5–5A with 388 turns.

The results in Figure 6-18 and Figure 6-19 show that the optimisation process successfully achieved a complete and uniform saturation of both electromagnetic cores. However, the magnetic flux density at the gap of both designs is well below the theoretical values calculated in the previous section.

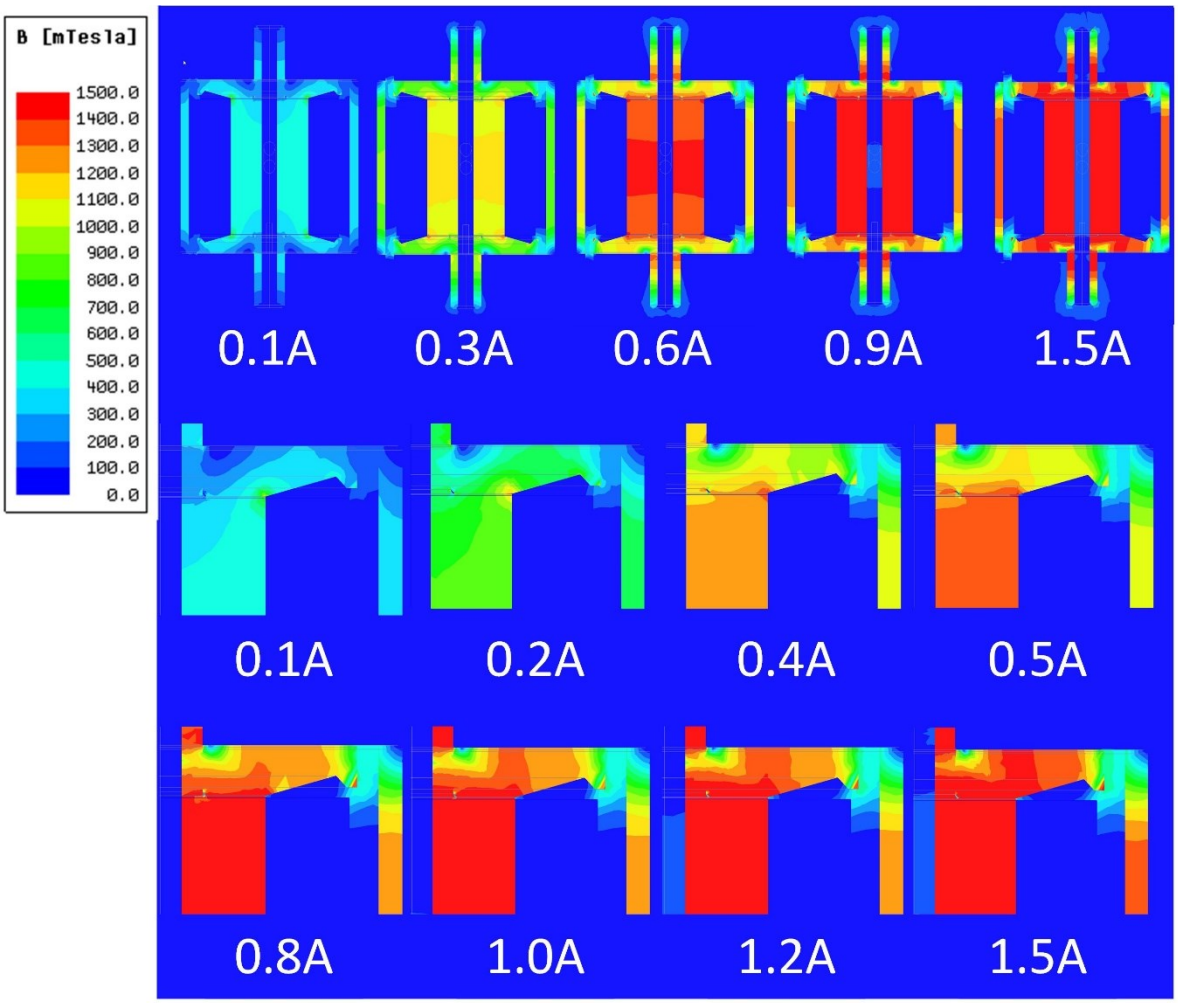


Figure 6-19. Magnetic flux FEM simulation showing side section, excitation current of 0.5–1.5A with 850 turns

While the annular design shows a smaller deviation with relatively uniform saturation, the values for the toroidal design are around 68% less than the predicted. This might be caused by the wrong estimation of the leakage parameter, which was linearly estimated from the previous prototype results.

A more detailed analysis of the FEM simulation revealed that the magnetic flux density at the centre of the toroidal plug is not entirely uniform, as it is shown in Figure 6-20. This is probably caused by the difference in size between the electromagnet core and the insert section. This problem might be solved in future iterations by having a bigger core size towards the end of the cores. The current size of the core still has plenty of space at the top and bottom to grow, without reducing the area available for coil windings.

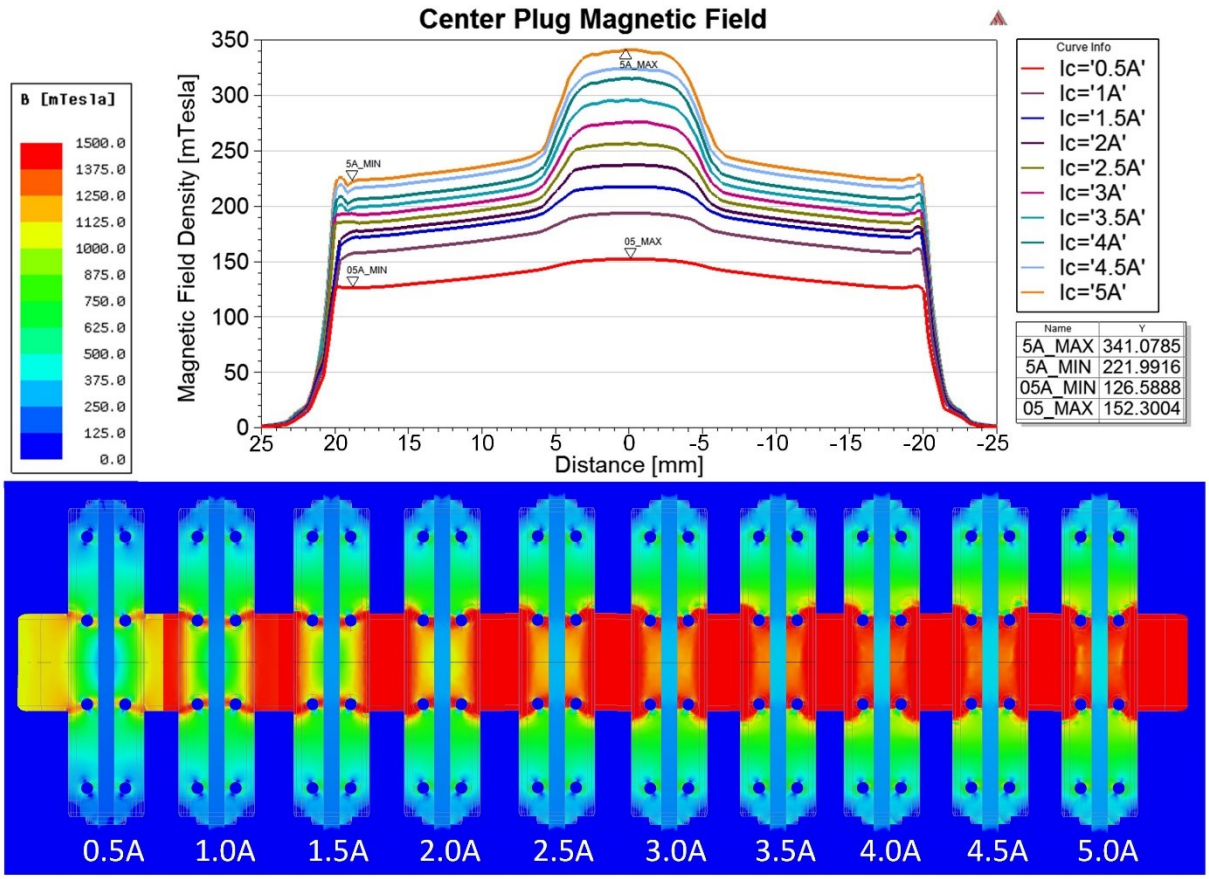


Figure 6-20. Magnetic flux density at the centre gap of the toroidal plug.

The simulation-based curves predict the trend of the experimental peak forces. This validates the revised flux values, and confirms that the problem lies mostly in the results from the reluctance model. Different approaches that could better account for the shortcomings of this model should be explored. Additionally, the hydraulic model should be also analysed to account for the non-linear behaviour of the MRF parameters.

## 6.10 Discussion & Remarks

The most relevant mechanical modifications done to the piston included a new sealing system to reduce friction, a double rod design to get rid of the accumulator, as well as other mechanical revisions. These modifications successfully improved the backdrivability of the piston by reducing the seals friction, reducing the contact diameter of the rod, and additional forces of the accumulator. They also achieved more stable forces during the push, and pull motions of the piston, due to the lack of an accumulator, and better design of the piston head. The modifications to the piston shape allowed for a simplification of the assembly, filling, and testing processes of the prototype. Nevertheless, some shortcomings were also introduced. The

double rod increased the overall friction of the system while in operation. In order to overcome this problem, future iterations should consider a different type of sealing system for the rods.

The optimisation of the toroidal head configuration was the most important factor of the improvement of this prototype. The shape of the passages was modified from square to rectangular, and the inserts were substituted for a permeable wall covering the complete surface of the MR plug. These modifications allowed for a more uniform distribution of the magnetic flux density inside the passages of the MR valves. This allows for a simpler modelling of the electromagnetic and hydraulic parameters. As a result, this also enabled the possibility to create an optimization method for the toroidal design.

The analysis of the new design brought to light two kind of optimisation targets. On one side the trade-off spaces allow the toroidal design to meet the specifications of specific applications. In this sense, the size of the passages allows the designer to set the necessary backdrivability and output force. On the other hand, there are parameters that have an optimal value. It follows that the size of the core can be optimised to achieve the maximum possible range of both of these properties. The right balance allows the coil to generate enough electromotive force, i.e. ampere turns, to achieve the desired magnetic flux density at the gap without avoiding the saturation of the core section.

Nonetheless, the toroidal exhibiting higher linearity in its force curves. This is one of the biggest advantages of the toroidal prototype, which can avoid the saturation of the MR fluid and the materials of the electromagnetic core despite high output forces. This advantage is partially attributed to the use of materials with higher magnetic saturation values. Ultimately, this characteristic permits for a wider variation of the design parameters, without sacrificing force performance, ultimately allowing for a greater degree of customisation options to meet different system requirements.

The preliminary tests after the optimisation of the prototype show that the designed achieved twice the force of previous iteration, with a twelve fold in energy efficiency. This validates the optimisation methodology, and puts the performance of the actuator in par with current MR dampers. Nevertheless, the toroidal has still a lower efficiency than the annular counterpart does. This is come as a result from the bobbin-shaped electromagnet core of the annular prototype fully using the space of the piston head. On the other hand, the toroidal has a donut like shape that leaves some empty space in the middle. This does not only limit the core

size, but also the number of coil windings in the core, significantly reducing the energy efficiency of the prototype. From this it can be concluded that the annular design is better suited for high power compact designs, while the toroidal would be prefer for stability over a wider range of force despite its energy efficiency.

Another important finding of this analysis is related to the material selection criteria. As far as current research has shown, most actuators focus in using high permeable materials in its construction. This type of materials allow to generate magnetic fields in a relatively efficient way, i.e. consuming few electromotive energy generates good amount of magnetic flux output. However, for actuators with limited space, such as the toroidal design, is better to have material with high saturation values. This allows to more effectively saturate larger areas in the passages. This results in a more powerful force output with a small sacrifice in the energy efficiency. Therefore, a careful selection of material is important depending in the application requirements and the type of actuator that one is planning to use.

These findings serve as an optimisation methodology for any kind of actuators based on this principle. They allow designers to set their targets and find optimal combinations to meet them. Nevertheless, this research did not account for different kinds of shapes for the holes. In the future, a deeper analysis should also include these parameters in order to have a more complete methodology for optimisation. This will allow for a more flexible and comprehensible design of future actuators.

## 6.11 Chapter Summary

The performance evaluation of the toroidal piston head configuration revealed that it had several shortcomings when compared with its conventional annular counterpart. In order to overcome them, a deeper analysis of the experimental data and the mathematical model revealed several areas of opportunity to improve the performance of the overall system. Additional to these findings, several other mechanical modifications were also necessary in order to improve it.

While several mechanical modifications were undertaken to improve the usability and hydraulic performance, the most relevant modifications were aimed to improve the performance of the toroidal piston head configuration. In the previous iteration, the construction and geometry of the toroidal assembly limited the force performance and made it difficult to

accurately model the actuator output parameters. In order to solve these problems, the geometry of the passages was changed to a rectangular shape. In this way, it was possible to change the insert section of the array. The use of a complete permeable wall, instead of the steel screw inserts, allows for a larger interaction area between the MR fluid and the magnetic field, as well as a more uniform distribution of the magnetic flux density inside the passages of the MR valves. Moreover, it also simplifies its construction while ensuring equal sealing performance.

Based on the new rectangular configuration the actuator models were updated using the same equations as before. The new model is then used to conduct an analysis of the relevant design parameter for the toroidal configuration. The analysis revealed that some of its dimensions have an optimal range of operation, while others depend solely on application requirements. It was concluded that there is an optimal balance between the cross section area of the electromagnet core and area available for the coil windings. On the other hand, the length and width of the gap are parameters related to the minimum and maximum output forces of the actuator. A careful selection of these parameters during the design stage can be used to set the backdrivability and output force range of the actuator.

An optimisation in Matlab is conducted using an iterative parameter algorithm. The results from the optimisation along with the mechanical changes previously described are used to built a two new prototypes. The toroidal and annular piston configurations are evaluated using the universal testing machine. The passive performance results showed that the prototype optimisation lead to an increased in peak force of 71%, 12 times better energy efficiency, when compared to the old design that needed 5A to produce 677N. The force values of both the toroidal and annular designs are now similar. Still, the toroidal configuration has a higher energy consumption due to the unused space in the toroidal piston head. This is mostly caused by the unused space inside the toroidal circuit. Nevertheless, the toroidal design exhibits better force linearity and less saturation of the magnetic cores, which makes it a suitable alternative to current designs.

The current optimisation severs as a design guideline for MR pistons based on the toroidal configuration. However, most of the concepts described in this chapter can also be applied to the design of other types of piston head configuration. This will help designers to implement MR pistons in a wider variety of applications, promoting the widespread adoption of the technology.

# 7 Actuator Experiments

The MRPA is a hydrostatic actuator that employs a novel piston head configuration based on a toroidal array of MR valves. This configuration was specially design to meet the high power actuation requirements to create a backdrivable, fully integrated and versatile system. Nevertheless, the performance of the initial prototype was limited by several factors. Therefore, a complete redesign of the MR piston was done through a methodology based on the findings from an empirical and theoretical analysis. The measurements done in the prototype demonstrated how the optimisation methodology successfully improved the toroidal assembly, achieving a performance similar, if not better than the one found in conventional MR dampers. Nevertheless, until now only the passive force characteristics of the MR piston has been evaluated.

This chapter describes in detail the experimental evaluation of the MRPA as a fully integrated actuator. It covers the complete description of the active test bench, was modified to accommodate the necessary instrumentation for the new experiments. Using the new setup is possible to conduct the speed and force control experiments previously published in [100]. Additionally, this study supplements experimental evidence to support the claims of force generation, active backdrivability during collisions and force control performance.

The empirical evidence gathered in this chapter will be used to support the claims that the MRPA is a feasible solution to the shortcomings of current actuation technology. The experiments will also bring light on the capabilities and limitations of the system. In the future, these findings will serve as a guide for the necessary improvements to deploy the actuator in real world applications.

## 7.1 Integral Experimental Setup

In order to evaluate not only the passive but also the active performance of the MRPA a new test bench was constructed. The new setup provides the necessary basis to achieve better control of the speed and force of actuator and the test bench, along with consistent data logging. Similar to the test setup presented in Chapter 4, the test setup is based on a linear actuator and a data acquisition (DAQ) board. However, since the MRPA consists also of hydraulic circuit several modifications to the original setup are needed.

From the diagram shown in Figure 7-1, it is clear that in order to actuate the MRPA it was necessary to develop a hydraulic pump system. This system is formed by the pump, motor and the necessary power electronics to supply power and control the speed and direction of the pump. Additionally, a new control strategy is necessary to simultaneously actuate the electromagnetic field and the pump. As a result, the control system consists of two parts, an electromagnet controller, and the pump controller.

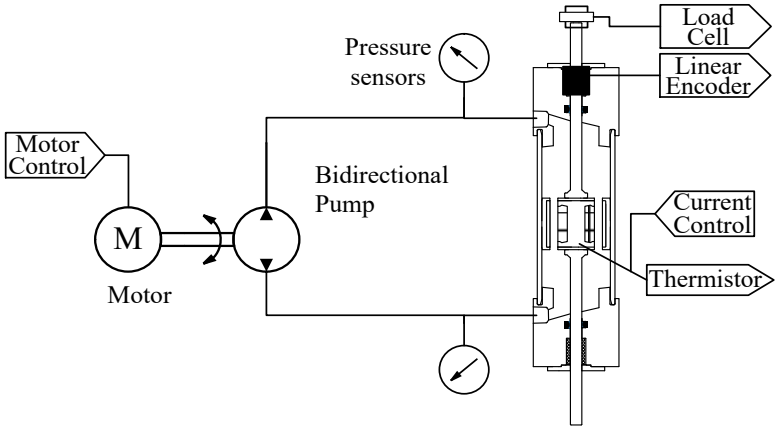


Figure 7-1. MRPA diagram schematic

### 7.1.1 Electromagnet Controller

It is responsible for regulating the current supplied to the electromagnetic circuit inside the piston head. It consists of a ESCON 50/5 controller connected to a 12 VDC power supply.

This setup allows the precise control and monitoring of the electromagnet current in a single integrated system. Thanks to the high frequency of operation of the ESCON controller is possible to achieve fast and stable current in the circuit.

### 7.1.2 Pump Selection

There are several kinds of hydraulic pumps in the market offering different kind of characteristics. In order to select an appropriate pump it is necessary to determine the hydraulic requirements of the system, most importantly the necessary flow rate and pressure of the pump. Additionally, the pump must be able to deal with the special characteristics of the MRF, which include its viscosity and high particle concentration.

After an extensive research of options including screw and vane pumps as the most likely candidates, a gear pump was selected. This kind of pump has a relatively low pulsation rate, can handle a wide range of viscosity, flow rate and pressure. Most importantly, it offers bidirectional variable flow control, and it is also available as an integrated system. The Oildyne 165 from Parker is a fully integrated hydraulic power unit compromising a 12VDC 800W electric motor, a bidirectional gear pump, internal relief valves and filters, and a reservoir tank.

Here is important to point out that the pump was not design to operate with MR fluids. Therefore, in order to protect and ensure its correct functionally, all the experiments were carried out using MRF-122EG from Lord Corporation, which have a nominal viscosity, $\mu$, of $0.042 \pm 0.02$ Pa–s@40°C, and a maximum yield stress of approximately 35kPa at 700 mT. This fluid has a lower viscosity and concentration of particles, which makes it more similar to the standard oil used for these type of pumps.

### 7.1.3 Pump Controller

The pumping system creates the necessary flow rate of MRF to move the piston at a given speed. This subsystem consists of a pump, a power supply, and a PWM drive.

In order to provide the necessary power to drive the pump a 200A 12VDC power supply from TDK lambda is employed. A full bridge PWM controller for permanent magnet DC motors from Kelly Corp. is used to regulate the current. EMI noise filters and safety devices are used to suppress electrical noise for the data acquisition system, and to ensure high current protection respectively.

### 7.1.4 Linear Actuator

An ASD-A2-0421 400W AC servo motor system from Delta drives the 2kN ball screw rod type linear actuator, LEY63. It is used to smoothly control the speed and force applied to the MRPA during the passive experiments, described in the subsequent section.

### 7.1.5 Instrumentation

In Figure 7-2 is possible to appreciate the complete control and instrumentation scheme used in the active test bench to test and monitor the performance of the MRPA. As it can be seen, the current sensors for the electromagnet and pump currents are omitted since they are implemented through observers depending in the PWM of the system.

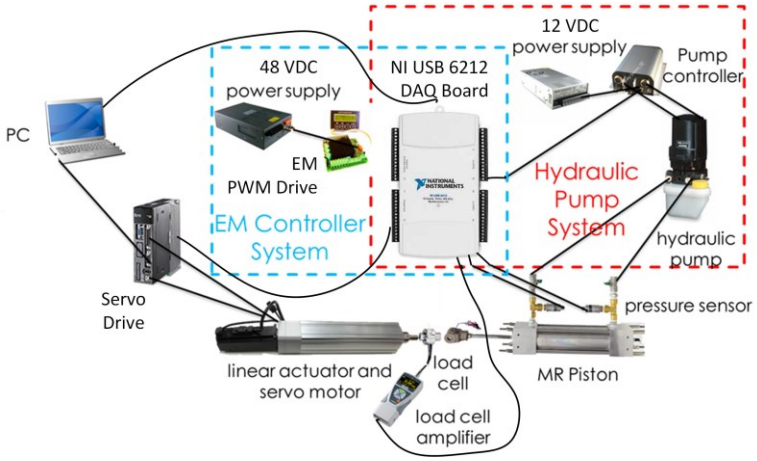


Figure 7-2. Instrumentation diagram for active test bench

A 2kN load cell, eLU-2000N, from IMADA is installed at the tip of the piston rod to measure the force of the actuator. It is connected to an ez-Connect amplifier to provide an analog reading. Two 250bar pressure sensors from Parker, PTDVB2501B1C2, are connected next to the MRPA ports to accurately monitor the pressure changes inside both piston chambers. A linear potentiometer, GEFRAN PZ34-A-150, is placed on top of the piston, and attached to the piston rod, to monitor the position and speed of the piston rod.

### 7.1.6 Data Acquisition System

A NI USB 6212 data acquisition (DAQ) board from National Instruments is connected to a PC to log all the data from the sensors, as well as to control the electromagnet, pump driver, and the linear actuator. This system allows for logging simultaneously all the inputs and outputs from the system at 1 kHz, to avoid the synchronization errors from previous studies.

In order to ensure correct measurement from the sensors noise filters and separate grounding is used for the overall instrumentation setup. Nevertheless, noise caused by ground loops could not be completely suppressed. In order to minimise its effect, the power supplied used for the sensors and the common ground of the board were implemented using a LiPo battery. In the future, a more comprehensive study of the instrumentation setup is necessary to ensure that the signals are measured with minimum electrical noise.

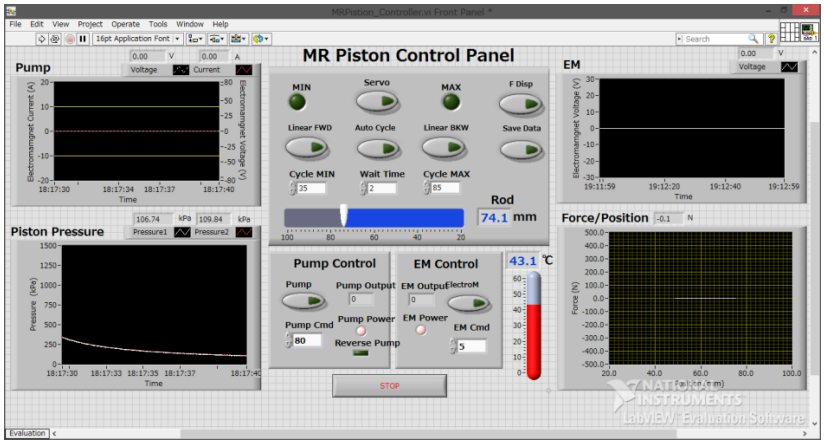


Figure 7-3. Data acquisition GUI done with LabVIEW

A LabVIEW GUI, shown Figure 7-3, was designed to monitor the system variables, log these variables into a file, implement the force and speed controllers, as well as to operate the system in a semi-automatic way during the experiments.

### 7.1.7 Integrated Test Bench

The assembled test bench including all the components is shown in Figure 7-4.

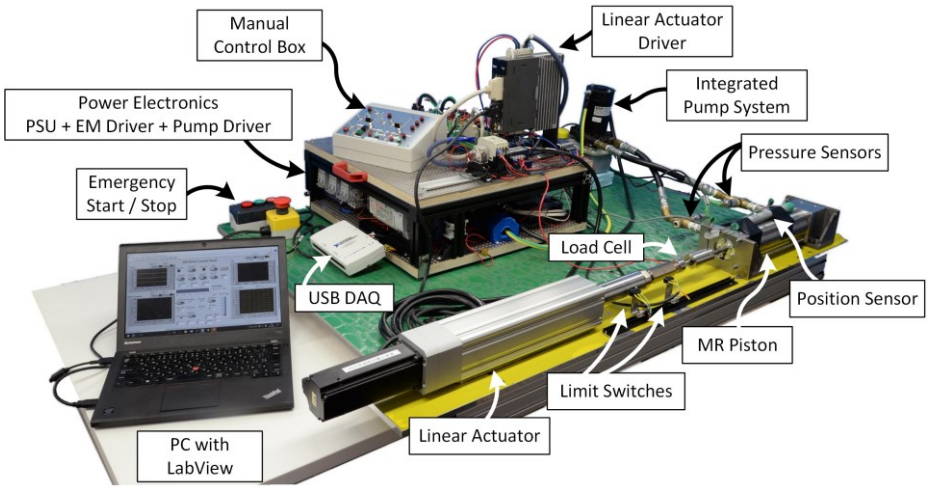


Figure 7-4. Active test bench including pump system

## 7.2 Open Loop Experiments

Several experiments are conducted to test the passive and active performance of the new actuator without a close control loop. These results show the maximum and minimum force and speed, as well as the response times of the electromagnet and pump. Later, these results are used to implement a simple controller. In the experiments, compression forces are positive, and speed is positive in the direction of the linear actuator, as shown in Figure 7-5. They are conducted at a standard temperature of 40ºC ± 2 to keep they oil viscosity constant.

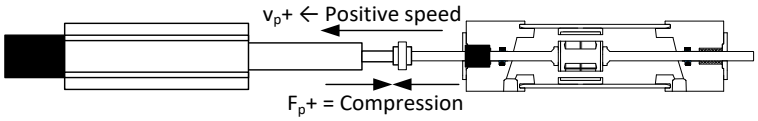


Figure 7-5. Piston speed and force direction diagram

### 7.2.1 Active System Results

In these experiments, the pump and electromagnet are operated simultaneously, while the piston movement is blocked by the linear actuator. Firstly, the electromagnet current (EMC) is set constant. Then, the pump voltage is increased from 0–80% in 5% steps of a 12VDC PWM signal. The output is restricted to 80% for the motor safety.

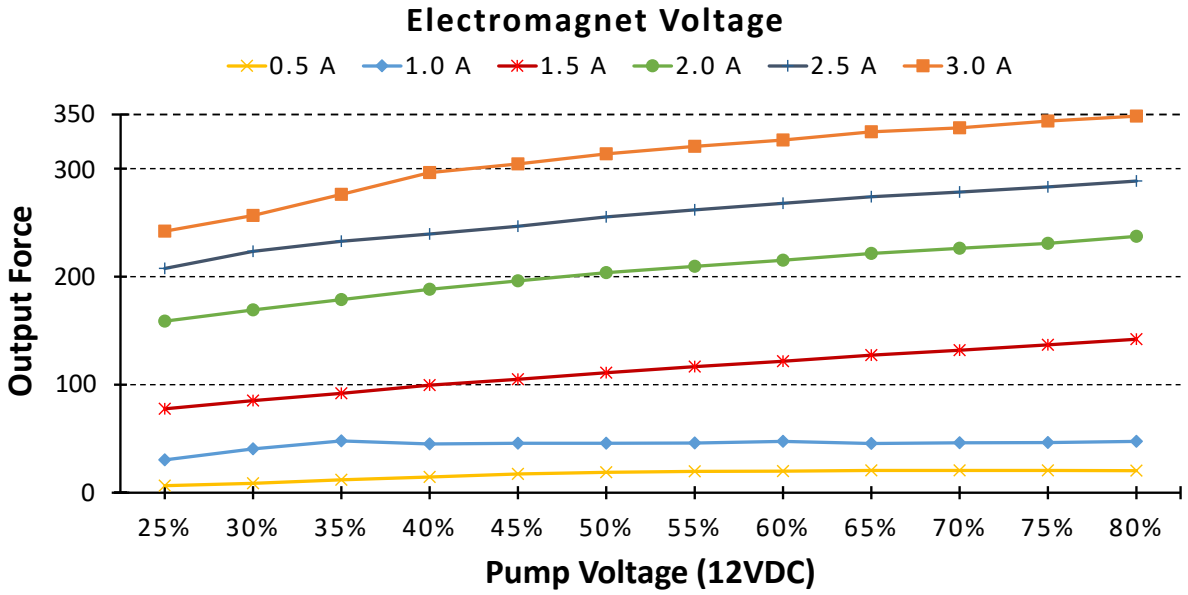


Figure 7-6. MRPA output force for different combinations of EM current and pump voltage

The results, Figure 7-6, show that the force strongly depends on the EMC. On the other hand, the effect of pump speed is more pronounced at higher EMCs. The combination of both variables can be exploited to achieve different modes of operation, e.g. high pump speeds can be used for fast response, while low speeds to reduce the energy consumption.

The figure also shows that the minimum combination required to overcome the piston friction is 0.5A for the EMC, and 3V for pump voltage (PV). The maximum force is approximately 350N. The forces develop by the actuator appear to be very linear, which is a very desirable characteristic that simplifies the control of the actuator.

### 7.2.2 Speed Step Results

In these tests, the MRPA is disconnected from the linear actuator, letting it move freely. The piston is fully retracted to a defined start position. At the beginning of the experiment, the pump is kept running at a set PV value, then the EMC is increased in steps. For every step of the current, the piston moves forward, then the PV is inverted to drive the piston backwards. After a complete cycle, a new current step is done.

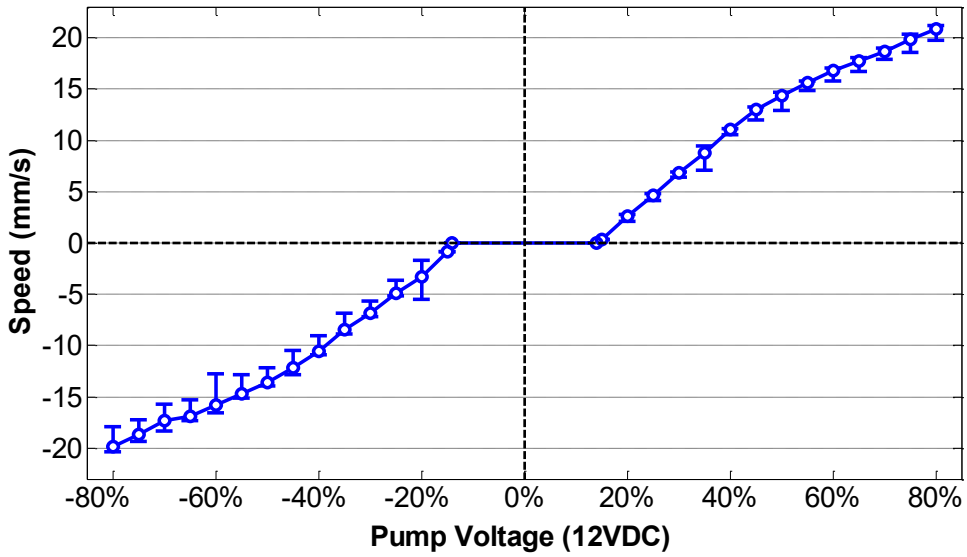


Figure 7-7. MPRA speed vs pump voltage characteristic, including EM current variance

The EMC current steps are 0.5A each, from 0A to 3A. On the other hand, the PV values are in steps of 5% from 0% to 80%. The plot in Figure 7-7 shows the average speed value for every PV. The average is calculated by adding all the EMC results for a given PV values, and

error bars represent the maximum and minimum values observed among all the EMC steps for a given PV.

The PV is almost linearly proportional to the MRPA speed, with a dead zone around 20% PV. The minimum speed achieved was -0.85mm/s in the backward motion, and 0.36mm/s for the forward motion. In both cases the minimum combination to break the system friction was 20% PV and 1.5A EMC. The maximum speed was -19.84mm/s and 20.88mm/s with 80% PV and 3A EMC for both directions. The speed appears to be relatively independent of the EMC used. However, its variation increases with the PVs. There is also a slight difference in the speeds achieved in the positive and negative directions.

This difference is still difficult to explain at the moment, with friction and system dynamics as the most likely explanations. A system with much lower friction could bring light to the cause of this phenomenon.

### 7.2.3 Backdrivability Test

In order to evaluate the backdrivable capabilities of the MRPA the piston is moved back and forward with a sinusoidal input of 100 mm/s. The current is varied to observe the range in which the MRPA can effectively control the force while been back driven by an external force. The results are shown in Figure 7-8.

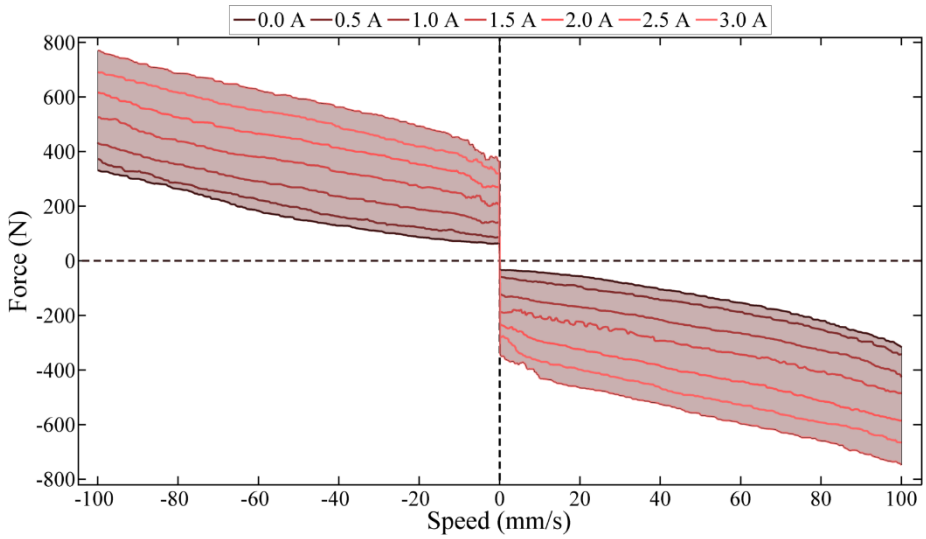


Figure 7-8. Backdrivable passive test for the toroidal prototype

The test revealed that the actuator has a wide range of operation in backdrivable motion. The range extends from 62N and –39N in the lower end when the actuator is in zero field mode, and reaching 770N and –747N when it is driven with a current of 3.0A.

This test revealed the deadband <62N ~ –39N> caused by the internal friction of the actuator. This band sets the minimum backdrivable force for the actuator. Inside this band it is not possible to control the forces of the actutor without using the pump. An intelligent controller could take advantage of the pump flow in order to counter balance the remaining friction force. In order to reduce this band it is necessary to improve the sealing system.

Given that the backdrivability of the actuator is one of the key parameters of this actuator a comparison with its annular counterpart is also presented. The testing conditions are similar, expect for the electromagnet currents, which are lower than in the annular. The results from the test are presented in Figure 7-9.

The results of this test show that the relation between the force and the speed of the piston are not as linear as with the toroidal prototype. This could be caused by the shear thinning of the MRF when is passing through the section of the gap affected by the magnetic field. In this respect the toroidal prototype has a distinct advantage. Since the toroidal prototype has a larger area affected by the magnetic field, the shear thinning effects of the speed is less pronounced.

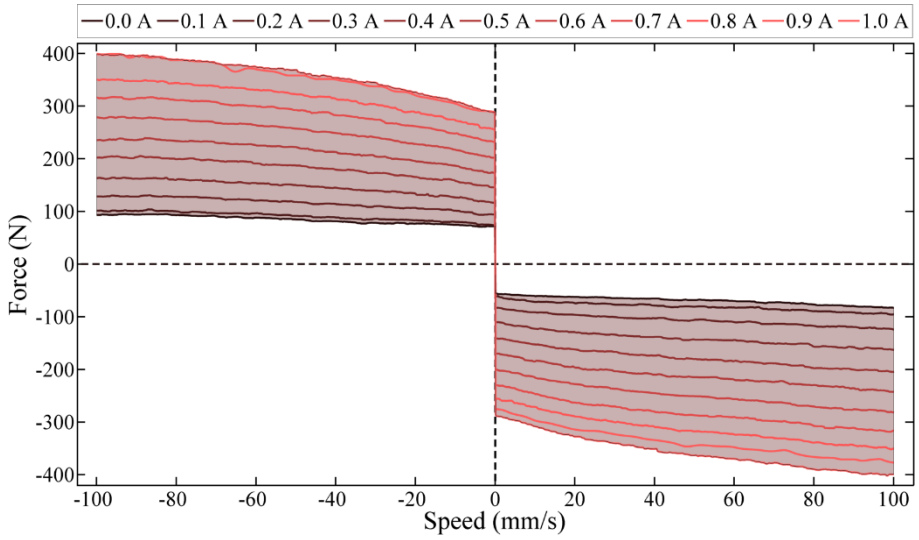


Figure 7-9. Backdrivable passive test for the annular prototype

It is important to note, that the forces of the annular prototype are lower than the ones reported after the optimisation was completed, in Figure 6-14. A probable cause of this discrepancy is the time the MRF spent inside the piston without moving. A long time between

the experiments may have caused some sedimentation or thinning of the fluid. Despite changing the fluid inside the piston, this behaviour did not improve. Further investigation about the operating conditions of the MRF must be research in the future in order to address this problem. This might be an important point to improve if the actuator is to be deployed in real world applications.

## 7.3 Close Loop Control

The close loop control was developed in order to precisely regulate the output force and speed of the actuator. The force controller is implemented using the load cell at the end of the piston rod as feedback signal. In this case, it is only possible to measure the output force when the piston rod is in contact with an object. On the other hand, as established in previous experiments the speed signal of the system is at the moment very noisy, which prevent us from implementing a close loop speed controller.

Based on the results obtained in the open loop experiments, a simple speed and force controllers are implemented to explore the possibility of using a PID system to improve the system response. For simplicity in the design, the force and speed variables are assumed to be independent. Thus, EMV is used to control the measured force in a close loop fashion, while the speed is controlled using PV open loop strategy.

### 7.3.1 Force PID Controller

This controller is implemented using the curves from the force step response. A known modification of the Ziegler-Nichols tuning method was used to get initial values for the controller, followed by manual tuning, as shown in Table 7-I.

Here the adjusted open loop gain Ko' is calculated as follows,

$$K_o' = K_o \frac{\tau}{T_{dead}}$$

Equation 7-1. Open loop gain for system with dead time

#### 7.3.1.1 Controller Tuning

The results from the initial calculations using the method described above are in the Table 7-I. These values were initially used to tune the controller, however it was instable. Therefore, a new approach using the resonant frequency of the system was used to find a suitable Kp. Then

the values of the integral and derivative terms were fine-tuned to adjust the response of the system. The final results are listed as manual values in Table 7-I.

TABLE 7-I - TUNING PARAMETERS OF THE FORCE CONTROLLER

| *Tuning Method* | $K_p$ | $T_i$ | $T_d$ |
|---|---|---|---|
| ***Ziegler-Nichols terms*** | $1.2K_o'$ | $2\tau$ | $0.5\tau$ |
| ***Values*** | 0.042 | 0.0.63 | 0.01575 |
| ***Manual values*** | 0.005 | 0.0016 | 0.0002 |

$K_o'$ is the adjusted open loop force gain, $\tau$ the force time constant, $T_{dead}$ the system dead time.

The parameters were put in the LabVIEW program with a constant controller frequency of 200 Hz. This is enough to achieve satisfactory results, however, as it will be described later, there are still several points that could be improved.

### 7.3.2 Independent Speed controller

For the speed, the derivative from the position sensor is fairly noisy, making it difficult to implement a close loop controller. Thus, an open loop strategy, using Equation 7-2, is implemented instead. The equations where calculated using the curves in Figure 7-7 and fitting a quadratic curves.

$$PV = \begin{cases} 0.0922v_p^2 - 1.4851v_p + 14.374 \ , v_p > 0 \\ 0 \qquad\qquad\qquad\qquad , v_p = 0 \\ -0.0814v_p^2 - 1.3592v_p - 15.302 \ , v_p < 0 \end{cases}$$

Equation 7-2. Curves for the speed controller

The implementation of the open loop controller done directly in LabVIEW using the input signal to select the appropriate equation. In future implementations, it will be necessary that this equation is paired with the electromagnet input/output, since no movement can be generated without the aid of some pressure difference.

### 7.3.3 Push Force Experiment

In order to test the force controller the piston movement is blocked. The pump output is set at PV of 20% or 80%; then, the desired force is entered, and the results measured. The error in the graph is the absolute relative to the input step. The time measured is the rising time of the signal to reach 90% of the value of the input step.

TABLE 7-II - FORCE CONTROLLER PERFORMANCE

| | ***Pump Output*** | | | | | |
|---|---|---|---|---|---|---|
| | ***80%*** | | | ***20%*** | | |
| ***Force Step (N)*** | ***Force (N)*** | ***Error (%)*** | ***$T_r$ (s)*** | ***Force (N)*** | ***Error (%)*** | ***$T_r$ (s)*** |
| $0 \rightarrow 30$ | 30.20 | 0.68 | 0.103 | 29.97 | 0.10 | 0.085 |
| $0 \rightarrow 150$ | 150.13 | 0.09 | 0.045 | 149.89 | 0.07 | 0.065 |
| $150 \rightarrow 200$ | 200.16 | 0.08 | 0.050 | 199.84 | 0.08 | 0.080 |
| $200 \rightarrow 0$ | 51.29 | N/A | N/A | 29.69 | N/A | N/A |
| $0 \rightarrow -30$ | -29.88 | 0.39 | 0.050 | -29.92 | 0.27 | 0.085 |
| $0 \rightarrow -150$ | -150.05 | 0.03 | 0.045 | -149.96 | 0.03 | 0.045 |
| $-150 \rightarrow -200$ | -200.06 | 0.03 | 0.045 | -200.07 | 0.03 | 0.050 |
| $-200 \rightarrow 0$ | -100.45 | N/A | N/A | -53.30 | N/A | N/A |

$T_r$ represents the time for the output force to rise to 90%, since the force step is triggered.
The error is calculated according to the desired input force

The results in Table 7-II show that the PID force controller can drive the piston to achieve the desired force with an accuracy above 99%, as long as the pump can provide enough flow and pressure to drive the piston. However, due to the internal friction of the piston, there is a dead band around 50N in the positive forces and -53N for the negative. Inside this region, which is also related to the flow rate of the pump, the MRPA cannot lower its force any further. In order to solve this problem, the pump must backdrive the MRPA.

It is also important to notice that the response of the piston is very fast despite the pump dynamics, which are slow (usually above 500ms as shown in the next section). This is a very important characteristic that demonstrates the capabilities of the system to achieve good control response, necessary for robotic applications where safety and reliable actuation are necessary.

### 7.3.4 Speed Controller Experiments

In this experiment, the force controller is turned off and the EMC is set to 2A constant value. The test starts when a speed step is inputted in the GUI. As the piston drives forwards or backwards, depending on the setting, the average speed is recorded.

The results are shown in Table 7-III. From the results, it is clear that the performance of the speed controller is lower than that of the force controller, in both reaction time and accuracy.

TABLE 7-III - SPEED AND COLLISION SAFETY RESULTS

| *Input* | *Output* | | |
|---|---|---|---|
| ***Speed Step (mm/s)*** | ***Speed (mm/s)*** | ***Error (%)*** | ***$T_r$ (s)*** |
| 0 → 8 | 7.63 | 4.58 | 0.515 |
| 0 → -8 | -7.60 | 5.02 | 0.520 |
| 0 → 17 | 17.68 | 3.97 | 0.515 |
| 0 → -17 | -17.86 | 5.09 | 0.440 |

$T_s$ represents the time for the output force to rise to 90%, since the speed step is triggered.
The error is calculated based on the input value

In this case, the current performance of the open loop speed controller is low, but it might be acceptable for simple tasks without needing sensor feedback. A better sense strategy and a more complete intelligent controller are necessary, perhaps using fuzzy or a neural network system. In the future, both speed and force controllers should be integrated in order to provide an integral solution that delivers the desired performance for particular applications.

### 7.3.5 Collision and Backdrive Experiments

This experiment is similar to the previous one. However, here the experiment is split in three stages. In the first stage, the piston moves forward with a fix current and pump voltage. When the piston makes contact with the linear actuator, the force current controller is activated, while the pump voltage remains constant. Then, the linear actuator waits approximately 700 milliseconds, for the force to stabilise, before it starts driving the piston back. The piston is backdriven approximately 27mm at a constant speed of 50mm/sec. After the linear actuator reaches the set position, it stops and waits 500 milliseconds. Finally, the linear actuator retracts to the origin position at a fast speed, causing to quickly lose contact with the piston. The experiments are repeated several times for both prototypes to compare their performance.

In both prototypes the experimental conditions are the same. The experiment consists of three target forces, set to 100N, 200N and 300N. For each target force, the pump is set to 30% and 70% of the nominal pump voltage, which is kept constant throughout the duration of the experiment.

The results from these experiments show the performance of the force current controller to compensate for the sudden changes in force during the collision and back drive operation of the MRPA. The results of the MRPA with toroidal head are shown in Figure 7-10.

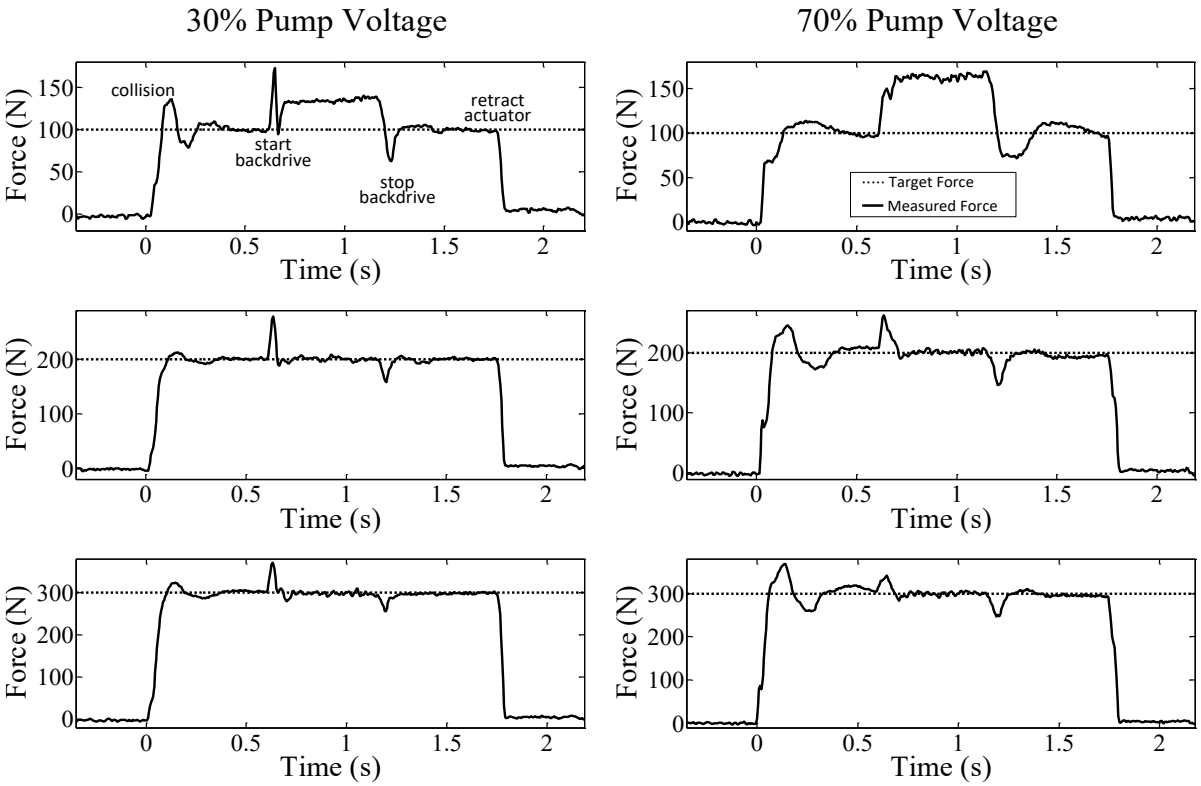


Figure 7-10. Collision and backdrivability force control experiments for MRPA with toroidal head

The experimental results for the toroidal prototype show that the MRPA can keep the target force under control during the collision and backdrive operations with slight deviations. The deviations from the 200N and 300N target forces are caused mostly by the slow performance in the PID based force current control loop. A better implementation of it will ensure that deviations are considerably minimised.

On the other hand, the deviations from the 100N target force are created by the pump controller, which is disabled at the moment. In order to reach the target force is necessary to have an intelligent controller that regulates the pump flow and direction according to the desired behaviour of the actuator. At the moment, the theoretical implementation of such controller is described in Section 7.4: Future Operation Modes.

The performance of the annular prototype is shown in Figure 7-11 for comparison. It can be seen that the annular prototype has better performance in the 100N target force experiment. This is due to the larger gap, which reduces the force dependency of the speed during the backdriving phase. On the other hand, the force controllers is slower to react during the collision phase.

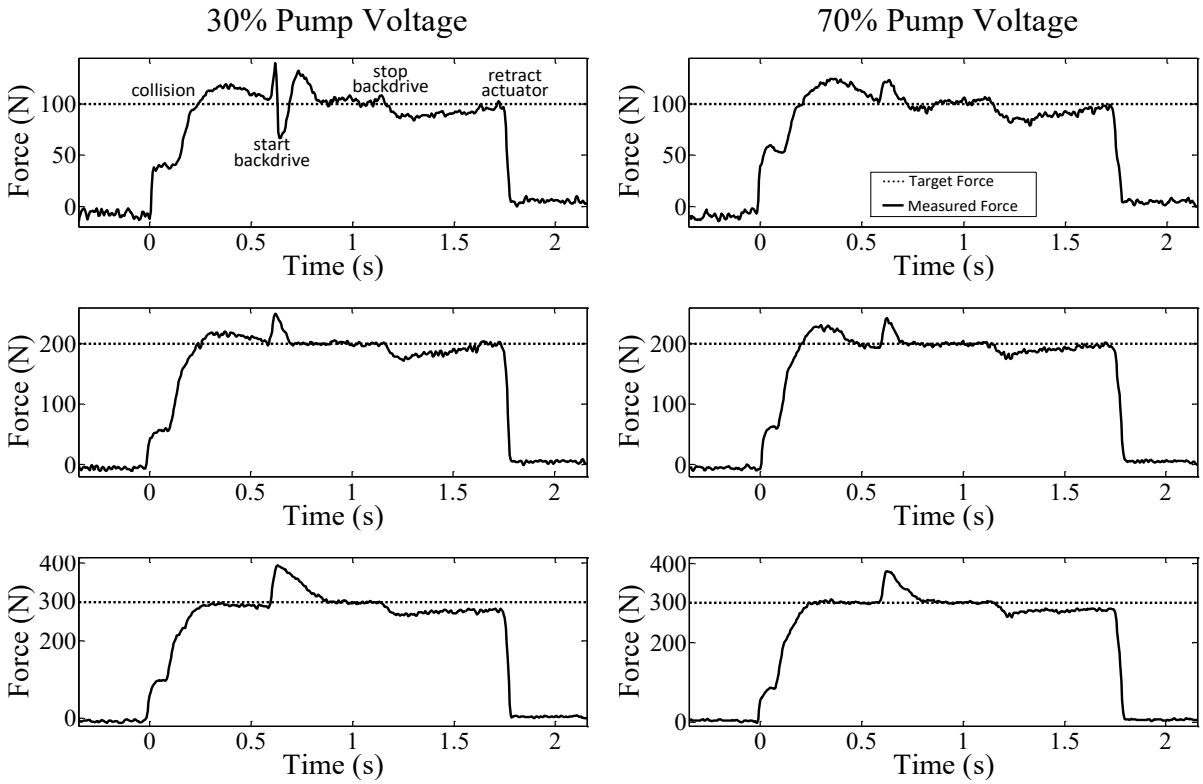


Figure 7-11. Collision and backdrivability force control experiments for MRPA with annular head

## 7.4 Future Operation Modes

The results from the experiments above hinted the existence of new operation modes for this kind of actuators. In order to realise a control strategy for the MR piston is necessary to have an understanding of these modes. So that in the future, a higher-level controller can be used to set behaviour of the system by automatically switching between these modes.

In this way, it should be possible for the new actuator to realise new possible control strategies. Depending on the application of the system a desired behaviour can be achieve by using different strategies such as compliant manipulation for safe human interaction, energy efficient scheme to minimise power consumption, or robust and precise manipulation when the former characteristics are not needed.

It is outside of the scope of this thesis work to present an implementation of this intelligent controller. However, its theoretical design and functionality will be described so that in the future it could be easily implemented.

### 7.4.1 Control modes of the piston

Depending on the conditions of these variables shown in Figure 7-12, the piston can work in the following modes described in Table 7-IV.

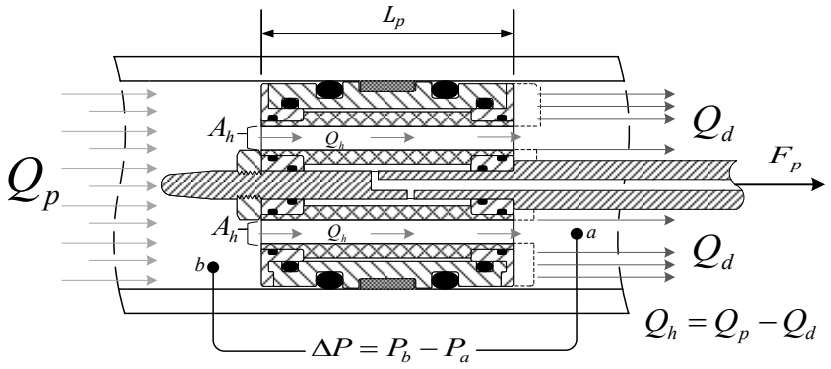


Figure 7-12. Simplified MRPA flow and hydraulic force diagram

TABLE 7-IV. MAGNETORHEOLOGICAL PISTON OPERATING MODES

| *Variable Status* | *NO Pressurised Inflow* $\boldsymbol{Q_p = 0}$ | *Pressurised Inflow* $\boldsymbol{Q_p > 0}$ |
|---|---|---|
| $\boldsymbol{Q_d = Q_p}$ | **Passive Hold**<br>The MR valve passages remain closed, holding the piston in position. | **Piston**<br>Same as a conventional piston, the pressurised fluid drives piston forward, while the MR valve produces the necessary magnetic field to remain close, i.e. $Q_h = 0$. |
| $\boldsymbol{Q_d < Q_p}$ | **Passive Push & Pull (MR Damper)**<br>Piston is pushed or pulled back by an external force. Push/pull force is controlled by varying magnetic field.<br>Push : $Q_h = -Q_d$<br>Pull : $-Q_h = Q_d$ | **Open Piston**<br>When the maximum pressure of the MR valve is surpassed, i.e. external force is bigger than the set force, then fluid starts flowing through the passages. The bigger the flow the higher is the force on the actuator.<br>Depending on $\boldsymbol{Q_d}$ 3 distinct sub-modes exist:<br>$\boldsymbol{Q_d < 0}$ → Active backdrive<br>$\boldsymbol{Q_d = 0}$ → Active hold<br>$\boldsymbol{Q_d > 0}$ → Active push |
| $\boldsymbol{Q_d > Q_p}$ | | **Extra Flow**<br>When piston is being pulled, then the pump can provide additional flow to reduce resistance. |

#### 7.4.1.1 Passive Hold

As described in the table above, this mode is used to keep the position of the piston static. Considering that the static friction ($F_f$) helps to keep the piston static, the MR piston acts in order to cancel out any external forces which have exceed the static friction in order to keep the position in a static position ($F_p = (F_e - F_f) > 0$). In this mode no fluid is pumped into the

piston ($Q_p = 0$) and the MR valves are kept closed ($Q_h = 0$). This ensures that the displacement of the pistons equals zero ($Q_d = Q_h + Q_p = 0$). In order for the MR valves to remain close the shear stress of the fluid is controlled to withstand the pressure generated by the external force $\left(\Delta P = F_p/A_p = f(\tau_y)\right)$. In this state minimal energy is being consumed, since the motor is not used at all, and the field is kept to the necessary minimum (no field is necessary if the external forces are less than the friction). Following there are some usability examples**:**

- Compared with a normal piston, the MR piston is safer. Setting a predetermined maximum force ensures that in case that a sudden external force occurs, such as the one cause by an impact, the MR piston can be safely backdriven. This is very useful when interaction with humans is necessary, since sudden unpredictable movements by the operator may lead to collisions with a robot or machines using this actuator.
- Compared to other hydraulic actuators, the fast response time of the MR fluid ensures a high control bandwidth against force disturbances, since they are cancelled out using the magnetic circuit alone without involving slow hydraulic mechanisms. Less energy is consumed by only using the magnetic circuit instead of activating the complete hydraulic circuit.
- Due to the mechanical construction with its inherited inertia and static friction offers stronger resistance to movement when compared to an MR damper. Here high shear stress values can be used to achieve a high stiffness, which is necessary in tasks that are more robust.
- Additionally this also means that less energy needs to be consumed when the friction is enough to hold the position of the MR piston.

#### 7.4.1.2 Passive Push & Passive Pull (Passive Backdrive)

Similar to the passive hold, in this mode no fluid is pumped into the piston (motor is off, therefore, $Q_p = 0$). However, the MR valve is opened, allowing the piston to be driven by an external force ($F_p + F_f < F_e$). Since no fluid is pumped into the piston, the fluid displaced by the movement of the piston head must be equal to the flow in the MR valve passages. In the case the piston is being pushed ($Q_h = -Q_d$), while in the case is being pulled it will be the opposite ($-Q_h = Q_d$). Here the MR valve is used to passively control the speed and/or force of the MR piston. This behaviour is similar to the one found in intelligent MR dampers in which the force depends on the speed and shear stress induced by the magnetic field ($F_p = f(\tau_y) +$

$\mu \cdot Q_h$), here $Q_h$ can be directly estimated from the piston head displacement measured by the position sensor ($Q_h = -Q_d = -\dot{x}A_p$). Following there are some usability examples**:**

- Different from a conventional MR Damper the passive force can easily be increased by pumping pressurised fluid. For example, if the MR piston is driven back by a very big force, then the speed could increase too much and it might cause an accident. In this case, the MR piston can quickly change to open piston mode, by pumping fluid into the MR piston, to provide extra fluid to generate more force and avoid the accident.
- Since the MR fluid has a fast response time, is possible to smoothly change between different piston modes, avoiding abrupt changes in speed or force, by carefully adjusting the magnetic field during the transitions.
- Likewise, when compared with a modified backdrivable piston, which uses valves and motors with complex control algorithms to emulate backdrivable behaviour, this mode has faster response time when a transition into other modes is necessary.
- Finally, this mode is more efficient when compared to the modified backdrivable piston mention above, since it requires lees computation power and also less electric power to actuate the system.

#### 7.4.1.3 Piston

In a similar way than a conventional piston, in this mode the piston is being driven by the pressurised fluid from the pump ($Q_p > 0$). The MR valve regulates the magnetic field always ensuring that it remains closed ($Q_h = 0$). In this case, the maximum speed of the piston is directly related on the pump flow rate ($\dot{x} = Q_p/A_p$). While the maximum allowed actuator force is controlled by the MR valve ($F_{pmax} = f(\tau_y)$ ). And although both variables are related, it is still possible to achieve many possible combinations that affect the compliant behaviour of the actuator. Since the actuator is always driving the piston against the friction force ($F_p > F_e + F_f$), it is important to note that output force of the actuator can either be determined in an straight forward manner by simply using the external force sensor, or by measuring the pressure difference and then subtracting the estimated friction force which is consider constant. Following there are some usability examples**:**

- In case a compliant behaviour is desired the magnetic field is kept to a minimum value, so that it is just enough to keep the MR valve closed at a given desired force. This ensures that the actuator remains as safe as possible in case of an unexpected collision.
- Additionally, keeping the field to the required minimum, also ensure less consumption of energy if an energy efficient strategy is required for a particular application.
- On the other hand, when high stiffness is necessary in a specific task, then the maximum shear stress may be set in the MR valve. This way the actuator can perform task where a high impact is necessary, for example during demolition tasks, debris removal, metal forging, or hammering
- As mention before, fast response and precise control of the magnetic field allow for quick and smooth transition to other modes. For example, even if collision occurs when high stiffness is set, the MR piston is still capable to instantaneously decrease the applied force by changing into open piston mode, which is much faster than activating valves to adjust the inflow of pressurised fluid as with conventional pistons.

#### 7.4.1.4 Open Piston

Similar to the piston mode, but in this case the passages of the MR valve are open ($Q_h \neq 0$). As in other modes the output force of the actuator ($F_p$) is determined by the shear stress ($\tau_y$) and the flow rate in the passages of the MR valve ($Q_h$). However, since both the inflow of pressurised fluid and the displacement of the piston head of the fluid variation affects the flow in the passages ($Q_h = Q_p - Q_d$), the correct measurement or estimation of these parameters is important to accurately control the output force of the MR piston ( $F_p = f(\tau_y) + \mu \cdot (Q_p - Q_d)$). Moreover, as it was shown in the table above there are three distinct sub modes of operation depending on the displacement of the piston head which will affect the apparent output force of the MR piston ($F_p{}'$):

**Active backdrive ($Q_d < 0$):** In sub-mode the piston is pushed back with an external force bigger than the piston and friction forces combined ($F_p' = F_p + F_f < F_e$).

**Active hold ($Q_d = 0$):** This sub-mode the piston is very similar to the passive hold, where the external forces which exceed the friction forces are balanced out by the piston force ($F_p' = F_p = (F_e - F_f) > 0$).

**Active push ($Q_d > 0$):** Similar to the piston mode this sub-mode produces forces exceeding the external and friction forces ($F_p' = F_p > F_e + F_f$).

Depending on the sensor setup different strategies can be used to determine the all the variables involved in the control. As it was mention before depending on the sensory setup it should be possible to directly measure each variable or estimate them based on related variables. Following there are some usability examples**:**

- Since both the pressurised inflow and the shear stress influence both the speed and force of the actuator a wide variety of combinations are available to produce a range of desired behaviours.
- Since the MR valves have a fast reaction time, the active piston mode allows to quickly change the speed and force of the actuator, by simply varying the shear stress of the fluid.
- For example, compared to a conventional piston higher accelerations can be achieve. The MR piston can be preloaded by increasing the inflow at a very low shear stress keeping a low output force, then suddenly closing the MR valve to enter the piston mode creating an almost instantaneous high force.
- The active backdrive and active piston sub-modes can be used to generate greater forces (past the $\tau_{max}$ limit) than the forces possible in passive backdrive and piston modes. By increasing the inflow of pressurised liquid the flow in the MR valve passages increases, which leads to an increased force. This is useful when the $\tau_{max}$ limit has been reached in other modes.
- Compared to the passive hold, in the active hold sub-mode is possible to generate forces even in a completely static position. This is advantageous when using force control with rigid static objects. For example, is possible to apply pressure to an object without deforming it.
- The active hold sub-mode also offers more flexibility to do smooth transitions to other operating modes by precisely controlling the MR valve. With faster reaction times is also possible to better response to disturbances in the external forces.
- This also offers enhance safe capabilities since is possible to almost instantaneously reduce the force being applied.
- Compared to other actuators, the active-backdrive sub-mode can save more energy because the pump usage may be reduced without loss of force.

#### 7.4.1.5 Extra Flow

Similar to the backdrive mode, the MR piston is being driven by an external force ($F_p + F_f < F_e$) and the MR valve is open MR valve is opened. This allows fluid to pass in an opposite direction to the displacement of the piston head, i.e. in the case the piston is being pushed ($Q_h = -Q_d$), while in the case is being pulled it will be the opposite ($-Q_h = Q_d$). However, pressurised fluid is pumped into the piston, in the same direction of the displacement, but at a lower rate ($Q_p < Q_d$). This decreases the amount of fluid in the passages ($Q_h$), reducing the braking force created by the piston head ($F_p = f(\tau_y) + \mu \cdot (Q_d - Q_p)$ ). This offer much more flexibility by allowing to achieve higher speeds than a conventional damper, while keeping a control of both the speed and the damping force independently by controlling the inflow rate and the shear stress of the MR fluid respectively. Following there are some usability examples**:**

- Fast reaction time of the MR valves allows a smooth control of the damping force.
- Compared to a MR damper where the minimum damping force is limited by the viscosity of the MR fluid. The MR piston can achieve smaller forces even at higher speeds in this mode, by reducing the amount of fluid passing through the MR valve passages.
- A sudden change in direction of the external force, can cause a transition from the active push sub-mode of the open piston mode into the extra flow mode. This situation could damage other systems, however the backdrivable nature of the MR piston allows this transition to occur smoothly, and once it is detected by the sensors it can be controlled accordingly without causing undesirable effects in the output, such as sudden changes in forces similar to impacts.
- This mode can also be used to release excessive pressure from the MR piston, in case an external force is backdriving it too strongly, helping to protect the system.

### 7.4.2 Operation Modes Advantage

As it can be seen, the MR Piston can provide superior safety due to its mechanical compliance. Especially when the passages are open, the maximum impact force can be limited using the appropriate magnetic field, i.e. shear stress.

It also provides superior reaction time compared to a conventional piston because the force can be accurately controlled by changing the magnetic field instead of the motor or valves, which have higher reaction times.

TABLE 7-V. CHARACTERISTICS OF THE PISTON OPERATION MODES

| | *Max Speed* | *Max Force* | *Reaction Time* | *Backdrivability* | *Collision Safety* |
|---|---|---|---|---|---|
| ***Passive Hold*** | N/A | ○○ | ○ | ○○ | ○○ |
| ***Passive Push/Pull*** | ○ | ○○○ | ○ | ○○○ | ○○○ |
| ***Extra Flow*** | ○○○○ | ○ | ○○ | ○○○ | ○○○ |
| ***MR Damper*** | ○ | ○○○ | ○○ | ○○ | ○○ |
| ***MR Piston*** | ○○○ | ○○○ | ○○○ | ○○○ | ○○○ |
| ***Open Piston*** | ○○ | ○○○○ | ○○○○ | ○○○○ | ○○○○ |
| ***Normal Piston*** | ○○○○ | ○○○○ | ○ | ○ | ○ |

In order to achieve the full potential of the MRPA is necessary to study in more detail the characteristics of every mode. Nevertheless, the current theoretical description of these operation modes is only a suggestion. Perhaps, there are other ways to describe the operation of the MRPA in a different variable space. Depending on the application requirements different kind of operation characteristics may be necessary. Therefore, special attention must be paid to the implementation of the controller when deciding which modes should be implemented and how they will interact among each other. Moreover, the correct design of the controller and its implementation will greatly influence the final performance of the MRPA.

### 7.4.3 Intelligent Controller Implementation

In order to realise a control strategy for the MR piston is necessary to have a higher-level controller to switch between the modes of operation previously described. A theoretical control strategy could be implemented as in Figure 7-13.

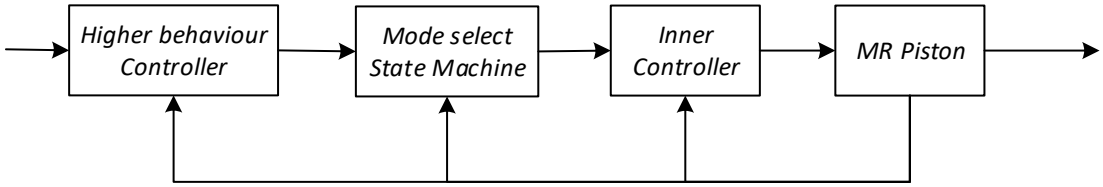


Figure 7-13. MRPA theoretical control strategy

In this theoretical controller, a state machine is used to switch between operating modes based on both inputs and outputs read from the actuator sensors. Meanwhile, a higher behaviour

controller adjusts the transition parameters of the state machine according to the commands of the user and other external sensors. Finally, the inner controllers transform the commands of the state machine into control variables, which can be directly applied to the system.

Example of common transition triggers for the state machine is shown in Table 7-VI.

TABLE 7-VI. COMMON TRANSITIONS FOR THE MR PISTON CONTROLLER

| | | ***Transition From*** | | | | |
|---|---|---|---|---|---|---|
| ***Transition to*** | | ***Passive Hold*** | ***Passive Push/Pull*** | ***Piston*** | ***Open Piston*** | ***Extra Flow*** |
| | ***Passive Hold*** | | Target position reached.<br>High stiffness needed. | Target position reached.<br>Less energy use needed.<br>High stiffness needed. | Target position reached.<br>Less energy use needed.<br>High stiffness needed. | Target position reached.<br>Less energy use needed.<br>High stiffness needed. |
| | ***Passive Push/Pull*** | Shear stress $\tau$ is overcome by an external force. | | External force starts driving piston back.<br>Backdrive for safety. | While force drives piston back less energy use needed. | More force or less speed needed.<br>Less energy use needed. |
| | ***Piston*** | New target position.<br>Movement with high stiffness needed. | New target position.<br>Sudden stop required.<br>Movement with high stiffness needed. | | Instantaneous acceleration or more speed needed.<br>Movement with high stiffness needed. | New force command to active drive load.<br>Instantaneous acceleration or more speed needed. |
| | ***Open Piston*** | $\tau_{max}$ not enough to hold position.<br>New target pos entered.<br>Movement with low stiffness needed. | $\tau_{max}$ not enough to generate desired backdrive force.<br>Prepare to change driving mode.<br>Movement with low stiffness needed. | Movement with low stiffness needed.<br>Faster response needed.<br>Prepare to change driving mode. | | New force or speed command. |
| | ***Extra Flow*** | - | Backdrive speed too slow.<br>Backdrive force too high. | Sudden change of direction in external force. | Backdrive speed too slow.<br>Backdrive force too high. | |

The inner loop of the controller strategy is similar to the one used in this chapter. However it has been extended to include the speed controller. This diagram, Figure 7-14, shows the interaction between the main variables used to model and control the behaviour of the MRPA.

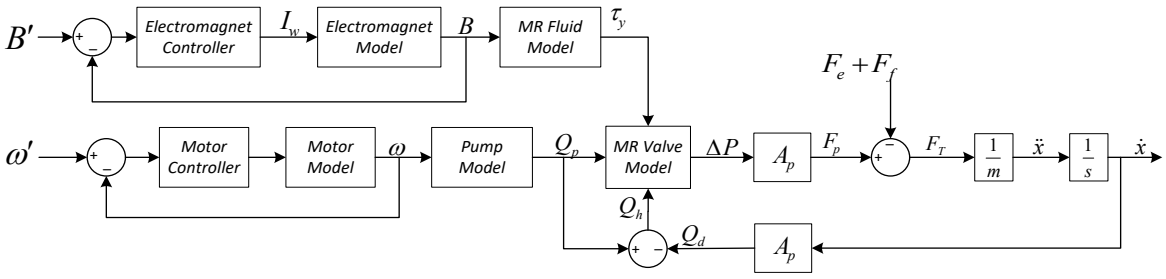


Figure 7-14. Inner loop of the control strategy

As it can be appreciated, the motor speed and the field are independent control variables, which affect the behaviour of the MR piston. By controlling these variables independently is possible to obtain a very precise control of the force and speed of the actuator, ensuring optimal response to the commands of higher controllers.

## 7.5 Discussion & Remarks

In conclusion, the experimental evidence support the premise that the new MRPA is a feasible alternative to current hydraulic actuators. It offers a wide range of force, while remaining backdrivable even during top forces. The simple control strategies used during its testing reinforce the idea that the toroidal piston head offers robust control of the force, without sacrificing force performance. However, as with other young technologies, further research is needed before the technology can be deployed in real world applications.

The passive force control experiments highlighted the improvements achieve during the optimisation of the piston. The force controller was not only able to achieve the same response as before, but it now the force range has been extended. On the other hand, the active tests show that the MRPA can achieve a semi-independent control of the force and speed characteristics. While the force can be mainly controlled by the electromagnet voltage, the actuator speed is directly related to the pump voltage. This is a very desirable characteristic, since it makes it possible to implement independent controllers for both variables.

The results from this preliminary analysis are used to create a close loop force controller, and an open loop speed controller for the pump. This is possible because the load cell provides accurate readings of the piston force. However, the piston speed is derived from a noisy position sensor, which difficult the implementation of the feedback signal for a close loop speed controller. Despite these limitations, the current performance of the controllers is remarkable.

Improvements of the instrumentation system could produce much better results than the ones observed in this paper.

The force controller is implemented using a simple PID controller with gains derived from the Ziegler-Nichols method and then fined tuned manually to achieve optimal performance. On the other hand, the speed controller is implemented using curve fitted to the experimental data. The results shows that the performance of such controllers is very satisfactory, achieving up to 99% accuracy within 0.5 seconds for the worst case, and 30ms for the force controller. However, in the future it is necessary to implement a state machine based controller in order to obtain a more satisfactory control of the system. Especially around the friction deadband, where the current controller does not offer any way to compensate for it.

The analysis of the force speed characteristics of the actuator revealed a relatively slow response to speed inputs. This is caused by the dynamics of the pump, which need to be improved. In this case, a system using valves could be an alternative if faster responses are required.

It is also important to mention that although the force and speed were treated as independent variables during the controller design, they have a strong interdependency. This is especially true at electromagnet currents and pump voltages. This interdependency can be exploit to create new operation modes never described before in literature. Theoretically, an intelligent controller could be implemented in order to switch between these modes, to provide different kinds of behaviours for the operation of the system. In this way, it could be possible to offer energy efficient operation, fast response times, softer backdrivability, or strong stiffness to mention a few examples. These modes of actuation could bring new control possibilities to the actuation field, enabling applications to perform tasks in ways that have not been possible before. The theoretical description of this controller is fully discussed in this paper, and its implementation can further enhance the development of the MRPA.

The fully integrated MRPA including the EHA was constructed taking into consideration the needs of powerful force output and the characteristics of the MRF. Therefore, a gear pump was used in order to avoid MRF for clogging the pump, as it would have likely happened with other pump technologies, such as piston pumps. Additionally, the pressure sensors and data acquisition systems were placed closer to the MRPA in order to have better measurements. In general, the system was made as compact as possible, but there is room for improvement of its

size. In general, it is necessary to optimise the hydraulic circuit by reducing the length and calibre of the pipes, which will help minimise the losses inside the circuit.

## 7.6 Chapter Summary

The MRPA has been develop to provide high power hydraulic actuation with backdrivable capabilities. The most important part of this actuator is the MR piston, which has been developed in this study. Thanks to an iterative development process the MR piston has finally been optimised to the point it matches the performance of other conventional technologies. Nevertheless, until this point only the passive force characteristics, i.e. damping performance, of the actuator has been tested. In order to determine this prototypes feasibility as an alternative hydraulic actuator, it is necessary to perform a comprehensive evaluation of the complete system.

The final evaluation of the MRPA is based on a system, which includes the necessary hydraulic system to drive the MR piston, as well as a modified test bench to evaluate its active performance. The hydraulic system compromises a bidirectional pump, a motor, and the necessary power electronics to supply power and control it. The modified test bench includes the necessary instrumentation to measure the piston variables, as well as the necessary GUI to control and log the data from the experiments. This new setup makes it possible to have full control of the electromagnet current inside the piston head, and the pump motor voltage using bidirectional PWM controllers. Additionally, the LabVIEW program allows to easily implement the necessary control scheme to drive both systems.

Several experiments are done to evaluate the open loop response of the system to different inputs. The information gathered from these tests shows that although the piston speed and force are interdependent variables, they can be controlled independently to a certain extent. This relation holds true mostly at low voltages, for both the electromagnet and the pump. In this sense, it can be assumed that the output force is closely related to the electromagnet current, while the piston speed is more closely related to the pump voltage. Using the data from the analysis a close-loop controller is implemented for the force, and a open-loop controller is implemented for the speed.

The MRPA force and speed controllers are tested using several experiments. The force step test revealed that the piston is able to achieve up to 99% accuracy within 0.5 seconds for

the worst case, and 30ms for the force controller. However, there is a dead band around 50N, caused by the actuator friction, where the system cannot achieve the desired force. These results agree with the backdrivability and collision tests, which also highlight the need to improve the friction performance of the actuator in order to enhance its backdrivable capabilities. Additionally, the slow response observed in the system seems to be cause by the slow dynamics of the pumping system. In order to improve the response, it might be necessary to use a unidirectional pump with conventional valves to direct the pumped fluid.

Finally, in this chapter it is discussed how the speed and force controller could be theoretically combined to create an intelligent controller. This controller could take advantage of the interdependency of the force and speed variables to create novel modes of actuations, which were discussed in detail in this study. These modes of actuation, could bring new control possibilities to the actuation field, enabling applications to perform tasks in ways that have not been possible before.

In summary, this chapter provides the necessary evidence to assess the performance of the complete actuation system. The experimental data supports the claims that the new MRPA is a feasible alternative to current hydraulic actuators. However, further research is needed in order to bring this technology into field applications.

# 8 COMPLIANT ROTATORY ACTUATOR

This section describes the concept, design, and construction of a new rotatory prototype. This prototype is based in the adaption of the technology developed throughout the previous sections of this works. It is presented to demonstrate how the MRPA technology can be adapted to create actuators with similar properties.

The work presented in this section is covered by the patent No. WSD – 16009, "回転型コンプライアント駆動装置". In this document the relevant information about the concept, novelty and utilization of the following design are published. Different from it, this thesis explain in detail the conceptualization process and the methodology followed to achieve a successful implementation of the technology.

This chapter is divided basically in the motivation to realise a new kind of actuator, the concept adaptation followed by a description of the preliminary design options, the mathematical evaluation of the proposed designs, and final design and construction of two alternative prototypes. Finally, a preliminary evaluation of the prototypes provides results to support the feasibility of the concept.

## 8.1 Motivation for Development

The original MRPA was develop with the intention of providing high power compliant actuation for medium size mobile application, such a small mobile construction machines, and disaster relief robots. These applications have relatively few degrees of freedom with relatively big bodies. These characteristics allow them to fit pistons of different length and diameter, making them a suitable target for this type of hydraulic actuators. Additionally, given the power requirements of such applications, they require actuators to produce forces in the order of kilo-Newtons. In this sense, pistons are also the preferred type of hydraulic actuator since they have the big cross-sections that maximise the pressure-generated forces.

Humanoid robots have different requirements than these high power applications. Usually, they have more degrees of freedom in spaces that are more restricted. This is especially true in their limbs, where many motors need to be integrated to actuate all the necessary motion to emulate the human body. On the other hand, their power requirements may be relatively low in comparison to the machines using pistons. Additionally, humanoid robots are usually placed in environments where they must interact with humans. Therefore, they are require to actuate with a higher degree of safety than construction oriented systems.

For these reasons, it is necessary to develop a new actuator that can meet the requirements of mobile humanoid robots [101]. The new actuator needs to be smaller in size, provide higher safety standards by increasing the backdrivability, and could have lower power output compared to the piston.

## 8.2 Concept Adaptation

The requirements detailed in the previous section provided the basis for the conceptualization of the new actuator. However, a detail analysis of the new requirements is necessary before a concrete actuator can be devised.

### 8.2.1 Size and Type of Actuator

The new actuator must be small to fit in the shoulder of a humanoid robot. The best way to fit in to the shoulder is by implementing a rotatory actuator [102].

### 8.2.2 Safety Considerations

The actuator must provide additional safety compared to the hydraulic piston. In this way, it should be easy to be backdriven and have the capacity to vary the damping coefficient fast. In order to further enhance the backdrivability the actuator must provide low friction. Finally, in order to avoid injuries during fast speed collisions it must minimise its weight [103].

### 8.2.3 Force and Power Requirements

The actuator will be implemented in the shoulder of humanoid robot. The main idea is to have a big humanoid robot that can work along humans assisting movement of heavy objects. On the other hand, aiming for very high forces will decrease the backdrivability of the system, since this is a trade-off relation during the actuator design. The right balance should be achieve when designing this step in order not to overstep the safety requirements stated above.

## 8.3 Concept Adaptation

The concept was adapted from the original MRPA, which formed by electro-hydrostatic-transmission between a bidirectional pump and modified hydraulic piston, as shown in the picture below.

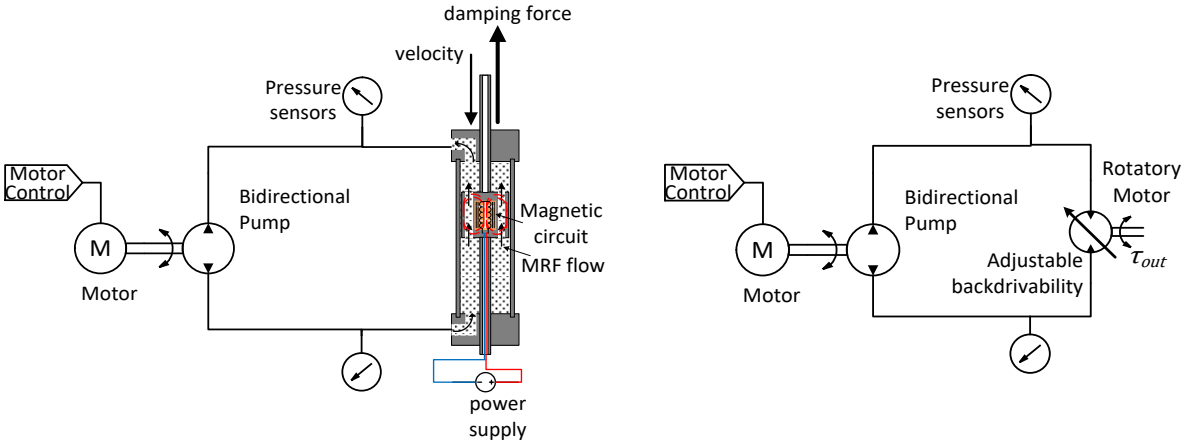


Figure 8-1. Hydraulic circuit comparing MRP with rotatory motor

The same hydrostatic transmission is used but the piston should be substituted for a rotatory motor as shown in the figure above. In order to realise such system it is necessary to select first a suitable rotatory motor for this application based on its requirements.

### 8.3.1 Adaptation Target

After looking at the requirements, it was decided to implement the system into a vane motor. Since it has the size, rotation input and necessary space are good to accommodate the new concept. The vane motor is simple, and is able to fit within the current constrains.

### 8.3.2 MR Piston Actuator Parts

The main parts of the actuator involved in the functionality are found inside the piston head. The MR piston head contains an integrated system to regulate the pressure difference between chambers. The systems consists in a toroidal array of magnetorheological valves that regulate the pressure drop between the piston chambers. They achieve this by controlling the magnetic field applied to the MR fluid moving through their passages. The figure bellows shows the principle of operation.

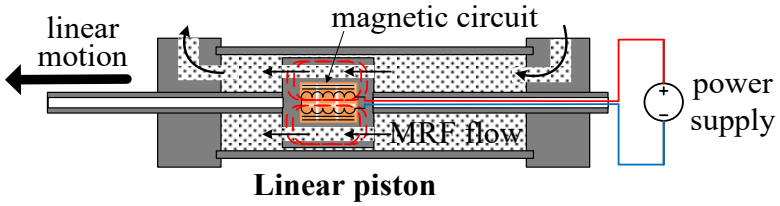


Figure 8-2. Schematic of the main parts of the MR piston concept

The piston head is the key part inside the MRP. Therefore, the new actuator must successfully implement its main functionality in order to work properly. The most important points is to effectively regulate the pressure difference between chambers. The pressure drop is related to the intensity of the magnetic field. Thus the head must:

- Generate the necessary electromotive force to produce enough magnetic field density.
- Create an magnetic circuit to transport and focus the magnetic field in the MRF gap
- The magnetic field must be perpendicular to the flow of MRF to maximise efficiency
- The electromagnetic circuit must minimise the magnetic leakage and contain the field to avoid it from affecting fluid outside the gap section

The points listed above are taken derive from the knowledge gather throughout the course of this research. As it has been previously proven in the optimisation sections, the efficiency of the adaptation of the concept depends mostly the balance between the magnetic core size and

the gap area. If all the points above are fulfilled a design can be considered to be a feasible alternative for implementation of the concept.

### 8.3.3 Adaptation of the Piston Head

The adaptation of the piston head is carried out by adapting the geometry of the MRP into the vane motor. In order to understand the adaption process is possible to bend the piston as to fit the circular shape of a typical vane motor, as seen in the figure below.

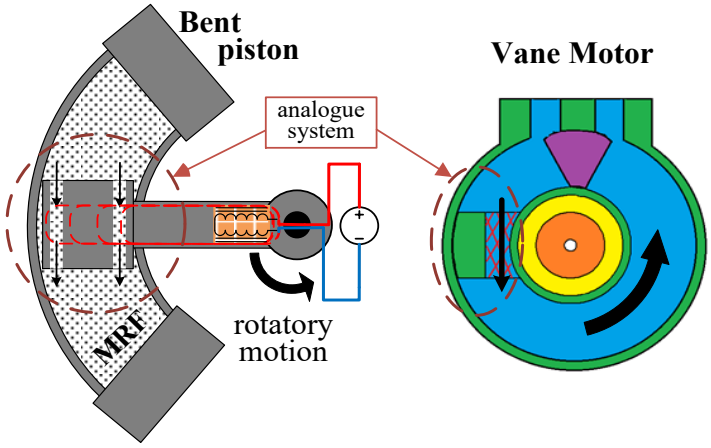


Figure 8-3. MR Piston concept adaptation into a conventional vane motor

As it can be seen in the picture the piston head can be adapted to a circular shape. In this way it allows the MRF fluid to move between chambers of the vane motor. In this sense, both system have an analogue functionally to control pressure and flow between chambers.

## 8.4 Implementation Candidates

The methodology above can be realised using two different alternatives. From the concept adaptation point of view, the most reasonable way to implement the MR valve is to create a gap in the motor vane. This conclusion is inferred from the similarities in the physical design of the piston.

Nevertheless, from a functional point of view the key point of the MR valve is to regulate the pressure drop between chambers. This implies that there is a connection between chambers, but it does not mean it has to be direct. Therefore, if a connection can be establish while satisfying the requirements from previous section then it should also be possible. There is the

possibility to connect both chambers through the centre shaft of the vane motor also. In this way, there are two way of achieving the same functionality.

### 8.4.1 Vane Hole Design

As it name suggest the vane hole design implements the MRF gap through the vane of the hydraulic motor. The picture below shows the main parts of the vane hole design.

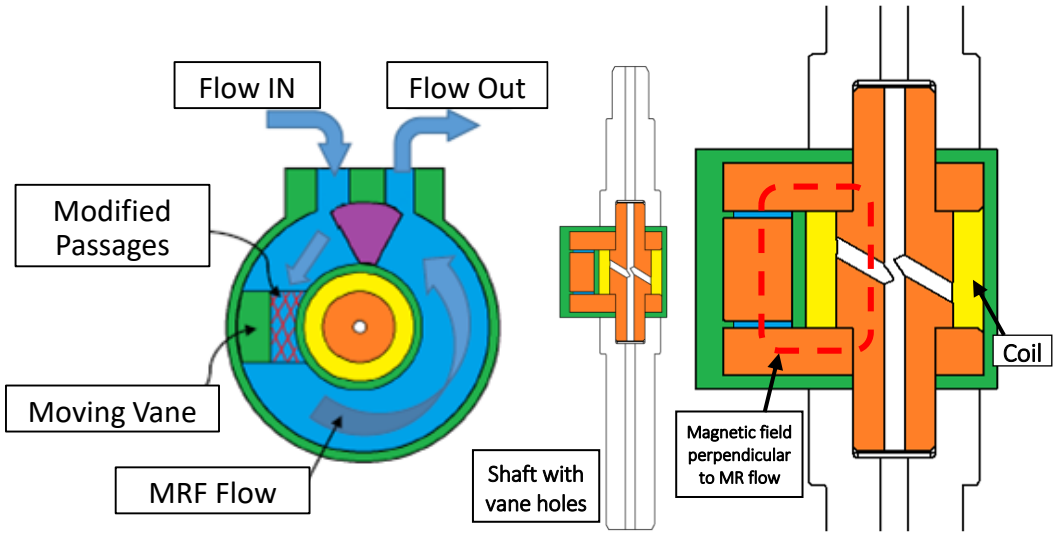


Figure 8-4. Vane hole design schematic details

The design allows for a big MRF gap, which improves backdrivability. Additionally it has quite a simple construction, due to the enclosed magnetic circuit.

### 8.4.2 Shaft Hole Design

The second alternative to connect both chambers of the vane motor is to implement a gap in the centre shaft of the motor.

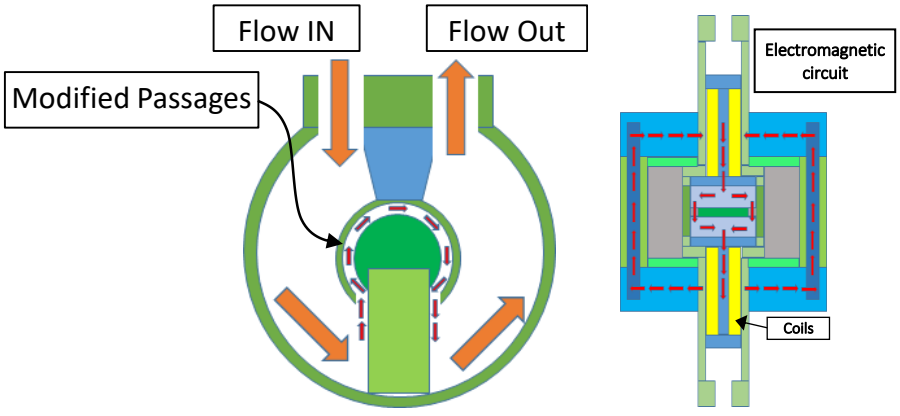


Figure 8-5. Shaft hole design schematic details

As it can be seen from the design the shaft hole type actuator needs to close the electromagnetic circuit using the vane motor frame. This configuration could potentially lead to lack of performance due to magnetic field leakage. Nevertheless, given the longer path of the fluid this actuator can potentially generate very high forces.

## 8.5 Actuator Design and Manufacturing

The actuator was design using the same principles and practices derived from the study before. Most of the practical design and construction issues are cover in Chapters 3 and 6. However here we make a brief summary of some of the important aspects. Additionally, information about the details of the implementation of the new design is provided.

### 8.5.1 Retrofit Conventional Vane Motor

The seal system, including the necessary manufacturing tolerances, is a key part of the hydraulic system. In the previous design it was completely design and built from scratch. The design process was time consuming and the manufacturing relatively expensive. Ultimately, the resulting performance of the friction system was under par to state-of-art commercial devices. In order to avoid this problem the new design is implemented by retrofitting a commercial vane motor.

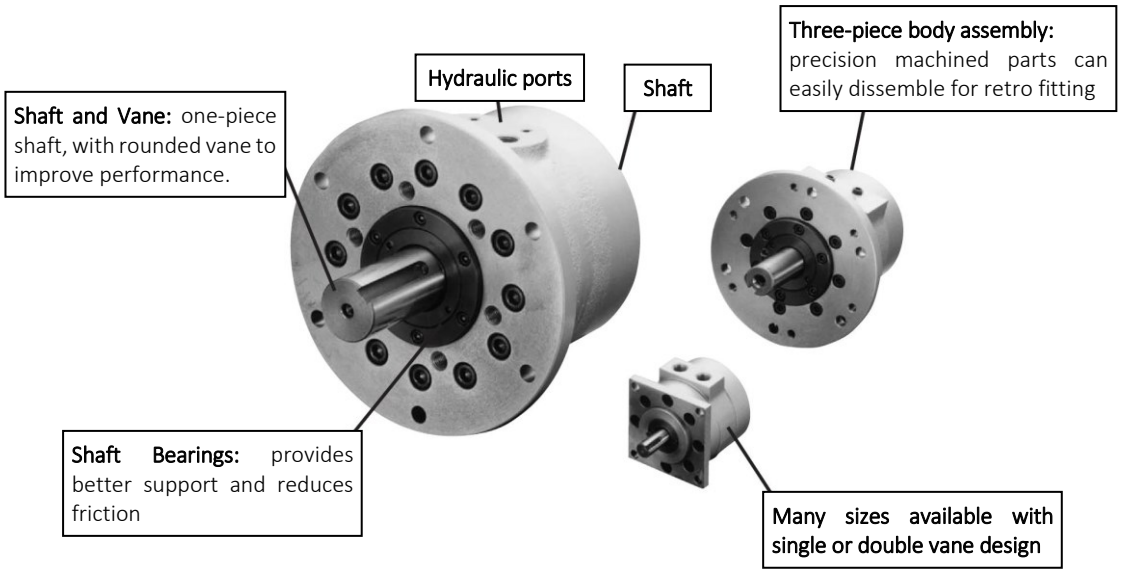


Figure 8-6. Base commercial vane motor used for retrofitting – Parker HRN Series

The motor already includes the necessary seals, tolerances, and bearings, as well as all the components necessary for assembly. The retrofitting process basically consist in replacing the shaft of the commercial vane motor with the new vane design. Additionally, the middle

section is also remanufactured using aluminium to reduce the friction of the MRF fluid caused by possible field leakage.

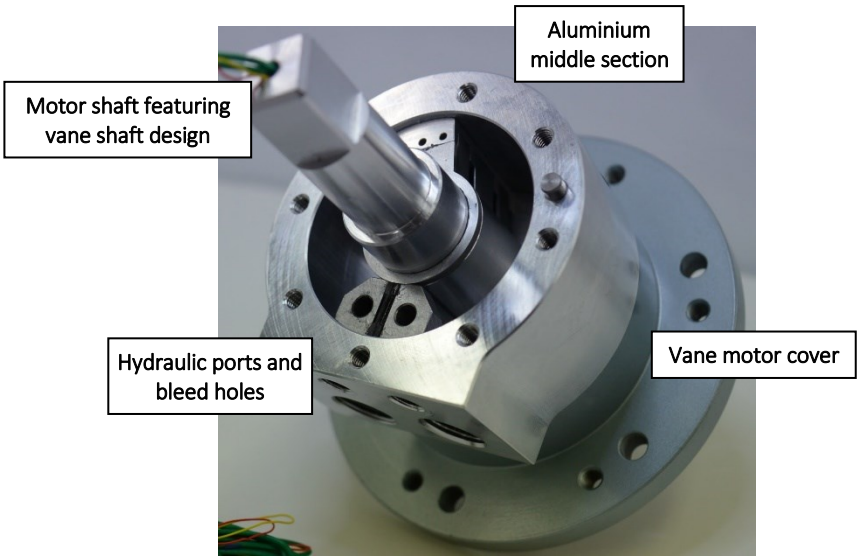


Figure 8-7. Retrofitted vane motor showing the new shaft featuring the vane hole design

In the figure above is clearly visible the vane motor part at the bottom, the new shaft featuring the vane hole design, and the remanufactured middle section in aluminium.

### 8.5.2 Prototype Assembly

The prototype was assembled using a concentric setup, which compromises, an encoder, the MR rotatory actuator, and an arm, as shown in the figure below.

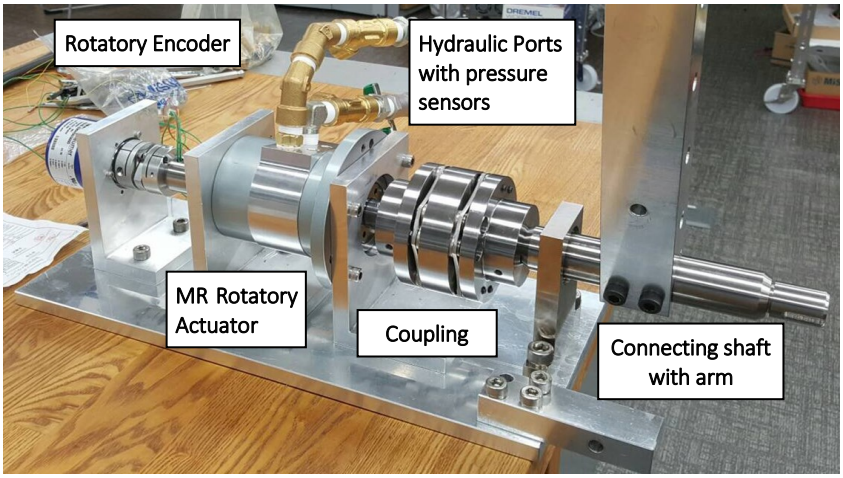


Figure 8-8. Magnetorheological Rotatory Actuator Assembly

All the parts of the assembly are built using high strength aluminium to prevent magnetic flux leakage, expect for the parts from the original vane motor, which are originally steel made. In the picture above it is possible to clearly appreciate the three parts of the vane motor. The middle section has been changed to fit the needs of the MR actuator.

## 8.6 Actuator Evaluation

The feasibility of the actuator is evaluated by measuring the generated torque in active mode. The results will show the capability of the new device to generate torque using the same principle as the linear actuator.

### 8.6.1 Test Bench for Rotatory Actuator

The test setup previously used in the linear actuator has been reused to fit the new actuator. The pump, electromagnet and data acquisition system remain as for the experiments in previous experiments. The modified experimental setup can be seen below.

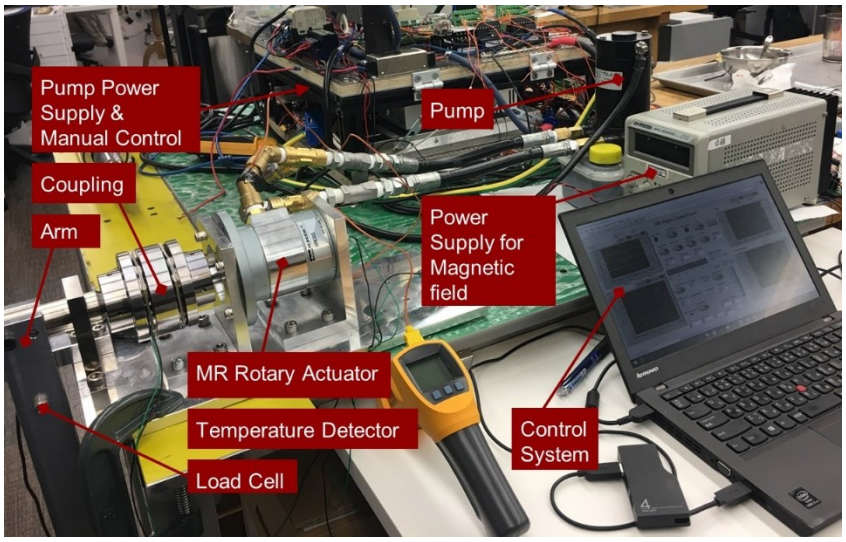


Figure 8-9. Test bench for the rotatory actuator

The torque sensor is placed at a predetermined distance of an arm connected to the shaft.

### 8.6.2 Experimental Results

The test presented in this study are still preliminary and are meant to serve as a proof of concept. A more detailed batch of experiment is necessary to fully assess the performance of the actuator. In this way, two test are performed to test the torque of the actuator.

In both tests the torque step response of the actuator is measured. In the first the steps used are pump steps. As it can be seen in the figure below the step response is not as linear when compared to the MRP.

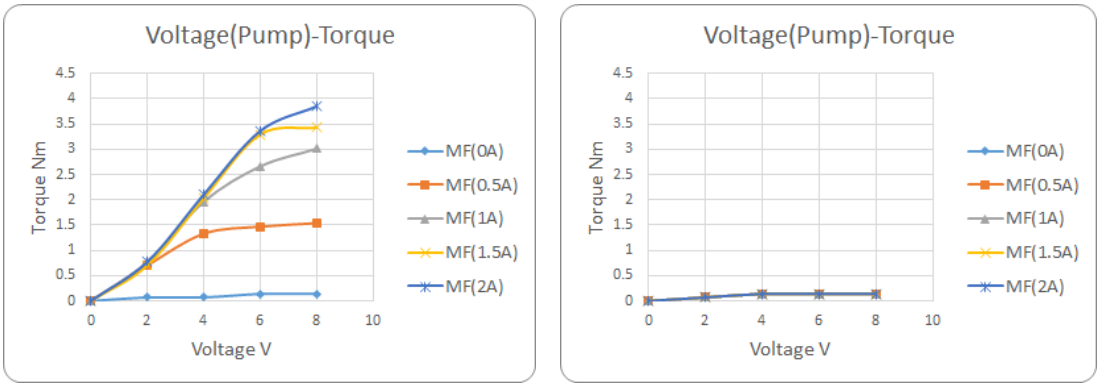


Figure 8-10. Output torque response to a pump voltage step for different EM currents. Left: vane hole type. Right: shaft hole type.

In the second experiment the pump is constantly running. Then a EMV step is introduced and the final stable torque is recorded.

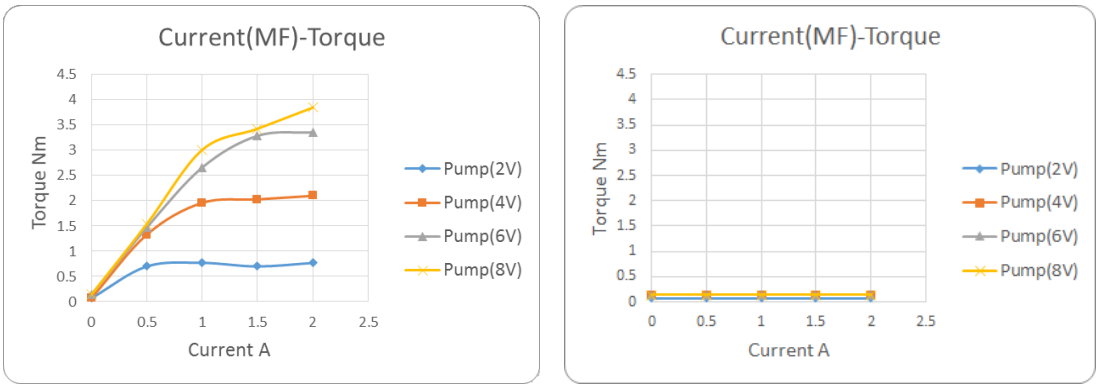


Figure 8-11. Output torque response to a EM voltage step for different pump voltage settings. Left: vane hole type. Right: shaft hole type.

In both experiments the shaft hole design was not able to generate enough torque. This means that it could not overcome the static friction, which is estimated at 4Nm (calculated from the vane hole design by comparing the pressure and torque measurements). The probable cause of this is a leakage in the many parts involved in its construction, or a poor performance of the electromagnetic circuit. Anyhow, this design should be reengineered in order to test its feasibility.

The results of the vane shaft design show the potential of the actuator to be implemented in a humanoid robot. However, the current torque performance is undermined by the friction of

the commercial vane motor. Since the motor is designed to operate at much higher pressures, it is causing excessive friction.

## 8.7 Discussion & Remarks

The adaptation of the MRPA concept into a rotatory vane motor demonstrates the flexibility and adaptability of the technology developed in this study. In previous chapters it was discussed how different the parameters of the MR piston could be changed to achieve different configurations that meet the requirements of specific applications. In this chapter, it is briefly described how the same functional and mathematical principles could be applied to completely modify the geometry of the MR piston to achieve backdrivable rotatory motion.

During the design and construction phases of this prototype the mathematical and simulation, models were used to estimate the feasibility and capabilities of two possible designs. These analysis suggested that there were two alternative for implementation with distinct characteristics. One that was more suited for backdrivability, while the other was able to reach higher forces. The preliminary results from both prototype showed that the vane-hole alternative was able to work as the models predicted. This clearly shows the potential of MR piston technology in different future applications. On the other hand, the shaft-hole design failed to achieve any output torque.

The discrepancy between the simulation and experimental data can be explained by the complexity of the electromagnetic circuit used to generate the magnetic field. In the case of the vane-hole type, the magnetic circuit path is perfectly closed by using the vane and shaft of the actuator. However, the shaft-hole type relies on longer path using the main body of the actuator. This assumes that the path can be perfectly closed using the tight screws, and that the permeability of all external components is high enough to sustain the field. Moreover, this design the sealing performance of this prototype depends on tightly fitting several parts, which increases the probability of having fluid and magnetic leakage. In the future, a less complex circuit with a more defined magnetic path should be able to correct this problem. Then, the shaft-hole design should be able to generate the expected performance.

In the future, the knowledge and techniques learnt during the adaptation of this technology will certainly serve as a base for its implementation in a variety of applications. This will help to widespread this technology, and further advance the research in this field.

## 8.8 Chapter Summary

The MRPA is a novel linear actuator that offer high power output with backdrivable capabilities. The current concept was develop throughout the course of this study. One of the relevant characteristics of the actuator is its versatility. This feature allows it to be customised to meet the requirements of specific applications. In order to demonstrate this, a new type of rotatory actuator is introduced in this chapter. The systems is based on the empirical and theoretical findings acquire through the course of the development of the original MRPA.

The development of the new actuator involved primarily the adaptation of the toroidal piston head configuration into the rotatory motion. In order to achieve this, the piston configuration was reshaped into a bent piston. This gave a perspective of the possible options to implement the system. Through this analogy, it was possible to understand that the most relevant feature of the MR piston was its ability to control the pressure difference between the piston chambers. Among the possible hydraulic systems that could realise such implementation, the hydraulic vane motor appear to be an ideal target for modification. These considerations resulted in the idea that it was possible to realise the same functionality using two different configuration inside the vane motor. One of then based in the original idea, placing the MR valve inside the motor vane. While a second more radical idea, was to implement the MR valve inside the central shaft of the motor.

Both of this ideas were design, modelled, simulated and built to test their feasibility. In order to simplify the implementation of the new rotatory prototype, a conventional vane motor was retrofitted with both designs. In this way, it was possible to avoid the tedious process of designing the prototype from scratch, while ensuring the sealing performance and optimal functionality of the new motor. The test bench of the MRPA was also adapted to accommodate the retrofitted vane motor and perform some preliminary test to determine the feasibility of the concept.

The results show that the vane type prototype is at the moment more suitable for implementation. The force measurements showed that it is able to achieve up to 4Nm torque despite the high friction caused by the sealing system in the conventional vane motor. On the other hand, the shaft hole design is currently no able to develop any measurable torque. This problem is attributed to the complex electromagnetic circuit used to generate the field at the

gap. Moreover, it is also speculated that there might be pressure leakage occurring between the many parts involved in its construction.

Nevertheless, this new concept prototype shows a higher potential for miniaturization, when compared with the MRPA. This makes especially suitable for implementation in medium size humanoid robots, which have limited space in its joints. Further development is necessary in order to achieve an stable, reliable and robust system that can be deployed in this and other possible applications where compact rotatory motion is required.

# 9 Conclusions & Future Work

In a world where safe robotic applications are becoming a ubiquitous need, there is still a limited amount of backdrivable actuation alternatives for mobile high power systems. This led to the development of a new actuation concept: an integrated MR piston actuator (MRPA) with theoretically adjustable backdrivability, and high output forces. The actuator was based in a novel design of MR damper piston head design specifically for active motion. It consists of a toroidal array of MR valves constructed of magnetically permeable and non-permeable materials selected for this particular application. This system was theorised to improve the energy efficiency while achieving a greater degree of configuration options when compared to other conventional systems. The theoretical and empirical evidence presented in this study supports the premise that it is feasible to realise adjustable backdrivable hydraulic actuators based on this concept. While the current potential of these early prototypes is still limited by some mechanical and optimisation related factors, they exhibit comparable performance to that of similar actuators in research.

## 9.1 Research Achievements

The most relevant benefits of the MRPA found in this study are attributable to the novel toroidal design in its piston head. The experimental evidence in chapters 4 and 6 shows that the toroidal does not only achieve similar force characteristics than that of the annular prototype, but also its force curves appear to have higher linearity. This is the result of the better utilization of the magnetic field in a larger active area, which avoids saturation of the magnetic materials, including the MR fluid. Moreover, this characteristic allows the MRPA to achieve much higher forces for short periods of time using high currents. All these characteristics can be used in practice to produce high forces with a stable yet inexpensive control scheme. This enhances the safety of applications despite the power output.

Additionally, the force experiments show that the toroidal design also provides adjustable backdrivability that further boosts the safety range of this actuator. The MRPA is able to keep backdrivable operation during passive and active tasks. Even in the case of unexpected collisions, a simple PID force controller was able to keep the interactions forces under control with very small overshoot. This demonstrates the safety and control advantages that adjustable backdrivability can bring to mobile applications in harsh environments. In this way is possible, to have reliable operation even in demanding situations with limited visibility, unreliable communication in tele-operated tasks, or simultaneous grasping with high power.

Another advantage of the toroidal design is its potential for customisation that allows it to modify its force output characteristics. In this study, an analysis and a practical example provide an insight into the different configuration options for the MRPA. The theoretical analysis presented in chapter 5 revealed the key parameter related to the actuator's performance. The hydraulic, electromagnetic, and visco-plastic models of the MRPA are constructed using explicit equations. This makes possible to understand the main variables affecting its performance. Together with an FEM analysis, they provide accurate estimation for the actuator performance. Later chapter 6 establishes the relations between the actuator parameters, and demonstrates how can they be optimise to achieve higher forces and efficiency. This example provides the basic design guidelines to follow when adapting the MRPA design to meet the requirements of particular applications. These models and guidelines are essential for the practical application of the prototype.

The design guidelines for the MRPA can even be applied beyond its geometrical design. This was verified by adapting the concept to a rotatory vane motor. During the conceptualization process two different approaches to implement the concept were discovered. The simulated prototypes displayed similar characteristics to its linear counterpart. One with higher forces, while the other with a more backdrivable output. Beside the high forces and backdrivable operation, these designs are smaller size. This makes them suitable for more mobile applications such as humanoid robots.

## 9.2 Research Limitations

The current performance of the MRPA prototype is still limited by several factors. Most of them can be easily solved by applying prevalent engineering knowledge and expertise in hydraulics systems and control theory. Nevertheless, there are some limitations that are intrinsic to the proposed design. It is important to understand the nature of both problems in order to successfully deploy the MRPA in real world applications.

The MRPA still has a higher energy consumption due to the unused space in the toroidal piston head, when compared to the annular design. The bobbin-shaped electromagnet core of the annular prototype fully uses the space of the piston head. On the other hand, the toroidal has a donut like shape that leaves some empty space in the middle. This does not only limit the core size, but also the number of coil windings in the core, significantly reducing the energy efficiency of the prototype.

Nevertheless, the current prototype has room for improvement. At the moment, the piston head employs seals to prevent MR fluid from entering it. These seals consume space and can be easily eliminated; given that the cable conduit and its connections remain sealed properly. Additionally, the centre space in the piston head can be considerately reduced by reducing the connecting piston rod. This could be possible by using more resistant materials for the piston rod, and using the toroidal passages as part of the mechanical support. These modifications will enhance the energy efficiency of the prototype, while preserving the advantages of the toroidal design, such as more linear forces and less saturation of the magnetic materials.

Friction is an important property of backdrivable systems. Poor friction performance significantly affects the backdrivability of the system. Although the current friction performance of the prototype is remarkable for a piston of its size, it can be improved to reduce

the minimum backdrivable force. Currently, the biggest source of friction in the systems are the piston rods. In order to improve their performance their diameter should be reduced. Additionally, the rod sealing packs should be redesign to eliminate the wipers, and use less tight o-rings. Perhaps, a study should be done to evaluate the possibility to allow for small leakage to occur, if it provides significant improvements to the friction performance.

The piston head also accounts creates significant friction. This can be reduced by employing a seal-less design based on a tampered head. This could potentially reduce the maximum stroke for a given piston size due to the centre alignment stability; but the gains in friction performance could justify it. Finally, the piston rod, cylinder and head should be machined and treated with coatings that enhance their friction performance with MR fluids. These improvements in the friction performance of the actuator will improve the backdrivability of the piston, and reduce the dead band in the force controller. These points are critical to simplify the control scheme, and ultimately enhance the intrinsic safety of the MRPA.

The hydraulic, electromagnetic, and visco-plastic models of the actuator are an useful tool to design and estimate the performance of the actuator. However, they are still sensitive to the correct estimation of the actuator parameters. Moreover, their results cannot be used to create a robust control strategy for the MRPA. Therefore, is necessary to apply state-of-art modelling techniques to achieve more accurate results. In order to create a model that can correctly estimate the flux leakage in the toroidal circuit is necessary to do precise measurements. A comprehensive analysis using hall sensors in several positions will bring insights and solutions to the problem.

Another uncertain part of the model is the accuracy of the parameter values. To clarify their values is necessary to have the permeable materials tested to have obtain their magnetization curves, which could have changed during the manufacturing process. More important is to evaluate the magnetization and yield stress curves, since they appear to considerable deviate from the manufacturer parameters. Finally, at the moment circular and rectangular shapes for the passages were evaluated. Modelling of additional shapes could open the door to new possible configuration options for the MRPA. These improvements, will not only enhance the accuracy of the models, but also improve the optimisation and design process. Additionally, they will ensure that the predictions, when varying other configuration options, are more accurate.

Finally, the size, weight, and level of integration of the current prototype are still not ideal. In order to improve this, a more compact pump with smaller hoses should be used. Integration of the sensors and power electronics is also a crucial step toward the miniaturization of the device. Additionally, the control scheme should also be simplified by using a microcontroller. These modifications will allow the prototype to directly be implemented into applications.

## 9.3 Future works

The recommendations presented in the previous section cover solutions to the problems found during the course of this research. In addition to these, there are other ideas and proposals to continue the development of the MRPA and backdrivable vane motor. These modifications will ensure that the actuator continue to mature to become a practical alternative for hydraulic robots in the future.

It is necessary to implement the system in a concrete application to evaluate its performance in different practical tasks. In this respect, it could be useful to cooperate with a company specialised in hydraulic systems. Their expertise and know-how could prove very useful to optimise, miniaturise the mechanical parts of the system.

A comprehensive analysis of the MRPA performance is necessary to evaluate its expected performance under operating conditions. Temperature influence the viscosity of hydraulic fluids. The effects of the operating pressure in the MR fluid has never been reported in research. This factor could also play a role during the operation of the MRPA. Thus, it is important to test the operational range of different fluids. Other important factor is the assessment of the wear of pump components due to micro-size particles in the MR fluid. Finally, the amount of leakage, and effects of contamination of the MRF fluid should also be included.

Insofar this research has employed MR fluids provided by LORD Corporation. However, there are several commercial and experimental alternatives to these fluids. Among them, nano-particle MR fluids show promising results in reducing the friction at the expense of small reductions in yield stress forces. These alternatives should be evaluated since they could also improve the operational life of the MRPA if it is deployed in a real application.

Finally, it is not only necessary to improve the force and speed controllers of the prototype, but to create an intelligent control scheme as well. The control scheme can be used

to provide smart context change between the operation modes of the piston described in this paper. In order to achieve this, a comprehensive study of a target application is necessary. Evaluating the energy, force, and safety needs of the system can be used to create an ad-hoc control scheme that simultaneously achieves these goals.

I hope that in the future this device can reach its full potential to bridge the gap in actuation system, offering many solutions for mobile applications where high power and safe backdrivable actuation are necessary.

# 10 References


[1] D. S. Walker, D. J. Thoma, and G. Niemeyer, “Variable Impedance Magnetorheological Clutch Actuator and Telerobotic Implementation,” in *2009 IEEERSJ International Conference on Intelligent Robots and Systems*, 2009, pp. 2885–2891.

[2] D. Torocsik, “Some Design Issues of Multi-plate magnetorheological clutches,” *Hungarian J. Ind. Chem.*, vol. 39, no. 1, pp. 41–44, 2011.

[3] A. S. Shafer and M. R. Kermani, “On the feasibility and suitability of MR and ER based actuators in human friendly manipulators,” in *2009 IROS IEEE/RSJ International Conference on Intelligent Robots and Systems*, 2009, pp. 2904–2909.

[4] P. Fauteux and M. Lauria, “Using a Dual Differential Rheological Actuator as a High-Performance Haptic Interface,” no. 5, pp. 2519–2520, 2010.

[5] J. Chen and W.-H. Liao, “A Leg Exoskeleton Utilizing a Magnetorheological Actuator,” in *IEEE International Conference on Robotics and Biomimetics*, 2006, pp. 824–829.

[6] M. H. Raibert and J. J. Craig, “Hybrid Position/Force Control of Manipulators,” *Trans. ASME, J. Dyn. Syst. Meas. Control*, vol. 102, no. 2, pp. 126–133, Jun. 1981.

[7] N. Hogan, “Impedance Control: An Approach to Manipulation,” *J. Dyn. Syst. Meas. Control*, vol. 107, no. 1, pp. 304–313, Mar. 1985.

[8] C. Ott, R. Mukherjee, and Y. Nakamura, “Unified Impedance and Admittance Control,” *2010 IEEE Int. Conf. Robot. Autom.*, pp. 554–561, May 2010.

[9] Y. Yao, Q. Huang, Y. Peng, and T. Oiwa, “Hybrid position, posture, force and moment control with impedance characteristics for robot manipulators,” *2011 IEEE Int. Conf. Mechatronics Autom.*, pp. 2129–2134, Aug. 2011.

[10] V. Duchaine, N. Lauzier, M. Baril, M.-A. Lacasse, and C. C. Gosselin, “A flexible robot skin for safe physical human robot interaction,” in *2009 IEEE International Conference on Robotics and Automation*, 2009, pp. 3676–3681.

[11] A. Albu-Schäffer and G. Hirzinger, “Cartesian impedance control techniques for torque controlled light-weight robots,” in *IEEE International Conference on Robotics and Automation (ICRA 2002)*, 2002, no. May, pp. 657–663.

[12] Y. Kobayashi, T. Watanabe, T. Ando, M. Seki, and M. G. Fujie, “Fractional impedance control for reproducing the material properties of muscle and its application in a body weight support system,” *2010 3rd IEEE RAS EMBS Int. Conf. Biomed. Robot. Biomechatronics*, pp. 553–559, Sep. 2010.

[13] M. Laffranchi, N. G. Tsagarakis, and D. G. Caldwell, “Safe human robot interaction via energy regulation control,” in *IEEE/RSJ International Conference on Intelligent Robots and Systems*, 2009, pp. 35–41.

[14] A. De Luca, A. Albu-Schäffer, S. Haddadin, and G. Hirzinger, “Collision detection and safe reaction with the DLR-III lightweight manipulator arm,” in *IEEE International Conference on Intelligent Robots and Systems*, 2006, pp. 1623–1630.

[15] R. Van Ham, T. G. Sugar, B. Vanderborght, K. W. Hollander, and D. Lefeber, “Compliant Actuator Designs - Review of Actuators with Passive Adjustable Compliance/Controllable Stiffness for Robotic Applications,” *IEEE Robotics & Automation Magazine*, no. September, pp. 81–94, Sep-2009.

[16] G. Endo, H. Yamada, and S. Hirose, “Development of a light duty arm with an active-fingertip gripper for handling discoid objects,” *2010 IEEE/RSJ Int. Conf. Intell. Robot. Syst.*, pp. 2600–2605, Oct. 2010.

[17] S. Haddadin, A. Albu-Schäffer, and G. Hirzinger, “The role of the robot mass and velocity in physical human-robot interaction - Part I: Non-constrained blunt impacts,” *Proc. - IEEE Int. Conf. Robot. Autom.*, pp. 1331–1338, 2008.

[18] H. B. Tokyo, “Design of Prograrnmable Passive Compliance Shoulder Mechanism,” pp. 348–353, 2001.

[19] G. A. Pratt and M. M. Williamson, “Series elastic actuators,” in *IEEE/RSJ International Conference on Intelligent Robots and Systems.*, 1995, vol. 1, no. 1524, pp. 399–406.

[20] T. A. McMahon, “The role of compliance in mammalian running gaits,” *J. Exp. Biol.*, vol. 115, no. 1, pp. 263–282, 1985.

[21] A. M. M. Omer, R. Ghorbani, H. Lim, and A. Takanishi, “Semi-passive Dynamic Walking for Biped Walking Robot Using Controllable Joint Stiffness Based on Dynamic Simulation,” in *2009 IEEE/ASME International Conference on Advanced Intelligent Mechatronics*, 2009, pp. 1600–1605.

[22] Y. Nakanishi, N. Ito, T. Shirai, M. Osada, T. Izawa, S. Ohta, J. Urata, K. Okada, and M. Inaba, "Design of Powerful and Flexible Musculoskeletal Arm by Using Nonlinear Spring Unit and Electromagnetic Clutch Opening Mechanism," *2011 11th IEEE-RAS Int. Conf. Humanoid Robot.*, pp. 377–382, Oct. 2011.

[23] H. Frontzek, E. Knubben, and E. Al., "Energy-efficient jump kinematics based on a natural model," 2014. [Online]. Available: https://www.festo.com/group/en/cms/10219.htm. [Accessed: 20-May-2003].

[24] K. Graichen, S. Hentzelt, A. Hildebrandt, N. Kärcher, N. Gaißert, and E. Knubben, "Control design for a bionic kangaroo," *Control Eng. Pract.*, vol. 42, pp. 106–117, 2015.

[25] A. Albu-Schaffer, S. Wolf, O. Eiberger, S. Haddadin, F. Petit, and M. Chalon, "Dynamic Modelling and Control of Variable Stiffness Actuators," *2010 IEEE Int. Conf. Robot. Autom.*, pp. 2155–2162, May 2010.

[26] R. Van Ham, B. Vanderborght, M. Van Damme, B. Verrelst, and D. Lefeber, "MACCEPA, the mechanically adjustable compliance and controllable equilibrium position actuator: Design and implementation in a biped robot," *Rob. Auton. Syst.*, vol. 55, no. 10, pp. 761–768, 2007.

[27] T. Morita and S. Sugano, "Design and Developme a new Robot Joint using Mechanical Impedance Adjuster," in *IEEE international Conference on Robotics and Automation*, 1995, pp. 2469–2475.

[28] T. Morita and S. Sugano, "Development of One-D.O.F. Robot Arm equipped with Mechanical Impedance Adjuster," in *IEEE/RSJ International Conference on Intelligent Robots and Systems*, 1995, pp. 407–412.

[29] S. S. Groothuis, G. Rusticelli, A. Zucchelli, S. Stramigioli, and R. Carloni, "The vsaUT-II: A novel rotational variable stiffness actuator," in *IEEE International Conference on Robotics and Automation*, 2012, pp. 3355–3360.

[30] J. W. Hurst, A. A. Rizzi, and D. Hobbelen, "Series elastic actuation: Potential and pitfalls," in *International Conference on Climbing and Walking Robots*, 2004.

[31] H. Kaminaga, T. Amari, Y. Katayama, J. Ono, Y. Shimoyama, and Y. Nakamura, "Backdrivability analysis of Electro-Hydrostatic Actuator and series dissipative actuation model," in *IEEE International Conference on Robotics and Automation (ICRA 2010)*, 2010, pp. 4204–4211.

[32] H. Sodeyama, K. Suzuki, and K. Sunakoda, "Development of Large Capacity semi-active Seismic damper using Magneto –Rheological Fluid.pdf," *J. Press. Vessel Technol.*, vol. 126, no. 1, pp. 105–109, Feb. 2004.

[33] J. Oblak and Z. Matjačić, "Design of a series visco-elastic actuator for multi-purpose rehabilitation haptic device.," *J. Neuroeng. Rehabil.*, vol. 8, no. 3, pp. 1–13, Jan. 2011.

[34] H. Kaminaga, S. Otsuki, and Y. Nakamura, "Development of High-Power and Backdrivable Linear Electro-Hydrostatic Actuator," *2014 14th IEEE-RAS Int. Conf. Humanoid Robot.*, pp. 973–978, Nov. 2014.

[35] H. Kaminaga, H. Tanaka, K. Yasuda, and Y. Nakamura, “Screw pump for Electro-Hydrostatic Actuator that enhances backdrivability,” in *11th IEEE-RAS International Conference on Humanoid Robots*, 2011, pp. 434–439.

[36] R. T. Foister, “Magnetorheological Fluids,” US 5,667,715, 16-Sep-1997.

[37] J. L. Pons, “Electro-and magnetorheological actuators (ERFs, MRFs),” in *Emerging Actuator Technologies: A Micromechatronic Approach*, Chichester, England: John Wiley & Sons, Ltd., 2005, pp. 205–243.

[38] D. Baranwal and T. S. Deshmukh, “MR-Fluid Technology and Its Application - A Review,” *Int. J. Emerg. Technol. Adv. Eng.*, vol. 2, no. 12, pp. 563–569, 2012.

[39] J. Blake and H. B. Gurocak, “Haptic Glove With MR Brakes for Virtual Reality,” *IEEE/ASME Trans. Mechatronics*, vol. 14, no. 5, pp. 606–615, Oct. 2009.

[40] Y.-M. Han, J.-S. Oh, J.-K. Kim, and S.-B. Choi, “Design and experimental evaluation of a tactile display featuring magnetorheological fluids,” *Smart Mater. Struct.*, vol. 23, no. 7, p. 77001, Jul. 2014.

[41] J. Gołdasz and B. Sapiński, “Modeling of magnetorheological mounts in various operation modes,” *Acta Mech. Autom.*, vol. 5, no. 4, pp. 29–39, 2011.

[42] P. Kuzhir, G. Bossis, and V. Bashtovoi, “Effect of the orientation of the magnetic field on the flow of a magnetorheological fluid. I. Plane channel,” *J. Rheol. (N. Y. N. Y).*, vol. 47, no. 6, pp. 1373–1384, 2003.

[43] R. Robinson, W. Hu, and N. M. Wereley, “Linking Porosity and Tortuosity to the Performance of a Magneto-Rheological Damper Employing a Valve Filled With Porous Media,” *IEEE Trans. Magn.*, vol. 46, no. 6, pp. 2156–2159, Jun. 2010.

[44] W. Hu, E. Cook, and N. M. Wereley, “Energy Absorber Using a Magnetorheological Bypass Valve Filled With Ferromagnetic Beads,” *IEEE Trans. Magn.*, vol. 43, no. 6, pp. 2695–2697, 2007.

[45] P. Kuzhir, G. Bossis, V. Bashtovoi, and O. Volkova, “Flow of magnetorheological fluid through porous media,” *Eur. J. Mech.*, vol. 22, no. 4, pp. 331–343, Jul. 2003.

[46] J. D. Carlson and M. R. Jolly, “MR fluid, foam and elastomer devices,” *Mechatronics*, vol. 10, no. 4–5, pp. 555–569, 2000.

[47] W. Li, “Design and Development of Magneto-Rheological Actuators with Application in Mobile Robotics,” The University of Western Ontario, London, ON, Canada, 2014.

[48] H. Tomori, S. Nagai, T. Majima, and T. Nakamura, “Variable impedance control with an artificial muscle manipulator using instantaneous force and MR brake,” in *IEEE International Conference on Intelligent Robots and Systems*, 2013, pp. 5396–5403.

[49] K. Voth, A. Wiehe, and C. Graf, “Realtime Compensation Methods for Hysteresis based Magnetorheological Actuators,” in *IEEE/ASME International Conference on Advanced Intelligent Mechatronics*, 2009, pp. 1010–1015.

[50] P. Yadmellat and M. R. Kermani, “Output Torque Modeling of a Magneto-Rheological Based Actuator,” in *18th International Federation of Automatic Control World Congress*, 2011, pp. 1052–1057.

[51] A. S. Shafer and M. R. Kermani, “Design and validation of a Magneto-Rheological clutch for practical control applications in human-friendly manipulation,” in *2011 IEEE International Conference on Robotics and Automation*, 2011, pp. 4266–4271.

[52] N. Najmaei, P. Yadmellat, M. R. Kermani, and R. V Patel, “Suitability of Small-Scale Magnetorheological Fluid-Based Clutches in Haptic Interfaces for Improved Performance,” *IEEE/ASME Trans. Mechatronics*, vol. 20, no. 4, pp. 1–12, Oct. 2014.

[53] N. Lauzier and C. Gosselin, “Series Clutch Actuators for Safe Physical Human-Robot Interaction,” in *Proceedings - IEEE International Conference on Robotics and Automation*, 2011, pp. 5401–5406.

[54] A. M. Clemente, A. F. Caballero, D. B. Rojas, D.-S. Copaci, and L. M. Lorente, “Elbow functional compensation using a lightweight magnetorheological clutch,” *2011 Annu. Int. Conf. IEEE Eng. Med. Biol. Soc.*, vol. 2011, pp. 5215–5218, 2011.

[55] T. Kikuchi, K. Oda, and J. Furusho, “Leg-Robot for Demonstration of Spastic Movements of Brain-Injured Patients with Compact Magnetorheological Fluid Clutch,” *Adv. Robot.*, vol. 24, no. 5–6, pp. 671–686, 2010.

[56] T. Saito and H. Ikeda, “Development of Normally Closed Type of Magnetorheological Clutch and its Application to Safe Torque Control System of Human-Collaborative Robot,” *J. Intell. Mater. Syst. Struct.*, vol. 18, no. 12, pp. 1181–1185, Dec. 2007.

[57] W. H. Li and H. Du, “Design and experimental evaluation of a magnetorheological brake,” *Int. J. Adv. Manuf. Technol.*, vol. 21, no. 7, pp. 508–515, 2003.

[58] G. Dirk, M. Aust, and J. Maas, “Novel Concepts for MRF based Clutch Systems with Integrative Functionalities,” in *2010 IEEE/ASME International Conference on Advanced Intelligent Mechatronics*, 2010, pp. 1191–1196.

[59] Y.-M. Han and S.-B. Choi, “Force-feedback control of a spherical haptic device featuring an electrorheological fluid,” *Smart Mater. Struct.*, vol. 15, no. 5, pp. 1438–1446, Sep. 2006.

[60] J. Yoo and N. M. Wereley, “Design of a High-Efficiency Magnetorheological Valve,” *J. Intell. Mater. Syst. Struct.*, vol. 13, no. 10, pp. 679–685, Oct. 2002.

[61] C. R. Liao, D. X. Zhao, L. Xie, and Q. Liu, “A design methodology for a magnetorheological fluid damper based on a multi-stage radial flow mode,” *Smart Mater. Struct.*, vol. 21, no. 8, p. 85005, Aug. 2012.

[62] M. Y. Salloom and Z. Samad, “Finite element modeling and simulation of proposed design magneto-rheological valve,” *Int. J. Adv. Manuf. Technol.*, vol. 54, no. 5, pp. 421–429, Oct. 2010.

[63] G. Hu, M. Long, L. Yu, and W. Li, “Design and performance evaluation of a novel magnetorheological valve with a tunable resistance gap,” *Smart Mater. Struct.*, vol. 23, p. 127001, 2014.

[64] D. T. Nosse and M. J. Dapino, “Magnetorheological Valve for Hybrid Electrohydrostatic Actuation,” *J. Intell. Mater. Syst. Struct.*, vol. 18, pp. 1121–1136, Nov. 2007.

[65] J.-H. Yoo and N. M. Wereley, “Performance of a Magnetorheological Hydraulic Power Actuation System,” *J. Intell. Mater. Syst. Struct.*, vol. 15, no. 11, pp. 847–858, Nov. 2004.

[66] H. P. Gavin, R. D. Hanson, and F. E. Filisko, “Electrorheological Dampers, Part I: Analysis and Design,” *J. Appl. Mech.*, vol. 63, no. 3, p. 669, 1996.

[67] H. P. Gavin, R. D. Hanson, and F. E. Filisko, “Electrorheological Dampers, Part II: Testing and Modeling,” *J. Appl. Mech.*, vol. 63, no. 3, p. 676, 1996.

[68] S.-B. Choi, M.-H. Nam, and B.-K. Lee, “Vibration Control of a MR Seat Damper for Commercial Vehicles,” *J. Intell. Mater. Syst. Struct.*, vol. 11, no. 12, pp. 936–944, Dec. 2000.

[69] J. Poynor, “Innovative Designs for Magneto-Rheological Dampers,” Virginia Polytechnic Institute and State University, 2003.

[70] J. W. Sohn, J.-S. Oh, and S.-B. Choi, “Design and novel type of a magnetorheological damper featuring piston bypass hole,” *Smart Mater. Struct.*, vol. 24, no. 3, p. 35013, Feb. 2015.

[71] S. A. Khan, A. Suresh, and N. S. Ramaiah, “Investigation on the Performance of MR Damper with various Piston configurations,” *Int. J. Sci. Res. Publ.*, vol. 2, no. 12, pp. 1–7, Dec. 2012.

[72] D. Case, B. Taheri, and E. Richer, “Dynamical modeling and experimental study of a small-scale magnetorheological damper,” *IEEE/ASME Trans. Mechatronics*, vol. 19, no. 3, pp. 1015–1024, 2014.

[73] D.-H. Wang and X.-X. Bai, “A magnetorheological damper with an integrated self-powered displacement sensor,” *Smart Mater. Struct.*, vol. 22, p. 14, May 2013.

[74] M. Mao, W. Hu, Y.-T. Choi, and N. M. Wereley, “A Magnetorheological Damper with Bifold Valves for Shock and Vibration Mitigation,” *J. Intell. Mater. Syst. Struct.*, vol. 18, no. 12, pp. 1227–1232, 2007.

[75] M.-H. Jin, D.-R. Lee, and T.-H. Kang, “Piston Valve Assembly of Continuous Damping Control Damper,” US 7,950,508 B2, 31-May-2011.

[76] S. Zhu, L. Tang, J. Liu, X. Tang, and X. Liu, “A novel design of magnetorheological damper with annular radial channel,” *Shock Vib.*, vol. 2016, no. 8086504, p. 7, Sep. 2016.

[77] A. Sadeghi, L. Beccai, and B. Mazzolai, “Innovative soft robots based on electro-rheological fluids,” in *IEEE/RSJ International Conference on Intelligent Robots and Systems*, 2012, pp. 4237–4242.

[78] G. Aguirre Dominguez, M. Kamezaki, M. French, and S. Sugano, “Development of a Backdrivable Magnetorheological Hydraulic Piston for Passive and Active Linear Actuation,” in *IEEE/RSJ International Conference on Intelligent Robots and Systems (IROS)*, 2015, pp. 6551–6556.

[79] N. Alle, S. S. Hiremath, S. Makaram, K. Subramaniam, and A. Talukdar, “Review on electro hydrostatic actuator for flight control,” *Int. J. Fluid Power*, vol. 17, no. 2, pp. 125–145, 2016.

[80] D. H. Wang and W. H. Liao, “Magnetorheological fluid dampers: a review of parametric modelling,” *Smart Mater. Struct.*, vol. 20, no. 2, p. 34, 2011.

[81] G. Daniel, C. Yoan, P. Zoltan, and P. Yves, “Bingham-papanastasiou and approximate parallel models comparison for the design of magneto-rheological valves,” in *IEEE/ASME International Conference on Advanced Intelligent Mechatronics*, 2014, pp. 168–173.

[82] E. Eberl and U. Eberl, “Parameters of transport of non-newtonian fluids through the pipes,” *Mining-Geological-Petroleum Eng. Bull.*, vol. 7, pp. 65–69, 1995.

[83] Q. S. Khan, *Design and Manufacturing of Hydraulic Presses*, vol. 2. Mumbai, India: Tanveer Publications.

[84] J. D. Carlson and M. J. Chrzan, “Magnetorheological fluid dampers,” US 5,277,281, 11-Jan-1994.

[85] B. Sapinski, “Magnetorheological fluid damper with radially shaped gap and contact less sealing,” *J. Theor. Appl. Mech.*, vol. 43, no. 2, pp. 223–240, Jan. 2005.

[86] G. Aguirre Dominguez, M. Kamezaki, and S. Sugano, “Proposal and Preliminary Feasibility Study of a Novel Toroidal Magnetorheological Piston,” *IEEE/ASME Trans. Mechatronics*, vol. PP, no. 99, 2016.

[87] J.-H. Koo, F. D. Goncalves, and M. Ahmadian, “A comprehensive analysis of the response time of MR dampers,” *Smart Mater. Struct.*, vol. 15, no. 2, pp. 351–358, 2006.

[88] O. J. Oaks and G. Cook, “Piecewise Linear Control of Nonlinear Systems,” *IEEE Trans. Ind. Electron. Control Instrum.*, vol. IECI-23, no. 1, pp. 56–63, Feb. 1976.

[89] H. Hu, C. L. C. Liang, and W. J. W. Jiong, “Control system design and performance test of a magnetorheological fluid fan clutch,” *Control Autom. ICCA 2010 8th IEEE Int. Conf.*, pp. 1409–1413, 2010.

[90] P. Yadmellat and M. R. Kermani, “Adaptive Control of a Hysteretic Magnetorheological Robot Actuator,” *IEEE/ASME Trans. Mechatronics*, vol. 21, no. 3, pp. 1336–1344, 2016.

[91] G. Aguirre Dominguez, M. Kamezaki, M. French, and S. Sugano, “Modelling and Simulation of a New Magnetorheological Linear Device,” in *IEEE International Symposium on Robotics and Intelligent Sensors (IEEE IRIS2015)*, 2015, pp. 235–240.

[92] X. Wang and F. Gordaninejad, “Flow Analysis of Field-Controllable, Electro- and Magneto-Rheological Fluids Using Herschel-Bulkley Model,” *J. Intell. Mater. Syst. Struct.*, vol. 10, no. 8, pp. 601–608, Aug. 1999.

[93] N. M. Wereley and L. Pang, “Nondimensional analysis of semi-active electrorheological and magnetorheological dampers using approximate parallel plate models,” *Smart Mater. Struct.*, vol. 7, no. 5, pp. 732–743, Oct. 1998.

[94] G. M. Kamath, M. K. Hurt, and N. M. Wereley, “Analysis and testing of Bingham plastic behavior in semi-active electrorheological fluid dampers,” *Smart Mater. Struct.*, vol. 5, no. 5, pp. 576–590, 1999.

[95] R. W. Phillips, “Engineering Applications of Fluids with a Variable Yield Stress,” University of California, Berkeley, Berkeley, CA, USA, 1969.

[96] G. A. Dominguez, M. Kamezaki, M. French, and S. Sugano, “An Iterative Design Methodology for the Performance Optimisation of Magnetorheological Piston Head Configurations,” in *IEEE/ASME International Conference on Advanced Intelligent Mechatronics, AIM 2016*, 2016, pp. 228–233.

[97] J. R. Brauer, “Reluctance Method,” in *Magnetic Actuators and Sensors*, IEEE, 2006, pp. 29–38.

[98] D. J. Inman and D. Leo, “Finite Element Analysis Based Modeling of Magneto Rheological Dampers,” Virginia Polytechnic Institute and State University, Blacksburg, Virginia, USA, 2002.

[99] G. A. Dominguez, M. Kamezaki, S. He, S. Sophon, A. Schmitz, and S. Sugano, “Design Optimisation and Performance Evaluation of a Toroidal Magnetorheological Hydraulic Piston Head,” 2016.

[100] G. Aguirre Dominguez, M. Kamezaki, H. Shan, and S. Sugano, “Performance Evaluation of a Compliant Magnetorheological Piston Actuator,” in *2016 IEEE/SICE International Symposium on System Integration (SII2016)*, 2016, pp. 254–259.

[101] Y. Ogura, H. Aikawa, K. Shimomura, H. Kondo, A. Morishima, H. Lim, and A. Takanishi, “Development of a new humanoid robot WABIAN-2,” in *2006 IEEE International Conference on Robotics and Automation (ICRA 2006)*, 2006, no. May, pp. 76–81.

[102] H. Iwata and S. Sugano, “Design of human symbiotic robot TWENDY-ONE,” *2009 IEEE Int. Conf. Robot. Autom.*, pp. 580–586, May 2009.

[103] M. Zinn, B. Roth, O. Khatib, and J. K. Salisbury, “A New Actuation Approach for Human Friendly Robot Design,” *Int. J. Rob. Res.*, vol. 23, no. 4–5, pp. 379–398, 2004.

# 11 Relevant Works

## Journal Paper

[1] G. Aguirre Dominguez, M. Kamezaki, and S. Sugano, "*Proposal and Preliminary Feasibility Study of a Novel Toroidal Magnetorheological Piston*", Transactions in Mechatronics, vol. PP, no. 99, Oct. 2016

## Conference Papers

[2] G. Aguirre Dominguez, M. Kamezaki, M. French and S. Sugano, "*Development of a backdrivable magnetorheological hydraulic piston for passive and active linear actuation*", 2015 IEEE/RSJ International Conference in Intelligent Robots and Systems (IROS2015), pp. 6551-6556, Oct. 2015

[3] G. Aguirre Dominguez, M. Kamezaki, M. French and S. Sugano, "*Modelling and Simulation of a New Magnetorheological Linear Device*", 2015 IEEE International Symposium on Robotics and Intelligent Sensors (IRIS2015), pp. 235-240, Oct. 2015

[4] G. Aguirre Dominguez, M. Kamezaki, H. Shan and S. Sugano, "*A Novel Toroidal Design for Magnetorheological Dampers*", The 2015 JSME/RMD International Conference on Advanced Mechatronics (ICAM2015), pp. 113-114, Dec. 2015

[5] G. Aguirre Dominguez, M. Kamezaki, M. French and S. Sugano, "*An Iterative Design Methodology for the Performance Optimisation of Magnetorheological. Piston Head Configurations*", 2016 IEEE International Conference on Advanced Intelligent Mechatronics (AIM2016), pp. 228-233, Jul. 2016

[6] G. Aguirre Dominguez, M. Kamezaki, Shan He, S. Somlor, A. Schmitz, S. Sugano, "*Design Optimisation and Performance Evaluation of a Toroidal Magnetorheological Hydraulic Piston Head*", 2016 IEEE/RSJ International Conference on Intelligent Robots and Systems (IROS2016), pp. 350-355, Oct. 2016

[7] G. Aguirre Dominguez, M. Kamezaki, H. Shan and S. Sugano, "*Performance Evaluation of a Magnetorheological Piston for Compliant Linear Actuation*", 2016 IEEE/SICE International Symposium on System Integration (SII2016), pp. 254–259, Dec. 2016

## Patents

[8] S. Sugano, M. Kamezaki, G. Aguirre / 菅野　重樹, 亀﨑　允啓, アギーレ　ゴンサロ, "*Compliant Actuator /コンプライアントアクチュエータ*", JP2016-142320A, Aug. 2016

[9] A. Schmitz, S. Bhavaraju, Y. Sakamoto, G. Aguirre Dominguez, S. Ritsuki, W. Wang, S. Sugano / シュミッツ　アレクサンダー, ババラジュ　ソウミヤ, 坂本　義弘, アギーレ ドミンゲス　ゴンサロ, 佐藤　立樹, 汪　偉, 菅野　重樹, "*Control System for a Robotic Arm / ロボットアームの制御システム*", 2015-134828, Jul. 2015

[10] M. Kamezaki, G. Aguirre, K. Otsuki, P. Zhang, S. Sugano / 亀﨑　允啓, アギーレ　ゴンサロ, 大槻　健史郎, 张　裴之, 菅野　重樹", "*Compliant Rotatory Drive Unit / 回転型コンプライアント駆動装置*', WSD-16009, Dec. 2016

## Co-Authored Papers

[11] M. Adachi, G. Aguirre Dominguez, T. Sasaki, R. Tsumura, T. Koshi, K. Mori, "*Novel Social Innovation Concept Based on the Viewpoint of the Infrastructure User*", 2015 IEEE 12th International Symposium on Autonomous Decentralized Systems (ISADS 2015), pp. 295-300, Mar. 2015

[12] M. Kamezaki, G. Aguirre Dominguez, J. Yang, H. Iwata, S. Sugano, "*Development of a tele-operation simulator based on virtual reality environment for advanced unmanned construction*", 2013 IEEE/SICE International Symposium on System Integration (SII), pp. 855-860, Dec. 2013

[13] S. Somlor, G. Aguirre Dominguez, A. Schmitz, M. Kamezaki, S. Sugano, "*A Haptic Interface with Adjustable Stiffness Using MR Fluid*", 2015 IEEE International Conference on Advanced Intelligent Mechatronics (AIM 2015), pp. 1132-1137, Jul. 2015

[14] A. Schmitz, S. Bhavaraju, S. Somlor, G. Aguirre Dominguez, K. Mitsuhiro, W. Wang, S. Sugano, "*A Concept for a robot arm with adjustable series clutch actuators and passive gravity compensation for enhanced safety*", 2015 IEEE International Conference on Advanced Intelligent Mechatronics (AIM), pp. 1322-1327, Jul. 2015

[15] 亀﨑 允啓, 何 山, アギーレ・ドミンゲス・ゴンサロ, フレンチ・モルガン, 菅野 重樹, "*能受動性を有するリニアアクチュエータのためのバックドライバビリティ磁性油圧ピストンの開発*", 日本機械学会ロボティクス・メカトロニクス講演会2016論文集(Robomec'16), 2P1-13b2, Jun. 2016

[16] 亀﨑 允啓, 何 山, アギーレ・ドミンゲス・ゴンサロ, 菅野 重樹, "*磁場解析に基づくMRピストンヘッドの構成パラメータとパフォーマンスの関連性評価*", 第17回計測自動制御学会システムインテグレーション部門講演会論文集(SI2016), Dec. 2016

# 12 Embodiment Informatics

In the dawn of the digital era, computer science developed at an unimaginable pace. The continuous miniaturization of computers with ever-increasing processing power has enabled more complex software applications to spread into a variety of consumer devices. Nowadays, these intelligent devices are capable to assist people in a variety of situations. However, in some situations the newly created digital world appears to overlook the human element. Interactions with the real world seem to be increasingly replaced by artificial relations taking place in the digital world. As a result, there is a trend that seeks to bridge the current gap between the digital and the real world. These days, there are more applications aiming to promote and improve our interactions, activities, and relations in the physical world.

In this scenario, the development of human centred technologies is becoming increasingly important for future applications. In order to achieve this, a multidisciplinary approach is necessary to ensure that these novel solutions can successfully address the technological and social expectations. In this respect, I personally see embodiment informatics not as an aim, but as a tool that allows us to integrate different perspectives. In this sense, embodiment informatics should not be focused the technological development itself, but rather in providing a methodology to pursue technological innovation through a curiosity driven

approach. Following this path, embodiment informatics can open the path to new technological frontiers, by striving to create bridges between physical objects and the data generated every day in the digital world.

Although big, the gap between the different aspects of the physical and digital world can be bridged by bringing together people from different backgrounds. By having different people involved in the development process, embodiment informatics tries to free us from the current research paradigms. In this way, this new methodology does not seek for new ways to apply our current knowledge, but it rather proposes novel creative strategies to communicate, assimilate, and try out ideas from other people. By doing so, the research of the physical and digital worlds can work together to complement and broaden their scope and reach. As the cooperation both research fields increases the gap between both worlds will certainly begin to close.

Embodiment informatics as a method has the potential to impact every aspect in the technology creation progress. For instance, one of the most common paradigms can be found in the design and development phases for new products. In a typical application development approach, first the mechanical structure of the prototype is conceptualised. Then, the necessary software is developed in order to control it. Although this process goes through several iterations to refine the product, the fundamental assumption is to design a software in order to control a mechanical device. However, by inverting the rolls between software and mechanical engineers new possibilities can be explored. This inversed approach could create applications that are tuned to respond to particular data algorithms. Then, it is possible to have machines that adapt to music trends on the internet, swarm robots that help to present cloud data, or haptic technologies tuned for VR scenarios. This is not the only scenario in which embodiment informatics serves as a powerful tool to enable a creative collaborative process for exploring new ideas. In the future as technology evolves embodiment informatics will certainly become a necessary instrument to curiously explore new frontiers in research and industry.

As it was mentioned before, embodiment informatics is a tool to enhance creative collaboration by bringing physical and virtual elements together. Therefore, embodiment informatics can also be seen as a tool that creates links between these two opposing concepts. Merging concepts from both worlds can lead to discover new possibilities of the application and conceptualization of technology. In order to achieve this, researchers in embodiment informatics must keep an open mind to find possible ways to apply technology to currently

unthinkable fields. Perhaps, using semantic data to represent real objects, or mechanical devices to represent information such in the case of haptic technologies in virtual reality, are common approaches today. But in the future, adding information to vegetables and fruits may sound like a bad science fiction movie, but until this possibility is explored one must keep an open mind for it. Perhaps it could be possible to embed certain information on the food's surface by using nano-machines. Or for example, using musical patterns to drive mechanical devices to achieve a particular task, such as controlling swarms. Information and embodiment must slowly extend their meaning to reach into many fields in order to realise its full potential. However, just mixing topics, people and research ideas does not ensure that new interesting technologies will be born. I believe that certain conditions must be met in order for collaborative creativity to occur.

In the current global economy, rigid planning, inflexible structures, and tight research schedules are the result of increased competition and strict budget controls from government and funding agencies. As a result, research has taken a rather market driven approach. Prioritising technology marketability and immediate applicability over curiosity to explore new frontiers. However, I believe it is important to remember that it is innate curiosity what has supported the evolution of technology, and with it, the advancement of humanity. In this sense, embodiment informatics should encourage freedom of exploration and creativity. This methodology must remind us that not everything must be useful, at least for the time being. Some discoveries that may not be applicable at the moment, later, when combined with other unrelated discoveries, can solve problems that could have never been solved by the application of a single technology. In this respect, I believe that embodiment informatics intrinsically points towards exploration, rather than the development of new technologies as a goal. In order to achieve this, embodiment informatics looks to bring many disciplines together in a flexible environment. In a way so that researches can have the freedom, flexibility, and time to collaborate and explore new ideas.

In respect with the research covered in this thesis, the involvement with embodiment informatics enabled me to improve and expand my research. The modelling of the complex phenomena involved in magnetorheological actuators presented several challenges throughout the research. The interaction with researchers working in the field of physical simulation provided insights about possible solutions to improve the accuracy of the mathematical models. Moreover, constant discussions about a variety of related topics allow me to realise new approaches to the problems faced during my research. Additionally, interaction with other

scientists allow me to realise other potential applications of my technology. In this way embodiment informatics acted as a tool that did not only improved the quality of my research, but also provided clues on other possible applications for it.

In conclusion, I personally do not see embodiment informatics as a technological aim in itself, but rather as a powerful tool to enable a creative collaborative process for exploring new ideas. In order for this methodology to work, the mind of a researcher must have the necessary freedom and time to interact, learn, and discuss in a highly open multidisciplinary environment. It is through this process that researchers will find new horizons to explore new frontiers for current information technologies to interact with the physical world. In the future, I believe that the fields of application of embodiment informatics will continue to grow providing new imaginative and surprising results. Just as the physical world can be extended in almost any imaginable direction, the research based in embodiment informatics can reach into other knowledge fields. In order to be able to see these possibilities we, as embodiment informatics researchers, must go to uncommon places to find inspiration. As we continue to grow in our careers we must never forget to continue to curiously listen, learn and research with an open mind towards other cultures, people, and fields of knowledge.

# 13 Appendices

# Appendices Contents

# A) MR Piston Prototype Early Version Drawings

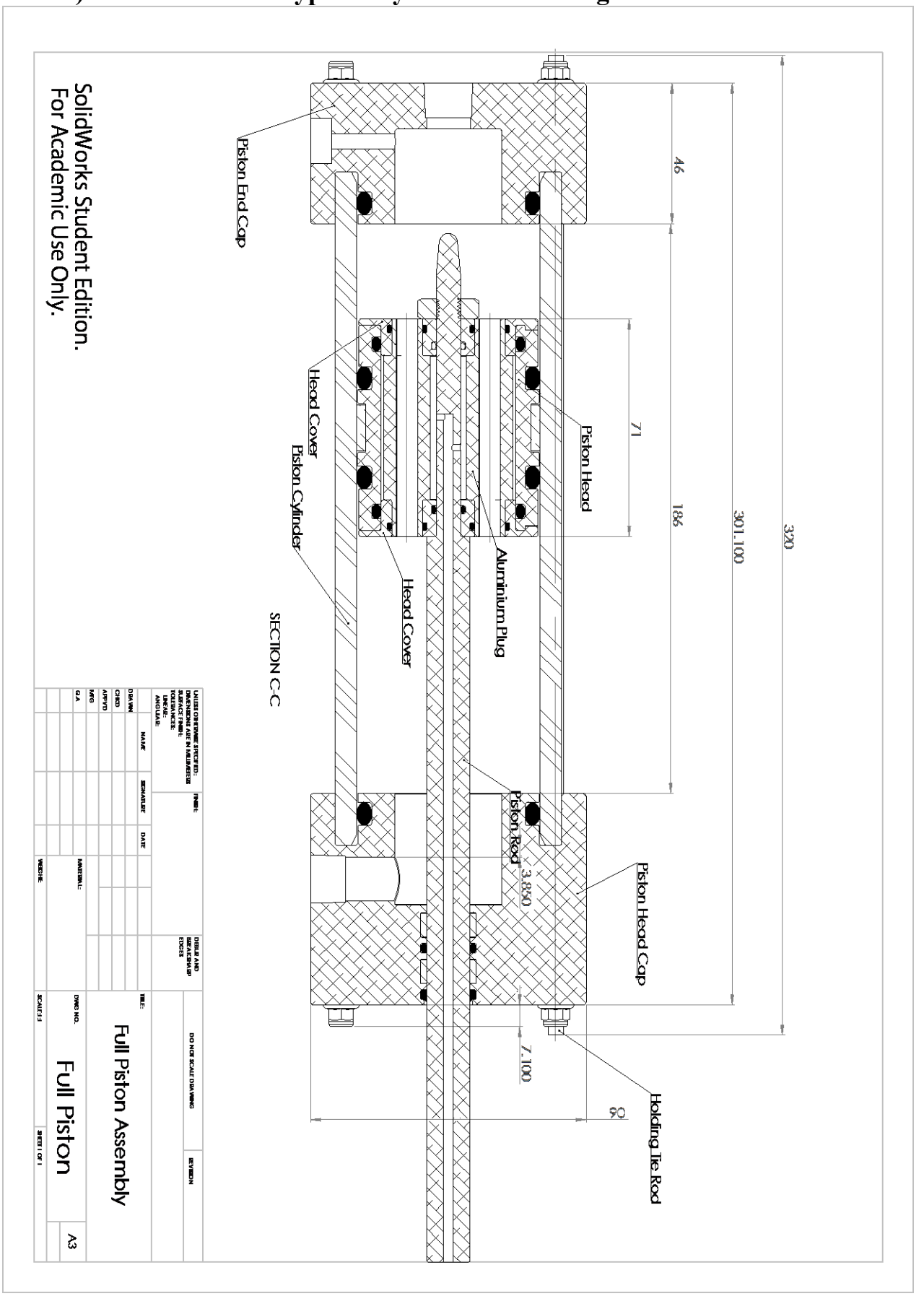

## B) MR Piston Prototype Optimised Version Assembly Drawing

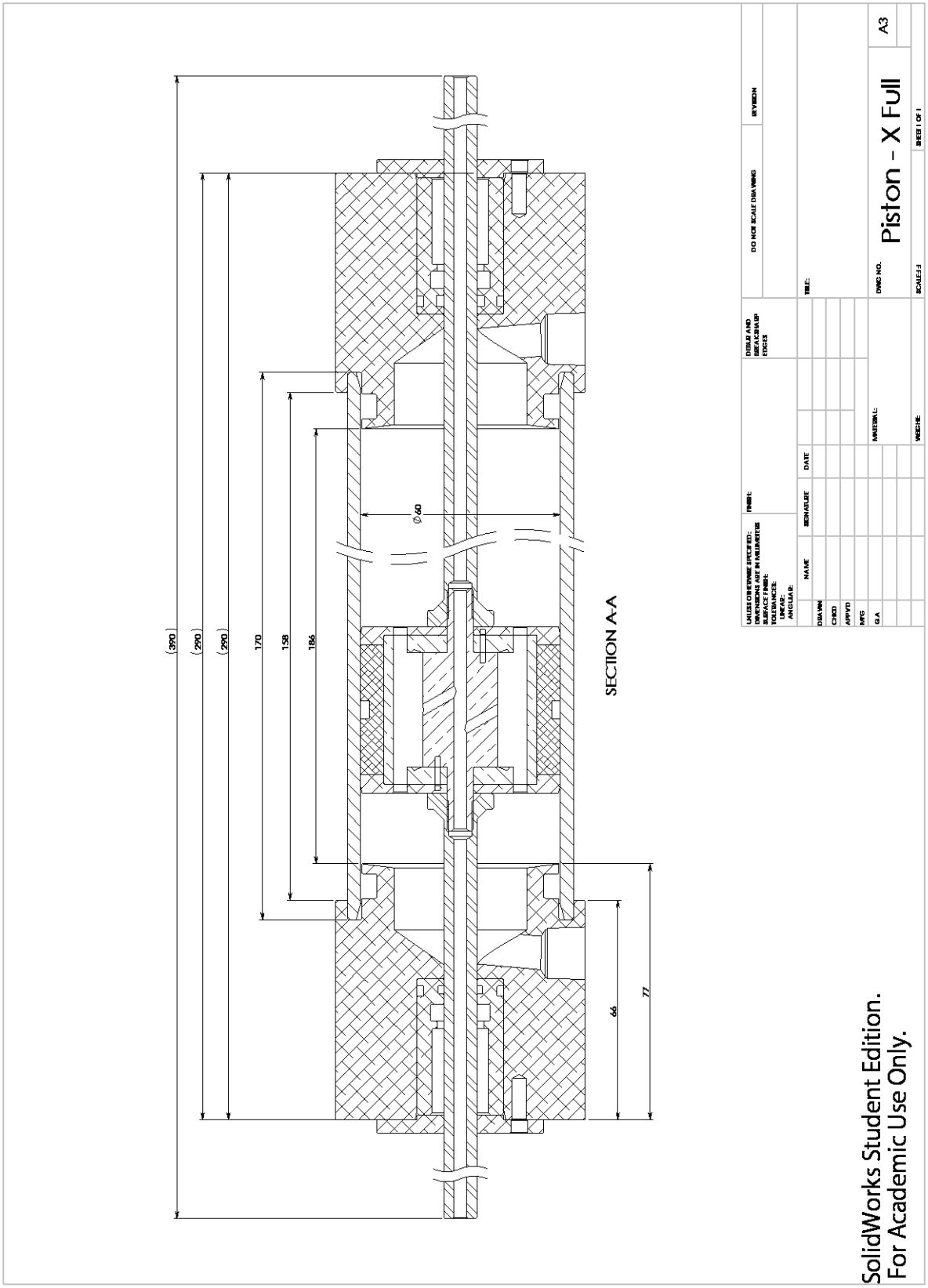

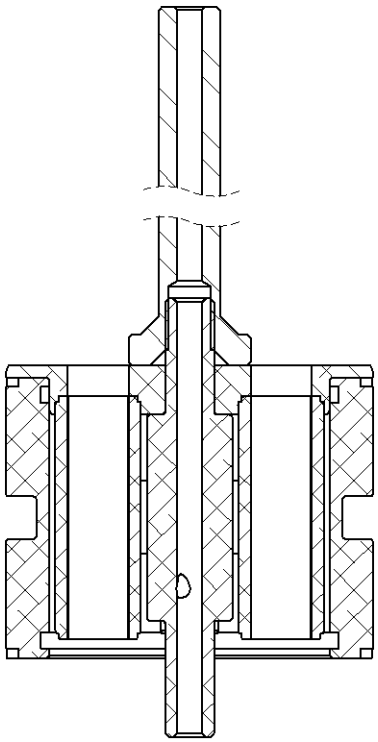

SECTION B-B

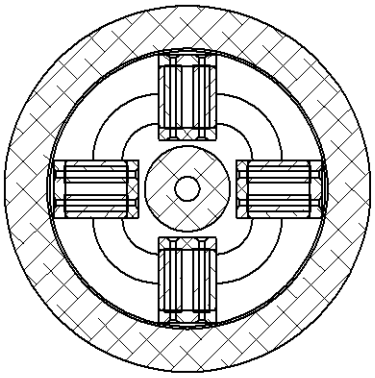

SECTION A-A

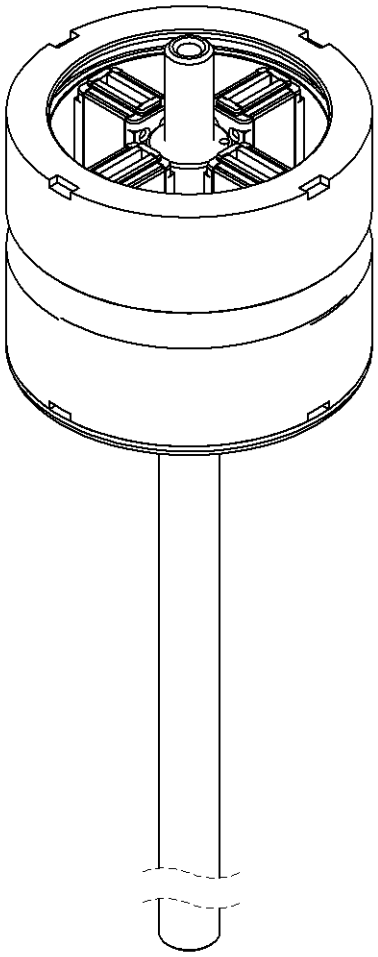

| | | | |
|---|---|---|---|
| UNLESS OTHERWISE SPECIFIED:<br>DIMENSIONS ARE IN MILLIMETERS<br>SURFACE FINISH:<br>TOLERANCES:<br>LINEAR:<br>ANGULAR: | FINISH: | DEBUR AND BREAK SHARP EDGES | DO NOT SCALE DRAWING / REVISION |

| | NAME | SIGNATURE | DATE |
|---|---|---|---|
| DRAWN | | | |
| CHKD | | | |
| APPVD | | | |
| MFG | | | |
| Q.A | | | |

MATERIAL:

WEIGHT:

TITLE:

Toroidal Assembly

DWG NO. Tor-PistonAseembly A4

SCALE:1:1 SHEET 1 OF 1

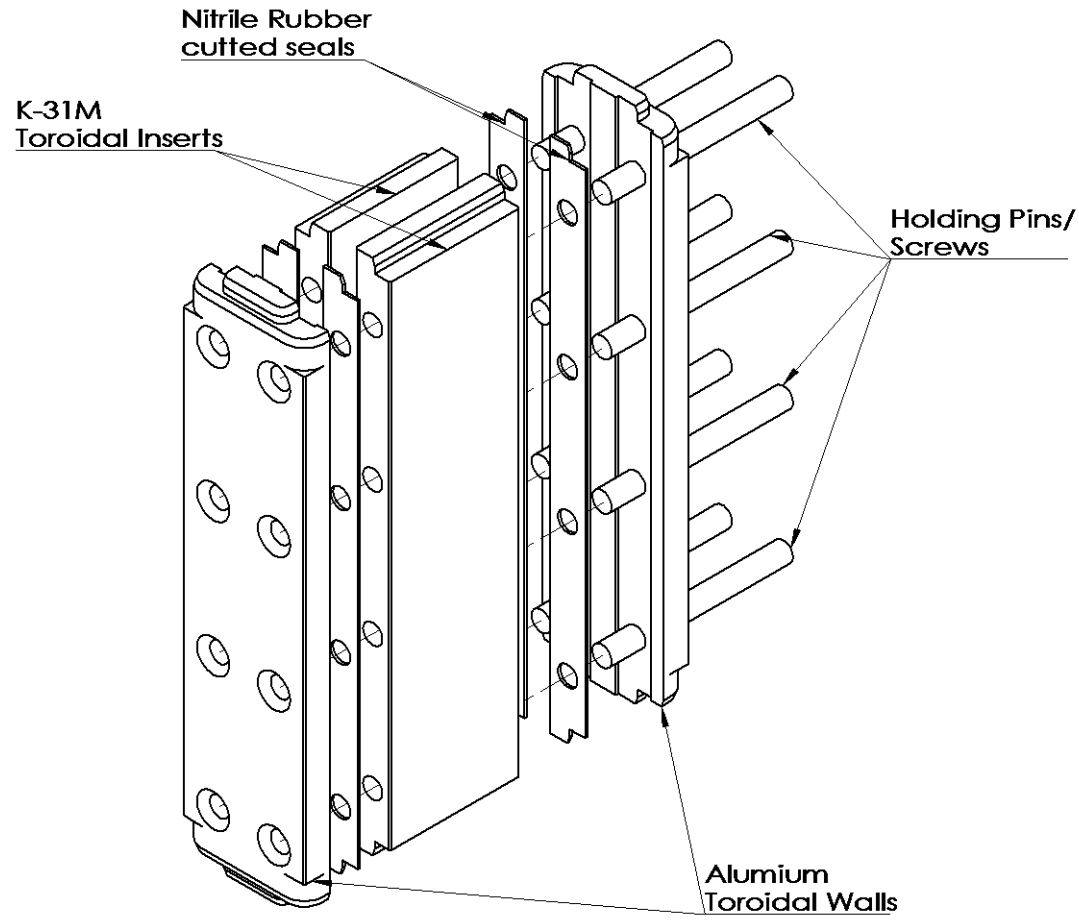


| | | | | | |
|---|---|---|---|---|---|
| UNLESS OTHERWISE SPECIFIED:<br>DIMENSIONS ARE IN MILLIMETERS<br>SURFACE FINISH:<br>TOLERANCES:<br>LINEAR:<br>ANGULAR: | FINISH: | | DEBUR AND BREAK SHARP EDGES | DO NOT SCALE DRAWING | REVISION |
| | NAME | SIGNATURE | DATE | TITLE: | |
| DRAWN | | | | Exploded View Plug | |
| CHK'D | | | | | |
| APPV'D | | | | | |
| MFG | | | | | |
| Q.A | | | MATERIAL: | DWG. NO. Toroidal Plug Assembly | 44 |
| | | | WEIGHT: | SCALE:2:1 | SHEET 1 OF 1 |

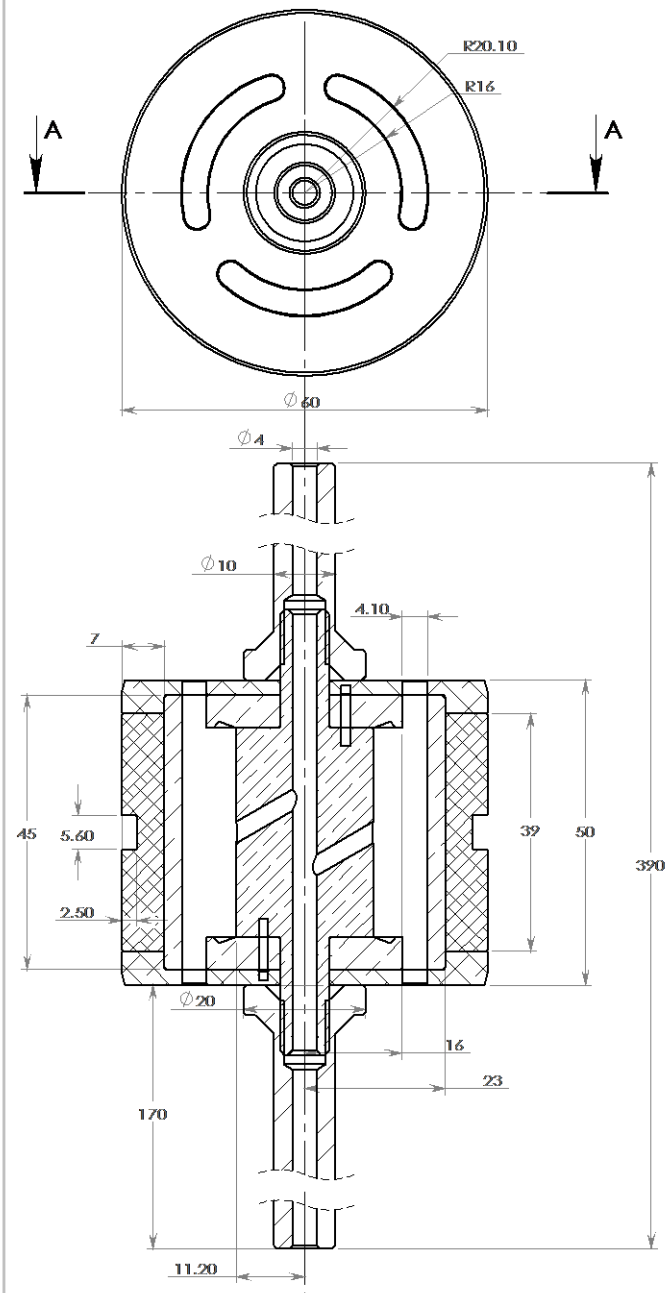


SECTION A-A

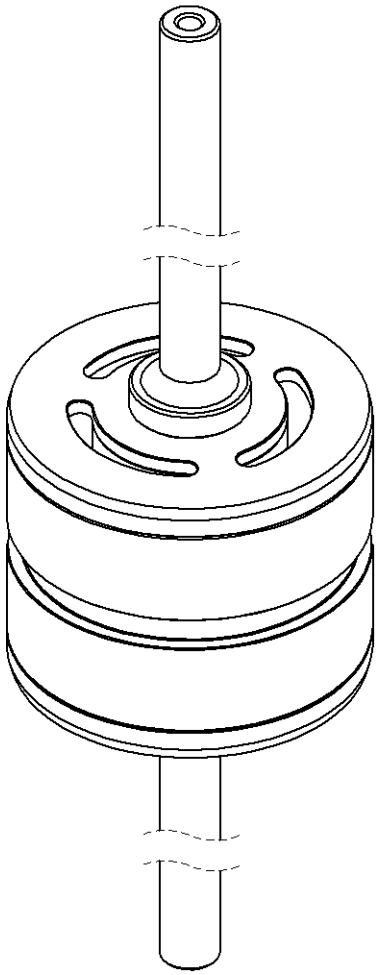

| | | | |
|---|---|---|---|
| UNLESS OTHERWISE SPECIFIED:<br>DIMENSIONS ARE IN MILLIMETERS<br>SURFACE FINISH:<br>TOLERANCES:<br>LINEAR:<br>ANGULAR: | FINISH: | DEBUR AND BREAK SHARP EDGES | DO NOT SCALE DRAWING / REVISION |

| | NAME | SIGNATURE | DATE |
|---|---|---|---|
| DRAWN | | | |
| CHKD | | | |
| APPVD | | | |
| MFG | | | |
| Q.A | | | |

MATERIAL:

WEIGHT:

TITLE:

F0 Assembly Set

DWG NO. Annular-PistonAssembly2

A4

SCALE:1:1

SHEET 1 OF 1

## C) Rotatory Actuator – Vane Hole Design Assembly Drawings

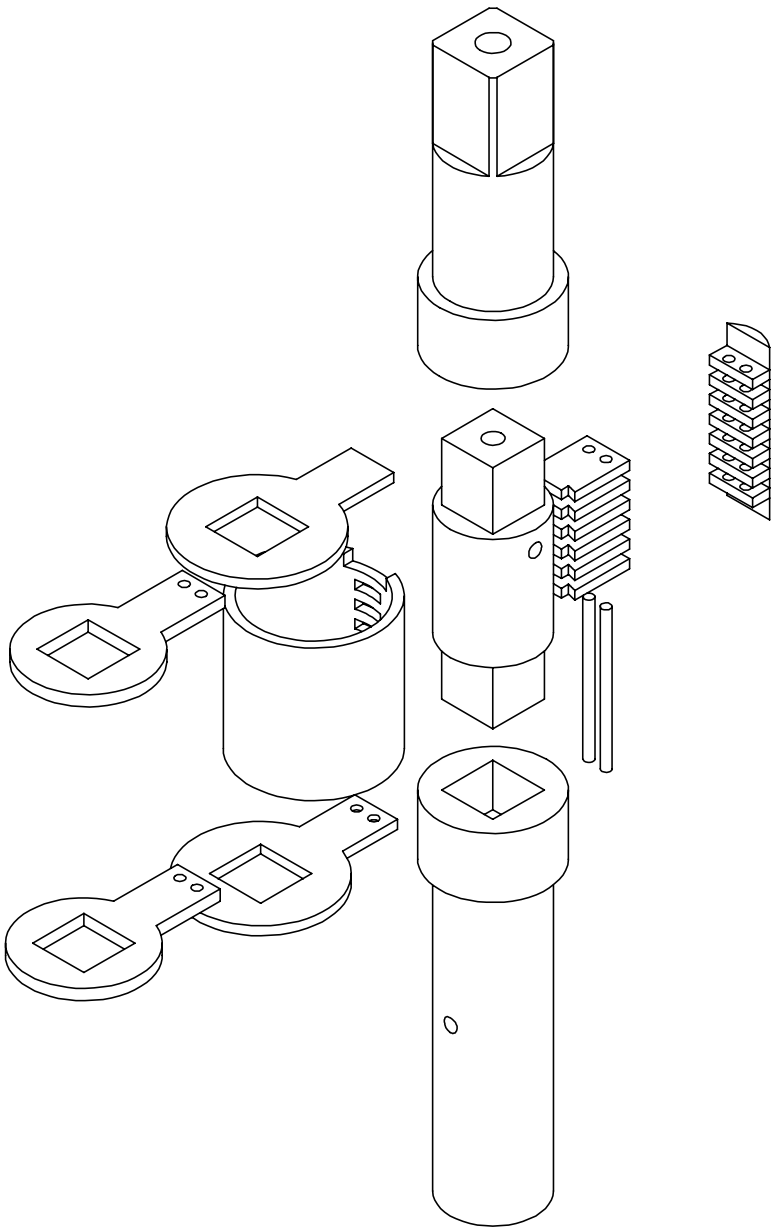

| | | | | | | | | |
|---|---|---|---|---|---|---|---|---|
| UNLESS OTHERWISE SPECIFIED:<br>DIMENSIONS ARE IN MILLIMETERS<br>SURFACE FINISH:<br>TOLERANCES:<br>LINEAR:<br>ANGULAR: | | | FINISH: | | | DEBUR AND BREAK SHARP EDGES | DO NOT SCALE DRAWING | REVISION |
| | NAME | SIGNATURE | DATE | | | | TITLE: | |
| DRAWN | | | | | | | | |
| CHK'D | | | | | | | | |
| APPV'D | | | | | | | | |
| MFG | | | | | | | | |
| Q.A | | | | | | | DWG NO. | A4 |
| | | | | | | | Explosion | |
| | | | | | WEIGHT: | | SCALE:1:2 | SHEET 1 OF 1 |